Characterisation of thermomechanical properties of bituminous mixtures used for railway infrastructures

Diego Alejandro Ramirez Cardona

N°d'ordre NNT : 2016LYSET009

THESE de DOCTORAT DE L'UNIVERSITE DE LYON
opérée au sein de
L'Ecole Nationale des Travaux Publics de l'Etat

Ecole Doctorale 162
Mécanique, Energétique, Génie Civil, Acoustique (MEGA)

Spécialité de doctorat : Génie Civil

Soutenue publiquement le 14/11/2016, par :
Diego Alejandro Ramirez Cardona

Characterisation of thermomechanical properties of bituminous mixtures used for railway infrastructures

Devant le jury composé de :

DAOUADJI, Ali	Professeur	INSA Lyon	Président
CANESTRARI, Francesco	Professeur	Università Politecnica delle Marche	Rapporteur
HARVEY, John	Professeur	University of California Davis	Rapporteur
CALON, Nicolas	Docteur	SNCF Réseau	Examinateur
DI BENEDETTO, Hervé	Professeur	ENTPE	Directeur de thèse
SAUZEAT, Cédric	Docteur	ENTPE	Tuteur
OLARD, François	Docteur	EIFFAGE Infrastructures	Invité

“En todo amar y servir”

“Alcanza la excelencia y compártela”

San Ignacio de Loyola

“In all things, to love and to serve”

Saint Ignatius of Loyola

I. Abstract and keywords

The research presented in this document was carried out in collaboration between the National School of Public Works (*Ecole Nationale des Travaux Publics de l'Etat* – ENTPE) of the University of Lyon and the French National Railway Company (*Société Nationale des Chemins de Fer* français – SNCF). The objective of this study is the characterisation of the thermomechanical properties of road base-course bituminous mixtures commonly used in France for their use in railway track structures. Linear Viscoelastic (LVE) and fatigue resistance properties have been investigated. The influence of moisture damage including freeze-thaw cycles on the properties of the studied mixtures was also studied.

LVE and fatigue resistance properties were obtained by means of sinusoidal tension-compression tests on cylindrical samples at the ENTPE/LTDS laboratory. A protocol for moisture conditioning of bituminous mixtures samples was developed based on the French and American standard test methods for moisture susceptibility and on the literature review on the subject. Moisture damage was assessed using complex modulus and fatigue tests. The LVE behaviour of the materials was described using the 2S2P1D (2 Springs, 2 Parabolic elements and 1 Dashpot) model developed at the ENTPE/LTDS laboratory.

Three road base-course mixtures available in the French market were studied: a GB3, a GB4 and a mixture called GB PMB (for Polymer-Modified Bitumen). The GB3 mixture stands as the reference material since it is commonly used for the base-courses of conventional roads in France. The GB4 mixture stands as a better performing material than the GB3. The specific studied GB4 formulation corresponds to that used as sub-ballast of the Brittany-Loire high-speed line (HSL) in western France. The GB PMB stands as an improved version of the GB3 in which the base bitumen is replaced by polymer-modified bitumen. The interest of the study of this third mixture is to assess the relevance of using PMB's in bituminous mixtures intended for railway platforms.

The test zone of the East-European HSL served as case study to identify the loading conditions and the behaviour of a bituminous sub-ballast layer in a French track. The several advantages of using bituminous mixtures as sub-ballast material identified in the literature are confirmed by the feedback from this test zone.

The results obtained show that the studied bituminous mixtures present excellent bearing capacities (stiffness) for their use as sub-ballast layers in France. The used moisture conditioning protocol did not alter the LVE behaviour of the materials. The good performance of the materials is then expected to be perennial regarding the effect of moisture on the LVE behaviour. With respect to fatigue resistance, the results show that the use of a PMB provides an important increase of the fatigue life as well as a reduction of the susceptibility to moisture damage. However, given the identified loading levels of the bituminous sub-ballast in a common French track structure, all three mixtures present adequate fatigue resistance properties.

Keywords: Bituminous mixture, viscoelasticity, fatigue resistance, sub-ballast layer, railway track.

II. Acknowledgements

I would like to spend a few words to thank all those who accompanied me during my PhD. Your encouragement and assistance has been crucial for the accomplishment of this thesis.

To my thesis advisor, Professor Hervé Di Benedetto, my sincere gratitude and esteem for believing in me and for his essential guidance and support thought these last three years and a half. It has been an honour to work and to exchange ideas with him. His work method, his approach to research, the scientific rigorousness, are just some of the valuable things he have though me that will be my tools to build a prosperous carrier from now on. His teachings have gone far beyond the scientific plan and they have improved the way I confront life and all its challenges. Thank you deeply professor.

My gratitude and consideration also go to Dr. Cédric Sauzéat, who has accompanied me in every step of this project. His advises and contributions to my theses were indispensable for its completion. His perseverance, patience, talent and sense of humour are an inspiration not only for me, but for the whole team at the laboratory.

To my "boss", Nicolas Calon, I would like to express my sincere admiration and my immense gratitude. I had always been curious about railways and I owe him the opportunity to have done my thesis in that field. His knowledge and love for railways helped turn my curiosity into passion. His trust in me and his constant interest for my work were precious source of motivation.

I also wish to thank all the other members of the PhD defense committee: Prof. Ali Douadji for presiding over the jury, Prof. Francesco Canestrari and Prof. John Harvey for having reviewed my dissertation and Dr. François Olard for having examined my work. I am truly honoured that you have agreed to participate in my defense and I am thankful for your appreciation and for the long journey that some of you had to make.

I would also like to thank the SNCF for its financial and material support of this project. My esteem goes to the whole team of the CIR division, which I was part of. I specially thank Dr. Gilles Saussine and Dr. Alain Robinet for taking me into your work team and for the many fructuous exchanges.

I also thank EIFFAGE Infrastructures for the material support of this project and for having given me the opportunity to discover the world of bituminous mixtures during my previous studies. In your laboratory, I learned the bases on which this study is built.

I couldn't forget to thank the PhD colleagues, faculty members, technicians and all those who are part of the ENTPE team. Thank you for all the enriching moments of chatting, debating, teaching, learning, eating, *coffee-breaking*, working together.

I wish to thank my family and loved ones. To my mom, dad and brothers, in spite of the distance, your support, teachings and love got me here and will keep me going further on through life. To my friends, thank you for sharing with me this moment of my life. You all are my infinite source of support and motivation.

Now, shall we?

III. Table of contents

IV. List of figures

V. List of tables

VI. Glossary and Symbols

a_T	Shift factor for the construction of master curves
C_1, C_2	Constants of the WLF equation
CT	Computed Tomography
DER	Dissipated Energy Ratio
E*	Complex modulus
E_1	Real part of the complex modulus
E_2	Imaginary part of the complex modulus
ITS	Indirect Tensile Strength
f	Frequency
F	Force
GB	*Grave Bitume*: French type of base-course bituminous mixture
j	Complex number so that $j^2=-1$
J(t)	Creep function
N	Number of cycles
PMB	Polymer Modified Binder
R(t)	Relaxation function
t	Time
T	Temperature
T_{ref}	Reference temperature
TGV	*Train à Grande Vitesse*: High-speed train
UGM	Unbound Granular Material
W	Viscous dissipated energy
ε	Strain
η	Viscosity
ν*	Complex Poisson's ratio
σ	Stress
φ	Phase angle
ω	Pulsation

VII. Introduction

The development of the railway transportation industry comes with an increase in circulation speeds, freight loads and traffic volume. Improving the track structure is then necessary in order to cope with the increasing solicitations and to ensure low railway operating costs, high passenger comfort and circulation safety during the entire lifetime of the railway. For ballasted tracks, sub-ballast layers are a crucial element for the mechanical performance of the track and for the protection of the subgrade. Using bituminous mixtures for sub-ballast layers has been acknowledged as a possible solution for the necessary enhancement of the track structure. Several studies and field experiences have identified some advantages of sub-ballast bituminous layers including vibration damping, reducing stress levels on the subgrade, constituting a low permeability layer over the supporting soil, among others. Tracks with bituminous sub-ballast layers have also shown lower maintenance needs than tracks with an unbound granular materials structure. In addition, constructive advantages have also been observed such as allowing the circulation of engines on the platform during the construction phase (European Asphalt Pavement Association (EAPA), 2014; Fang, Fernández Cerdas, & Qiu, 2013; Huang, Lin, & Rose, 1984; Robinet & Cuccaroni, 2012; Rose & Bryson, 2009).

In 2004, the French National Railway Company (SNCF) designed a 3km long experimental zone with a bituminous mixture sub-ballast layer in the East-European High-Speed Line (EE HSL) that connects Paris to eastern France. This HSL has been in service since 2007 with circulation of French TGV and German ICE passenger trains at a commercial speed of 320 km/h. By 2013, its average annual daily traffic (AADT) was estimated at 112 trains per track. So far, the test section has presented a very good behaviour and, most interesting, a significant reduction and a better efficiency of the maintenance operations compared to the surrounding sections made with conventional granular materials. The success of the EE HSL test section encouraged the use of bituminous sub-ballast layers in various sections of four major French HSL projects, three of which should be in service by 2017.

Regarding geometry degradation of ballasted tracks, several authors highlight the need to understand the ballast and subgrade deterioration mechanisms in order to improve maintenance efficiency while preserving the viability, comfort and safety of the railway. A necessary step to understand the degradation process of tracks with bituminous sub-ballast layers is to characterise the mechanical behaviour of bituminous mixtures under railway traffic loading conditions.

Road base-course bituminous mixtures are used in France for the construction of HSL sub-ballast layers. These materials are mostly conceived for highway pavement loading conditions, which differ largely from those of HSL trackbeds. The differences include the constant compression effort due to the ballast and superstructure weight; the dynamic phenomena due to high-speed circulation and the greater axle loads, the unique loaded trajectory due to the fact that trains are a guided transport system, among others. Moreover, these mixtures are exposed to weather conditions during their service life unlike in highway pavements where they are protected by the overlaying wearing course. Taking into account all of these factors when characterizing the mechanical behaviour of bituminous mixtures is crucial for drawing

conclusions on their performance as sub-ballast layers and, therefore, their role in the degradation process of the track structure.

Aware of this, the French National Railway Company (SNCF), owner and manager of the French railway network, launched this research in collaboration with the National School of Public Works (ENTPE), member of the University of Lyon. The objective of this study is to characterize the thermomechanical behaviour of bituminous mixtures intended to be used in railway platforms. Commonly used road base-course materials were studied in order to assess whether they present adequate properties for railway applications, or whether specially designed mixtures for railways are needed.

More specifically, viscoelastic and fatigue resistance properties were characterized for three different mixtures: a GB3, a GB4 and a mixture called GB PMB (for Polymer-Modified Bitumen). The GB3 mixture was chosen as the reference material since it is commonly used for the base-courses of conventional roads in France. The GB4 mixture stands as a better performing material than the GB3 normally used for highways or high traffic roads. The specific studied GB4 formulation corresponds to that used as sub-ballast of the Brittany-Loire high-speed line (HSL) in western France. The GB PMB stands as an improved version of the GB3 in which the base bitumen was replaced by polymer-modified bitumen. The interest of the study the GB PMB mixture is to assess the relevance of using PMB's in bituminous mixtures intended for railway platforms. The study of these materials allows observing the influence of air void content, binder content and binder polymer-modification in the thermomechanical properties of bituminous mixtures, in the light of their aptitude to be used in railway platforms.

This manuscript is organised in six sections. The first one presents a literature review on bituminous materials and their different properties as well as their use in railway infrastructures. Special attention is given to moisture susceptibility of bituminous mixtures. The second section presents the EE HLS case study and the conclusions from the experience feedback. The third section presents the tested materials and the tests carried out at the laboratory for the characterisation of their thermomechanical properties. The results from the complex modulus tests are presented in section 4 of this manuscript and those from the fatigue tests in section 5. Finally, general conclusions are drawn and perspectives for future studies are proposed in chapter 6.

1 Literature review

1.1. The bituminous mixtures and their components

Bituminous mixtures are composite materials for which determining the mechanical behaviour is a complex task. Mechanical properties of bituminous mixtures depend on their volumetric composition, on the characteristics of their components and on the working conditions, especially temperature and loading application time. When used in railways, this translates into a track structure whose mechanical behaviour depends not only on the quality of its components, but also on traffic circulation and climatic conditions.

This section exposes what a bituminous mixture is, describes its components and explains the most relevant methods for characterising their mechanical properties. The relation between the properties of each component and the global behaviour of the bituminous mixture is highlighted.

1.1.1. Definition of bituminous mixture

A bituminous mixture is defined as a composite material consisting of mineral aggregates and bitumen (Corté & Di Benedetto, 2004; Di Benedetto & Corté, 2004). The aggregates are considered as the mineral structure or "skeleton" of the material, while the bitumen provides cohesion to the whole system. In reality, the cohesion is provided by the mixture of bitumen and fine particles of the aggregates, which is called mastic. Air is also present in the interstices of the material.

Bituminous mixtures are predominantly implemented in road pavement structures. Depending on the construction methods, and on traffic and environmental conditions, different additives can be added to the mixture in order to improve certain properties. The most commonly used ones are polymers to modify the bitumen structure, warm mix additives to reduce mixing and compaction temperatures, anti-stripping agents to reduce the loss of binder-aggregate adhesion in presence of water, and emulsifiers which are necessary for the cold-mix production and pavement surface treatments (Mangiafico, 2014).

1.1.2. The aggregates

The aggregates are the main constituent of bituminous mixtures representing approximately 95% of the total mass of the material and 80% to 85% of its volume (Corté & Di Benedetto, 2004). They are defined by the European Standard (EN 13043, 2003) as mineral materials used in the construction industry and they can arise from natural sources, like alluvial deposits, or be extracted from quarries by mechanical procedures. Depending on its origin and on the extraction procedures, the aggregates can have either round or crushed aspects. Normally, quarry-extracted aggregates have crushed aspect and alluvial ones have round aspect. Natural aggregates can be further processed to obtain a certain grain size, according to which they are classified into different homogeneous granular classes. The addition and mixing of different granular classes gives origin to the granular "skeleton" of the bituminous mixture (Corté & Di Benedetto, 2004). The skeleton is made of the inter-granular contact through which the efforts are transmitted from the loaded surface of the pavement to the subgrade. The form, angularity, surface texture and hardness of the aggregates will then be determinant for the mechanical behaviour of bituminous mixtures. Rotation and displacements of the aggregates in the compacted mixture must be reduced and the internal friction angle increased in order to obtain optimal performances. Angular grains provide higher internal friction angle than round ones. The mechanical resistance of the mineral material (mother rock) itself is also important so that the aggregate will not fail under the traffic solicitations (Sohm, 2013).

The different granular classes are defined by a minimum (d) and a maximum (D) grain size. The D/d ratio is set to 1.4 to avoid excessive size dispersion within each class. The grain sizes are determined through Particle Size Distribution (PSD) analysis using an arrangement of standard sieves. Three grand classes are defined by the European Standard (EN 13043, 2003):

Table 1-1. Granular classes of aggregates according to the European Standard (EN 13043, 2003)

Class name	D [mm]	d [mm]
Gravel	≤45	>2
Sand	≤2	>0.063
Fines	0.063	-

Special attention has to be given to the fines. They are defined as all particles with a diameter smaller than 63 µm and might be present in all aggregates as they can be described as dust. To identify the real fines content of aggregates, dusting procedures can be carried out at the laboratory. Given their important specific surface area (SSA), fines interact with a great part of the bitumen added to the mixture and constitute the mastic which, as enounced before, provides cohesion to the mixture. The properties of the mastic, given by the fines-bitumen affinity and proportions, are determinant for the stability of the mixture and resistance to several distresses, such as rutting (Corté & Di Benedetto, 2004; Sohm, 2013).

Two types of fines are considered by the European Standard (EN 13043, 2003):

- Natural fines which are naturally produced during the breaking and crushing of the mineral materials to obtain the desired particle sizes. They are mainly contained in the materials characterised as sand. Sands and gravels can then have a portion in mass of particles smaller than 63 µm. The fines content needs to be specified by the fabricant if it

surpasses 3%. In a bituminous mixture, this kind of fines represents normally 4% to 6% of the total mass of the mixture (Tapsoba, 2012).

- Added fines which are industrially fabricated and are, as their name indicates, added to the mixture design in order to complete the required fines content to achieve specific mechanical performances. These are also called added filler and usually represent from 1% to 6% of the mixture mass. Fillers play a densifying role within the mixture. The most used ones are hydrated lime and limestone since they present very good adhesive properties with bitumen (Tapsoba, 2012).

Concerning mineralogical composition, the aggregates that are rich in clay or ferromagnetic minerals (basic aggregates) are more sensible to wear and fragmentation than those rich in feldspars and quartz (acidic aggregates). These hard minerals provide the aggregate with high resistance properties. Granitic, volcanic, limestone containing low clay minerals and some sandstone aggregates are then usually used for construction as they are highly resistant to fragmentation (Chevassu, 1969). It is generally admitted that aggregates with good intrinsic properties also resist well to freeze-thaw cycles, as they can withstand thermal induced stresses (Corté & Di Benedetto, 2004; Lamothe, 2014). However, basic aggregates are usually found to provide lower moisture susceptibility, in terms of stripping, than acidic ones (c.f. section 1.4) (Khan, Grenfell, Collop, Airey, & Gregory, 2013). The study by (Buchanan, 2000) found that mixtures with granite aggregates showed better fatigue resistance than mixtures with limestone aggregates due to the higher effective binder content of mixtures with granite.

Fine particles, or filler, are a crucial component of mixture design. The mastic behaviour will highly depend on the filler grain size, mineralogical nature and content. Filler contents higher than 50% of the mastic mass were found to increase the stiffness of the mastic due to packing optimization. This effect is increased at high temperatures and/or low loading frequencies (Rayner & Rowe, 2004; Soenen & Teugels, 1999). This is a clear evidence of the temperature and time dependence of the mastics behaviour (c.f. section 1.3).

At low temperatures, (Anderson et al., 1994; Lackner, Spiegl, Blab, & Eberhardsteiner, 2005) observed that nor filler nature nor its size had any influence on the mastic properties. However, quartz filler was found to increase the mastic stiffness compared to sandstone filler. Quartz filler grains were also smaller than limestone's which is related to a more effective reduction of air voids content and to an increase of the binder-filler interface surface. Small grain sizes were further associated with the increase in stiffness in (Chen & Peng, 1998; Shashidhar & Romero, 1998).

An increase in stiffness has been observed by several authors when replacing limestone filler by hydrated lime (Bari & Witczak, 2005; Y.-R. Kim, Little, & Song, 2003; Lesueur, Petit, & Ritter, 2013; Little & Petersen, 2005). For bituminous mixtures at 15°C and 10 Hz, this increase is estimated in 18% when replacing 1/3 of the limestone filler by hydrated lime. This effect increases as the material temperature rises or the loading frequency decreases (Phan, Di Benedetto, Sauzéat, & Lesueur, 2016).

1.1.2.1. Aggregate characterisation

In order to characterize the aggregates, laboratory tests are carried out to assess their resistance to fragmentation and wear, amongst other properties.

a. Resistance to fragmentation test (EN 1097-2, 2010)*:*

The resistance to fragmentation is measured by the "Los Angeles" coefficient which indicates whether the aggregates are prone or not to breakage under traffic loadings. During the test, the aggregates are introduced in a metal barrel that turns at a 30 rpm rate. Standard steel balls inside the barrel impact the aggregates as the barrel turns. The coefficient is calculated based on the amount of fines generated during the test.

b. Resistance to wear test (EN 1097-1, 2011)*:*

The resistance to wear of aggregates is assessed trough the "Micro Deval" test under dry or wet conditions. The test results indicate the susceptibility to wear of the aggregates due to the interactions between each other and to the contact with the pneumatic wheels.

c. Polished stone value test (EN 1097-8, 2009)*:*

This test allows determining the resistance to polishing of the gravels used in surface courses. A plate with a mosaic of gravel is subjected to accelerate polishing and the polished stone value is found by means of the difference in friction of the specimen before and after polishing.

1.1.2.2. Mix design parameters concerning aggregates

Grains size distribution in the mixture can be expressed by means of a grading curve. This distribution can be either continuous or discontinuous depending on the desired performances and characteristics of the mixture, specially resistance and compactness (Baaj, 2002). Bituminous mixtures are usually identified by their nominal maximum grain size, defined as the largest sieve size retaining some material during the PSD analysis (Roberts, Kandhal, Brown, Lee, & Kennedy, 1996). Therefore, a 0/14 mixture has a nominal maximum grain size of 14 mm. Nominal maximum size differs from maximum size in that the latter corresponds to the smallest sieve size through which 100% of the aggregates pass.

A continuous grading means that all the granular classes, or fractions, are present. A discontinuous grading means that there is a low quantity of one or some fractions. When a fraction is completely missing, the grading curve is said to be gap-graded. An example of 0/20 gap-graded grading curve is presented in Figure 1.1.

Conceiving a discontinuous grading curve can be seen as optimizing the aggregates packing and is justified by the densification of the compacted mixture. When well-conceived, it maximizes the amount of inter-particle interaction and optimizes air void content. This potentiates the load distribution network within the material increasing its stiffness. Optimizing air voids means allowing only the necessary void content to prevent bleeding and rutting of the compacted mixture (Krishnan & Lakshmana Rao, 2001; Lira, Jelagin, & Birgisson, 2013). Examples of packing optimization in bituminous mixture design can be found in (Goode & Lufsey, 1962; Nijboer, 1948; Olard, 2012; Vavrik, Pine, Huber, Carpenter, & Bailey, 2001). However, it was observed

that not all inter-granular contacts equally contribute to the load distribution. In particular, the research by (Cundall, Drescher, & Strack, 1982; Jaeger & Nagel, 1992; Roque, Birgisson, Kim, & Guarin, 2006; Santamarina, Klein, & Fam, 2001; Sauzeat, 2003) identified the existence of principal chains that effectively transmit stress and strain and of secondary chains that prevent the principal chains from breaking.

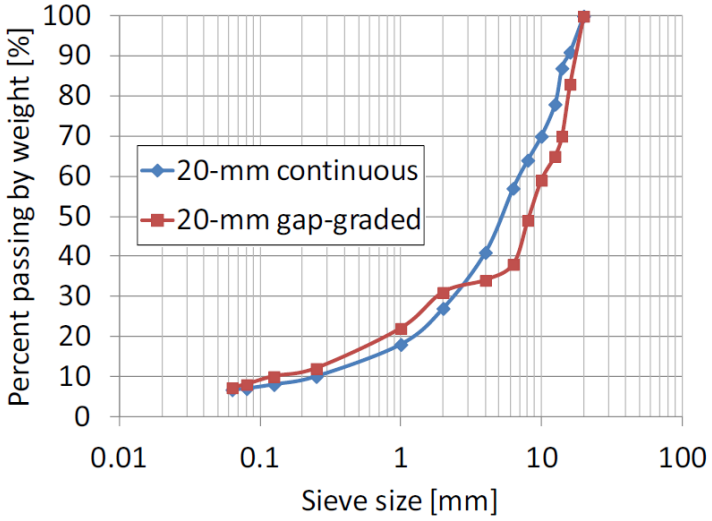

Figure 1.1. Continuous and gap-graded grading curves (Mangiafico, 2014)

1.1.3. Bituminous binders

Bituminous binders are adhesive materials containing bitumen. According to the World Road Association (formerly called Permanent International Association of Road Congresses - PIARC), a bitumen is a "a very viscous or nearly solid, virtually involatile, adhesive and waterproofing organic material derived from crude petroleum or present in natural asphalt, which is completely or nearly completely soluble in toluene" (World Road Association, 2007). In this definition, the term “asphalt” is used in the American way, referring to a material found in the nature containing bitumen (as in rock asphalt). In American English, it is also common to shorten the term “asphalt cement” to simply “asphalt” in order to refer to the bitumen as a building material. Outside America, the word “asphalt” refers to the mixture of bitumen and aggregates used to build road surfaces.

The most relevant characteristic of bitumen is the progressive variation with temperature over a large consistency range, which will be addressed as “temperature susceptibility”. Bitumen has a glassy solid aspect at temperatures below 0°C, but becomes a low viscosity Newtonian fluid at temperatures over 80°C. At intermediate temperatures, the transition from solid to fluid is progressive and allows the bitumen to present different behaviours within the viscoelastic domain, both linear and non-linear. Since viscoelasticity is a time-dependent behaviour, the loading application time also influences the properties of bitumen, which is addressed to as “kinematic susceptibility”. For pavement applications, the load application times can vary from many hours (stopped vehicle) to fractions of second (moving vehicle). The temperature and kinematic susceptibilities of bitumen are passed on to bituminous mixtures. Hence, different pavement distresses are associated with certain temperature and circulation conditions.

Permanent deformations are associated with high temperatures and long loading times, fatigue cracking is associated with intermediate temperatures and repeated loading, and thermal cracking and fragile rupture are associated with very low temperatures and very short loading times (Sohm, 2013).

Bitumen ageing refers to the variations of the chemical composition of bitumen over time. These occur during the service life of the bituminous mixture (long-term) but also during its manufacturing phase (short-term). Long-term ageing is due mainly to the exposition to oxygen, UV-radiation, moisture, temperature changes, etc. Short-term ageing is due to the high temperatures used for pavement manufacturing. Aged bitumen is harder and more brittle than when newly manufactured (Collop, Choi, & Airey, 2008).

1.1.3.1. Origins and production

Bitumen originates from non-pyrolysis processes, distinguishing it from pyrolysis materials such as coal tar and pitch. Coal tar is often confounded with bitumen because of their similar black and viscous appearance. Nevertheless, the chemical properties of bitumen are very different from those of coal tar.

Bitumen can be found in nature either in rocks naturally impregnated with it (rock asphalt) or in well-defined surface deposits (lake asphalt). Due to its rareness, natural bitumen is scarcely used in pavement engineering. The main source of bitumen is crude oil refining. Nevertheless, according to the French Refined Bitumen Association (*Groupement Professionnel des Bitumes* - GPB), only 10% of the 1300 known crude oils in the world are suitable to produce bitumen of adequate quality in commercial quantities (Groupement Professionnel des Bitumes, 2013).

The most common crude oil refining process consists in separating its components depending on their molecular weight. Light fuel fractions are first separated from heavier non-boiling fractions by atmospheric distillation at temperatures between 300°C and 350°C. Eventual remaining fuel fractions in the residue are withdrawn by vacuum distillation (350°C – 425°C) in order to avoid thermal cracking of the heavy fractions of crude oil. This heavy residue can then be further processed by air rectification or by solvent de-asphalting. Air rectification, or blowing, is made at temperatures around 280°C in order to increase the average molecular weight of bitumen components by means of oxidation reactions. Depending on the degree of oxidation; two products can be produced: oxidized bitumen and air-rectified bitumen. The former is used for roof waterproofing and the latter for paving applications. Solvent de-asphalting is done in order to separate the paraffin present in the crude oil distillation residues. Propane or butane is used to solve the paraffin, making the polar and aromatic components to precipitate. Bitumen is obtained from the insoluble part. Mixtures of air-rectified bitumen and de-asphalted bitumen are then made in order to obtain a final product with specific properties, specially its consistency (hardness) (Eurobitume, 2016; European Asphalt Pavement Association & National Asphalt Pavement Association, 2011).

1.1.3.2. Chemical composition of bitumen

Bitumen is a complex material, a mixture of high molecular weight hydrocarbons consisting primarily of carbon (82-88%), hydrogen (8-11%), heteroatoms such as oxygen (0-1.5%), sulphur (0-6%), nitrogen (0-1%), and heavy metals. There is no single bitumen molecule, but it is possible to separate its components into two broad chemical groups called asphaltenes and maltenes, based on their solubility and polarity. Maltenes can be further decomposed into three families called saturates, aromatics and resins. Chromatography techniques are widely used to define the constitution of bitumen by a method called SARA fractionation as it allows identifying the fractions of saturates, aromatics, resins and asphaltenes (Corté & Di Benedetto, 2004; European Asphalt Pavement Association & National Asphalt Pavement Association, 2011; Read & Whiteoak, 2003).

The asphaltenes can be described as a dark, amorphous solid phase insoluble in n-heptane that constitutes between 5% and 25% of the bitumen mass. Its content has a significant influence in the rheological behaviour of bitumen. High asphaltene content produces harder bitumen with lower penetration grade, higher softening point (cf. Section 1.1.3.4) and, therefore, higher viscous behaviour. These are highly polar molecules of 5 to 30nm in size and with a molecular mass ranging between 1000 and 100000 g/mol (Corté & Di Benedetto, 2004; Read & Whiteoak, 2003).

The resins have a solid or semi-solid dark aspect and represent between 13% and 25% of the bitumen mass. Considered as molecules with a marked polarity, they are responsible for the adhesive properties of bitumen. They are 1 to 5 nm in size with a molecular mass of 500 to 50000 g/mol. Aromatics are the main bitumen component, constituting 40% to 65% of its mass. Their aspect at room temperature is that of a viscous red to yellow liquid. Aromatics molecules have a molecular mass of 300 to 2000 g/mol. Saturates are non-polar viscous light-coloured oils representing 5% to 20% of the bitumen mass (Corté & Di Benedetto, 2004; Read & Whiteoak, 2003).

Bitumen structure is usually considered as a colloidal system consisting of high molecular mass asphaltene micelles dispersed or dissolved in a lower molecular mass oily medium composed of maltenes (Read & Whiteoak, 2003). High molecular mass resins are partially absorbed by asphaltene micelles and act as a stabilising solvating layer around the micelles. Away from the centre of the micelle, there is a gradual transition from less polar resins to a less aromatic oily medium formed by the maltenes. If the maltenes are in sufficient quantity and have an adequate solvating power, the asphaltene micelles will be fully peptised and, therefore, will have good mobility within the bitumen. In this case, the bitumen structure is said to be of sol-type, as shown in Figure 1.2(a). On the opposite case, when the maltenes fraction is not present in sufficient quantity or does not have adequate solvating power, the asphaltene micelles associate to form an irregular open packed structure leaving voids filled with intermicellar fluid of mixed composition. This structure is called gel-type, as schematized in Figure 1.2(b). Air-rectification and oxidation processes impart gel-type characteristics to bitumen (Labout, 1950). In fact, atmospheric and vacuum distillation lead to removal of saturates and concentration of asphaltenes. After air-blowing, the aromatics content decrease, the asphaltene content increase and saturates and resins contents remain substantially of the same order.

The maltenes fraction imparts an inherent viscosity to the bitumen that depends on the molecular mass of the fractions: the higher the molecular mass, the higher the viscosity. The presence of asphaltenes and the degree of asphaltene micelles association increase the bitumen viscosity. The chemical bonds between asphaltenes weaken when the temperature increases and the gel-type structure of certain bitumen can almost disappear at a sufficiently high temperature. As for sol-type structures, the asphaltenes dispersion is improved with the increase of the temperature. Consequently, bitumen viscosity falls as temperature increases. Nevertheless, this viscosity decrease is reversible as asphaltenes bonds are restored when bitumen cools. Temperature dependence can be reduced by a high saturates content as they reduce the ability of the maltenes to solvate the asphaltenes. At a constant resins to aromatics ratio and constant asphaltenes content, increasing saturates content also softens the bitumen. On the contrary, adding resins hardens the bitumen and increases its viscous behaviour. At ambient and intermediate temperatures, it is then possible to conclude that the rheology of bitumen is controlled by the association degree of asphaltene micelles and the relative amount of other molecules (resins, saturates, aromatics) available to stabilise these associations (Airey, 2010; Read & Whiteoak, 2003; Traxler, 1961).

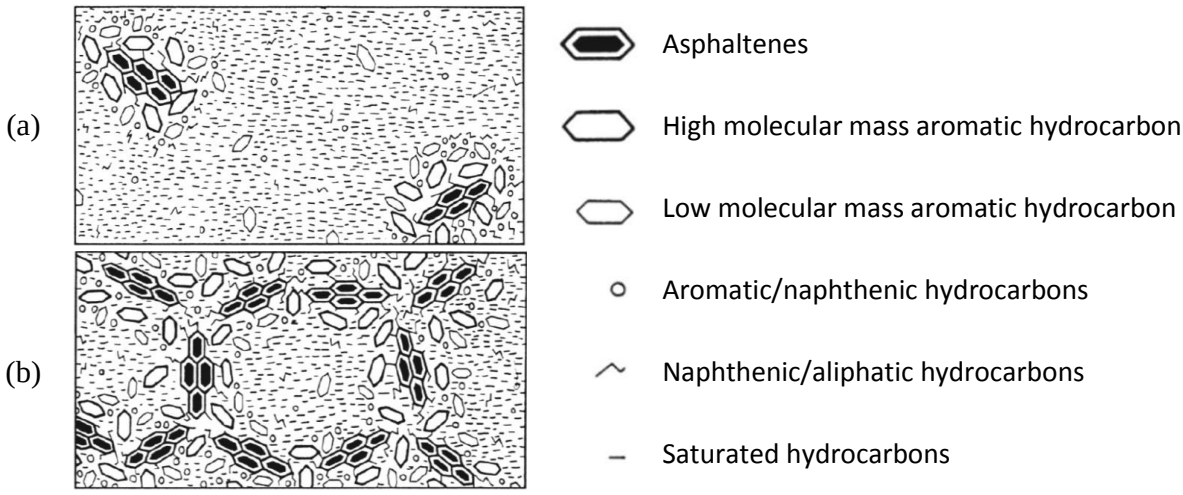

Figure 1.2. Schematic representation of sol-type (a) and gel-type (b) bitumen structures (Read & Whiteoak, 2003).

Up until now, even if physical properties can be related to chemical composition, it is impossible to describe bitumen generally in terms of chemical components concentration. Defining bitumen specifications in terms of chemical components (e.g. minimum asphaltene content) is then of very little relevance (Read & Whiteoak, 2003).

1.1.3.3. Types of bitumen

Depending on the refining and manufacturing process, several types of bitumen are available in the market (European Asphalt Pavement Association & National Asphalt Pavement Association, 2011; Mangiafico, 2014):

- Pure bitumen: Obtained only from the atmospheric and vacuum distillation of a selected crude oil. These are the most commonly used binders in pavement engineering.

- Cutback bitumen: Pure bitumen whose viscosity has been reduced temporarily by mixing it with volatile solvents, such as kerosene, so it can penetrate more effectively granular material layers or to allow spraying at low temperatures. It is commonly used for tack coating and spray sealing. Once applied on the surface to coat, the solvents evaporate and the hardness of the remaining bitumen is restored to values close to the original bitumen's.
- Fluxed bitumen: Bitumen whose viscosity has been reduced by mixing it with non-volatile oils. It is differs from a cutback bitumen in that the flux oil has low volatility and does not evaporate at ambient temperature. As the cutback bitumen, fluxed bitumen can be applied at lower temperatures and is commonly used to waterproof layers under new pavement or for tack coating. They can also be used to make cold-mix patching material that can be stored for long periods.
- Air-rectified bitumen: Bitumen subjected to mild oxidation in order to increase the average molecular weight of its components. Air-rectification, or blowing, increases the asphaltenes concentration and modifies the penetration grade.
- Multi-grade bitumen: Bitumen whose thermal sensitivity has been reduced by refining processes, such as air-rectification. They present properties of bitumen with different penetration grades at high and low temperatures (i.e., soft bitumen behaviour at low temperatures and hard bitume behaviour at high temperatures).
- Bitumen emulsions: Mixture of two immiscible components, bitume and water, where the dispersed phase can be either one of them, depending on the relative concentrations. An emulsifying agent, normally surfactants, is used to maintain the emulsion stable. They are used in roofing and waterproofing operations as well as in pavement engineering at ambient temperature.
- Modified bitumen: Bitumen whose rheological properties have been modified by adding non-bituminous agents. The most commonly used additives are adhesion agents, crumb rubber, polymers, poly-phosphoric acid, sulphur and waxes.

Polymer modification is a currently common practice intended to improve some of the characteristics of pure bitumen. The modification is made by introducing one or several polymers, elastomers or plastomers, usually between 2% and 7% in weight. The two most common types of polymers used in pavement engineering are SBS (Styrene-Butadiene-Styrene) and EVA (Ethylene-Vinyl Acetate), which are, respectively, an elastomer and a plastomer. An elastomer presents a substantial elastic recovery after being subjected to a strain lower than its rupture point (e.g., rubber), while a plastomer does not exhibit such recovery (e.g., polyethylene). SBS-polymer modification can then have a more significant influence on the rheological properties of pure bitumen, compared to EVA modification (Jasso et al., 2015; Stastna, Zanzotto, & Vacin, 2003; Zanzotto, Stastna, & Vacin, 2000). SBS-polymers can present a linear or radial structure, with polystyrene blocs occupying the two ends of a polybutadiene block. Cross-linking is used to create a uniform network of SBS molecules.

When mixed with bitumen, polymers tend to absorb a part of the maltenes fractions and swell, while the asphaltenes are not absorbed at all. When observed through fluorescent microscopy, the absorbed aromatic oils give a light colour to the polymer-rich phase and the residual maltenes and asphaltenes appear in a dark colour, forming what can be considered as a continuous bitumen-rich phase. Figure 1.3 shows the impact of polymer content in the polymer-modified bitumen (PMB) morphology. At low polymer content (Figure 1.3(a)) the polymer phase

is dispersed in the continuous bitumen one. On the contrary, at high polymer content (Figure 1.3(c)), the polymer phase becomes the continuous phase where the bitumen one is dispersed. At intermediate polymer content, the PMB presents a rather unstable structure with neither the polymer nor the bitumen phases dominating the overall system (Figure 1.3(b)). According to Airey (1999), similar observations have been made for SBS and EVA PMBs, though the structure morphology depends also on other aspects besides polymer content such as the polymer nature (swelling potential) and the base bitumen nature (composition of the maltenes fraction).

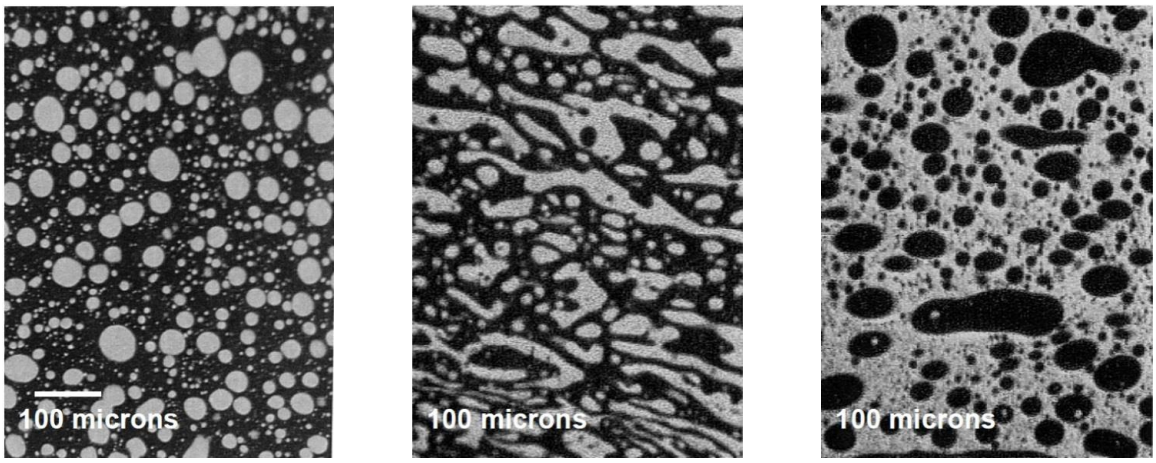

(a) (b) (c)

Figure 1.3. Fluorescent microscopy images of a polymer-modified bitumen (PMB) with 3% EVA (a), 5% EVA (b) and 7% EVA (c) – obtained at 100x magnification (Airey, 1999).

1.1.3.4. European classification of bituminous binders

In Europe, bitumen are conventionally characterised by monitoring their response to specific loadings at precise test conditions, especially temperature. These semi-empirical tests do not measure fundamental mechanical properties of bitumen. The most commonly used are described hereafter:

a. Needle penetration test (EN 1426, 2007)*:*

The needle penetration test aims to classify bitumen according to its consistency, which is evaluated by measuring the penetration depth of a standard needle in a bitumen sample at 25°C. During the test, a load of 100 g is applied on the needle for five seconds (cf. Figure 1.4). The penetration depth is measured in 1/10mm and allows placing the bitumen in one of the standard penetration grade classes. These classes are defined by lower and upper penetration depth thresholds. For example, the class 50/70 comprises all bitumen whose needle penetration test result at 25°C is comprised between 50/10 mm and 70/10 mm. Table 1-2 presents some of the standard penetration grade classes.

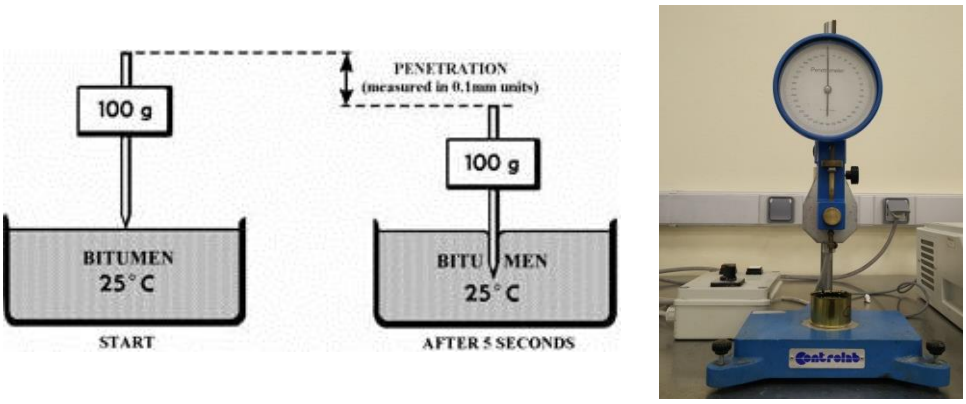

(a) (b)

Figure 1.4. Needle penetration test scheme (a) (University of Minho, 2009) and test device (b)

Table 1-2. Penetration grade classes and consistency perception of the most used bitumen in France (Tapsoba, 2012)

Penetration grade class (in 1/10mm)	**Consistency perception**
10/20	Hard bitumen
15/25	
20/30	
35/50	
50/70	Semi-hard bitumen
70/100	
160/200	Soft bitumen

b. Softening point test (EN 1427, 2007)*:*

The softening point or "ring and ball" test is used to identify the temperature for which a bitumen ring, on which a standard steel ball reposes, reaches a specific deformation while its temperature increases. The temperature increase rate is set at 5°C/min. The softening point, or "ring and ball" temperature, is denoted as TRB. Figure 1.5 presents a scheme of the test principle and a picture of the test device.

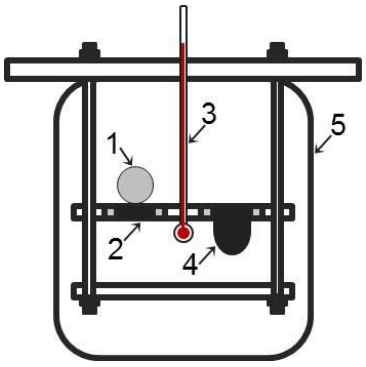

1. Steel ball
2. Ring with bitumen sample at room temperature
3. Thermometer
4. Deformed bitumen sample at elevated temperature
5. Glass vessel with water

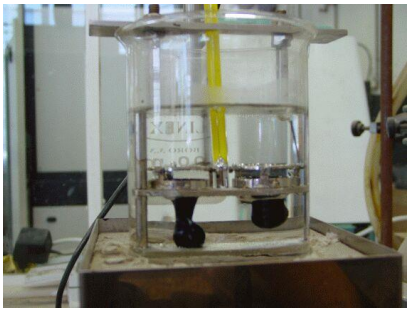

(a) (b)

Figure 1.5. Softening point test scheme (a) and test device (b) (University of Minho, 2009)

c. Fraass braking point test (EN 12593, 2015)*:*

The Fraass breaking point test is used to identify the temperature for which a crack develops in a bitumen sample under repeated bending, while its temperature decreases. The sample is made by laying a 0.5 mm tick bitumen layer on a thin steel plate (41 mm x 20 mm). The temperature decrease rate is set at 1°C/min. The "breaking point" corresponds to the temperature for which the first crack appears. It is used as an approximated measure of the threshold between ductile and fragile conditions of the bitumen. Figure 1.6 presents a scheme of the test.

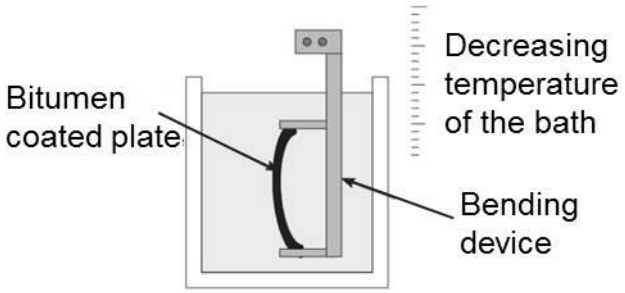

Figure 1.6. Softening point test scheme (Tapsoba, 2012)

The European classification method of bitumen is based on the penetration grade classes explained before. Three standards comprise the classes in which bitumen can be classified: (EN 12591, 2009) sets the requirements for paving bitumen, (EN 13924-1, 2016) sets the requirements for special hard paving bitumen and (EN 13924-2, 2014) for special multi-grade paving bitumen. The main drawbacks of this classification are that it is based on semi-empirical tests that do not account for fundamental properties of the bitumen and that are made at one single temperature, in spite of the temperature dependence of bitumen behaviour.

A different classification method is used in the United States: the Superpave (Superior Performing Asphalt Pavements) Performance Grade (PG) method. The system was developed in the framework of the Strategic Highway Research Program (SHRP) (Anderson et al., 1994). It includes tests methods that measure fundamental properties of the materials, allowing a classification based on bitumen performance. It relies on the concept of "critical temperature", that is, the temperature for which material properties allow road pavement distresses to occur. This applies for both bituminous mixtures and bituminous binders.

1.1.3.5. Classification of bituminous binders based on performance characterisation tests (Superpave)

The American Association of State Highway and Transportation Office (AASHTO) adopted the AASHTO M320 specification to regulate the PG binder classification (AASHTO M320, 2010). Three road pavement distresses are considered and associated to a service temperature range: permanent deformation or rutting for high service temperatures, fatigue cracking for intermediate temperatures and thermal cracking for low service temperatures. The method assumes that these distresses can be ascribed to different binder properties, depending on temperature conditions and ageing characteristics. Binders are then classified according to the

two critical temperatures (high and low) for which permanent deformation and thermal cracking can occur in pavements built with the studied bitumen. Hence, a bituminous mixture made with PG 64-22 bitumen can present rutting problems beyond 64°C and thermal cracking below -22°C, for example.

The mechanical tests required by the PG method to determine the critical temperatures and, therefore, classify bitumen, are shown on Table 1-3.

Table 1-3. Rheological tests for bitumen classification according to the performance-based method – (Anderson, D'Angelo, & Walker, 2010; Lamothe, 2014; Mangiafico, 2014)

Test name	Standard	Related mixture characteristic or pavement distress	Bitumen ageing condition	Test temperature (T) range	Mechanical parameter value verification or utility
Rotational viscometer (RV)[A]	(AASHTO T316, 2013)	Pumpability, mixability and workability	Non-aged	135°C (High T)	Viscosity for mixing and compacting temperatures definition
Dynamic Shear Rheometer (DSR)	(AASHTO T315, 2012)	Permanent deformation (rutting) (25mm plate)	Non-aged	52°C – 76°C (High T)	$G^*/\sin\delta$ > 1kPa
			RTFO[+] aged		$G^*/\sin\delta \geq$ 2.2kPa
		Fatigue cracking (8mm plate)	RTFO[+] and PAV[++] aged	4°C – 40°C (Intermediate T)	$G^*/\sin\delta \leq$ 5MPa
Multiple Stress Creep Recovery (MSCR)	(AASHTO TP70, 2013)	Permanent deformation (rutting)	RTFO[+] aged	52°C – 64°C (High T)	J_{nr} and MSCR Recovery - good correlation with rutting potential
Bending Beam Rheometer (BBM)	(AASHTO T313, 2012)	Thermal cracking	Non-aged[B] RTFO[+] and PAV[++] aged	-36°C – 0°C (Low T)	Creep stiffness S ≤ 300MPa at 60s m-value ≥ 0.3
Direct Tension Tester (DTT)	(AASHTO T314, 2012)	Thermal cracking	RTFO[+] and PAV[++] aged	-36°C – 6°C (Low T)	Failure stress

[+] Rolling Thin Film Oven test (AASHTO T240, 2013): Short-term ageing.
[++] Pressure Ageing Vessel (AASHTO R28, 2012): Long-term ageing.
[A] Not used for bitumen classification but for bituminous mixture manufacturing temperatures.
[B] Not used for bitumen classification but for control purposes.

Since the PG method aims to classify binders according to the performance of the bituminous mixture of which it is part, the mechanical tests considered by the Superpave specification are made on aged bitumen. Two ageing procedures are performed to simulate bitumen ageing during service life. The Rolling Thin Film Oven (RTFO) procedure (AASHTO T240, 2013) simulates short-term ageing due to mixing and compacting procedures at high temperatures during the pavement construction phase. The RTFO samples are prepared by introducing small amounts of unaged bitumen in cylindrical glass bottles that are placed in a rotating carriage, within an oven. The oven is set at 163°C (325°F). As the carriage turns (at 15 RPM), the bitumen in the glass

bottles spreads on the bottle walls forming a thin homogeneous bitumen layer. The bitumen samples are also exposed to a continuous air flow of 4 000 ml/min. The continuous carrousel rotation allows the samples to be continuously exposed to airflow and prevents the formation of a surface “skin layer” as it slowly mixes the sample. The test lasts 85 minutes. After RTFO, a mass loss evaluation can be made in order to identify the amount of volatile components lost during the ageing process. The mass loss has to be inferior to 1% according to the PG specifications.

The Pressure Ageing Vessel (PAV) procedure (AASHTO R28, 2012) simulates long-term ageing due to service conditions (7 to 10 years). The ageing factor concerned by the PAV procedure is oxidation. RTOF aged bitumen is placed in stainless steel pans inside a pressured vessel at 2.1 ± 0.1 MPa (300 psi). The temperature inside the vessel is either 90°C, 100°C or 110°C and the bitumen is aged for 20 hours. RTFO and PAV tests are recognized by the European Standard for bituminous binders ageing.

The Rotational Viscometer (AASHTO T316, 2013) is used to determine the viscosity of bitumen at high temperatures. It is not used for the PG classification, properly speaking, but it allows ensuring that the bitumen is fluid enough, at manufacturing temperatures, for pumping and mixing (Roberts et al., 1996). The test principle is to determine the viscosity by measuring the torque required to maintain a constant rotational speed of 20 RPM of a cylindrical spindle submerged in the bitumen at constant temperature.

The Dynamic Shear Rheometer (DSR) is used to identify the rheological properties of bitumen. The test is performed at high and intermediate temperatures according to the anticipated service conditions of the bituminous mixture which contains the studied binder. The test uses a thin bitumen sample in between two circular plates. The lower plate is fixed while the upper turns back and forth in an oscillatory movement, creating a shear stress in the bitumen sample. DSR measures the binder complex shear modulus (G*) and its phase angle (δ). The norm of G* is the bitumen resistance to deformation when repeatedly sheared and its phase angle is the lag between the applied stress and the resulting shear strain. PG classification method imposes a minimum G*sinδ value for original and RTFOT aged bitumen. This value is accessed by a DSR test at high temperatures using 25mm in diameter circular plates. It corresponds to a minimum stiffness required for the binder to be considered as resistant to permanent deformations. The maximum G*sinδ value is determined by a DSR test performed at intermediate temperatures on RTFOT+PAV aged bitumen. For this temperature range, the test has to be done with 8mm in diameter plates as to have exploitable data. This maximum G*sinδ value corresponds to the maximum stiffness of the long-term aged bitumen in order to limit fatigue cracking. For both cases high elasticity is desirable, which is reflected in low phase angle (δ) values.

The G*sinδ parameter is measured in the linear viscoelastic (LVE) behaviour domain of bitumen. Given the fact that rutting is defined as a permanent deformation of the transversal profile of a pavement structure (Di Benedetto & Corté, 2004), it is a phenomenon that does not occur within the LVE domain. This has been identified as a shortcoming of the DSR test in defining rutting resistance of bituminous mixtures. In fact, low correlation has been found between the expected rutting potential according to PG classification method of bitumen and real developed ruts in roads. Another inconvenient of the DSR test is its inability to capture the benefits of polymer-modification on rutting resistance (Anderson et al., 2010; Anderson, 2014). The efforts to overcome these shortcomings lead to the development of the Multiple-Stress Creep-Recovery (MSCR) test.

The MSCR test (AASHTO TP70, 2013) consists of a DSR test where a stress is applied to the bitumen sample for 1 second, followed by a unloaded rest period of 9 seconds. The test starts at a low stress level of 0.1 kPa during 10 creep/rest cycles and then the stress is increased to 3.2kPa for another 10 creep/rest cycles. It uses the creep and recovery concept to evaluate the binder's potential for permanent deformation. For PG classification purposes, it is done on RTFO aged samples at high temperatures. Two parameters are determined for each loading cycle: the non-recoverable creep compliance (J_{nr}) and the percentage of recovery (MSCR Recovery). The test results are reported as the average of the ten measures at each stress level. Both parameters show much better correlation with real rutting field measurements than G*sinδ, particularly for PMBs (Anderson et al., 2010).

The Bending Beam Rheometer (BBR) (AASHTO T313, 2012) evaluates low temperature stiffness and relaxation properties of bitumen. The test consists in loading the middle of a bitumen beam immersed in a cold bath liquid. The beam deflection is measured over time. For PG classification method, the test is carried on RTFOT+PAV aged bitumen. The test is correlated to thermal cracking as this distress occurs when the bituminous mixture is unable to rapidly relax contraction stresses created by a decrease in temperature. The critical cracking temperature is determined by combining the BBR results with the Direct Tension Test's (DTT). The BBR test critical temperature is 10°C lower than the lowest temperature yielding maximum creep stiffness at 60 s of 300 MPa and an m- value of at least 0.3. The m-value is a measure of the stress relaxation rate through plastic flow. This means that the BBR test is performed at a temperature 10°C higher than the one that appears in the binder classification.

The DTT test (AASHTO T314, 2012) measures the stress and strain at failure of a I-shaped RTFOT+PAV aged bitumen sample by direct traction at constant elongation rate. The test is conducted at low temperatures, for which the bitumen failure is brittle or brittle-ductile. In order to calculate the critical cracking temperature, the creep stiffness time-dependent function is obtained from the BBR test results and then converted to a stress relaxation modulus. The thermal stress produced in the bituminous mixture containing the studied bitumen is then predicted by affecting the relaxation modulus by a constant. This predicted stress is then compared to the failure stress observed from the DTT test results.

Bitumen has to maintain optimal performances during its service life in spite of the potential ageing caused by volatilisation of some of its components and oxidation. Complementary tests can be carried out on bitumen in order to verify the elasticity recovery and passive adhesion properties, which are related to the bituminous mixture durability. Canadian standard specifies two tests to measure these properties. A modified ductility test is used to measure the elasticity recovery properties of bituminous binders (LC 25-005, 2004). This test allows predicting the long-term behaviour of bituminous binders regarding temperature variations, which is then directly related to its durability when exposed to freeze-thawing cycles (Lamothe, 2014). The passive adhesion test (LC 25-009, 2009) aims to evaluate the stripping potential of a bitumen-coated aggregate according to the aggregate origin. It allows having an idea of the moisture susceptibility of bituminous mixtures. High passive adhesive properties would mean low water infiltration into the bitumen-aggregate interface. Passive adhesion is highly dependent on the crude oil and on the fabrication procedures of bitumen (Lamothe, 2014).

1.1.4. The air voids

Air voids are the spaces not occupied with mastic, bitumen or aggregates in the compacted bituminous mixture. This definition concerns the interstitial voids and does not take into account the porosity of the aggregates. The air voids of a compacted bituminous mixture are rather coarse with an average equivalent diameter between 0.5 and 1.9 mm (Arambula, 2007; Castelblanco Torres, 2004; Kassem, 2008; Masad, Castelblanco, & Birgisson, 2006; Masad, Muhunthan, Shashidhar, & Harman, 1999; Mauduit et al., 2010; Walubita, Jamison, Alvarez, Hu, & Mushota, 2012).

Air void content is defined then as the ratio of the volume of voids filled with air respect to the total volume of the mixture. According to the Asphalt Institute, as cited in (Chen, Lin, & Young, 2004), the desired air void content ranges between 5% and 8%, with average value of 7%, for common dense bituminous mixtures right after compaction. Usually, air voids content decreases to values between 3% and 5% during service life due to traffic loading.

Two other volumetric properties of bituminous mixtures can be enounced: voids in mineral aggregate (VMA) and voids filled with bitumen (or asphalt using the American notation) (VFA). The former is defined as the ratio of the volume of voids between the aggregate particles (including the spaces filled with bitumen) with respect to the total volume of the mixture. The latter corresponds to the ratio of only the volume of voids filled with bitumen with respect to the total volume of the mixture. Figure 1.7 shows a scheme of the volumetric properties of bituminous mixtures.

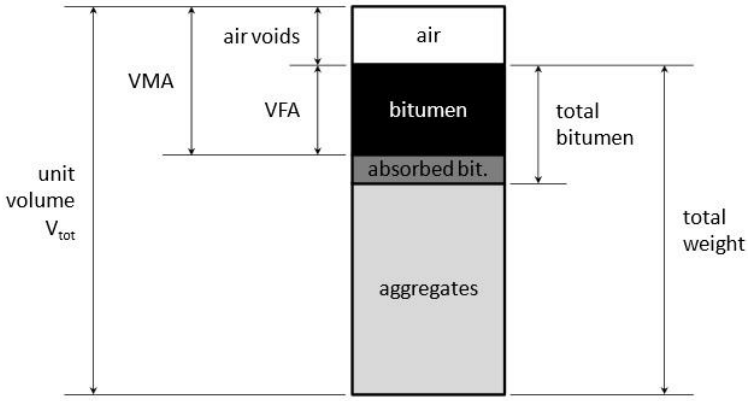

Figure 1.7. Scheme of the volumetric properties of bituminous mixtures (Mangiafico, 2014)

Air voids in bituminous mixtures can be characterised in terms of the total air voids content, the voids average size, the amount of interconnected voids and the ratio between connected and total voids (Alvarez-Lugo & Carvajal-Munoz, 2014). Samples of the same mixture with the same total air voids content but different voids distribution, may present very distinct mechanical properties (Masad, Jandhyala, Dasgupta, Somadevan, & Shashidhar, 2002). It is also important to differentiate the voids that are connected to the exterior from those who are not. (Chen et al., 2004) uses the term “effective” to describe the interconnected voids that allow water to pass through the bituminous mixture. Semi-effective voids are then those who allow water to penetrate the mixture but not to pass through it, and impermeable ones are those not connected to the exterior of the material. Figure 1.8 schematizes the three types of air voids in

terms of connectivity. The effective and semi effective voids into which water easily penetrates are also referred to as “outside” voids due to the fact that they are not taken into account when calculating the real volume of the specimen, using hydrostatic weighing. Only the impermeable voids, or voids connected by very tortuous paths, are then taken into account in the bulk density calculation. These are referred to “inside” voids.

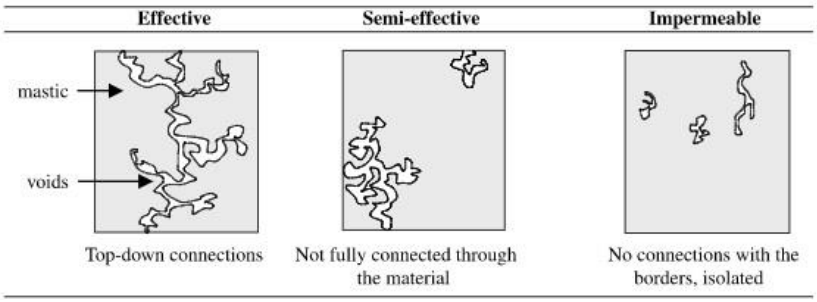

Figure 1.8. Air voids classification in terms of connectivity as adapted by (Caro, Masad, Bhasin, & Little, 2007) from (Chen et al., 2004)

Air voids characteristics have been found to have an important influence on the performance of bituminous mixtures. Some notable properties affected by air void content and distribution are stiffness, fatigue resistance, permeability, permanent deformation resistance, moisture susceptibility, bleeding and thermal cracking (Alvarez-Lugo & Carvajal-Munoz, 2014; Arambula, 2007; Castelblanco Torres, 2004; Chen et al., 2004; Dubois, De la Roche, & Burban, 2010; Kassem, 2008; Mangiafico, 2014; Masad et al., 1999; Monismith, 1992; Partl, Flisch, & Jönsson, 2007; Romero & Masad, 2001; Walubita et al., 2012).

Stiffness values tend to increase with the decrease in air voids total content (Bazin & Saunier, 1967; Di Benedetto & De la Roche, 1998; Moutier, 1991). As for fatigue resistance, the effect of air voids content depends on the characteristics of the mixture and the loading mode. For strain controlled fatigue tests, decreasing the air void content reduces the fatigue life of dense mixtures; on the contrary, it increases the fatigue life of mixtures with low bitumen content (Doan, 1976). For stress controlled tests, fatigue life tends to increase when air voids content is reduced for all mixtures. Nevertheless, voids distribution and connectivity within the material is also important. Heterogeneous voids distribution creates heterogeneous strain and stress fields which can lead to earlier fatigue failure of the material. Air voids characteristics can then have significant influence on the fatigue resistance properties of bituminous mixtures, even more than binder content in some cases (Harvey, Deacon, Tsai, & Monismith, 1995; Masad et al., 1999; Romero & Masad, 2001).

With respect to rutting, it is recommended for most compacted mixtures to have air void content lower than 9% and higher than 2%. Some specially designed mixtures can have higher voids content. Repetitive loading due to traffic can cause after-compaction settlement in undercompacted mixtures or viscoplastic deformation (creep rutting) in overcompacted ones. The latter are also susceptible of bleeding, a non-reversible distress characterized by the migration of bitumen to the surface of the bituminous mixture layer, reducing the skid resistance of the wearing course. Bleeding depends on the temperature susceptibility of the binder but also on the pressure gradient created in the bituminous layer when loaded. The gradient is increased

when the air voids are reduced (in size and quantity) pushing the binder to migrate to the surface of the layer (Krishnan & Lakshmana Rao, 2001; Lamothe, 2014).

Considering durability, air void content should be as low as possible in order to prevent premature ageing of the binder film and moisture infiltration into the mixture. Voids distribution is also important regarding durability as high voids connectivity increases moisture diffusion in the material, facilitating moisture damage (Arambula, 2007; Caro, Masad, Bhasin, & Little, 2010; Cooley, Brown, & Maghsoodloo, 2001; Mallick, Cooley, Teto, Bradbury, & Peabody, 2003; Masad et al., 2002; Roberts et al., 1996).

Permeability of bituminous mixture depends on the air voids content as well as on voids connectivity. In general, mixtures with air voids contents less than 5% are considered impermeable, while mixtures with air voids contents higher than 15% are considered as "free-draining" or completely permeable. Values in-between, especially close to 8%, are considered as "pessimum" air voids contents in terms of permeability. This concept will be further developed in section 1.4. Regarding connectivity, voids are unlikely to be interconnected in bituminous layers compacted to less than 7% air void content (Arambula, 2007; Arambula, Masad, Martin, & Lytton, 2007; Chen et al., 2004; Terrel & Al-Swailmi, 1993).

Air voids content and distribution depend on the granular distribution and binder content, as well as on compaction procedure and effort (Caro, Masad, Bhasin, & Little, 2008). This supposes a major problem for the study of bituminous mixtures as the fabrication procedures in the laboratory are different from those in the field. Therefore, the expected behaviour of bituminous materials, based on laboratory test results, sometimes differ from the observed behaviour of the material in the field. Some of the most common sample fabrication procedures, and their influence on air voids, are described later in this section.

Properly characterising the air voids in the compacted mixture is then crucial for the study of bituminous mixtures. There exist several methods to characterise air voids, some of which are addressed below.

1.1.4.1. Air voids characterisation methods

The commonly used methods for measuring air voids content are based on density and volumetric measurements of the material and of the samples. However, they only give quantitative information and voids size, distribution in space and interconnectivity are usually unknown (Krishnan & Lakshmana Rao, 2001). Lately though, imaging technology and non-destructive methods have been used to characterize the internal structure of granular materials (Alvarez-Lugo & Carvajal-Munoz, 2014; Masad et al., 1999). Some of the most relevant techniques used for this purpose are treated in this section.

a. Bulk density by volumetric measurements

The compactness of a bituminous mixture sample is defined as the ratio of the bulk density of the sample respect to the maximum density or "true density" of the mixture. This method is included in the European Standard (EN 12697-6, 2012). The air voids content (V) is then defined as:

$$V\% = 100\left(1 - \frac{Bulk\ density}{Maximum\ density}\right) \quad [1\text{-}1]$$

This method implies the determination of the bulk and maximum densities of the sample. The sample volume, used to determine its bulk density, can be measured by assuming a certain geometric form for the sample or by hydrostatic weighing. The maximum density of the mixture can be calculated based on the densities of each of its components or by a volumetric method using a pycnometer, as stipulated by the European standard (EN 12697-5, 2009).

b. *Scan by X-ray Computed Tomography*

X-ray computed tomography (CT) is a non-destructive technique used to characterize the internal structure of opaque objects. The principle of the measure is as follows: a source emits an X-ray of a known intensity which passes through the studied specimen and is then received by a detector (c.f. Figure 1.9). When the beam passes through the sample, some of the radiation is absorbed by the material or scattered so that the received beam has lower intensity than the one emitted by the source. The intensity attenuation coefficient at a certain point is directly related to the density of the sample at that point. Using mathematical processes, the variations of attenuation can be converted into a map of the spatial density distribution inside the material. Voids can then easily be differentiated from mastic and aggregates due to the difference in density. Taking measurements for a full rotation of the sample, allows creating 2-dimensional images of a cross section of the sample. The internal structure of the sample can then be identified through image treatment of the assembly of multiple cross section images (Arambula, Masad, & Martin, 2007; Caro et al., 2008; Masad et al., 2002).

Comparing results from X-ray CT and from volumetric measurements, the latter tend to slightly underestimate total void content. According to (Kringos, Azari, & Scarpas, 2009), this difference can be attributed to inaccuracies of the volumetric measurements or to image resolution limits. In general terms, total air void content measured with both techniques compare very well (Masad et al., 1999). The advantage of the scanning procedure is the access to information on the voids connectivity and size, rather than higher precision on the total air void content estimation. It allows, for example, identifying potential paths (interconnected voids) for moisture infiltration and their tortuosity, which can be useful information for the study of moisture susceptibility of bituminous mixtures. This method also allows identifying the aggregate gradation in the sample, as well as the network of mineral particles in contact with each other (Alvarez-Lugo & Carvajal-Munoz, 2014; Caro et al., 2008; Masad et al., 1999).

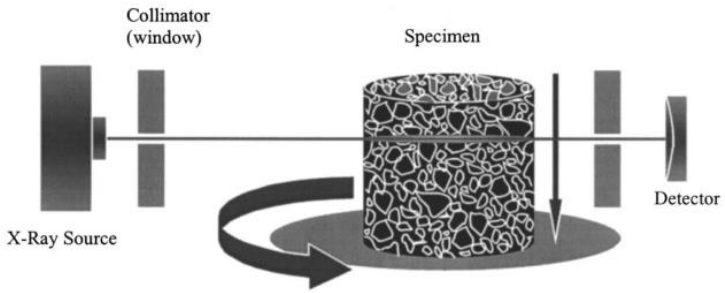

Figure 1.9. Computed tomography system scheme (Masad et al., 2002)

c. Bulk density by gamma rays

The determination of density using gamma radiation is now a common practice in geotechnics. The European Standard (EN 12697-7, 2002) has adopted this method to measure air voids content of bituminous mixture samples. The measurement equipment; a vertical gamma-densitometer bench, consists of a frame holding the specimen holder, which adapts to prismatic and cylindrical specimens, and a carriage holding a radiation source and a detector, both on the same vertical axis (c.f. Figure 1.10). The equipment measures the specimen's thickness and the radiation (emitted and detected), and controls the carriage movements. The measurement principle is based on the detection of the decrease in the narrow beam gamma photons emitted by a radioactive Cesium 137 source. The number C of the photons, the count rate after passing through the sample, is correlated with the density of the specimen through a mathematical relation (Dubois et al., 2010; Tan & Fwa, 1991).

Figure 1.10. Vertical gamma-densitometer bench (Dubois et al., 2010)

1.1.4.2. Specimen fabrication methods

The characteristics of air voids in bituminous mixtures depend on the compaction effort, the mixture temperature, the aggregate gradation and grains shape, but also on the compaction method. Aggregate orientation and the homogeneity of air void distribution depend on the compaction method; hence, great differences can be found between samples of the same material but differently compacted. Mechanical properties of compacted bituminous mixtures

strongly depend on the internal structure, especially on the arrangement of the aggregate skeleton in the compacted mixture.

Laboratory compaction methods have then to reproduce at the laboratory the voids distribution observed in the field. In general, vertically cored field samples tend to have larger void content in their top quarter and uniform void distribution in the rest of the specimen. Horizontal voids distribution is rather homogeneous (Arambula, 2007; Arambula, Masad, & Martin, 2007; Castelblanco Torres, 2004; Dubois et al., 2010; Masad et al., 2002; Tashman, Masad, D'Angelo, Bukowski, & Harman, 2002; Walubita et al., 2012). An important effort to understand the impact of the sample fabrication processes in the material's internal structure and air voids characteristics is found in the literature. A discussion on four commonly used compaction methods in laboratory is proposed in this section.

a. Marshall compactor

The Marshall compactor is described in the (ASTM D1559-89, 1989) standard. The compaction hammer consists in a 4 536 g sliding weight with a free fall of 457.2 mm, with a circular flat tamping face. The mixture to be compacted is placed in a cylindrical mold of 101.7 mm of inside diameter and 76.2 mm in height. Extension collars are used to fit the mixture at the beginning of the procedure. The molds are heated to the compacting temperature to avoid temperature loss of the mixture.

Bituminous mixture samples fabricated using the Marshall compactor have been found to have high quantities of outside voids with respect to the inside ones. This means that Marshall specimens can have high direct exposition to water even if its internal air voids content (by bulk density determination method) is low. According to (Kringos et al., 2009), outside pores are, in average, 45% of the internal voids of a Marshall specimen. This study also showed that the specimens have higher air void content on the top compared to the bottom and that this compacting mechanism tends to create void clusters, which translates into a very asymmetric and inhomogeneous repartition of voids within the specimen. The variability of the voids structure from one sample to another may cause also high variability and feeble repeatability of mechanical tests performed on this kind of samples.

b. Gyratory compactor

Gyratory compactors were developed as a result of the necessity to include shear effort to the loose mixture during the compaction procedure. Shear effort was observed to orientate the aggregates in order to maximize the density of the mixture. Gyratory compactors aim to simulate the density of a bituminous mixture layer after field compaction (Prowell & Brown, 2006).

In France, the mix design procedure is based on the Gyratory Shear Compacting Press (PCG from its French name "*Presse à Cisaillement Giratoire*") (c.f. Figure 1.11). The PCG applies vertical pressure on the ends of a cylindrical sample, which are kept parallel to each other. One end is fixed, while the other rotates describing a circle. The sample is then compacted as a rotating oblique cylinder with a gyration angle of 1°. The applied vertical compressive effort

is of 0.6 MPa. The sample height and the effort to maintain the 1° gyration angle are recorded after every cycle. The density of the sample after every cycle is calculated assuming constant sample mass and diameter. A rate of 6 gyrations per minute is recommended by the French normativity (NF P98-231-2, 1992). The PCG results are correlated to density values achieved on-site with rubber tired or vibratory rollers for a given thickness of the bituminous mixture layer. The correlation is made between the number of roller passes and the number of PCG gyrations. In this way, a mixture can be designed to have target on-site air voids content, for a specified compacting effort, based on the PCG test results (number of gyrations to attain the target air void content). Normally, this target value is set to 3% to 4% for cold and mountainous regions, and to 6% to 7% for regions with hot weather (Prowell & Brown, 2006).

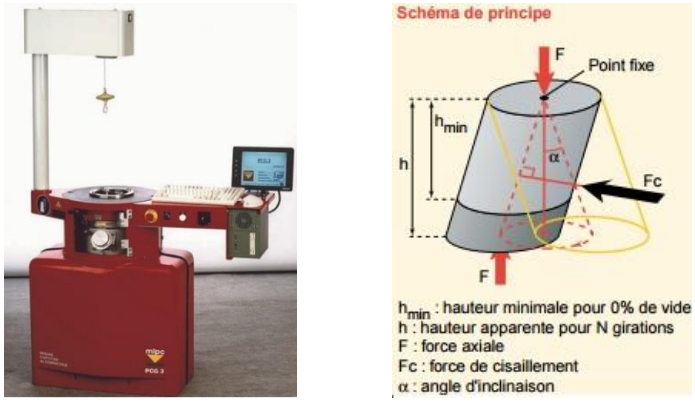

(a) (b)

Figure 1.11. Gyratory Shear Compacting Press - PCG (a) and compaction principle scheme (b) (IFSTTAR, 2016b)

In the American Standard, the Superpave Gyratory Compactor (SGC) (ASTM D6925-15, 2015) works under the same principles as the French PCG but at a rate of 30 gyrations per minute. After an extensive study comparing field cores with samples made with different laboratory compaction methods in terms of air void content and mechanical properties, the SHRP decided to implement the gyratory compactor for the fabrication of bituminous mixture samples. The study concluded that the SGC was the most convenient, the fastest and the cheapest compaction method from the ones available. The study also found rolling wheel compactors to be equivalent to gyratory compaction in terms of mechanical performance and void content of the samples. The gyration rate difference of the SGC with respect to the French PCG lays on the necessity for minimizing sample fabrication time. The increase from 6 to 30 gyrations per minute was found not to generate statistically relevant modifications to the characteristics of the specimens (Harman, Bukowski, Moutier, Huber, & McGennis, 2002; Hughes, 1989; Prowell & Brown, 2006).

Compared to Marshall specimens, SGC ones are found to have rather well distributed air voids. The internal voids are rather uniform in size in the middle part of the sample, with bigger voids in the top and bottom parts. The voids size distribution with respect to their position in the sample form a “bath tub”shape graphic, as shown in Figure 1.12, which is more evident with the increase of the compaction effort. The study made by (Masad et al.,

2002) found that the voids size was uniform within the central 8 cm of 12 cm tall cylindrical specimens.

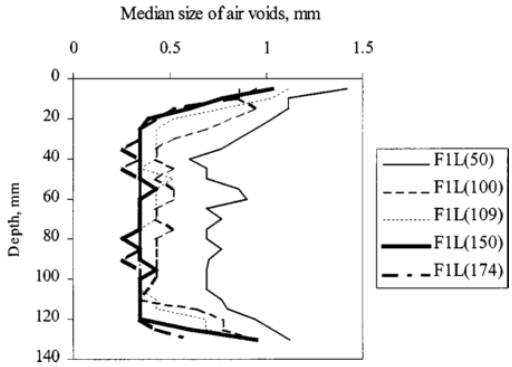

Figure 1.12. Median distribution of air void size with respect to position in the sample at different number of gyrations (50, 100, 109, 150 and 174) (Masad et al., 2002)

SGC specimens have almost half of the outside voids content of Marshall specimens, which means that they have much less direct contact with water and oxygen(Kringos et al., 2009). Due to better air voids distribution and less direct contact with moisture, gyratory compacted samples are then expected to resist better to moisture conditioning and to present more repeatable mechanical test results, compared Marshall ones.

c. Linear kneading compactor

The linear kneading compactor (LKC) is a linear driven kneading machine used to fabricate bituminous mixture slabs. It is intended to simulate the action of a rolling pavement compactor used in the field. The loose mixture is placed in a rectangular mold on a sliding table and compaction plates are positioned on top of it. Compaction effort is made by a rolling wheel which applies a force on the top of the plates while the sliding plate moves back and forth with the mold. The successive downward motion, of one plate after the other, creates a linear compression wave on the mixture and the kneading action avoids aggregate breakage (CP-L 5116, 2014). Slabs fabricated by linear kneading were found to have an bigger voids sizes at the bottom of the slabs than at the top (Masad et al., 2002). This would imply that moisture conditioning and ageing might happen non-uniformly in these slabs.

d. *Roller compactor*

Roller compacting is usually considered to be the laboratory compacting method that creates the specimens with the most similar mechanical properties as field cores (Hartman, Gilchrist, & Walsh, 2001; Hunter, McGreavy, & Airey, 2009; Sousa, Deacon, & Monismith, 1991). Like the kneading compactor, this method is used to fabricate bituminous mixture slabs which can be directly tested, for rutting tests for example, or cored to obtain cylindrical specimens. The slabs are compacted with equivalent loads to those used on a road construction site by field roller compactors. The European Standard (EN 12697-33+A1, 2007) considers either the

use of steel rollers or pneumatic wheels to apply the vertical force to compact the loose mixture (c.f. Figure 1.13). The positions of the wheel and the number of passes at each position are defined in order to attain the target compactness. Horizontally cored cylindrical samples were found to have a very homogenous air void distribution. The same observation has been made for field cores (Dubois et al., 2010).

Figure 1.13. BBPAC roller compactor from IFSTTAR and CEREMA French research institutes (IFSTTAR, 2016a)

1.1.5. Types of bituminous mixtures for road pavement

Bituminous mixtures are mostly used in road pavement applications. Road pavements are a multilayer structure which can be divided into two main layers: the base course and the wearing course. The wearing course mainly assures the good adhesion between the pneumatic wheels and the pavement surface while the base course plays a more structural role by supporting and distributing the efforts to the subgrade. Since their functions are different, specific mixture formulations exists for each layer.

The European Standard (EN 13108-1, 2007) sets the composition and performance requirements for both wearing course and base course bituminous mixtures.

1.1.5.1. Wearing course bituminous mixtures

The wearing course, also called surface course, is the top layer of the pavement structure. It is then in direct contact with climate agents (solar radiation, water, temperature) and with the vehicle's wheels. Wearing course materials have to withstand the stresses induced by traffic and the environment without presenting distresses such as cracking or rutting. They must assure the good state of the road surface and the driving comfort and security. For this, their macro-structure has to provide a rough texture to ensure adequate skid resistance. In most cases, wearing course materials need to be impermeable to keep water out of the pavement structure. The average wearing course thickness ranges between 3 cm to 9 cm. Some French denominations of wearing course bituminous mixtures are:

- BBSG (*béton bitumineux semi-grenu*): Semi-coarse conventional wearing course mixture.
- BBM (béton biutmineux mince): Mixture with a high mastic portion for manually laid thin surface layers of low traffic roads (2.5 cm to 5 cm).

- BBTM (béton bitumineux très mince): High durability mixture with high binder content for very thin wearing course layers of high traffic roads (1.5 cm to 3 cm)
- BBME (béton bitumineux à module élevé): High modulus wearing course material.
- BBDR (béton bitumineux drainant): Highly draining mixture for quick water evacuation.

The European Standard (EN 13108-1, 2007) specifies minimum and maximum values for binder, aggregates and void content of each formulation. In general, these mixtures have high to moderate binder content (TL≥5%) and their maximum aggregate size is either 10 mm or 14 mm. They are also easily compacted. For the most commonly used material, the BBSG 0/14, the air voids content at 80 gyrations of a PCG sample has to be comprised between 4% and 9%. Due to the high binder content, a minimum air void content value is necessary to prevent rutting of the wearing course. This high binder content also decreases their susceptibility to moisture. In terms of resistance, most of the wearing course mixtures must meet a minimum module value of 5 500 MPa at 15°C and 10 Hz, except for the BBME which has higher modulus requirements. With respect to fatigue resistance, the Standard imposes a minimum ε_6 value of 100 µm/m with the 2-points flexion test on prismatic specimens at 10°C and 25 Hz. The ε_6 value is the strain amplitude that causes the specimen failure after one million loading cycles.

For high traffic roads, a binding layer can be used to assure the binding of the base and wearing courses. The BBSG is a typical mixture design for this application.

1.1.5.2. Base course bituminous mixtures

Base course materials need to have high bearing capacity since the base course is responsible for the transmission and distribution of the loads onto the subgrade so that it is not exposed to excessive stresses and strains. It is the most important structural component of a road pavement. Base course materials are then characterized by high modulus values and good fatigue resistance, but no macro-texture specifications are required. Two main base course materials families are comprised within the European Standard (EN 13108-1, 2007):

- The GB (*grave bitume*) classes 2, 3 and 4.
- The EME (*enrobé à module élevé*) classes 1 and 2.

The maximum aggregate size of base course mixtures can be 14 mm, 20 mm or, in some cases, 10 mm. Hard binders are usually used in this kind of mixtures. The different classes of GB are characterised by specific minimum values of modulus and fatigue resistance shown in Table 1-4. These values are all referenced to the same tests and test conditions described before for the wearing course materials.

The performance differences follow the specifications for void and binder content. Table 1-4 clearly shows that the best performing mixtures present lower maximum allowed voids content at the PCG and higher minimum binder content. The standard allows then less air void content and imposes higher binder content to achieve better mechanical performances. The most used GB in France is the GB3, which is a reference material for base course applications. The GB4 and EME2 mixtures are used for roads with special traffic conditions such as heavy traffic or high-speed traffic.

Table 1-4. Specifications for base course mixtures according to the European Standard (EN 13108-1, 2007)

Mixture	Minimum modulus |E*| value at 15°C and 10 Hz [MPa]	Minimum ε_6 value at 10°C and 15 Hz	Maximum voids content of the PCG sample after 100 gyrations [%]	Minimum binder content for a 0/14 mixture [%]
GB2	9 000	80	11	3.8
GB3	9 000	90	10	4.2
GB4	11 000	110	9	4.5
EME2	14 000	130	6	5.5

Compared to wearing course materials, it is clear that regular base course mixtures have lower binder content, higher modulus values and less fatigue resistance. Base course mixtures are also less easily compacted than wear course mixtures, probably due to the difference in binder content. For a railway structure, only the base course is necessary to assure the optimal load transmission to the subgrade. Since there is no wheel-pavement contact, the wearing course can be suppressed which represents a considerable cost saving due to the high binder content of wearing course mixtures. Nevertheless, assuring the adhesion of the pneumatic wheel to the pavement is not the only task of the wearing course; it also protects the base course from weather agents.

1.2. The use of bituminous mixtures for railway trackbeds

The development of the railway transportation industry comes with an increase in circulation speeds, freight loads and traffic volume. Nowadays High-Speed Trains (HST) can circulate at commercial speeds up to 350km/h and future projects consider increasing this limit up to 400km/h. The construction on new High-Speed Lines (HSL) for passenger transportation will open the conventional lines to the transportation of merchandise. The necessary works to adapt these lines and their infrastructures (usually very old ones) to freight traffic require new building techniques. Improvements in the track structure are then necessary in order to cope with the increasing solicitations and to ensure low railway operating costs and higher passenger comfort and safety. In the case of ballasted tracks, two approaches can be considered: improving the track design as a whole or improving the structural components of the superstructure and of the platform. Regarding the second approach, the use of innovative sub-ballast layers and of low stiffness rail-sleeper-ballast systems constitutes an interesting scenario (Teixeira, Lopez-Pita, Casas, Bachiller, & Robuste, 2006).

Track substructure design is crucial for the good behaviour of the track and maintenance costs optimisation. In almost all European countries, a minimum bearing capacity of 80 MPa is required for sub-ballast layers when the soil characteristics are optimal. This minimum requirement increases to 120 MPa for low quality soils. In conventional track design, increasing the bearing capacity of the platform is achieved by increasing the thickness of the sub-ballast layers made with unbound granular materials (UGM), or by using cement-treated granular

materials (gravel or soil) if the terrain conditions are very inconvenient. Some advantages of using sub-ballast layers include the prevention of rainwater infiltration into the layers below the embankment, the reduction of high stresses in the embankment, the protection of the upper part of the earth-works from freezing and the reduction of ballast fouling (Buonanno & Mele, 2000).

The use of bituminous mixtures for sub-ballast layers has been identified as a possible solution for the necessary enhancement of the track structure. Studies and field experiences have identified some advantages of sub-ballast bituminous layers including vibration damping, reducing stress levels on the subgrade and constituting a low permeability layer over the soil layers, which leads to a reduction in the maintenance needs. In addition, constructive advantages have also been observed such as allowing the circulation of engines on the platform during the construction phase (EAPA, 2014; Fang et al., 2013; Huang et al., 1984; Robinet & Cuccaroni, 2012; Rose & Bryson, 2009).

The earliest uses of bituminous mixtures in rail industry consisted in railroad of highway crossings, bridge or tunnel approaches and rehabilitation of turnouts, where conventional track designs did not perform satisfactorily.

In Europe, the arrival of high-speed passenger transportation incited the research of new track designs, some of which used bituminous sub-ballast layers as it is the case of the first Italian HSL: the Rome to Florence “Direttissima”, in service since 1977. By the same period, bituminous mixtures started to regain interest for American freight lines due to the sudden increase in tonnage, axle-loading and traffic volume that followed the deregulation of the freight system. The experiences from these countries, dating already from almost 40 years, show a good long-term performance of bituminous materials in railway tracks. Until now, many other countries have started to use bituminous materials as a way to cope with the increasing tonnage, speed and frequency of rail traffic (Di Mino, Di Liberto, Maggiore, & Noto, 2012; EAPA, 2014; Rose & Souleyrette, 2015; Rose, Teixeira, & Veit, 2011; Teixeira, López Pita, & Ferreira, 2010).

Nowadays, three basic types of trackbeds including a bituminous mixture layer are being used. The first consists of a bituminous layer under the ballast layer, replacing the UGM sub-ballast. It is the case of the Italian, French and Spanish track examples that are presented later in this section. A variation of this track configuration consists in a combination of bituminous and granular sub-ballast. The bituminous layer is thinner than in the previous configuration and it is not as large as the whole trackbed. It reposes on a granular sub-ballast layer that covers the whole width of the trackbed, which is not as thick as that of the conventional configuration. In this way, the ballast reposes on the bituminous layer at the centre of the trackbed and on the granular sub-ballast at the track borders. It is the case of some track designs in the USA. The second type of track configuration consists of a thin layer of bituminous mixture under the ballast which separates it from the UGM sub-ballast avoiding ballast fouling. It is the case for the Japanese track structure. The third type is the ballast-less configuration with the sleepers anchored to the bituminous layer, as the GETRAC® system developed in Germany (Rose et al., 2011).

1.2.1. Examples of bituminous mixtures used in railway trackbeds

1.2.1.1. Tracks with bituminous layers as part of the bearing structure

Bituminous layers are nowadays used as part of the structure of railway tracks in many different countries including Italy, France, Spain and the USA.

In Italy, in the 70's, the Italian Railway Company (Ferrovie dello Stato) decided to use a bituminous mixture sub-ballast layer in the design of the "Direttissima" HSL as it was the most economical solution to assure the high stiffness requirements of the platform. Compared to the bituminous layer, the cement-treated gravel sub-ballast presented several disadvantages. It presented higher sensitivity to freezing during the construction phase than the bituminous mixture and it had to be protected from bad weather with bituminous emulsions or membranes. Additionally, the cement-treated gravel could not be used as access way to the construction site by the construction engines before its completion and maturation. Moreover, for this specific case, the bituminous solution represented aggregate cost savings of 40% with respect to the cement-treated gravel one. The used bituminous mixture had a 50/70 pen grade bitumen at a binder content ranging between 4.1% and 4.7%. The voids content was set to 2%. The bituminous layer was laid and compacted with conventional road construction equipment.

Several advantages of this track design were identified. The safety and the structural reliability of the track were improved by the high stiffness of the bituminous mixture and by the fact that the bituminous layer provides a uniform bearing capacity. Ballast is also better confined and the risks of ballast fouling are eliminated. Moreover, the bituminous track height was lower than that of a conventional granular one. Bituminous mixtures were also found to have excellent damping properties, leading to an attenuation of solid-borne vibrations transmitted to the embankment (Buonanno & Mele, 2000; Teixeira et al., 2010). Finally, (Buonanno & Mele, 2000) affirm that the high tension resistance of bituminous mixtures helps reducing the tension stress suffered by the ballast layer, inducing less wear and tear of the ballast grains and, therefore, reducing the need for track maintenance. Given the good behaviour of the "Direttissima", the use of a 12 cm thick bituminous sub-ballast layer over a highly compacted soil of at least 80 MPa bearing capacity (c.f. Figure 1.14), was henceforth generalized for all Italian HSL projects. The complete HSL Italian network comprises nowadays nearly 1 200 km of tracks with sub-ballast bituminous layers (Buonanno & Mele, 2000; Teixeira et al., 2010).

Figure 1.14. Schematic cross section of a typical Italian HSL track with bituminous sub-ballast layer (adapted from (Rose et al., 2011))

In Spain, four trial sections with sub-ballast bituminous layer have been built in the Madrid-Valladolid, the Barcelona-Figueras (near the French border), the Valladolid-Burgos and the Alicante-Murcia lines. The Madrid-Valladolid HSL became operational in December 2007, and the Barcelona-Figueras HSL in 2013. Both track structures use a Spanish S20 bituminous road-base mixture for the 12 cm to 14 cm thick sub-ballast layer, which lay over a 30 cm thick form layer on top of a subgrade on minimum bearing capacity of 80 MPa (cf. Figure 1.15). The Sils-Riudellots site in the Barcelona-Figueras HSL has an important instrumentation and the results from a 4 years monitoring study will serve to validate the use of bituminous sub-ballast layers for future Spanish HSL projects. For the moment, the Spanish Rail Infrastructure Agency ADIF has defined some technical specifications for bituminous mixtures to be used as sub-ballast. These include the use of binders of grade 50/70 or 70/100, added filler content higher than 50% of the natural filler in the aggregates, binder content higher than 4.75% and fatigue resistance ε_6 by 4-point flexion test of at least 120 µm/m (EAPA, 2014; Rose et al., 2011).

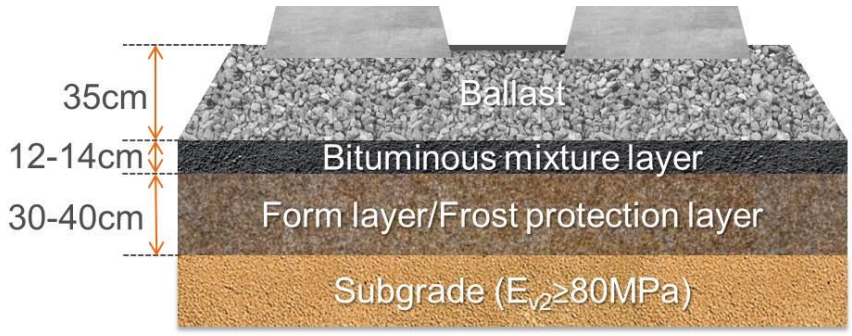

Figure 1.15. Schematic cross section the Spanish HSL test sections with bituminous sub-ballast layer (adapted from (Rose et al., 2011))

According to (Rose et al., 2011), the typical sub-ballast bituminous mixture layer in the United States is 3.7 m wide and 12.5 cm to 15 cm thick. The thickness can rise up to 20 cm if the soil conditions are poor. Ballast thickness over the bituminous layer ranges from 20 to 30 cm, which are similar values to those used in Europe. As for the mixture specifications, dense-graded road base-course mixtures are the most commonly used, with maximum nominative aggregate size of 2.5 cm to 3.7 cm. The binder content is usually 0.5% higher than the reference road base-course mixture and they have air void content between 1% and 3%. High compactness is intended to assure sufficient strength and impermeability of the material. Rutting is believed not to be of concern due to the large area of load repartition by the ballast. Bleeding and flushing are not of concern either, in spite of the high binder content, as there is no direct contact with wheels. Regarding temperature variations, (Rose et al., 2011) states that extremes are minimized by the overlaying ballast. In the past decade over 322 km of bituminous sub-ballast layers have been built for new projects in the mid-west area of the United States; mostly for heavy freight traffic. Other American notable applications of bituminous mixtures include three railway tunnels in the Norfolk Southern (NS) Heartland Corridor. These tunnels have a history of soft support and drainage problems which required several maintenance operations. The track design with a bituminous trackbed was retained for the renovation works due to its low structure height and to the good drainage properties (Rose & Souleyrette, 2015).

The French experience with bituminous materials in trackbeds is developed in Chapter 2. The first 3 km long French trial track with bituminous sub-ballast layer, built in the East-European (EE) HSL, is the case study of this thesis. The French HSL experience with bituminous sub-ballast layer has been exported to Morocco for the construction of a section of the Tangiers-Casablanca HSL, the first line of the high-speed Moroccan network project.

Interesting design tendencies can be identified from the presented examples of the different exposed countries. All of the presented track designs include the use of a high binder content bituminous mixture of around 4.5%. This binder content level corresponds to that commonly used for the French *Grave-Bitume* (GB) type 3 mixtures. In the case of the United States, since the binder content of the sub-ballast layer is systematically higher than for road layers, the authors state that rutting is not an expected problem due to the load repartition over a large surface through the ballast. However, due to the angularity of the ballast grains, punching of the bituminous layer surface could be increased if the high binder content affects the mechanical properties of the mixture by making them softer than the reference road mixture. Punching could have negative effects on the bituminous layer such as the triggering of cracks or the deformation of its surface creating zones where water could accumulate or infiltrate. If the objective of increasing the binder content of 0.5% with respect to the reference road mixture is to decrease its susceptibility to water, this deserve further attention.

High binder contents increase the impermeability of the mixtures and this is seen as a solution for the problem of water infiltration. However, this rises up the question of water pressure build-up in the case of water coming from below the bituminous layer trough the granular layers. Drainage systems of the underground water are then of special importance for these kinds of tracks. Even if the bituminous layers are designed to be impermeable and to have excellent surface draining properties, water remains a great risk for the integrity of the track. All the precautions should be taken to reduce the exposition to water of the bituminous materials.

The Spanish mixture design does not impose specific voids content but sets a minimum fatigue resistance value of ε_6=120 µm/m according to the European normativity for testing of bituminous materials (EN 12697-24, 2012). This is a fatigue resistance value excepted from high performance mixtures. Given the relationship between voids content and fatigue resistance, the Spanish mixture should have very low voids content in order to cope with this requirement. In the case of the Italian and American designs, the target voids contents of around 2% also contribute to the high fatigue resistance of the mixtures. Even if it is not always specified, the presented examples agree on the fact that low voids content mixtures are preferable for sub-ballast applications.

The difference in the bearing capacity of the subgrade for the presented examples could be attributed to the all-ready existing specificities of the conventional track designs of each country. This would explain why the Italian track includes a “supercompattato” layer over a 40 MPa subgrade, while the Spanish one includes a form 30 cm thick layer over an 80 MPa subgrade. In both cases the resulting bearing capacity of the layers under the bituminous one round up to 120 MPa. There is then a trend in the presented examples of assuring a high bearing capacity granular base for the bituminous layer. This seems prudent since the granular layers below the bituminous one should not subside to ensure a continuous support. Moreover, the results from numerical simulations of the track (c.f section 1.2.3) stand that the soil failure could be attained before the bituminous material’s (Alfaro Albalat, Montalban Domingo, Villalba Sanchis, Real

Herraiz, & Villanueva Segarra, 2011), highlighting the importance of a good quality granular support of the bituminous layer to ensure a long service life of the track.

The French design adopted for the 3 km long trial track with bituminous sub-ballast layer of the EE SHL does not differ much from the Spanish and Italian cases. The mixture adopted for the test section has very low voids content (around 3%) and high binder content of a French GB. Also concerned by the service life of the bituminous structure, the used mixture has an extended fatigue life compared to the reference road GB (fatigue resistance value of ε_6=110 μm/m). More information on this is given in Chapter 2.

1.2.1.2. Tracks with bituminous layers as a barrier between the ballast and granular sub-ballast

This kind of use of bituminous mixtures in railways is different from what was previously discussed. The requirements for the bituminous mixtures intended to separate the ballast and the subgrade are then different and do not make part of the scope of this study. However it is very interesting to observe the different applications of bituminous materials in railway tracks.

In Japan, bituminous materials are widely used in the construction of both high-speed and conventional lines. For the Japanese design, the bituminous layer intends to assure the track geometry and to serve as firm support for the ballast that separates it from the sub-ballast. A scheme of the cross section of a typical Japanese HSL structure with bituminous sub-ballast layer is presented in Figure 1.16. This design has been used for over 40 years due to capacity of the bituminous layer to distribute loads and facilitate drainage. Despite the very low thickness of the bituminous layer (~5 cm), reduced load levels at the subgrade have been observed in comparison to conventional tracks made with UGM. In Figure 1.16, the thickness of the crushed stone layer ranges between 15 cm to 60 cm depending on the quality of the subgrade. The used method in Asia to control the compaction qualities of the granular materials is the plate loading test which measures the reaction modulus k_{30}. Even though a relationship between E_{v2} and k_{30} values was proposed by (D. Kim & Park, 2011), more information is needed to provide the equivalent E_{v2} value of the subgrade of this configuration. As estimation of the order of magnitude, a k_{30} of 130 MN/m3 would be equivalent to an E_{v2} around 128 MPa. The roadbed (bituminous layer + crushed stone capping layer) design methods are described in the “Design Standard for Railway Structures (Earth Structures)”. Before the 2007 revision, this standard defined a single bituminous layer thickness. Nowadays, the standard is based on the materials resistance to fatigue cracking which allows defining a layer thickness for each project based on the roadbed performance requirements (Momoya, 2007; Momoya, Horike, & Ando, 2002; Rose et al., 2011).

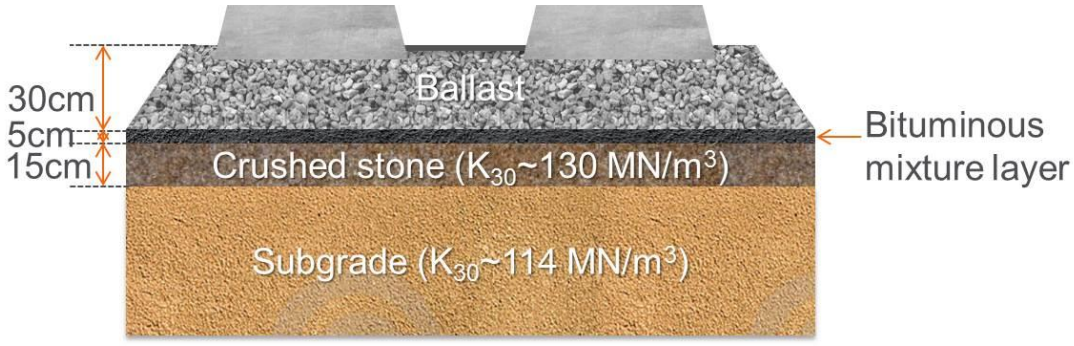

Figure 1.16. Schematic cross section of a typical Japanese HSL track with bituminous sub-ballast layer (adapted from (Rose et al., 2011))

The Austrian Federal Railways have also shown great interest in bituminous mixtures. Their use in Austrian trackbeds is usually conceived as a way of separating the subgrade from the superstructure and the thickness of the bituminous layer varies from 8 cm to 12 cm. For the Austrians, the economic investment in bituminous materials must be balanced by the gain in other aspects such as avoiding water penetration to the substructure, avoiding ballast fouling, obtaining optimal track stiffness and homogenizing the stress at the substructure due to the continuous support of the ballast. The experience of a bituminous sub-ballast layer laid in 1963 allowed assessing the low maintenance needs of the bituminous layer itself: no maintenance operations had been necessary by 2011.

Life-cycle and return on investment studies have been carried out, taking into account construction and long-term maintenance costs. These studies are based on the analysis of track quality evolution which depends on the initial quality and on the deterioration rate of the track over time. The study from (Holzfeind & Hummitsch, 2008) found that tracks with bituminous layers had lower degradation rates (of around 33%) than high quality conventional tracks. The initial quality of both trackbeds was similar. For Austrian standards, this reduction of the deterioration leads to the increment of the time between levelling, lining and tamping operations from 3 to 5 years, and to an increase of the service life of 17%. The study also demonstrated the stability of the economic efficiency of using bituminous sub-ballast layers (Rose et al., 2011).

1.2.1.3. Ballast-less tracks with bituminous mixtures

This kind of configuration is out of the scope of this study, however, the fact that bituminous mixtures can be used for ballast-less tracks is evidence of its versatility and adaptability to numerous contexts. The examples presented below are then intended just to inform the reader of their existence.

The most evident example is found in Germany. The German railway company, the Deutsche Bahn, encourages the research of alternatives to conventional ballasted tracks in order to lower maintenance costs and preserve natural resources. The most recently proposed alternative is the GETRAC® system (c.f. Figure 1.17), a ballast-less track system including a bituminous mixture support layer with concrete ties anchored into the mixture(EAPA, 2014; Rose et al., 2011).

(a)

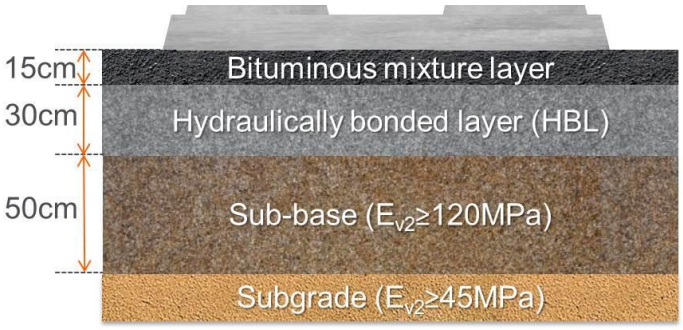

(b)

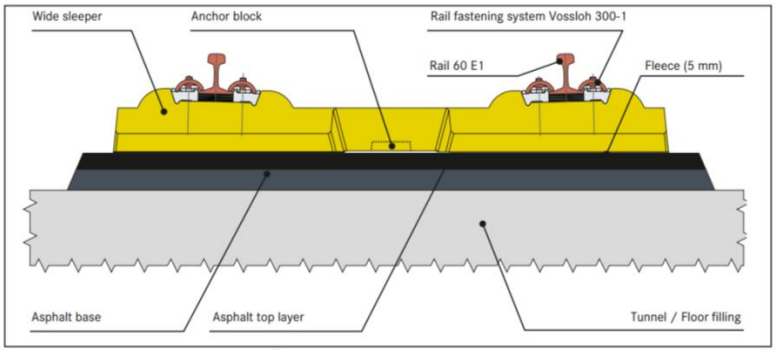

Figure 1.17. Schematic cross section the GETRAC® A3 ballast-less track with HBL (a) and scheme of the application of GETRAC® system to tunnels (adapted from (Rail.One GmbH, 2012))

In France, the Lingolsheim trial ballast-less track for freight traffic constitutes a revolutionary case for the French network. This test zone is only 150 m long but it is the only ballast-less track with bituminous mixture platform in France.

1.2.2. Identified advantages of the use of bituminous sub-ballast layers

There are many advantages form an economic point of view of using bituminous sub-ballast layers. In general, no especial equipment is needed for the construction since construction methods of sub-ballast bituminous layers are similar to those of highways, using paving laydown equipment and roller compactors. The costs of a structure with bituminous material can be lower than those of a structure with only new granular materials if high-quality material is far from the construction site and transportation costs are high (Alfaro Albalat et al., 2011; EAPA, 2014; Rose et al., 2011; Teixeira et al., 2010). For the Spanish context in 2011, (Alfaro Albalat et al., 2011) estimated that sub-ballast layers made from granular materials coming from distances higher than 60 to 80 km were more expensive than bituminous ones. The dimensions (thickness and width) of a bituminous mixture layer are normally smaller than those of a high stiffness UGM sub-ballast layer. This allows an important economy in material volume and costs estimated by (Alfaro Albalat et al., 2011) in around 200 m^3/km/track. Since the construction procedures are the same as for highways, there is few manual work and high reliability in the respect of the track geometry and layer smoothness. The good drainage properties of the bituminous layer allow reducing the lateral slope of the sub-ballast to 3% which allows reducing the volume of the ballast layer, compared to conventional structures (4%). According to (Alfaro Albalat et al., 2011) this ballast saving could be equal to, at least, 5% of the bituminous layer cost.

Initial costs of bituminous tracks can then be similar of higher than those of conventional ones depending on the context. However, the greatest interest of bituminous sub-ballast layers lays on the lifetime operating costs. The French experience of the EE HSL showed an important reduction of the maintenance needs of the bituminous track section compared to neighbouring conventional track sections (c.f. chapter 2). These observations are in concordance with the studies made based on the Austrian and Italian experiences.

From the international and national experiences, several technical advantages of using bituminous mixtures in track design are well identified. These include providing continuous support and improving loading distribution to reduce stress at the subgrade, increasing the ballast confinement, improving drainage properties of the trackbed, avoiding moisture diffusion into the subgrade and maintaining constant its water content, reducing the track geometry variations, being trafficable during the construction phase and reducing maintenance efforts during service life. Bituminous trackbeds are now considered as a state of the art technology for HSL and for heavy tonnage freight lines (Rose & Souleyrette, 2015). Future developments include the use of Reclaimed Asphalt Pavements (RAP), cold mixtures with modified binders, further development of the ballast-less (even sleeper-less) bituminous track, amongst others.

1.2.3. Numerical modelling of railway tracks with a bituminous layer

Numerical modelling of railway tracks is a common practice to evaluate the stress generated in the different constituents of the track due to train circulation. Estimating the stress levels in each component allows correctly dimensioning the structure.

The track structure usually consists of a rail, a rail fastener, a sleeper and a multi-layered support including the ballast layer, the sub-ballast, the capping layer and the subgrade. Ballast and sub-ballast layers constitute the trackbed. Rail traffic is usually modelled by the application of two consecutive concentrated loads on the rail. The distance between the two loads depend on the bogie geometry of the considered train. The reactions to the loading (stress, strain, acceleration, deflection) are obtained by superposing the singular reactions to each of the concentrated loads. In the case of using a finite element method (FEM), rail and sleepers are usually modelled as beam elements. The fastener is modelled as a spring (Rose, Li, & Walker, 2002).

For the support layer, the ballast can be considered as a non-linear elastic material when the track is new and as a linear elastic material when the track has been used and the ballast compacted by the traffic action. The UGM sub-ballast is modelled as an elastic material. Despite the viscoelastic behaviour of bituminous mixtures, these are usually (and wrongly) described by elastic equations in track modelling. Since the material's behaviour depends on temperature, different elastic modulus values are taken into account depending on the season of interest. Nevertheless, this does not take into account the frequency dependence of the mechanical behaviour of the material. Viscoelastic models should be integrated to simulation software to be accurate when modelling railway tracks with bituminous materials. Finally, the capping layer and subgrade, both granular materials, can be modelled as elastic ones.

The works of (Alfaro Albalat et al., 2011; Di Mino et al., 2012; Fang et al., 2013; Huang, Rose, & Khoury, 1987; Momoya et al., 2002; Teixeira et al., 2006) are some examples of the application of numerical models for bituminous track structure analysis.

Two parameters are usually taken into account to evaluate the behaviour of tracks with bituminous layers. The first one is the tensile strain at the bottom of the bituminous layer as it can cause cracking in a sudden way or through damaging after repeated loading. The second is the vertical compressive stress at the subgrade soil as it can cause excessive setting and deformation of the platform. The service life of the structure will depend on how long the bituminous mixture will withstand the repeated strain or on the subgrade's bearing capacity over time. Both failure criteria are similar to those used for road design but due to the difference in design life time and in the loading and environmental conditions, the same thresholds as for road designs should not be taken into account for railway track dimensioning (Huang et al., 1987; Rose et al., 2002).

The research by (Teixeira et al., 2006) evaluated the effect of bituminous sub-ballast layers in terms of three parameters: the vertical stresses on the ballast, the tensile strains in the sub-ballast layer and the vertical stresses on the subgrade. They used the finite elements model based KENTRACK computer program, which considers the track structure as an elastic multilayer assembly. They identified an optimal sub-ballast thickness of 12 to 14cm using conventional bituminous mixtures. The studied track structure was found adequate for meeting the Spanish high-speed railways standards (Teixeira et al., 2010).

The KENTRACK program had already been used by (Huang et al., 1987) to propose a design method for bituminous sub-ballast layers considering the strain at the bituminous layer and the stress at the subgrade. (Rose et al., 2002) also used KENTRACK in the evaluation of a track with bituminous mixture. The results of their track simulations compared well to in-situ measurements from a trial track, thus confirming the ability of the program to predict performance values of both conventional and bituminous trackbeds.

Furthermore, (Fang et al., 2013) concluded that the optimal position of the bituminous layer is under the ballast layer and right above the upper subgrade. For this, they used a finite element method to calculate vertical stresses and transversal and longitudinal tensile strains in each layer of various track configurations. The results showed that placing the bituminous layer under the ballast provides the most total stress reduction in the trackbed as well as the most vibration attenuation. Compared to conventional trackbeds, the bituminous layer was found to greatly decrease the vertical acceleration of the top of the subgrade and to be beneficial to the long-term track behaviour and vibration control.

With the aim of optimizing the required volume of material for HSL new projects, (Alfaro Albalat et al., 2011) determined the optimal thickness of bituminous sub-ballast layers. They used the ANSYS FEM software to simulate the track behaviour under high-speed trains loading. Elasto-plastic constitutive laws were used for soil and granular materials and a viscoelastic model for the bituminous sub-ballast. The results of this research showed a minimum bituminous layer thickness ranging between 12 cm to 14 cm, depending on the loading case. They also observed that the vertical stress levels on the sub-ballast bituminous layer are equivalent to a fraction of those imposed by high-pressure truck tires on highway pavements. Regarding lifetime, the simulation showed that the failure by fatigue happens first in the subgrade than in the bituminous layer. This means that the theoretical service life of a track with a bituminous mixture layer is equivalent to that of a conventional track and that it is not defined by the fatigue resistance of the mixture.

(Di Mino et al., 2012) used a 2-dimensional dynamic model to analyse the behaviour of a track with bituminous sub-ballast layer containing dry asphalt rubber. They modelled the bituminous layer as a continuous viscoelastic beam. They assessed the shear stress behaviour of the ballast layer and the flexural behaviour of the bituminous one. Four bending point tests were used to characterize the viscoelastic behaviour of the bituminous mixture at typical ambient temperature conditions of southern Italy. The simulation results from this study show a reduction of 40% of the dynamic pressures at the subgrade for the track with 12 cm thick bituminous sub-ballast compared to the conventional track. This confirms the fact that the bituminous layer distributes better the loads on the subgrade. The study also concluded on the theoretical possibility of using of rubber in bituminous mixtures for railway track bed.

In Japan, slab tracks are widely used in order to reduce maintenance costs of the railway network. However, concrete slab tracks are very noisy. In (Momoya et al., 2002) a bituminous slab track is proposed as a solution to reduce noise emissions. For this study, a 20 m long test track (c.f. Figure 1.18) was built in the laboratory to assess, on the one hand, the noise reduction, and on the other, its mechanical behaviour. Regarding noise production, the results of motor car running tests showed that the maximum sound level of the bituminous track was lower than that of conventional slab tracks. From a mechanical point of view, the setting of the track was observed under static and dynamic loading. For this last one, a dynamic loading car (DYLOC) was used. The tests results showed that the settlement of the track with the bituminous layer was smaller than that of the conventional ballasted track under static loading and that no cracks were observed in the bituminous layer after dynamic loading. The authors concluded that the proposed track with a 20 cm thick bituminous layer was a good alternative for low maintenance track design. A FEM software was used to simulate the mechanical tests on the trial track. The simulation results compared well with the experimental ones which validated the model.

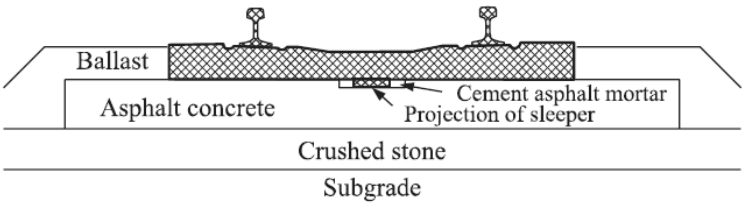

Figure 1.18. Cross section of the proposed track design by (Momoya et al., 2002) as an alternative to Japanese concrete slab tracks

Numerical models are then a valuable tool to estimate the behaviour of new track designs. As observed from the works presented, the ability of FEM based software to reproduce the real behaviour of tracks need to be validated by comparing the simulation result to those of test tracks. Once calibrated, these models can be used to assess different properties including service life. Given the fact that real service life can only be assessed after a long time period, its estimation through validated numerical models can be very useful. The results from the presented works agree on the fact that a 12 cm to 14 cm thick bituminous mixture (as the ones presented in section 1.2.1) would be suitable for HSL common service life standards. This is in accordance with the good behaviour of the Italian and French bituminous tracks already in service.

1.2.4. Relevant characteristics of railway track design

Railway track distresses can be categorized in two families. The first one comprises the failures due to overpassing the subgrade's bearing capacities; the second one comprises the failures due to the malfunction of one or many trackbed structural components. Subgrade distresses can be prevented by reducing the vertical pressure, by improving drainage to avoid water content variations or by using thicker and better quality trackbed layers (sub-ballast, ballast). Structural components failures can be minimized by optimizing the track stiffness through the design and selection of high quality fasteners, pads, sleepers, etc. In order to optimize the track design, models are often used to characterise the pressure levels and load transmission at each level of the structure such as the rail base-fastener, fastener-sleeper or sleeper base-ballast interfaces.

One common symptom of distresses in the track is its excessive deflection, which causes accelerated movements of the track components. This acceleration increase causes wear of ballast through inter-granular friction. Normally the dysfunction of one of the track components triggers the accelerated deterioration of the other components and a global track dysfunction. The use of a stiff platform can help reducing track deflections; however, a platform too stiff can promote ballast breakage. The ideal track structure provides a balance of stiffness and flexibility (Rose et al., 2002).

The effective load applied to the track is not only dependent on the vehicle tonnage but also on the circulation speed and of the spacing between axles of the train. High speeds promote dynamic phenomena that causes load amplification. The train geometry defines the load repartition on the vehicle's axles; therefore, the tracks have different responses to different circulating trains. Axle load is determinant to calculate acceleration, speed and displacement amplitudes of a track element when loaded by a passing train. Track quality should then be optimized for the specific traffic on a railway line.

For conventional trackbeds made only with unbound granular materials, the loading frequency is not considered as a determinant parameter of its dynamic behaviour. This wouldn't be the case for a track with bituminous sub-ballast layer since the behaviour of bituminous mixtures is dependent on the frequency and on the temperature (c.f. section 1.3).

Recently though, researchers have studied the behaviour of the interlayer, a naturally-formed sub-ballast layer containing fines and wore ballast grains located between the clean ballast and the subgrade, and found that its mechanical behaviour is influenced by the loading frequency. In this regard, for old tracks containing interlayers, the plasticity index of the fines particles becomes a parameter of importance in order to determine the frequency dependency of their dynamic behaviour (Bolton & Wilson, 1989; Lamas-Lopez, Alves Fernandes, et al., 2014; Lamas-Lopez, Cui, et al., 2014; Selig & Waters, 1994). Figure 1.19 presents the excited wavelengths by different train geometries at different circulation speeds. The work of (Lamas-Lopez, 2016; Lamas-Lopez, Cui, et al., 2014) allowed the identification of the wavelength excited by the distance between the axis of a bogie as the one that gives the most energy to the system. Therefore, the frequency associated with this wavelength would be determinant of the behaviour of frequency-dependant materials in railway tracks such as bituminous mixtures. However, given the fact that the other excited wavelengths also give energy to the system, the answer of bituminous mixtures to a passing train would be influenced by a mixture of loading frequencies. This is worth of further investigation.

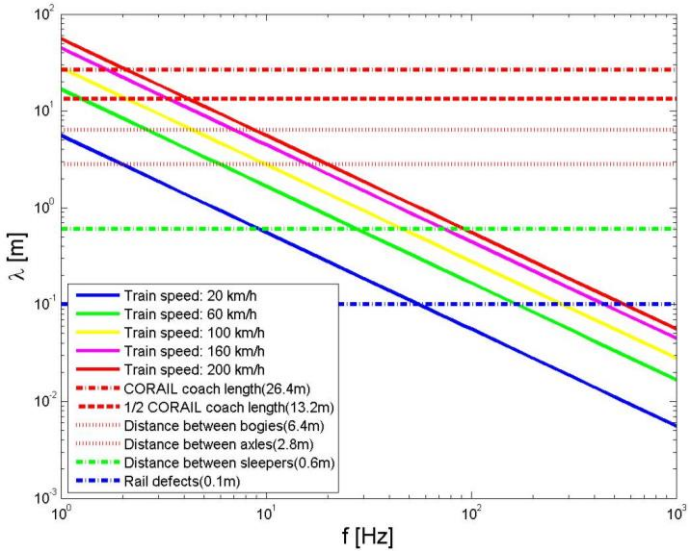

Figure 1.19. Excited wavelength (λ) according to train speed and geometry (Lamas-Lopez, 2016)

1.2.5. Differences between rail and road traffic loading conditions on bituminous layers

In order to understand the degradation processes of railway tracks using bituminous layers, it is necessary to characterize the mechanical behaviour of bituminous mixtures for typical loading conditions of rail traffic. Using the hypothesis and feedback from the road industry experience can help at a first approach but specific standards and specifications issued from railway experience are required to assure optimal track design.

Figure 1.20 illustrates the typical model used to study the action of traffic loads on a road pavement structure. It is based on the elastic layered theory (Di Benedetto & Corté, 2004). The layers behave as slabs and bend when loaded, generating horizontal tensile stresses and strains at the bottom of each layer and vertical compressive stresses and strains in the bulk section. Road design aims to limit these tensile strains at the bottom of the bituminous layers to avoid tensile cracking and fatigue, as well as limiting the compressive stresses at the subgrade to avoid permanent deformation of the support. In road design the bituminous layer thickness has a determinant effect on the critical tensile strain value. The thicker the layer, the lower the developed strain in it.

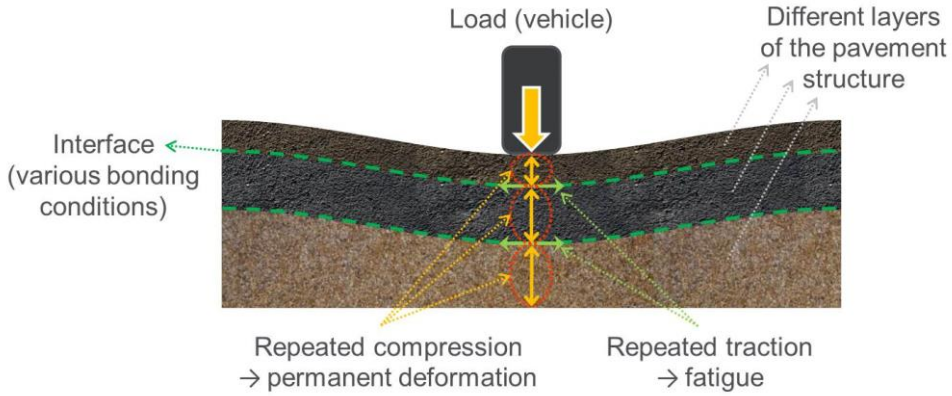

Figure 1.20. Scheme of the effect of traffic loads on a road pavement structure (adapted from (Di Benedetto, 1998)

In railways, a constant vertical effort is applied on the bituminous sub-ballast layer due to the weight of the superstructure (ballast, sleepers, rail). This acts as a confinement pressure of the material which would have to be taken into account when assessing fatigue cracking properties of bituminous sub-ballast layers (Huang et al., 1984). As in roads, the bituminous layer in the railway track design also confines the subgrade, increasing its bearing capacity.

Regarding circulation speed, in France, trains can circulate at speeds up to 350 km/h for passenger TGV trains and up to 160 km/h for freight trains. High-speed train circulation induces dynamic phenomena on the bituminous mixture that contributes to load amplification. This is not observed in highway pavements.

Axle loads are significantly higher in railway traffic than in road traffic. French TGV and freight trains have maximum axle loads of 17 ton and 22.5 ton, respectively. In the USA, the average weight of freight trains is 16 ton (Rose et al., 2011). These loads are very high compared to the 13 ton maximum axle load taken into account for French road pavement design. Due to the time-dependent behaviour of bituminous mixtures (creep), the application of such high loads for extended periods of time is of concern from a track permanent deformation point of view. Such is the case of train stations and technical centres where trains are stopped for long time periods.

However, load distribution is a more important difference than load amplitude between roads and ballasted railway tracks. In roads, the axle load is directly applied to the pavement on small circular areas, whereas in railways the load is distributed by the rail-tie-ballast system over a much wider surface. The European Asphalt Pavement Association (EAPA) states that the load applied to the sub-ballast bituminous layer is lower than in road pavements. As an example, an 11.5 ton/axle loaded truck applies a 0.8 MPa stress on a surface of around 710 cm^2. On a railway, the same concentrated load of 11.5 ton results in a stress at the bottom of the sleeper of only around 0.25 MPa. The stress at the bituminous layer will then be smaller. Despite this, the longer expected service life of a railway track of 100 years, compared to 25 to 30 years for a road pavement, imposes a careful track design to avoid maintenance needs of the bituminous layer which are practically impossible (EAPA, 2014).

The larger load distribution surface affects also the development of compressive strains at the top of the subgrade. When the load is applied over a large area, the vertical compressive strains depend largely on the horizontal stresses, which vary in an irregular manner with respect to the bituminous layer thickness. This is very different from road structures, where the compressive strains depend almost exclusively on the vertical stresses which decrease as the layer gets thicker. This implies that the vertical strains at the top of the subgrade layer should not be used as a design parameter for railway tracks with bituminous sub-ballast layers. Instead, vertical stress should be used, even though its critical value not only depends on the bituminous layer thickness but also depends on the subgrade bearing capacity. A specific criterion for railway structures on allowed compressive stress needs to be stablished taking also into account the fact that the bituminous layer is confined by the superstructure weight (Huang et al., 1984).

Fatigue and vertical stress criteria have to be adapted as more information is collected from the return on experience of in-service tracks with bituminous sub-ballast layers. This highlights the importance of research programs including on-site measurements such as those in the Spanish Barcelona-Figueras and the French Brittany-Loire HSLs.

The bituminous mixtures used for railway trackbeds are road base-course mixtures. In road applications, these materials are covered by the wearing course which offers an effective protection from weather conditions such as moisture and UV radiation. The exposition of base-course mixtures to these factors can accelerate their degradation process and; therefore, shorten the service life of the track and cause the loss of all the formerly discussed advantages of using bituminous layers in railway track design, especially the reduction of maintenance needs. Given the fact that loading is supposed to be lower in bituminous sub-ballast layers than in road base-courses, degradation due to the exposition of the materials to weather constitutes a crucial issue for the viability of this technique.

1.2.6. Effect of weather conditions on bituminous mixtures

Weather conditions can alter the mechanical behaviour and trigger degradation processes in the bituminous mixture.

Temperature has several effects on pavements containing bituminous materials. Figure 1.21 is a schematic representation of the effects discussed hereafter:

- Bituminous mixtures are materials whose mechanical behaviour depends on their temperature (c.f. section 1.3). In particular, their stiffness increases when temperature decreases and vice-versa.
- Bituminous mixtures undergo thermal expansion and contraction when subjected to temperature changes, as do most materials. This phenomenon is particularly detrimental for bituminous materials when temperature is quickly reduced to extreme low values as they can present thermal cracking from internal thermal stress accumulation. When in contact with other materials, or at the contact between distinct bituminous layers, the contact friction opposes the movement created by the contraction-dilation. Restrained thermal contraction leads to stress build-up and eventually to thermal cracking. The generated cracks in deeper layers can develop and be transmitted to the upper layers, such is the case represented in Figure 1.21, where the bituminous layer reposes on a cement-treated capping layer. This phenomenon is known as reflective cracking. Thermal cracking is helped by the embrittlement of the material at low temperatures.
- Different thermal contraction between distinct adjacent bituminous layers can also lead to a shear debonding of the layers.
- Water present or captured within the pores of the bituminous material freezes and thaws with temperature oscillations. These freeze-thaw cycles cause progressive degradation of the material affecting its performance.
- Water can also cause the deterioration of the cohesive and adhesive properties of the bituminous mastic through a complex combination of physical and chemical processes (c.f. section 1.4). The direct exposition to UV radiation and oxygen can accelerate chemical modifications of the material affecting its properties.

In Figure 1.21, the schema represents a road pavement structure where a wearing course overlays the base course materials. In the case of a ballasted track, if the ballast completely covers the bituminous layer, it would protect the bituminous mixture from UV exposition but not from moisture infiltration. According to the studies and experiences reviewed in this section, the bituminous layer seems to be well protected from extreme temperature variations in a sub-

ballast position. Nevertheless, characterising temperature and moisture susceptibility of bituminous materials is crucial for a good and rational bituminous track design.

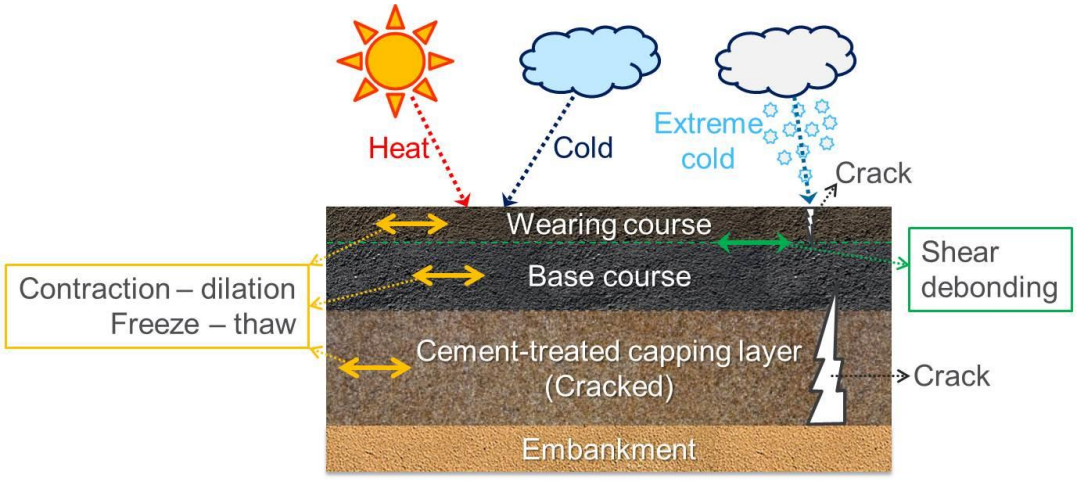

Figure 1.21. Schematic representation of thermal loads and corresponding pavement response (adapted from Di Benedetto, 1998)

1.3. Thermo-mechanical properties of bituminous mixtures

Under the effect of traffic and climate conditions, pavement structures are subjected to several phenomena. Bituminous materials have a complex nature and behave according to the applied type of solicitation. In particular, mechanical loads and temperature effects are treated in this section. In the context of this thesis, two aspects of the thermomechanical behaviour of bituminous mixtures are developed: the linear viscoelasticity and the resistance to fatigue properties.

1.3.1. Behaviour domains of bituminous mixtures

Bituminous mixtures can be considered as composite materials, therefore their properties depend on the properties of the components and on the interaction between them. From a macroscopic approach, bitumen can be seen as a continuous, homogeneous isotropic material. Under cyclic loading, its behaviour is influenced by mainly three factors:

- Temperature (T)
- Strain amplitude (ε)
- Number of loading cycles (N)

Bitumen's behaviour is complex and depends on the combination of these factors. Figure 1.22 presents the different mechanical behaviours that bitumen can present with respect to temperature and strain amplitude values (Di Benedetto, Delaporte, & Sauzéat, 2007b; Olard, Di Benedetto, Dony, & Vaniscote, 2005). The temperature T_g corresponds to the glass transition temperature defining the temperature limit between the brittle and ductile states. Figure 1.23 presents the behaviour domains of bitumen, at a given temperature, with respect to the number of loading cycles and to the strain amplitude.

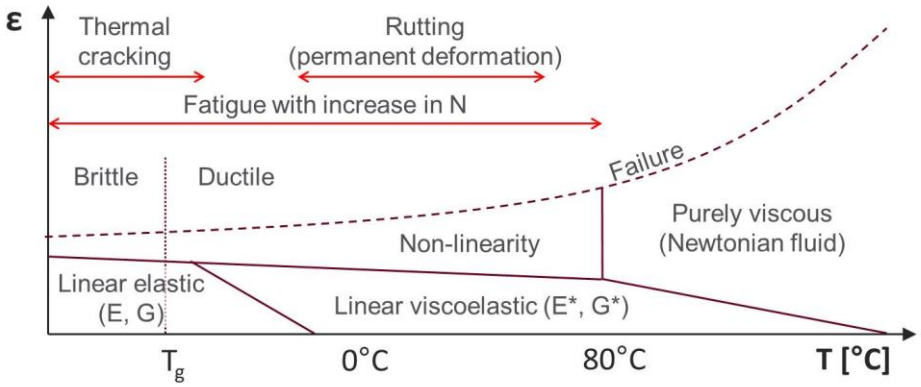

Figure 1.22. Different mechanical behaviours of bitumen with respect to the temperature and strain amplitude (adapted from (Olard et al., 2005))

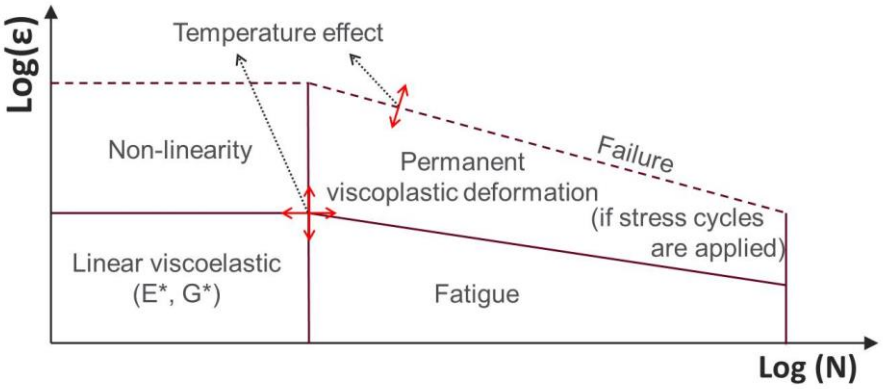

Figure 1.23. Different mechanical behaviours of bitumen with respect to the number of loading cycles and strain amplitude (adapted from (Mangiafico, 2014))

Bitumen presents linear viscoelastic (LVE) behaviour for small strain amplitudes ("small strain" domain), average service temperatures and few loading cycles (of the order of 100). The LVE domain is characterised by the complex modulus E* or G* (c.f. section 1.3.2). However, at very low temperatures, bitumen can be considered as an elastic material, neglecting the viscous component of its response to mechanical solicitations. This is the domain where thermal cracking occurs.

As the number of loading cycles within the "small strain" domain increases, fatigue mechanisms are triggered which can lead to failure (N in the order of 1 000). Non-linearity is observed for large strain amplitudes being 1% the approximate limit between large and small strain amplitudes for bitumen (Airey, Rahimzadeh, & Collop, 2003). Accumulation of permanent deformation of the material is created when the cyclic loading is not centred on a zero stress value. This is the case of traffic loads on a pavement structure as they create repetitive compressive stresses, which leads to a permanent deformation distress called rutting.

At very high temperatures, bitumen softens and presents the behaviour of a Newtonian fluid, with a nil elastic component.

Bitumen is responsible for a great part of the properties of bituminous mixtures. In Figure 1.24, the different behaviour domains of bituminous mixtures reflect those of bitumen. The threshold values for strain amplitude and for number of loading cycles that delimit each behaviour domain are shown as an order of magnitude. The transition between domains is not abrupt but rather progressive. The impact of the granular skeleton is evident in the strain limit between the LVE behaviour and the domain of non-linearity.

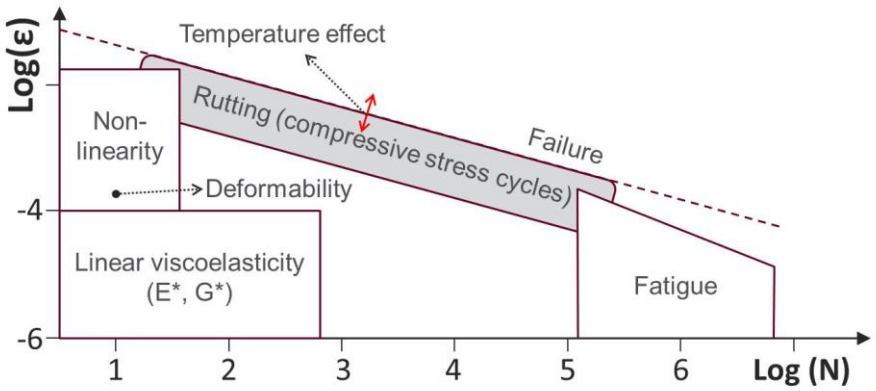

Figure 1.24. Different mechanical behaviours of bituminous mixtures with respect to the number of loading cycles and strain amplitude (adapted from (Di Benedetto et al., 2013))

Taking into account the solicitations to which bituminous mixtures are subjected during their service life in road pavements, 4 thermomechanical properties have to be characterised in order to assure an optimal pavement design (Di Benedetto & Corté, 2004). It also applies for railway platforms. These are:

- Stiffness dependence on temperature and loading characteristics.
- Fatigue degradation for the considered loading mode.
- Permanent deformation resistance for the service conditions.
- Crack propagation especially at low temperatures for which the material is prone to thermal cracking.

The most common approach to study bituminous materials, is to consider them as homogeneous, isotropic, viscoelastic, linear and thermo-susceptible (Di Benedetto & De la Roche, 1998).

Bituminous mixtures are considered homogeneous from a macroscopic approach in spite of their composite nature. This hypothesis is valid in the scale of pavement structures as the component sizes are very small compared to the pavement structure dimensions. In laboratory tests, however, a ratio of 10 between the nominal maximum value of the mixture and the specimen size is usually recommended.

Isotropy refers to the uniformity of properties in spite of the analysed direction. The hypothesis of isotropy for bituminous mixtures can be debated as the compaction processes provide certain anisotropy expressed in the density gradient with the depth of the bituminous layer and in the privileged grain orientation along the compacting direction. Indeed, modulus values from samples cored in three different directions were found to differ from each other (Doubbaneh,

1995). To minimize the effects of anisotropy, specimens for laboratory tests are cored from the middle of the layers or slabs and in the compaction direction (Baaj, 2002).

Under traffic loading, bituminous mixtures usually present viscoelastic behaviour. Further explained in section 1.3.2, this means that the material has a predominant viscous behaviour for slowly applied loads, and a predominant elastic behaviour for rapidly applied loads. For in-between loading rates, the material's reaction is a mixture of both behaviours. As seen in Figure 1.24, for small strain amplitudes, this transition follows a linear tendency. Pavement design methods aim to keep the strain levels at the bituminous layers as low as possible, reason why the behaviour of bituminous mixture is considered linear. Laboratory tests reproduce these small strains to characterize the LVE behaviour. The LVE behaviour hypothesis allows describing the response of the bituminous mixtures in the time domain. It is used to assess stiffness values or energy dissipation properties at specific strain or stress signals from the passing of a vehicle over the structure (Baaj, 2002).

1.3.2. LVE behaviour of bituminous mixtures

Viscoelasticity is a time-dependent behaviour presented by the materials with elastic and viscous responses to an applied strain. As shown in (Salençon, 2009) the typical response of a viscoelastic material subjected to constant strain is presented in Figure 1.25. When an instantaneous strain is applied at t_0, the viscoelastic material presents an also instantaneous stress response, which is typical of elastic materials. However, if the strain level is maintained constant until t_1, the stress level in the material progressively decreases due to its viscous properties. This is called stress relaxation. Moreover, if at t_1 the strain level is abruptly brought back to zero, the elastic stress developed in the material is higher than the residual stress level, which results in a total stress after discharge with an opposite sign with respect to that before unloading. After t_1, the strain level is maintained constant at zero and thus the stress progressively decreases until a complete stress recovery at an infinite time (i.e. $\sigma_\infty \rightarrow 0$ at $t \rightarrow \infty$). This principle is valid for materials whose properties do not change with time while undisturbed (i.e. $\varepsilon=0$). This kind of materials is referred to as non-ageing materials.

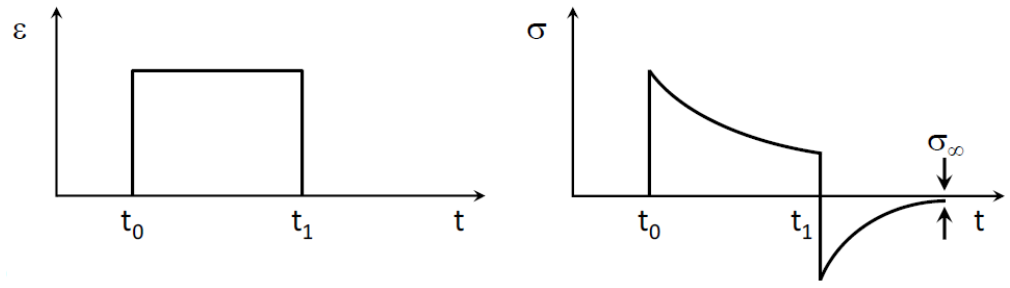

(a) (b)

Figure 1.25. Typical stress response (b) to a maintained constant strain (a) of a viscoelastic material (Mangiafico, 2014)

A linear viscoelastic material has to verify the Boltzmann superposition principle. According to this principle, the total stress response to various deformations is the addition of the stress responses to each discrete deformation. Likewise, the total strain responses to various stresses

are additive (Salençon, 2009). In a simple way, this means that the strain is directly proportional to the stress (Lakes, 2009). Table 1-5 summarizes the Boltzmann superposition principle.

Table 1-5. Boltzmann superposition principle summarized

Action		Response
$\varepsilon_1(t)$	→	$\sigma_1(t)$
$\varepsilon_2(t)$	→	$\sigma_2(t)$
$a\varepsilon_1(t) + b\varepsilon_2(t)$	→	$a\sigma_1(t) + b\sigma_2(t)$

1.3.2.1. Stress control loading – The creep function

Creep is defined as the time-dependent deformation of a material subjected to a constant stress. During a creep test, a constant instantaneous stress σ_0 is applied to the material at t_0 (c.f. Figure 1.26). The stress function depends on the Heaviside function H(t) as seen in equation [1-2]. The stain (ε) response of the material is given in equation [1-3].

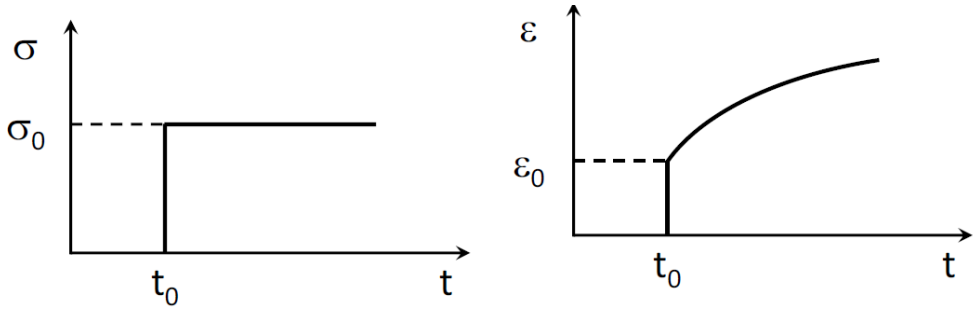

(a) (b)

Figure 1.26. Creep test for a LVE material: imposed stress (a) and strain response (b) (Mangiafico, 2014)

$$\sigma(t) = \sigma_0 H(t - t_0)$$

$$\text{where } \begin{cases} H(t) = 0 & t < 0 \\ H(t) = 1 & t \geq 0 \end{cases} \qquad [1\text{-}2]$$

$$\text{so that } \begin{cases} H(t - t_0) = 0 & t < t_0 \\ H(t - t_0) = 1 & t \geq t_0 \end{cases}$$

$$\varepsilon(t) = \sigma_0 J(t_0, t) = \sigma_0 J(t - t_0)$$

where $J(t_0, t)$ is the creep function at any instant t for the applied stress at t_0. For a non-ageing material the creep function becomes dependant of only one variable as $J(t_0,t)=J(t-t_0)$. [1-3]

When the applied stress is not constant but variable (dσ(t)), the variation of the strain dε(t) at an instant τ is noted as shown in equation [1-4]. For LVE materials the Boltzmann principle implies

that the total strain response is equal to the sum of the individual responses to discrete stress variations, as in equation [1-5].

$$d\varepsilon(t) = d\sigma(\tau)J(t-\tau) \quad [1\text{-}4]$$

$$\varepsilon(t) = \int_{t_0}^{t} J(t-\tau)\, d\sigma(\tau) \quad [1\text{-}5]$$

Assuming $d\sigma(t)$ differentiable, the strain response can be written as shown in equation [1-6] after integrating equation [1-5] by parts.

$$\varepsilon(t) = \sigma(t)J(0) + \int_{t_0}^{t} \sigma(t)\frac{\partial J}{\partial t}(t-\tau)d\tau \quad [1\text{-}6]$$

The first term of equation [1-6] represents the instantaneous response of the material and the second term represents the memory of the stress history which expresses the time-dependent behaviour. For a solid material the creep function tends to a limit value for $t \to \infty$, for a liquid it can increase infinitely.

1.3.2.2. Strain control loading – The relaxation function

Inversely from the creep function, the relaxation function is the time-dependent stress response to a constant strain. During a relaxation test, a constant instantaneous strain ε_0 is applied to the material at t_0 (c.f. Figure 1.27). Likewise equations [1-2] and [1-3], strain and stress functions are shown in equations [1-7] and [1-8].

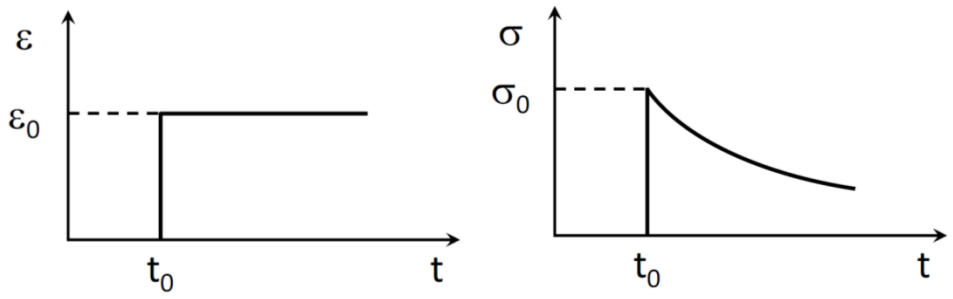

(a) (b)

Figure 1.27. Relaxation test for a LVE material: imposed strain (a) and stress response (b) (Mangiafico, 2014)

$$\varepsilon(t) = \varepsilon_0 H(t-t_0) \quad [1\text{-}7]$$

$$\sigma(t) = \varepsilon_0 R(t-t_0) \quad [1\text{-}8]$$

where $R(t-t_0)$ is the relaxation function at any instant t for the applied strain at t_0 for a non-ageing material

In the case of a non-constant strain history, a similar approach as that taken for the creep function can be applied for the solution of the relaxation function. The stress at any instant t for a given strain history is given in equation [1-9].

$$\sigma(t) = \varepsilon(t)R(0) + \int_{t_0}^{t} \varepsilon(t)\frac{\partial R}{\partial t}(t-\tau)d\tau \qquad [1\text{-}9]$$

Once again, the first term is the instantaneous response to a given strain and the second term takes into account the strain history.

1.3.2.3. Calculations – The Laplace-Carson transform

The strain and stress functions for a LVE material (equations [1-6] and [1-9]) can be transformed using the Laplace-Carson transform to make them easier to use. This transform turns integral equations into algebraic ones, simplifying calculations (Corté & Di Benedetto, 2004). The Laplace-Carson transform, denoted $\tilde{f}$, of a generic time-dependent function f(t) is defined in equation [1-10].

$$\tilde{f}(p) = p\int_0^{\infty} f(t)e^{-pt}\,dt \qquad [1\text{-}10]$$

where p is a complex variable corresponding to time in the transform domain

The transformed strain and stress functions are then similar to the equation of elasticity:

$$\tilde{\varepsilon}(p) = \tilde{J}(p)\tilde{\sigma}(p) \qquad [1\text{-}11]$$

$$\tilde{\sigma}(p) = \tilde{R}(p)\tilde{\varepsilon}(p) \qquad [1\text{-}12]$$

1.3.2.4. Behaviour under cyclic loading – Complex modulus and Poisson's ratio

Equation [1-13] expresses the function of a sinusoidal loading under strain control of amplitude ε_{01}. Given the viscous properties of bituminous mixtures, there exists a phase lag (φ) between the imposed strain and the stress response as shown on equation [1-14]. The stress response is also sinusoidal and of amplitude σ_{01}. Both strain and stress functions have the same pulsation $\omega=2\pi f$, with f the sinus frequency. The subscript "1" means the direction of the loading and the subscript "2" means the direction perpendicular to the loading. In a 3-dimensional case, the directions "2" and "3" are both perpendicular to the loading.

$$\varepsilon_1(t) = \varepsilon_{01}\sin(\omega t) + \varepsilon_{average1} \qquad [1\text{-}13]$$

$$\sigma_1(t) = \sigma_{01}\sin(\omega t + \varphi) + \sigma_{average1}(t) \qquad [1\text{-}14]$$

Equations [1-13] and [1-14] refer to the general case where the central value of the strain signal ($\varepsilon_{average1}$) is not equal to zero. Under the hypothesis of LVE behaviour, the application of the Boltzmann principle allows dissociating the two components of the strain and stress signals as

schematized in Figure 1.28 and Figure 1.29. The central value of the stress signal ($\sigma_{average1}$) is time dependant as it constitutes the relaxation of the stress induced by ($\varepsilon_{average1}$).

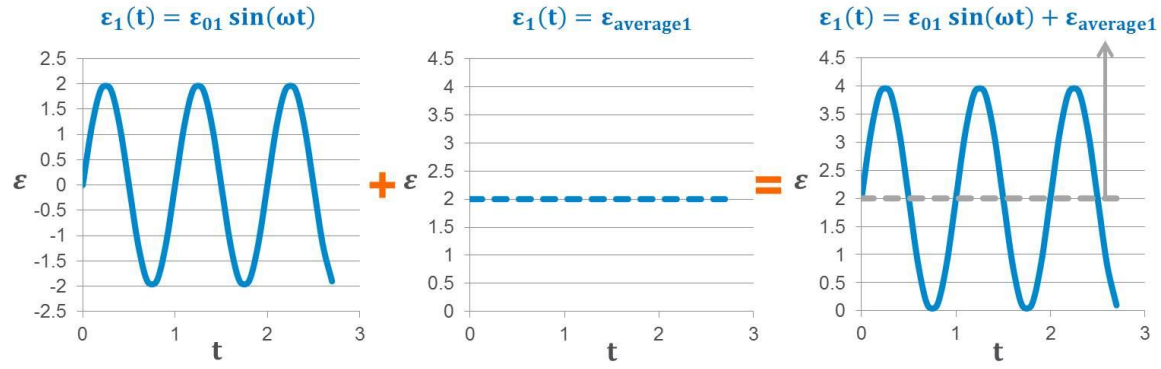

Figure 1.28. Boltzmann principle applied to the strain signal of a strain controlled loading

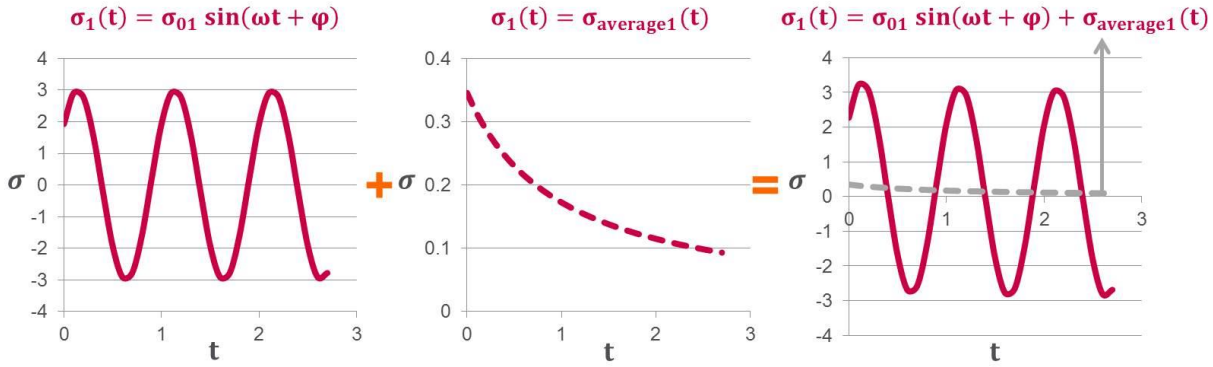

Figure 1.29. Boltzmann principle applied to the stress signal of a strain controlled loading

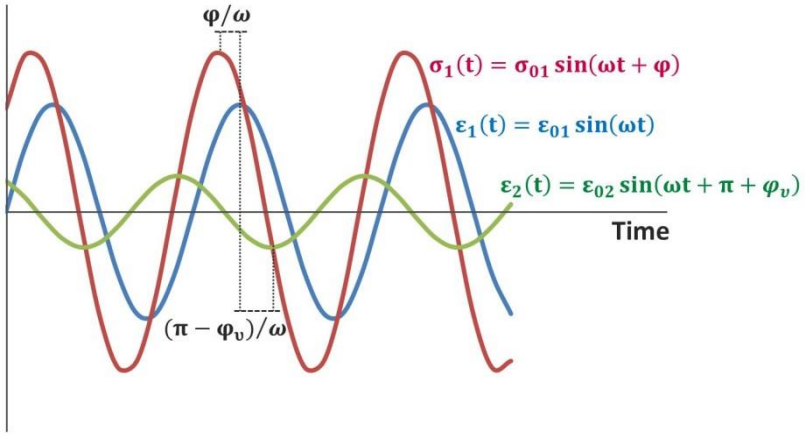

Figure 1.30. Schematic representation of the measurements from a sinusoidal loading on a LVE material

In order to calculate the complex modulus (or the complex Poisson's ratio) only the sinusoidal component of the strain signal is needed. The term $\varepsilon_{average1}$ is then neglected for these calculations. As for the $\sigma_{average1}$ term, its variation during a loading cycle is very small compared to the stress signal amplitude. Its influence on the complex modulus (or complex Poisson's ratio)

can also be neglected. Figure 1.30 shows a scheme of the strain and stress signals used for the calculation of the complex modulus and complex Poisson's ratio.

By using complex notations, a complex number j defined by j^2=-1 can be introduced and equations [1-13] and [1-14] can be rewritten as:

$$\varepsilon_1^*(t) = \varepsilon_{01} e^{j\omega t} \quad [1\text{-}15]$$

$$\sigma_1^*(t) = \sigma_{01} e^{j(\omega t+\varphi)} \quad [1\text{-}16]$$

Equation [1-12] can then be written as:

$$\sigma_1^*(t) = \widetilde{R}(j\omega) \cdot \varepsilon_1^*(t) \quad [1\text{-}17]$$

The Carson transform of the relaxation function ($\widetilde{R}$) at a point "jω" is classically known as the complex modulus (E*) of the LVE materials, as seen in equation [1-18].

$$E^* = \widetilde{R}(j\omega) = \frac{\sigma_{01}}{\varepsilon_{01}} e^{j\varphi_E} = |E^*| e^{j\varphi_E} \quad [1\text{-}18]$$

Since E* is complex, it can be also expressed in terms of its real and imaginary parts, E_1 and E_2 respectively:

$$E^* = E_1 + jE_2 = |E^*| \cos\varphi_E + j|E^*| \sin\varphi_E \quad [1\text{-}19]$$

E_1 is called the "storage modulus" and it represents the recoverable part of the energy stored by the material during loading. It is the elastic component of the LVE behaviour. E_2 is called the "loss modulus" and represents the energy lost due to internal friction. It is the irreversible viscous component of the LVE behaviour.

The phase angle φ characterises then the LVE behaviour as much as the norm of E*. When φ=0, the material presents a perfectly elastic behaviour, while when φ=90° the material is purely viscous. For intermediate values the material presents LVE behaviour.

Similarly to E*, when subjected to a sinusoidal shear strain γ(t) the shear stress τ(t) is also sinusoidal and shifted of a ϕ phase angle. The complex shear modulus G* is defined in equation [1-20]. According to the isotropy hypothesis for bituminous materials, E* and G* are related as in equation [1-21].

$$G^*(\omega) = \frac{\tau_0 e^{j(\omega t+\varphi_G)}}{\gamma_0 e^{j\omega t}} = |G^*| e^{j\varphi_G} = G_1 + jG_2 = |G^*| \cos\varphi_G + j|G^*| \sin\varphi_G \quad [1\text{-}20]$$

$$G^* = \frac{E^*}{2(1+\nu^*)} \quad [1\text{-}21]$$

For a cylindrical sample, the complex Poisson's ratio ν* is defined as the ratio between the axial and radial strains, as shown in equation [1-22]. The Poisson's ratio phase angle is denoted as φ_ν.

$$\nu^*(\omega) = |\nu^*| e^{j\varphi_\upsilon} = \upsilon_1 + j\upsilon_2 = |\upsilon^*| \cos\varphi_\upsilon + j|\upsilon^*| \sin\varphi_\upsilon \quad [1\text{-}22]$$

Poisson's ratio depends on the frequency and temperature of the bituminous material. Its phase angle has negative values close to zero, indicating that axial and radial strains are almost on the

same phase but with a slight delay with respect to axial strain. (Di Benedetto, Delaporte, & Sauzéat, 2007a). The evolution of the complex modulus and Poisson's ratio with frequency and temperature gives the complete LVE characterisation of the material (Corté & Di Benedetto, 2004).

Laboratory tests include thus various temperature and loading frequency conditions. Different graphical representations are used to show the variation of E* and ν* with frequency and temperature. The most commonly used plots for E* (likewise for ν* and G*) are:

- Isothermal curves: They are obtained by plotting the $|E^*|$ or φ_E values against the corresponding test frequency for each tested temperature. Each plotted curve corresponds then to a single temperature. Both axes are generally in logarithmic scale.
- Isochronal curves: They are complementary to the isothermal curves and represent the $|E^*|$ or φ_E values against the corresponding test temperature. Each plotted curve corresponds then to a single test frequency. The norm values axis is generally in logarithmic scale while the temperature one is not.
- Cole-Cole plot: This plot represents the E_2 values against the E_1 values. It is then a complex plane. The axes are usually in linear scale so the variation of E_1 and E_2 is more evident when the material presents high stiffness and a more elastic behaviour at test conditions of low temperatures/high frequencies.
- Black diagram: This plot represents the phase angle values against the complex modulus norm values. Presented on a semi-logarithmic scale ($\log|E^*|$ vs φ_E), it highlights the behaviour of the bituminous mixtures at test conditions of low frequencies/high temperatures.

Examples of all these plots are presented in section 4, where the complex modulus test results are presented.

1.3.3. Energy dissipation

When subjected to loading and unloading cycles, linear viscoelastic materials dissipate some energy during each loading cycle. Therefore, stress-strain curves of the loading and unloading phases do not superpose (c.f. Figure 1.31). In the case of a linear elastic material, both curves superpose as all the stored energy during loading is returned during unloading and there is no dissipation.

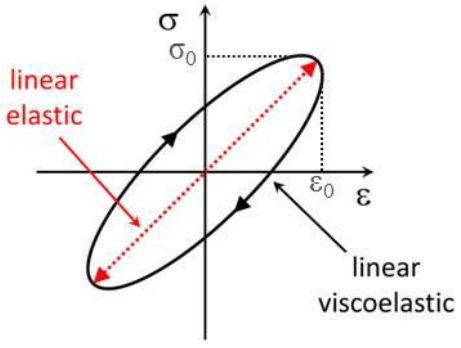

Figure 1.31. Hysteresis for sinusoidal loading of elastic and LVE materials (Mangiafico, 2014).

The energy dissipated per unit of volume during a loading cycle (W) corresponds to the area within the stress-strain curve. Equation [1-23] is the expression for W in the case of a LVE material subjected to sinusoidal loading.

$$W = \pi \sigma_0 \varepsilon_0 \sin(\varphi) \qquad [1\text{-}23]$$

1.3.4. Time-Temperature equivalence principle

Under the hypothesis of LVE behaviour, E* and G* are dependent on two independent variables: frequency (f) and temperature (T). The complex modulus test results presented as isotherm curves usually indicate that a same |E*| value can be attained at different combinations of frequency and temperature conditions. This is also valid for the Poisson's ratio and the phase angles. This means that there are couples of f and T for which $E^*(f_1,T_1)=E^*(f_2,T_2)$ is valid, with $(f_1,T_1)\neq(f_2,T_2)$. Moreover, various authors (Ferry, 1980) have observed that the tests results plotted in the Cole-Cole plot or in the Black space formed a continuous unique line, independently of the tested temperatures or frequencies. Materials that show this behaviour are referred to as "thermo-rheologically simple" (Corté & Di Benedetto, 2004).

For this kind of materials, the influence of temperature and frequency can be reduced to a single variable (c.f. equation [1-24]). The most commonly chosen one is the equivalent frequency (f_{eq}). For materials having this property, it is said that the "Time Temperature Superposition Principle" (TTSP) is respected.

$$E^*(f,T) = E^*\big(f\, h(T)\big) = E^*(g(f)\, T)$$

$$\text{then} \qquad [1\text{-}24]$$

$$f_1\, h(T_1) = f_2\, h(T_2) \;\text{ and }\; T_1\, g(f_1) = T_2\, g(f_2)$$

Using the f_{eq} reduced variable, the TTSP allows using the isotherm curves to build a unique |E*| curve that is characteristic of the material for an arbitrarily chosen reference temperature (T_{ref}). On a log|E*| against log(f_{eq}) plot, this single curve, called "master curve", is built by the translation of the isotherms along the horizontal log(f_{eq}) as to superpose all the points with the same ordinate (|E*|) values. This translation is operated by multiplying the tested frequency of each point by a dependent coefficient denoted a_T. This shift factor depends on the temperature of the isotherm to shift and on the reference temperature. Equation [1-25] shows the mathematical procedure to obtain f_{eq} through the shifting procedure. Figure 1.32 shows an example of |E*| master curve construction with its associated shift factor a_T.

$$f_{eq} = f_i \frac{f(T_i)}{f(T_{ref})} = f_i\, a_t\big(T_i, T_{ref}\big) \qquad [1\text{-}25]$$

This procedure allows accessing to the material's behaviour at a very large frequency domain. Since an increase in temperature is equivalent to a decrease in the loading frequency, the material's behaviour at quasi static loading conditions can be accessed in a much shorter time than what a low frequency test would take. In the same way, tests at very low temperatures allow describing the material's behaviour at very high frequencies which are physically impossible to apply with standard laboratory equipment.

For the present study, the Williams, Landel and Ferry (WLF) (Williams, Landel, & Ferry, 1955) equation was used to fit the a_T values. This is an empirical equation where two constants (C_1 and C_2) are determined for each material with respect to the chosen T_{ref} (c.f. equation [1-26]). The value of the shift factor for $T=T_{ref}$ is 1 as no shifting is needed. In order for the WLF equation to be used over a large range of temperatures, the fit must be performed on experimental data obtained at temperatures over and below the glass transition temperature.

$$\log(a_T) = \frac{-C_1(T - T_{ref})}{C_2 + T - T_{ref}} \qquad [1\text{-}26]$$

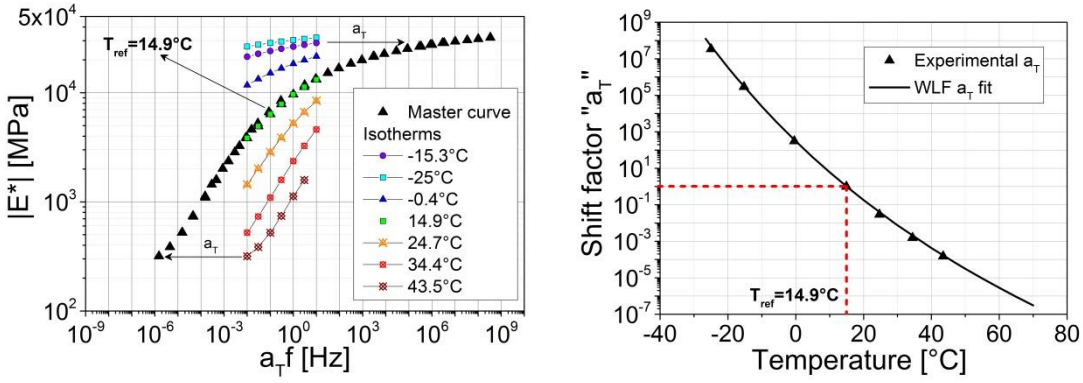

Figure 1.32. Master curve building from isotherm curves (a) and shift factor a_T obtained for a bituminous mixture (adapted from (Ramirez Cardona, Pouget, Di Benedetto, & Olard, 2015))

The same procedure is used to build phase angle and Poisson's ratio master curves. The a_T values are the same as the ones found for |E*|, validating the TTSP in the tri-dimensional case (Q. T. Nguyen, Di Benedetto, Sauzéat, & Tapsoba, 2013). Moreover, if a reference frequency is chosen instead of a reference temperature as single variable, isochronal master curves can be obtained.

Some bituminous materials, such as highly polymer-modified bitumen, are not thermo-rheologically simple and the TTSP is not validated for them. Complex modulus results obtained from these materials do not present a unique curve in the Cole-Cole and Black plots. However, if master curves can still be built, then the material is said to comply with the "Partial Temperature Superposition Principle" (PTTSP) (Di Benedetto, Olard, Sauzéat, & Delaporte, 2004; Olard & Di Benedetto, 2003; Olard et al., 2005).

1.3.5. The 2S2P1D model

Any assembly of springs and dashpots is considered as an analogical LVE model. The springs represent the elastic component of the LVE behaviour and the dashpots the Newtonian viscous one. Such models are theoretical and only provide a mathematical approximation of the real material behaviour (Gallegos & Martinez Boza, 2010). More information on the different rheological models used to describe the LVE behaviour is found in Appendix I.

The 2S2P1D rheological model is a generalization of the Huet-Sayegh model (Huet, 1963) and consists of 2 springs, 2 parabolic creep elements and 1 dashpot. It was developed in the Laboratory of Civil Engineering and Construction (LGCB) of the ENTPE/University of Lyon.

The 2S2P1D model has been found to be a suitable tool for the description of the linear viscoelastic behaviour of most bituminous materials over a wide range of frequencies and temperatures (Carret et al., 2015; Gudmarsson, Ryden, Di Benedetto, & Sauzéat, 2015; Mangiafico et al., 2014; Mounier, Di Benedetto, & Sauzéat, 2012; Pham et al., 2015; Ramirez Cardona, Di Benedetto, Sauzeat, Calon, & Saussine, 2016; Ramirez Cardona et al., 2015; Yusoff et al., 2013; Zhao, Ni, & Zeng, 2014).

(a)

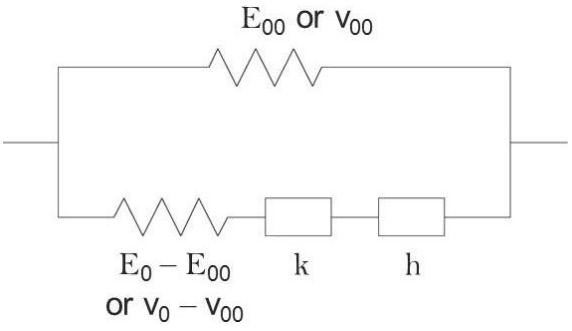

(b)

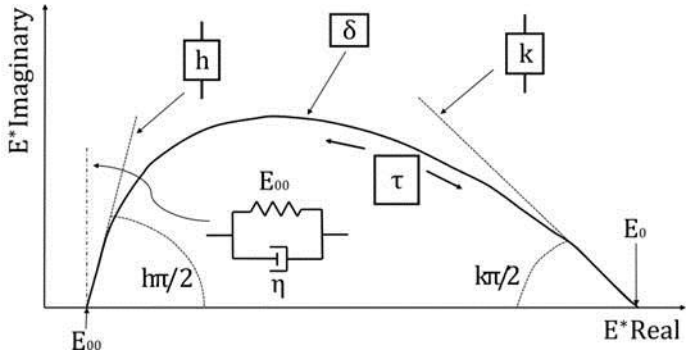

Figure 1.33. Analogical representation of the 2S2P1D Model (a) and 2S2P1D model parameters on the Cole-Cole plot of bituminous materials (b) (Mangiafico, 2014)

The model needs only seven parameters to describe the LVE of bituminous materials in the 2-dimensional case. These are:

- The static modulus E_{00} ($\omega \rightarrow 0$), which is associated with the behaviour at low frequencies and/or high temperatures.
- The glassy modulus E_0 ($\omega \rightarrow \infty$), which is associated with the behaviour high frequencies and/or low temperatures.
- The calibration constant δ.
- The constant τ, which depends on the temperature. It can be expressed as a function of the shift factor.
- The constants k and h, which are defined such that $0 < k < h < 1$.
- The constant β, which depends on the viscosity of the dashpot as shown in equation [1-27].

If the effect of temperature is to be taken into account, the WLF constants C_1 and C_2 are also needed. Finally, for a 3-dimensional case, the parameters ν_0 and ν_{00} have to be introduced to describe the Poisson's ratio. These are the static and glassy Poisson's ratios, respectively (Di Benedetto et al., 2007a) (c.f. equation [1-28]).

$$E^*(\omega) = E_{00} + \frac{E_0 - E_{00}}{1 + \delta(j\omega\tau)^{-k} + (j\omega\tau)^{-h} + (j\omega\beta\tau)^{-1}} \quad \text{with } \eta = (E_0 - E_{00})\beta\tau \qquad [1\text{-}27]$$

$$\upsilon^*(\omega) = \upsilon_{00} + (\upsilon_0 - \upsilon_{00})\frac{E^*(\omega) - E_{00}}{E_0 - E_{00}} \qquad [1\text{-}28]$$

A total of 11 parameters are then needed to fully characterise the LVE behaviour of bituminous materials over the whole temperature and frequency domain. Figure **1.33**(b) presents the influence of the h, k, τ, δ, E_{00} and E_0 parameters on the shape of the Cole-Cole plot for a bituminous material.

1.3.6. Fatigue of bituminous mixtures

The passing of vehicles' axles generates low amplitude strains in the bituminous layers. These repeated loadings are of short duration and do not cause the immediate rupture of the bituminous material. Nevertheless, the material's properties are degraded by the repeated loadings which entail the appearance of micro-cracks. After a certain number of applied loadings, these micro-cracks evolve into macro-cracks that cause the material's failure. This progressive weakening of the material properties leading to failure is known as fatigue damaging (Di Benedetto & Corté, 2004). A considerable research effort is found in the literature concerning the characterisation of the fatigue behaviour of bituminous materials (Baaj, 2002; De la Roche, 1996; Di Benedetto, de La Roche, Baaj, Pronk, & Lundström, 2004; Kim, Lee, & Little, 1997; Li, Lee, Kim, 2011; Piau, 1989, among others).

In a pavement structure, due to the multilayer approach, the stresses and strains generated at the bottom of the bituminous layers are held responsible for the occurrence of fatigue. The French design method for bituminous layers is based on the comparison of these strains with the material's fatigue resistance estimated with laboratory tests.

The classic test to assess the fatigue resistance properties of bituminous mixtures consists in subjecting a specimen to repeated loadings, of a certain level that does not cause its immediate rupture, and to note the number of loading cycles withstood by the specimen before failure. This number of cycles is usually referred to as "fatigue life" and it is associated to the strain (or stress) level of the test. By testing the same material at different strain (or stress) levels, different values of fatigue life are obtained. The most common representation of these values is the Wöhler curve, which plots strain (or stress) amplitude (ε_0) against the number of loading cycles before failure (N_f) (c.f. Figure 1.34).

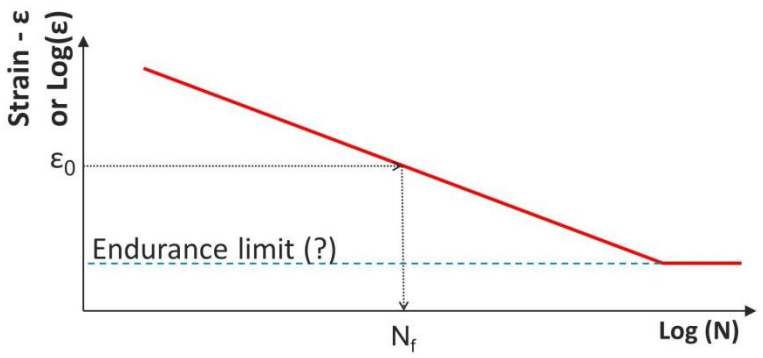

Figure 1.34. Wöhler curve scheme (for a strain controlled test)

The Wöhler curve is described by the following linear relation in the case of a linear scale of the strain (or stress) axis:

$$\log\varepsilon = \alpha - \beta \log N \qquad [1\text{-}29]$$

Despite the fact that this representation was first proposed for metallic materials (Wöhler, 1870), it remains valid for fatigue tests performed under strain control mode on bituminous materials. The slope of the Wöhler curve is negative as it is observed that the fatigue life decreases with the increase of the strain amplitude.

Some authors affirm that some materials do not present fatigue damage if they are subjected to strain levels lower than a certain threshold value called “endurance limit” (Carpenter, Ghuzlan, & Shen, 2003; Prowell et al., 2010, amongst others) (c.f. Figure 1.34). For such low stain levels, the material is said to have infinite fatigue life. However, there is no consensus on the existence of this endurance limit.

When loadings of different amplitude (S_i) are applied to the same material, the combined effect on fatigue life can be considered as the accumulation of the contributions of each discrete loading. This can be estimated with the so-called Palmgren-Miner hypothesis (Miner, 1945) (equation [1-30]). To apply this hypothesis, it is required to know the fatigue life (N_i) associated to each loading amplitude (S_i) and the number of cycles endured by the material at each amplitude (n_i). Although it has been proven that this hypothesis is not accurate, it is widely used as a first approach due to its simplicity. The main downside is that the loading history is not taken into account whereas it has a strong influence on the material’s behaviour (Mangiafico, 2014).

$$C = \sum_{i=1}^{k} \frac{n_i}{N_i} \qquad [1\text{-}30]$$

Fatigue tests can be carried out in the laboratory or in-situ. In-situ tests aim to describe the behaviour of the material under service conditions, therefore they are carried out in instrumented pavement structures or in full-scale trial tracks loaded by accelerated traffic simulation devices (De la Roche et al., 1994). Laboratory tests aim to investigate the fundamental fatigue resistance properties of the materials. Different laboratory tests are proposed and each one uses a different loading mode. The most common ones are bending,

tension-compression and shear tests. The fatigue life values are highly affected by the test loading mode (Di Benedetto, de La Roche, et al., 2004), therefore the simple comparison of results obtained from different tests can be misleading and is not recommended. In-situ tests present real stress and strain signals, while laboratory tests use simple cyclic loadings describing sinusoidal, square or haversine signals, being the sinusoidal wave the most commonly used. The influence of the wave form was studied by (Homsi, 2011; Raithby & Sterling, 1972; Said, 1988).

In all cases, fatigue phenomena is very complex and laboratory fatigue tests present high variability causing significant scatter in Wöhler curves for bituminous mixtures. This fatigue life value uncertainty is taken into account in the pavement design method by means of correcting coefficients. For high scatter values, these coefficients increase the layer thickness in order to cope with the eventual overestimation of the mixture fatigue resistance.

The European Standard (EN 12697-24, 2012) promotes the use of bending tests to assess the fatigue resistance properties of bituminous mixtures. Bending tests aim to simulate the repeated bending of the bituminous layers under traffic loading. These tests are considered as non-homogeneous tests since the stress and strain levels are not identical in every point of the sample, the idea of a bending loading mode being to concentrate the strain and stresses in one point of the sample. For a two-points bending test under deformation control mode, a prismatic specimen with very accurate dimensions is required in order to control the location of the point with maximum strain. The sample is then instrumented at that specific point (c.f. Figure 1.35). One advantage of this method is that the crack position is imposed and, therefore, the crack developing procedure is almost always observed in the measurements. However, the non-homogeneity of the bending tests is cause of a very high scatter in the fatigue test results, which leads to a thickening of the bituminous layers for pavement design. In order to reduce the uncertainty of the fatigue life value, a great number of tests at the same deformation level need to be done. Because of this, the fatigue characterisation is very long and costly. Another drawback of bending tests is the necessity of samples with perfect geometry which are also very expensive and difficult to manufacture.

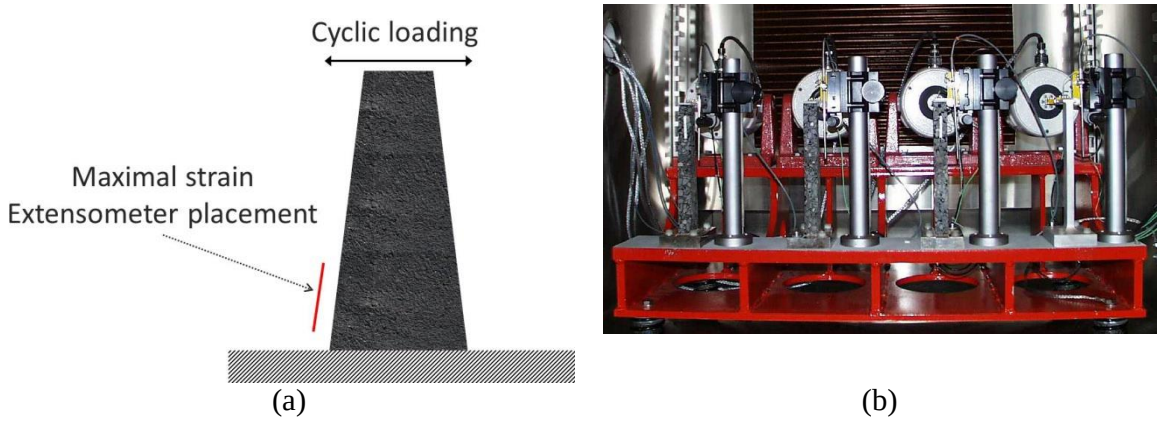

Figure 1.35. Scheme (a) and laboratory equipment for the two-points bending fatigue test

The tension-compression test on cylindrical samples is an alternative to the bending tests. Due to the axial tension-compression loading, stress and strains are the same at every point of the sample, with the exception of the samples top and bottom edges where it is attached to the test equipment. This test can be done either in strain control mode (setting a constant strain level

and measuring the stress evolution during the test) or in stress control mode (setting constant stress level and measuring the strain evolution during the test). For stress-controlled tests, the strain increases during the test. For strain-controlled tests, the stress decreases during the test. Figure 1.36 shows the schemes of the stress and strain evolution for each of this test control modes. Stress-controlled tests with cyclic signals not centred on zero must not be used to characterise fatigue resistance as the constant stress leads to accumulation of permanent deformation of the bituminous material. Stress-controlled tests present also a quick macro-crack development due to the concentration of stress at the tip of the crack. The rupture of the specimen is then abrupt once the first macro-cracks appear during this kind of tests. On the contrary, the evolution of the macro-crack during strain-controlled tests is slow.

The results of the tension-compression fatigue test present less dispersion and also allow accessing to the intrinsic fatigue behaviour of the material (Olard, 2003). Fewer tests at the same strain level are then required, thus reducing the time and cost of a fatigue characterisation study.

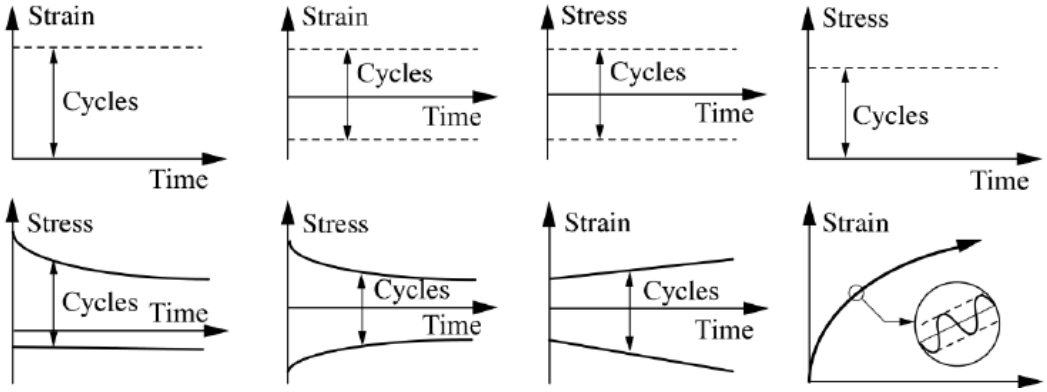

Figure 1.36. Strain and stress evolution during fatigue tests performed in strain control mode (a) and stress control mode (b) (as adapted from (Di Benedetto & Corté, 2004) in (Mangiafico, 2014))

During a fatigue test, a stiffness loss is observed as the number of applied loading cycles (N) increase. This loss is characterized by three distinguishable phases in a |E*| against N plot (c.f. Figure 1.37). Likewise, the phase angle evolution also presents three distinguishable phases (Baaj, 2003; Di Benedetto, Ashayer Soltani, & Chaverot, 1996; Di Benedetto, de La Roche, et al., 2004).

- Phase 1: During the first loading cycles, the material adapts to the recently applied cyclic loading. An important stiffness loss is observed during this phase mainly due to the action of biasing phenomena such as heating, thixotropy and non-linearity and not to fatigue damaging. According to recent research (Di Benedetto, de La Roche, et al., 2004; Mangiafico, 2014) this modulus loss can be completely recovered if the test is stopped. As for phase angle, it increases rapidly during this phase.
- Phase 2: After the stabilisation of the sample, the modulus value decreases steadily and almost linearly as the number of applied loading cycles increase. As for phase angle, it increases in an also quasi-linear trend. Even if biasing phenomena is still present, this phase is usually referred to as the real fatigue damaging phase where micro-cracks

develop inside the sample. For a homogeneous test, micro-cracks develop homogeneously inside the material.

- Phase 3: This phase is characterised by the propagation of macro-cracks generated from the accumulation of micro-cracks. During this phase, the test can no longer be interpreted according to continuum mechanics assumptions. The LVE properties of the sample can no longer be accessed as for the phases 1 and 2. The stress concentration at the tips of the cracks controls the crack propagation speed. The test can no longer be considered as homogeneous due to the presence of macro-cracks, therefore |E*| values in this phase cannot be considered as an intrinsic property of the material. In a |E*| against N plot, a rapid decrease of |E*| is observed before attaining the physical rupture at the end of the test. As for phase angle, it decreases abruptly.

Figure 1.37 presents the typical form of a fatigue curve. The modulus norm values are normalised by the initial modulus value, which is taken as the intercept with the ordinates axis of the linear regression on the cycles 60 to 110 on a |E*| against N plot. This value is used in order to minimize the effect of non-linearity in the normalisation procedure.

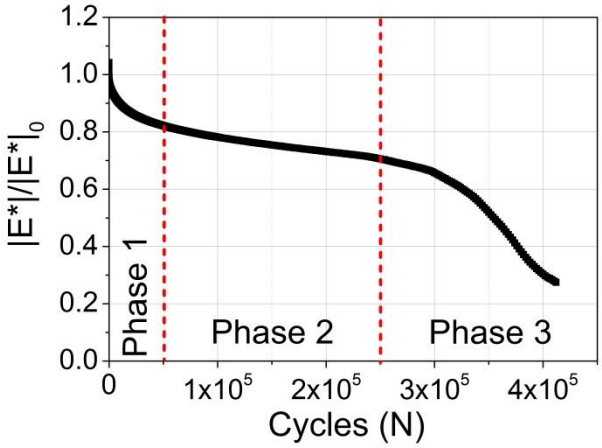

Figure 1.37. |E*| evolution of a bituminous mixture during a tension-compression fatigue test with the three phases of the test represented

1.3.7. Fatigue failure criteria based on global measures

Physical failure of the specimen is not the only failure criterion for bituminous mixtures. The most commonly used one is the reduction of 50% of the initial |E*| value. Several failure criteria can be proposed and it is important to note that, depending on the used failure criterion, the specimen's fatigue life can vary a lot. For example, it is possible for the 50% reduction of the modulus norm to be observed somewhere in the 2nd phase, before attaining the macro-cracks development. It is also possible, and rather common for tension-compression tests, to attain the physical rupture of the specimen without reaching the 3rd phase of the fatigue test. Several failure criteria are proposed in this thesis to analyse the fatigue test results. Those explained in this section are based on the global behaviour of the sample during the tests.

1.3.7.1. Classical approach – $N_{f\text{-}50\%}$

This is the simplest criterion to establish the fatigue life from a fatigue test. It is prescribed by the European Standard (EN 12697-24, 2012) for bituminous mixtures. It consists simply in determining the number of cycles for which the sample presents a reduction of 50% of its initial complex modulus norm value. This criterion is criticized due to the fact that the |E*| loss percentage is arbitrarily chosen and does not take into account the effect of biasing phenomena occurring during fatigue tests (Di Benedetto et al., 1996; Di Benedetto, de La Roche, et al., 2004; Kim et al., 1997).

1.3.7.2. Second inflection point (SIP) or phase angle peak criterion – $N_{f\text{-}\varphi Max}$

This criterion was proposed by (Kim, Little, & Lytton, 2003) who identified two inflection points in the |E*| against N plot of a fatigue test. The first inflection point appears at the end of the initial modulus loss. The second inflection point (SIP) is located before the physical rupture of the sample and corresponds also to the peak of the phase angle (c.f. Figure 1.38). It is believed to be representative of a change of the mechanical behaviour of the material due to fatigue damage accumulation.

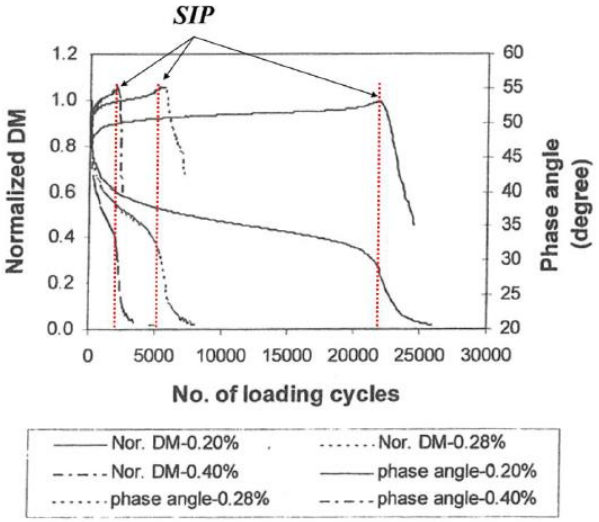

Figure 1.38. Example of identification of the SIP for three different fatigue tests at three different strain amplitudes (as adapted from (Kim, Little, & Lytton, 2003) in (Mangiafico, 2014))

1.3.7.3. Energetic approach – $N_{f\text{-}Wn}$ & $N_{f\text{-}r2Wn}$

This method is based on the evolution of the dissipated energy per loading cycle (c.f. section 1.3.3) over the duration of the test. It consists in identifying a representative trend change in the evolution of the Dissipated Energy Ratio (DER) (Hopman, Kunst, & Pronk, 1989) which is defined as:

$$DER = \frac{\sum_{i=1}^{N} W_i}{W_N} \qquad [1\text{-}31]$$

Where N is the considered cycle and W_N is the energy dissipated during the considered cycle

In a DER against N plot, the DER presents a quasi-linear evolution with the increase of N from the beginning of the test until a certain point when the tendency changes as shown in Figure 1.39. For strain-controlled tests, DER increases quickly after the tendency change until it develops a linear tendency with higher slope than the initial trend. The failure criterion is then defined by the intersection between the linear fitting of the first part of the test and the linear fitting of the final part of the test.

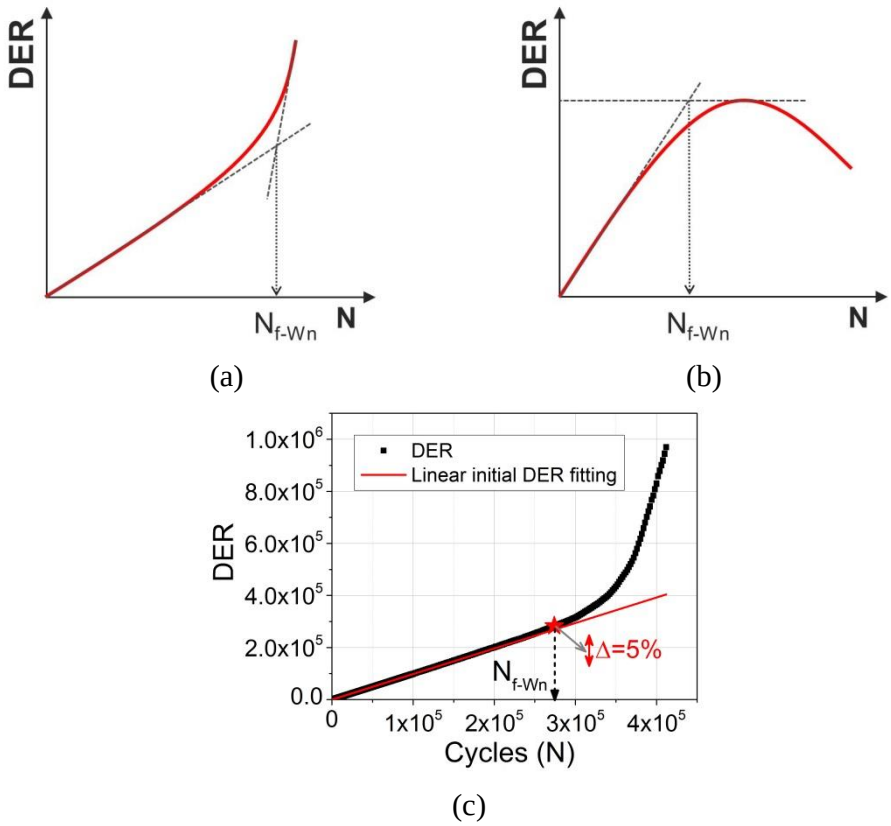

Figure 1.39. Scheme of fatigue life determination according to the energetic approach for a strain-controlled test (a) and a stress-controlled test (b), and example of the used criterion for this thesis (tests results from a fatigue test on a GB3 sample) (c)

For stress-controlled tests, DER reaches a maximum point after which it decreases. The failure criterion is then defined as the intersection between the linear fitting of the first part of the test and the horizontal line passing by the DER peak (c.f. Figure 1.39). Further developments of this criterion have led to the proposal of the N_f determination by a relative variation of the DER value at a cycle N with respect to the linear fitting of the first part of the test (Bocci, Cardone, Cerni, & Santagata, 2006; Soenen, de La Roche, & Redelius, 2003).

For this thesis two criteria are defined based on the DER evolution. The first one ($N_{f\text{-}Wn}$) is defined as the DER variation of 5% with respect to the expected value at the considered cycle N obtained from the DER linear fitting of the cycles 60 to 10 000 (c.f. Figure 1.39(c)). The second one ($N_{f\text{-}r2Wn}$) is defined as the variation of 1% of the coefficient of determination of the DER experimental points, which is equal (or very close) to 1 at the beginning of the test.

1.3.7.4. Change of concavity of the fatigue curve – $N_{f\text{-}concavity}$

This criterion is similar to the SIP criterion in identifying the inflexion point of the |E*| against N plot that marks the end of the second phase of the fatigue test. However, this criterion is based on a slope change of the linear |E*| trend during the second phase. The slope is calculated for representative intervals of loading cycles in the second phase. The length of the intervals depends on the length of the test's second phase and it's chosen as that who allows identifying the inflexion point of the fatigue curve. The slope of one interval is compared to that of the precedent interval. A remarkable trend change is considered when the relative difference (Δb_i) between the slope of one interval (b_i) and that of the precedent one (b_{i-1}) exceeds 20% (in absolute value). The first cycle of the considered interval is then marked as the end of the second phase of the fatigue test. Since the sample is no longer homogeneous in the third phase, the end of the second phase is also considered as the failure of the sample.

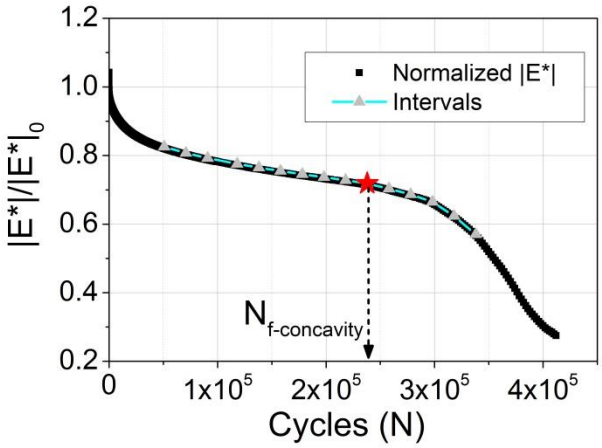

Figure 1.40. N_f determination using the failure criterion based on the concavity change of the |E*| against N curve (Normalized |E*| values)

1.3.8. Fatigue criteria based on local measures

Analysing the evolution of the measures from each extensometer during the fatigue tests can reveal changes in the local behaviour of some parts of the sample. These changes are related to the hypothesis that homogeneity is lost when macro-cracks are developed in the sample. This is equivalent to the passage from the second test phase to the third.

The tension-compression strain-controlled fatigue test on cylindrical samples requires the use of at least three extensometers disposed at 120° from each other to measure the strain in the sample. The considered strain value for the test control is the average value of the three strain amplitudes measured by the three extensometers. Since the test is homogeneous, the measurements from each extensometer are very similar in amplitude until the homogeneity is lost. The development of a macro-crack on one side of the sample causes the measurements from the nearest extensometer to derive and thus the strain field can no longer be considered as homogeneous. For this thesis, three threshold values are proposed to define the loss of homogeneity in the strain field.

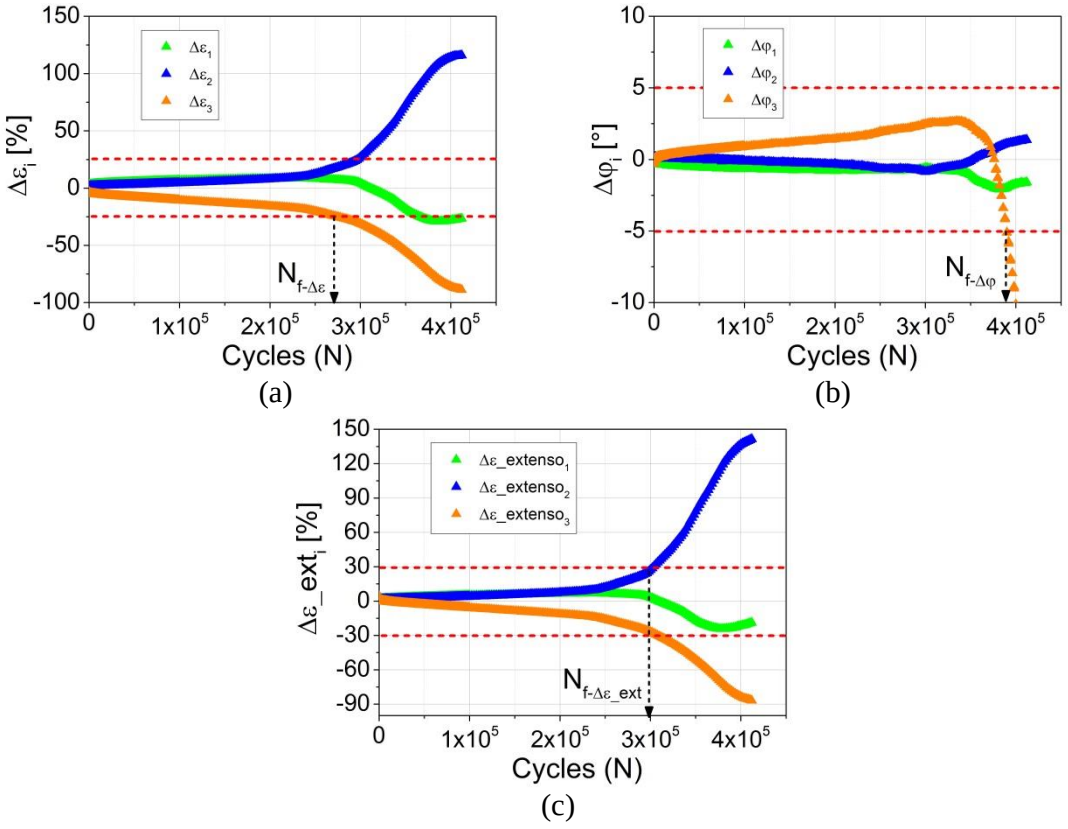

Figure 1.41. N_f determination using the failure criteria based on the loss of homogeneity in the strain field

The first considers the relative difference ($\Delta\varepsilon_i$) between the strain amplitude of one extensometer (ε_i) and the average amplitude from the three extensometers (ε_0) at the considered cycle (N). When one of the extensometers presents a $\Delta\varepsilon_i$ value exceeding 25% (in absolute value), the strain field is considered to be heterogeneous and the sample failure attained ($N_{f\text{-}\Delta\varepsilon}$). An example is shown in Figure 1.41(a).

$$\Delta\varepsilon_i = \frac{\varepsilon_i - \varepsilon_0}{\varepsilon_0} \qquad [1\text{-}32]$$

A similar approach is used for the definition of the second threshold value taking into account the evolution of the phase angle of the strain signal of each extensometer. When the difference ($\Delta\varphi_i$) between the measured phase angle of one extensometer (φ_i) and the phase angle of the average strain (φ) exceeds 5° (in absolute value), sample failure is attained ($N_{f\text{-}\Delta\varphi}$) (c.f. Figure 1.41(b)).

$$\Delta\varphi_i = \varphi_i - \varphi \qquad [1\text{-}33]$$

The third threshold value considers the relative difference ($\Delta\varepsilon\_ext_i$) between the strain amplitude of one extensometer (ε_i) and the initial value (ε_{i_0}) measured by the same extensometer taken as the value measured at the 60th cycle (N_{60}). When one of the extensometers presents a $\Delta\varepsilon\_ext_i$ value exceeding 30% (in absolute value) the sample is considered to have failed ($N_{f\text{-}\Delta\varepsilon\_ext}$). An example is shown in Figure 1.41(c).

$$\Delta\varepsilon\_ext_{\_i} = \frac{\varepsilon_i - \varepsilon_{i\_0}}{\varepsilon_{i\_0}} \quad [1\text{-}34]$$

1.3.9. Biasing effects non-linked to fatigue phenomena

During a fatigue test, different biasing phenomena affect behaviour of the material. Fatigue damage of the materials in the laboratory is accelerated compared to what happens under real traffic conditions. The continuous loading of laboratory tests does not consider the resting periods (where no load is applied) observed in real working conditions. In order to interpret fatigue tests results, it is necessary to isolate the transient reversible phenomena non-related to fatigue damage occurring during continuous loading (Di Benedetto et al., 1996; Di Benedetto, de La Roche, et al., 2004). The concept of biasing effects has been introduced to define these phenomena. These include non-linearity of the material's behaviour, self-heating and thixotropy (Delaporte, Van Rompu, Di Benedetto, Chaverot, & Gauthier, 2008; Di Benedetto, Nguyen, & Sauzéat, 2011; Q. T. Nguyen, Di Benedetto, & Sauzéat, 2012). Mangiafico (2014) observed that 90% of the total variations of |E*| and φ during fatigue tests are completely reversible and due to biasing phenomena.

1.3.9.1. Non-linearity

The threshold strain value below which the behaviour of the bituminous mixtures is considered as linear viscoelastic is usually set at 100 µm/m (Airey et al., 2003). However, because of the internal structure, the bituminous binder located within the inter-aggregate spaces can be subjected to local strain levels significantly higher than the overall strain in the mixture (Kose, Guler, Bahia, & Masad, 2000). The mixture behaviour can show sensible non-linearity even for relatively low global strain levels. It has been observed that the effects of non-linearity are identical to the effect of increasing the number of loading cycles applied to the material during the phase 1 of a fatigue test. Since these effects can be confused with fatigue damage, they have to be taken into consideration when analysing fatigue tests (Di Benedetto et al., 2011; Doubbaneh, 1995; Gauthier, Bodin, Chailleux, & Gallet, 2010; Q. T. Nguyen, 2011).

1.3.9.2. Thixotropy

Some materials present a decrease of their consistency or their viscosity when subjected to a shear stress after a long rest period. If the viscosity loss is completely recovered when the stress is stopped, the material is said to be thixotropic. Bituminous materials have been found to present thixotropy and its effects on the materials behaviour can be assimilated as that of an increase in temperature. This modulus loss can be of important proportions, to the point that thixotropy is signalled as the main cause of modulus loss during laboratory fatigue tests (Delaporte et al., 2008; Di Benedetto et al., 2011; Mangiafico, 2014; Soltani & Anderson, 2005)

1.3.9.3. Self-heating

Viscoelastic and elasto-plastic materials present a temperature increase when subjected to repeated loading or when subjected to a loading higher than the yielding limit of the material (Oldyrev, 1971). This temperature increase is referred to as self-heating and it has been observed in a significant measure during fatigue tests on bituminous materials (Bodin, Soenen, & De la Roche, 2004; Mangiafico, 2014; Petersen, Link, Lundström, Ekblad, & Isacsson, 2004). Given the temperature dependency of bituminous materials, this self-heating has an effect on the mechanical behaviour of the sample and cannot be considered as fatigue damage. Since fatigue damage is seen as a modulus loss, it is important to note that an increase of 1°C of the temperature of the sample causes a modulus loss of approximately 5%. According to (Bodin et al., 2004; Q. T. Nguyen et al., 2012), self-heating effects are not negligible specially during phase 1 of fatigue tests. Nevertheless, (Mangiafico, 2014) observed that self-heating has a lesser effect on the behaviour of the samples during fatigue tests than thixotropy and non-linearity.

1.3.10. Fatigue damage analysis

The fatigue damage analysis method proposed by (Baaj, 2002; Di Benedetto, de La Roche, et al., 2004) is intended to correct the influence of biasing effects when analysing tension-compression tests on cylindrical samples of bituminous mixtures.

Damage amount (D) at a considered cycle N is calculated in terms of |E*| decrease as shown on equation [1-35]:

$$D(N) = \frac{|E_0^*| - |E_N^*|}{|E_0^*|} \quad [1\text{-}35]$$

Where $|E_0^*|$ is the initial value of the norm of the complex modulus and $|E_N^*|$ is the value of the norm of the complex modulus at the cycle N

This method is based on the hypothesis that the biasing effects can be estimated by monitoring the energy dissipation values per cycle W. The damage rate is corrected according to the estimated biasing effects.

The method considers three intervals (i=[0,1,2]) of the second phase of the |E*| against N plot:

- Interval 0 [cycles 40 000 to 80 000]
- Interval 1 [cycles 50 000 to 150 000]
- Interval 2 [cycles 150 000 to 300 000]

Depending on the test duration, the highest entire interval must be used. Several parameters are then calculated for the considered interval:

- $|E^*_0|$: the initial value of the norm of the complex modulus calculated by extrapolation of the linear fitting of the values of the cycles 50 to 250.
- $|E^*_{00i}|$: the initial value of the norm of the complex modulus calculated by extrapolation of a linear fitting of the values within the considered interval.

- a_{Ti}: the normalized damage rate corresponding to the slope of the linear fitting of the considered interval as:

$$a_{Ti} = \frac{d|E^*|/dN}{|E^*_{00i}|} \quad [1\text{-}36]$$

- W_{00i}: the initial value of the dissipated energy calculated by extrapolation of a linear fitting of the values within the considered interval.
- a_{Wi}: the normalized energy dissipation evolution rate corresponding to the slope of the linear fitting of the considered interval as:

$$a_{Wi} = \frac{dW/dN}{W_{00i}} \quad [1\text{-}37]$$

- a_{Fi}: the corrected fatigue damage rate, calculated as:

$$a_{Fi} = a_{Ti} + a_{Wi} C_i \frac{|E^*_0| - |E^*_{00i}|}{|E^*_{00i}|} \quad [1\text{-}38]$$

$$\text{were } C_i = \left[\frac{4}{5}, \frac{3}{4}, \frac{2}{3}\right] \text{ depending on the considered interval}$$

This method is independent of the test control mode allowing the comparison between both types of test.

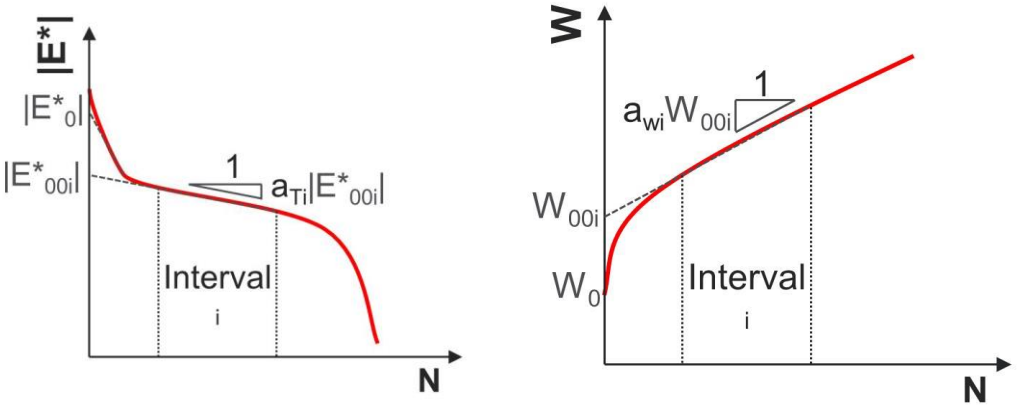

(a) (b)

Figure 1.42. Scheme explaining the determination of the parameters for the fatigue damage analysis: Complex modulus parameters (a) and energy dissipation parameters (b) - The energy dissipation scheme corresponds to a stress-controlled test

The cumulated damage at the transition between phases 2 and 3 of the fatigue test can also be estimated. For this, the uncorrected damage value D_{III} is calculated as:

$$D_{III} = \frac{|E^*_0| - |E^*_{III}|}{|E^*_0|} \quad [1\text{-}39]$$

Where $|E^*_{III}|$ is the value of the norm of the complex modulus at the transition between the phases 2 and 3 of the fatigue test

The corrected damage at the end of the transition (D_{IIIc}) can then be obtained from equations [1-38] and [1-39] as:

$$D_{IIIc} = D_{III} - C_i \frac{|E_0^*| - |E_{00i}^*|}{|E_{00i}^*|} \quad [1\text{-}40]$$

Recent studies showed that the D_{IIIc} value does not depend on the loading amplitude of the fatigue test. It represents an amount of damage for which the material fails under the tension-compression fatigue test conditions (Mangiafico, 2014; Tapsoba, Sauzéat, & Di Benedetto, 2013).

1.4. Moisture susceptibility and ageing of bituminous mixtures

The principal aspects of moisture susceptibility and ageing of bituminous mixtures are presented in this section. The influence of mixture components is highlighted through a literature review on the subject. The principal standard tests to assess moisture susceptibility of bituminous mixtures are exposed as they are the base of the moisture conditioning procedure used during this study.

1.4.1. Definition of moisture damage for bituminous mixtures

The most accepted definition of moisture damage of bituminous mixtures is probably that proposed by (Kiggundu & Roberts, 1988). The authors define moisture damage as "the progressive functional deterioration of a pavement mixture by loss of the adhesive bond between the asphalt cement and the aggregate surface and/or loss of the cohesive resistance within the asphalt cement principally from the action of water". Indeed, according to (Copeland, Youtcheff, & Shenoy, 2007), moisture damage can occur in two forms: as the weakening of the adhesive bond between the binder or the mastic and the coarse and fine aggregate, or as the degradation of the bituminous mastic. Cohesive and adhesive bonds are equally important to characterize the moisture susceptibility of bituminous mixtures.

Adhesion between aggregates and binders can be explained by four theories: chemical reaction, surface energy, molecular orientation and mechanical adhesion (Terrel & Shute, 1989). Chemical reaction is based on the generally accepted hypothesis that the acidic and basic (polar) components of both bitumen and aggregate surface attract to each other and form water-resistant bonds. Surface energy and molecular orientation are synergistic theories because both assume that adhesion is facilitated by a reduction in the surface energy at the aggregate surface as bitumen is adsorbed to it. This surface energy determines the degree of wettability of the aggregate by bitumen and water. Calculating the adhesive bond based on surface energy is very complex (Kiggundu & Roberts, 1988; Little & Jones, 2003). Finally, mechanical adhesion is a simple theory stating that the adhesive bond is determined by the physical characteristics of the aggregate surface such as texture, porosity or absorption, cleanness or absence of surface coatings, particle size, etc (Terrel & Al-Swailmi, 1993). The improvement of the mechanical bond synergistically improves the chemical bonds between bitumen or mastic and aggregates (Little & Jones, 2003).

Cohesive strength of the mastic depends on its rheology, defined by the interaction of the bituminous binder and the mineral filler (Kim, Little, & Lytton, 2003). Mastic design, which aims to optimize the amount of suitable filler with respect to the amount and nature of the bitumen, is then crucial to avoid moisture-related distresses in the mastic.

In any case, moisture damage cannot be explained by a single theory as it is a very complex phenomenon that involves several mechanisms of different nature (Kiggundu & Roberts, 1988).

1.4.2. Mechanisms of moisture damage

The weakening of the adhesive bond between the aggregate and the binder is called “stripping”. At least five different stripping mechanisms have been identified: detachment, displacement, spontaneous emulsification, pore pressure and hydraulic scour (Kiggundu & Roberts, 1988; Little & Jones, 2003; Terrel & Al-Swailmi, 1993). The strength loss due to adhesive bond weakening was observed to be very high (D. Cheng, Little, Lytton, & Holste, 2002).

Detachment is the separation of the binder film from the aggregate surface by a thin film of water in-between (Majidzadeh & Brovold, 1968). It defers from displacement in that the binder film is not broken. The reason it happens is that the aggregate surface presents higher affinity, or wettability, for water than for bitumen as water has lower viscosity and lower surface tension (Arambula, 2007; Hicks, 1991). The difference in wettability lays also in the fact that most bituminous binders have low-polarity and develop relatively weak bonds with the aggregate surface. In presence of water, water molecules easily replace the binder as they are highly polar and develop strong bonds with the aggregate surface. This effect is represented in Figure 1.43, where it can be observed that the contact angle (θ) between aggregate and bitumen increases with time in presence of water until the contact between the two materials is loss.

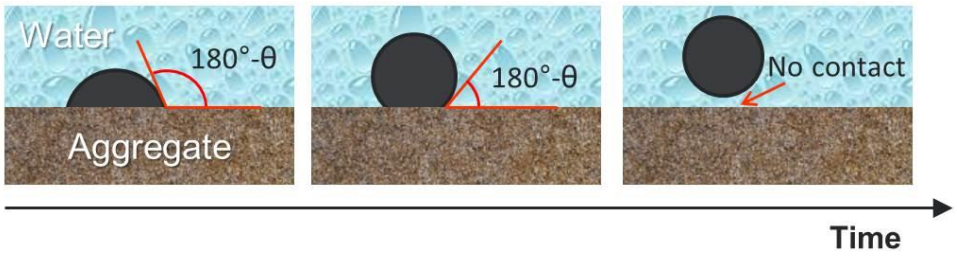

Figure 1.43. Schematic representation of the effect of water on an bitumen drop in contact with the aggregate surface (adapted from (Hicks, 1991))

The adhesive bond was also found to be highly influenced by the pH of the water in the system as it changes the contact angle and the wettability of the binder. Higher pH values of the water were found to be correlated to higher stripping potential (Kiggundu & Roberts, 1988). Spontaneous emulsification is the formation of an emulsion of water droplets in the bitumen. The adhesive bond between aggregate and binder is broken when the emulsion formation penetrates the substrata and the emulsification rate depends highly on the nature and viscosity of the binder, but also in the presence of additives (Little & Jones, 2003). The deterioration of the adhesive bond can also be triggered by the build-up in pore pressure caused by entrapped water in the materials interstices when loaded. This increase in pore pressure can disrupt the

binder film and create micro-cracks that lead to displacement. Finally, hydraulic scour is the stripping of the pavement surface by the action of pneumatic tires in the presence of water (Little & Jones, 2003). This last distress mechanism is not expected in a railway track structure.

The reduction of the cohesive strength of the mastic is caused by the moisture saturation and build-up pore pressure in the mixture (Terrel & Al-Swailmi, 1993). As for the adhesive bond, pore pressure can create micro-cracks that damage the mastic and accelerate the crack growth rate. This damaging rate is influenced by the diffusion of water into the mastic and by its water-holding potential. Mastics with the most capacity to hold water were found to present the most moisture-related damage (D. Cheng et al., 2002).

1.4.3. Factors affecting moisture damage

Two main stages of the moisture damage mechanism were identified by (Caro et al., 2008). The first stage corresponds to the moisture infiltration and transfer through the material, and the second to the alteration of the internal structure of the material in response to the presence of water, which leads to a reduction of its mechanical properties. In order to characterise the moisture susceptibility of bituminous mixtures it is then necessary to identify the different factors that govern these two stages of moisture damage.

According to (Solaimanian, Kennedy, & Elmore, 1993) there are five main factors that determine the moisture susceptibility of bituminous mixtures. These factors have been regrouped into two categories by (Arambula, 2007):

- Internal factors
    - The aggregates characteristics and properties
    - The bituminous binder characteristics
    - The mixture design
- External factors
    - The environmental conditions to which the material is subjected during service
    - The nature and volume of traffic

The interaction between mineral aggregates and bituminous binder, which is related to the stripping potential, is of special interest for this study as it can be decisive in the selection of the materials for railway bituminous mixtures. The study by (Canestrari, Cardone, Graziani, Santagata, & Bahia, 2010) proposed a modified Pneumatic Adhesion Tensile Testing Instrument (PATTI) for evaluating the adhesive and cohesive properties of different bitumen-aggregate combinations and the effects on moisture damage on them. They observed that non-conditioned PATTI specimens never presented cohesive failure. However, for moisture conditioned specimens, the bitumen-aggregate affinity controlled the transition from cohesive to adhesive failure.

With respect to mixture design, compactness and binder content are of importance as they are determinant for the exposition of the material to moisture. The amount of water, its residence period and the moisture transfer mechanisms in the mixture are strongly dependent on its volumetric properties.

Regarding environmental conditions, the authors have observed that an increase of the humidity of the environment (regular rains, snow accumulation, high relative humidity) causes greater damage in bituminous materials due to higher exposition to moisture (Barra, Momm, Guerrero, & Bernucci, 2012; Sengoz & Agar, 2007). The materials cannot then be considered as impermeable and insensitive to weather conditions and have to be conceived to withstand them during service life. The environmental conditions to which bituminous layers are subjected in French track structures are assessed through the study case presented in section 2 of this thesis.

Traffic loading characteristics play an important role in the occurrence of pavement distresses related to moisture. Stripping potential can be increased by the increase of the axle loads and of the traffic volume. Cyclic loadings can cause high pore pressures in the interstices filled with water which has an erosive effect on the mastic, accelerating the damaging of the material (Kringos et al., 2009; Mehrara & Khodaii, 2013; Solaimanian, Harvey, Tahmoressi, & Tandon, 2004). Several environmental factors of concern where identified by (Terrel & Al-Swailmi, 1993) including precipitations, ground-water sources, temperature fluctuations and freeze-thaw cycles. Railway traffic loading characteristics are taken into account for the analysis of the laboratory test results carried on to characterise the thermo-mechanical behaviour of bituminous mixtures used for railway infrastructure (c.f. sections 4.3 and 5.3).

1.4.3.1. Influence of aggregate characteristics

The nature of the aggregates has been identified in the literature as an important factor to assure the good adhesion of bitumen to its surface.

The mineralogical composition of aggregates will determine its degree of affinity for water over bitumen (hydrophilic nature). It is generally accepted that acidic aggregates are more hydrophilic and basic aggregates are more hydrophobic. Acidic aggregates are those with high contents of silica, like granite and sandstone. Basic aggregates have high contents of carbonates and alkaline earth metals like limestone. Bitumen is a generally acidic or electronegative material, thus it usually creates chemical bonds with aggregates of basic nature that are more difficult to break by water than those created with acidic aggregates (Barra et al., 2012; Little & Jones, 2003; Sengoz & Agar, 2007).

Several ways of assessing the influence of the mineralogical composition of aggregates are found in the literature. Using the indirect tensile strength (ITS) test, (Cheng, Shen, & Xiao, 2011) compared the moisture resistance of mixtures containing aggregates from different sources, a schist and a granite with high contents of Al_2O_3 and SiO_2, and a limestone with higher contents of CaO and MnO. They observed that the mixture with aggregates with low content of Al_2O_3 and SiO_2 performed twice as better during the ITS test than the rest of the studied mixtures. Similar conclusions were made by (Bagampadde, Isacsson, & Kiggundu, 2005). The authors found that aggregates composed of at least 30% of CaO, MgO and Fe_2O_3 provided low moisture susceptibility compared to aggregates composed of metals, feldspars and mica, which were catalogued as highly sensible to stripping. According to (Bagampadde et al., 2005), the aggregates composed by ferromagnesian minerals at around 70% systematically perform better in terms of moisture susceptibility. No clear correlation was found for the contents of silica and alumina but they are interesting to characterise as they are electronegative charged compounds and abundantly found in most of the rocks composition.

Mixtures with aggregates with high content of carbonates were also found to perform better to the AASHTO T283 test procedure than those with sandstone aggregates (Kringos et al., 2009). A study by (Khan et al., 2013) highlights the fact that mixtures with aggregates of basic nature sensitively presented higher stiffness after conditioning than mixtures with acidic ones. The authors used the Nottingham Asphalt tester (NAT) to perform direct tensile strength tests on moisture conditioned samples of mixtures with granitic and limestone aggregates. Using a modified PATTI device, (Canestrari et al., 2010) did not observe adhesive failure for bitumen-limestone aggregate combinations after moisture conditioning. This indicates that the binder affinity for limestone aggregates is higher than for acidic ones.

Surface energy analysis has been used to study the relation between the mineralogical nature of the aggregates and their adhesive bond with bitumen and mastic. (Cheng et al., 2002) compared the bond energy per unit of mass of acidic and basic aggregates and found that the calcareous ones had far greater energy values than the siliceous ones. This highlights the importance of the synergy between physical and chemical properties as when the energy values are taken in units per surface area the results are reversed. Similar conclusions were observed by (Cheng, Little, Lytton, & Holste, 2003) using a mathematical model. The model results where validated by permanent deformation tests under cyclic loading on two mixtures with aggregates of the two different natures. Furthermore, (Hefer, Bhasin, & Little, 2006) proposed a method to find the optimal aggregate-binder combination with regard to moisture resistance based on their surface energy properties.

Nevertheless, the chemical bond between water and aggregate is always stronger than that between bitumen and aggregate so that all aggregates are prone to stripping.

Aggregates surface is also important for the adhesive bond with bitumen and mastic. Crushing rocks to manufacture aggregates creates high energy at the fracture surface of fresh grains due to the breakage of the internal chemical bonds of the mother rock. Water, oil and contaminants in the air, such as dust, are immediately attracted to these high energy new surfaces. Theoretically, careful manipulation of new aggregates can help maintaining their surface energy at high levels to facilitate stronger bonds with bitumen during mixing. Nevertheless, most of them adsorb moisture present in the air and create a water films on the surface. Heating the aggregates was then observed as a solution to remove this outermost absorbed water. Heating also diminishes the bitumen viscosity, thus improving wettability and adhesive strength at the interface with the aggregate. The use of dusted and clean aggregates is also of importance since impurities at the surface of the aggregates can prevent a direct contact of the binder and the aggregate (Bagampadde et al., 2005; Little & Jones, 2003; Majidzadeh & Brovold, 1968).

1.4.3.2. Influence of binder characteristics

Regarding the composition of bitumen, the amount of functional groups that are easily absorbed by the surface of the aggregate and of those which are easily displaced by water can serve as indicator of the moisture susceptibility to moisture damage (Kanitpong & Bahia, 2008). However, estimating the mechanical performances of bituminous mixtures based only on the chemical nature of aggregates and binders is, for the moment, impossible.

The influence of bitumen properties on the stripping potential was found to be less important than that of the aggregates' (Caro et al., 2008; Sengoz & Agar, 2007). Carboxylic acids and sulfoxides are generally undesirable since they create bonds with the aggregate in a dry state, but these are easily broken in the presence of water. On the contrary, nitrogen and phenol bases usually present low desorption (Bagampadde & Karlsson, 2007; Little & Jones, 2003). A slight correlation between bitumen stiffness and stripping potential was found by (Airey, Collop, Zoorob, & Elliott, 2008) for some combinations of bitumen and aggregates. The study by (Canestrari et al., 2010) concluded that, in general, higher asphaltene contents lead to better cohesive and adhesive strength. Moreover, they observed that polymer-modified bitumen showed less moisture sensitivity in terms of cohesion loss.

The presence of water in the fabrication process of bitumen, as is the case for foamed bitumen, was found to increase the moisture susceptibility of the mixtures (Caro, Beltrán, Alvarez, & Estakhri, 2012). Ageing of the bituminous binder and mastic increases their susceptibility to moisture damage (Little & Jones, 2003).

However, a strong influence on moisture susceptibility was found for the thickness of the binder film around the aggregates (Little & Jones, 2003). According to (Sengoz & Agar, 2007) there is an ideal interval for the film's thickness between 9.5 µm and 10.5 µm which corresponds to a binder content of about 5.5% depending on the aggregate used. The binder film thickness is also related to the type of moisture failure developed in the mixture. Adhesive failure usually occurs in thin films and cohesive failure in thick ones. The thicker the film, the less cohesive strength it presents, and the thinner the film, the lower the adhesive tensile strength is (Lytton, Masad, Zollinger, Bulut, & Little, 2005). Indeed, (Partl, Pasquini, Canestrari, & Virgili, 2010) concluded that the low moisture sensitivity in terms of fatigue damage of open graded mixtures with rubber binder was probably due to their high binder content that produced a thicker bituminous film around the aggregates, compared to traditional mixtures.

Anti-stripping agents can be used to improve the moisture resistance of bituminous mixtures when the components at disposal are not optimal. According to (Kanitpong & Bahia, 2008), anti-stripping agents significantly increase the adhesion between bitumen and aggregates in presence of water.

1.4.3.3. Influence of mixture characteristics

The mixtures characteristics and the fabrication methods also have an important influence on its moisture susceptibility.

Air voids content, size and distribution within the compacted mixture have been observed as a determinant factor for moisture damage. The presence of voids increases the total surface of the material that is in contact with water. Moreover, air voids content determines the drainage capacity of the mixture. Mixtures with relatively high air voids content, between 6% and 15%, usually are more susceptible to stripping than draining mixtures with voids content between 15% and 25%. In the latter type of mixture, the water flows through the material, thus the exposition time to moisture is shorter than for non-draining mixtures (Stuart, 1990).

The "pessimum" air voids was proposed by (Terrel & Al-Swailmi, 1993). It corresponds to an air voids content range between 8% and 10% for which a great amount of bituminous are

compacted. Above this range, bituminous mixtures have interconnected voids allowing free water flow when the material is loaded. Below it, bituminous mixtures are considered as almost impermeable from a macroscopic point of view and thus do not saturate with water. Bituminous mixtures within the pessimum air voids range have interconnected voids that do not allow free flow but can get saturated. When loaded, saturated mixtures build-up pore pressure that damages the material, as discussed before. Heterogeneous moisture damage can happen when trapped water locally exposes the material to moisture over long periods (Arambula, 2007; Arambula, Masad, Martin, et al., 2007; Chen et al., 2004).

Air voids size was found to be correlated to moisture damage by (Birgisson, Roque, & Page, 2003; Masad et al., 2006). The results of their studies showed the existence of a pessimum void size for which moisture damage is maximized. Permeability was found not to be directly proportional to moisture damage as mixtures with intermediate permeability values (between 10^{-4} and 10^{-2} cm/s) presented high moisture damage being in the pessimum size range (Arambula, 2007; Chen et al., 2004; Masad et al., 2006). The schematic representations in Figure 1.44 show the evolution of moisture damage with air void content, air void size and permeability according to (Masad et al., 2006; Terrel & Al-Swailmi, 1993).

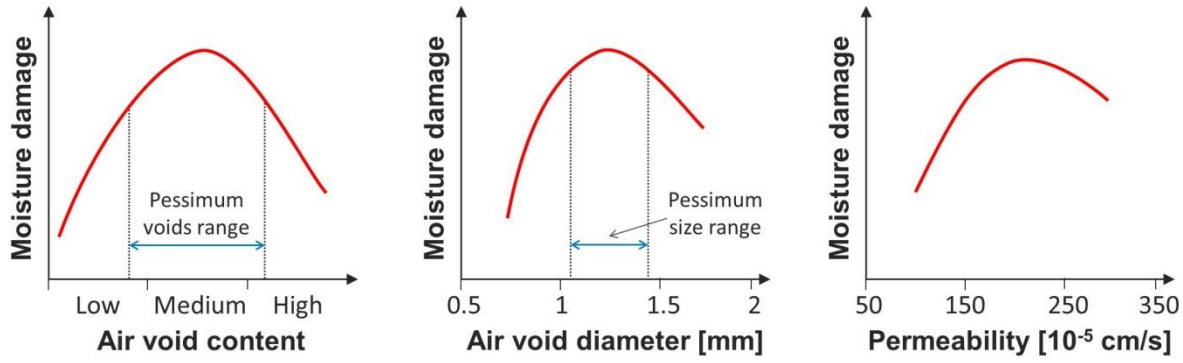

(a) (b) (c)

Figure 1.44. Schematic representation of the pessimum air void content range (a), of the pessimum air void size range (b) and of the nonlinear relation between permeability and moisture damage (adapted from (Arambula, 2007))

Air voids are very variable and dependent of many different factors. Aggregate segregation, bleeding, poor compaction, amongst other factors, can alter the amount and distribution of air voids in a compacted bituminous material (Solaimanian et al., 2004). This high variability has been identified by the authors as a possible source of scatter in the results of moisture susceptibility tests on bituminous mixtures and as a possible explanation for the unexpected bad (or good) moisture resistance of in-service bituminous layers.

Voids distribution was found to be highly dependent on the compaction method (Masad et al., 2002) (c.f. section 1.1.4). Pneumatic wheel roller compactors create, for example, an increasing gradient of voids size and content with the layer depth. (Kringos et al., 2009) considers the heterogeneity in air voids as the main source of the recurrent dispersion of the Modified Lottman test results which is considered by the American Standard (AASHTO T 283, 2014).

The study by (Masad et al., 2002) also shows a great influence of the granular skeleton grading on the mixtures density. Comparing the maximum density lines of various mixtures, they concluded that coarse graded mixtures presented bigger voids than fine graded ones.

Water transport through the material depends on its volumetric properties. Water infiltration at the surface of a bituminous layer is the principal source of moisture for in-service bituminous mixtures. Capillary rise and vapour diffusion are other identified sources (Caro et al., 2008). The amount of infiltrated water to the core of the material and the infiltration speed depend on the voids content and connectivity. In order to determine in a more precise way these factors, the authors use Computed Tomography (CT) techniques to scan the materials (Arambula, Masad, & Martin, 2007; Kringos et al., 2009; Tashman et al., 2002). This allows identifying the real amount, size and distribution of air voids in the samples.

Using CT-scan, (Khan et al., 2013) observed that permeability and voids connectivity of the mixtures increase with the increase of the design voids content. They also highlighted that saturation levels obtained by simple mass comparison of dry and surface-dried specimens are coherent with values obtained by CT-scan. Furthermore, the authors carried out tensile strength tests on moisture conditioned samples and observed a decrease in the saturation level of the samples after the mechanical test. They defined the retained saturation level as the portion of it that is not lost after mechanical testing. For mixtures containing basic aggregates, the saturation level does not seem to have any effect on stiffness. On the contrary, stiffness values of moisture conditioned samples of bituminous mixtures containing acidic aggregates decrease considerably with the increase of the retained saturation level. Stripping of the acidic aggregates might be the source of the performance differences between mixtures with basic and acid aggregates. They also carried out tests to compare the properties of bitumen before and after moisture conditioning using distilled water at 20°C under vacuum conditions during 30 min. They observed that the bitumen recovered from conditioned samples was considerably aged in comparison with the original new bitumen. This was a clear evidence of the effect of moisture conditioning on the bituminous mixtures properties.

Three different test methodologies were used by (Barnes & Trottier, 2010) to assess the moisture resistance properties of bituminous mixtures with different voids contents. According to the authors, the ITS test, coupled with visual inspection of the fracture planes of the samples, was found to be the most suitable methodology to characterize the moisture susceptibility of mixtures with air voids between 5% and 10%. However, for more compacted mixtures, they recommend the surface wave test. They concluded that the complex modulus is not a suitable parameter to characterize the moisture susceptibility as it is poorly sensible to moisture damage. Nevertheless, this conclusion was only based on modulus values at 25°C and 25 Hz. Bitumen ageing, stripping and loss of cohesive strength might cause important modulus variations at high and low frequencies.

1.4.4. Evaluation of moisture susceptibility of bituminous mixtures

Several laboratory tests have been proposed to assess the moisture susceptibility of bituminous mixtures. In this section, a literature review is presented as to highlight the advantages and disadvantages of the most commonly used test methods. Special attention is given to the

standard French and American test methodologies as they are the base for the conditioning methodology used in this study.

1.4.4.1. The French standard moisture susceptibility test

In France, moisture susceptibility tests of bituminous mixtures are defined by the European Standard (EN 12697-12, 2008). The standard comprises three different methods and a moisture conditioning procedure. Two of the methods are intended for compacted mixtures; they use the simple compression test and the indirect tensile strength test (ITS), respectively. Moisture susceptibility is measured as the ratio of the mechanical performance of moisture conditioned samples with respect to non-conditioned ones. The third method in the European Standard is intended for mixtures made with bitumen of low viscosity ($\eta \leq 4000$ mm^2/s at 60°C) which is why it is out of the scope of this study.

In this thesis, conditioned samples can also be referred to as “wet” samples and non-conditioned ones can be referred to as “dry” samples.

French authorities recommend the use of the simple compression test, also called the “Duriez” test. The test uses cylindrical samples of either 120±3 mm or 80±3 mm in diameter and a height to diameter ratio of at least 0.5. The samples are fabricated by compacting loose mixture in a cylindrical mould under axial loading. The samples mass has to be 3 500±4 g or 1 000±4 g, depending on the diameter. The bulk density of each sample is determined by hydrostatic weighting and two groups of samples with similar geometry and density are formed, each one of at least 4 samples. One group is conserved in a chamber at 18±1°C and 50±10% of relative humidity for 7 days. The other is placed in a vacuum chamber at 47±3 kPa of residual pressure. After 1 hour, water is allowed into the vacuum chamber while the pressure level is maintained. The samples are left under these conditions for 2 hours, and then they are immersed in a water bath at 18±1°C for 7 days with a tolerance of two hours. The difference in temperature between the water bath and the chamber where the dry samples are stocked cannot be superior to 1°C. The samples whose volume increases of 2% during vacuum are discarded.

Simple compression test is carried out on every sample at a rate of 1mm/s. A ratio of compressive strength is calculated between the dry and wet groups. This ratio, called immersion-compression ratio (i/C), has to be superior to 0.8 for the mixture to be accepted for road applications. This means that the moisture conditioning process cannot cause a resistance loss in the material of more than 20%. Right after taking the sample out of the water bath, its surface is dried and its mass measured in order to calculate the saturation.

$$i/C = \frac{C_w}{C_d} \qquad [1\text{-}41]$$

Where C_w is the average compressive strength of the conditioned samples and
C_d the average compressive strength of the non-conditioned ones

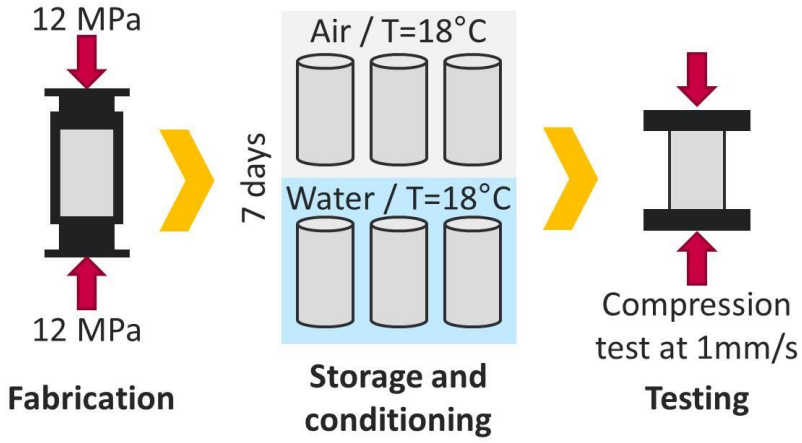

Figure 1.45. Schematic representation of the Duriez test procedure

1.4.4.2. The American AASHTO T 283 test

The American standard (AASHTO T 283, 2014) considers the Modified Lottman test for assessing the moisture susceptibility of compacted bituminous mixtures. The test consists in comparing the resistance to indirect tensile stress of non-conditioned samples with respect to conditioned ones. Samples are made of loose mixtures that have been subjected to a curing period of 16 h at 60°C, followed by 2 h at 135°C. The cured mixture is then compacted with a Marshall compactor to form cylindrical specimens with air voids content between 6.5% and 7.5%. Half of the compacted specimens (at least 3) are kept unconditioned while the other half is subjected to vacuum for a short amount of time until attaining a saturation level between 55% and 80%. Saturation is estimated as:

$$S' = \frac{100(W_{ssd} - W_d)}{\frac{V\%}{100} E \rho_w} \quad [1\text{-}42]$$

Where S' is the saturation level, W_{ssd} is the mass of the sample after vacuum, W_d is the mass of the dry sample, V% is the air voids content in percentage, E the volume of the dry sample and ρ the density of water.

The partially saturated samples are then wrapped in plastic bags and subjected to a freezing cycle at -18°C for 16 h. The samples are then submerged in a water bath at 60°C for 24 h. The conditioned samples are then finally put back in a water bath at room temperature for 2 additional hours before testing.

The ITS test consists in applying a constant compression effort at a rate of 50.8 mm/min alongside the flank of the sample placing sideways between two steel bars. The test is made at 25°C. The compressive load induces then indirect tensile stress in the horizontal direction of the sample until it fails. The maximum applied load is registered to calculate the tensile strength (S_t) as shown in equation [1-43].

$$S_t = \frac{2P}{\pi t D} \quad [1\text{-}43]$$

Where P maximum applied compressive load, t is the sample height and D its diameter

The tensile strength ratio between the performances of dry and wet samples (TSR) is calculated as:

$$TSR = \frac{S_{t\_w}}{S_{t\_d}} \quad [1\text{-}44]$$

Where S_{t_w} is the average tensile strength of the conditioned samples and S_{t_d} the average tensile strength of the non-conditioned ones

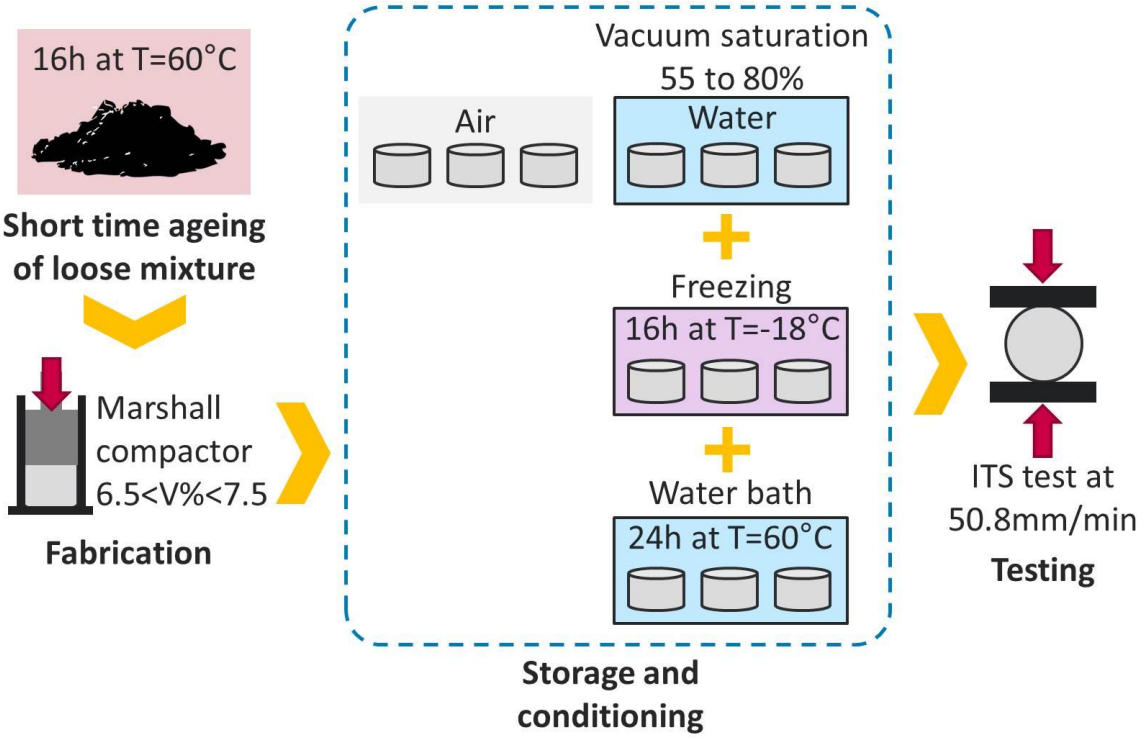

Figure 1.46. Schematic representation of the AASHTO T283 test procedure

According to the Superpave standard, the minimum TSR recommended value is 0.8 (Asphalt Institute, 1995). The AASHTO T283 procedure is nowadays one of the most used methods to assess moisture susceptibility of bituminous mixtures. The Lottman test differs from its modified version in that vacuum saturation is done for of 30 min instead of until certain saturation level is attained, and in that the test is done at 12°C instead of 25°C. The loading rate is also lower for the Lottman test than for the modified version. The ASTM standard (ASTM D4867, 2014) adopted a modified version of the AASHTO T283 test where the curing period of the loose mixture was eliminated.

Between the AASHTO T283 and the Duriez test procedures several differences are of importance. Besides the different loading mode, the Duriez test does not appeal to high temperatures or freeze-thaw cycles as does the AASHTO T283 in order to accelerate the moisture damage occurrence. However, the exposition time to moisture is higher in the Duriez procedure.

1.4.4.3. Other moisture susceptibility test procedures

The preoccupation for stablishing the resistance of bituminous mixture to moisture damage dates back to the 1920's. Nowadays, many different test methodologies have been developed. Two great families of moisture susceptibility tests can be distinguished: those made on loose mixture samples and those made on compacted mixture specimens. The advantage of the latter is that it allows taking into account the effect of the physical properties of the material and the effect of pore pressure induced by traffic loading (Solaimanian et al., 2004).

In parallel, the different tests can be classified as quantitative or qualitative. Qualitative tests are based on observation to evaluate the resistance to moisture of the mixtures whereas quantitative tests are based on the measurement of a certain parameter which is used to compare the mixtures performance. The French Duriez test is then a quantitative one, part of the compacted specimen family, using the immersion-compression ratio as parameter of resistance to moisture damage.

One of the first tests was proposed by Saville and Axon in 1937, as cited in (Solaimanian et al., 2004), and was called the "boiling test". It consisted on a qualitative test made on bitumen coated aggregates. These were submerged in a boiling water bath intended to accelerate moisture damage and reproduce the effects of the exposition to moisture on the long term. Moisture damage acceleration through high temperature water baths has been a recurrent technique in laboratory tests since then (Solaimanian et al., 2004).

In 1950, the immersion-compression test was the first homologated test by a standardization organization: The American Society for Testing and Materials (ASTM). New test methodologies were proposed during the 1960's and 1970's, all of them recognizing the importance of simulating field conditions and accelerating the moisture conditioning of the samples. (Jimenez, 1974) proposed a conditioning method including saturating the sample by partial vacuum and the use of a mechanical cyclic test in order to simulate the repetitive loading of traffic. Latter, (Lottman, 1978) introduced a conditioning procedure including high temperature water baths and freeze-thaw cycles, as well as the use of the indirect tensile test on cylindrical samples. As seen before, this protocol was adopted by the standard of the American Association of State Highways and Transportation Officials (AASHTO T 283, 2014). By the same time, the Hambourg Wheel Tracking Device (HWTD) was developed in Germany by Esso A.G., which combines the effects of rutting and moisture damage by simulating traffic loading with a turning steel wheel on a submerged bituminous mixture sample. The test was latter introduced into the United States and it was found to be a good screening test for moisture susceptibility, however, it is limited in the way that it does not provide information on the fundamental properties of the materials and that it is only suitable for the case where moisture comes from rainfall and during the hottest periods of the year. It is then not suitable for simulating moisture damage caused by infiltrated water during cold periods (Aschenbrener, 1995; Solaimanian et al., 2004).

In the 1990's, (Al-Swailmi & Terrel, 1992) developed the Environmental Conditioning System (ECS) as part of the Asphalt Research Program of the Strategic Highway Research Program (SHRP) at the University of Oregon. This test allows subjecting the bituminous mixture samples to several conditioning cycles and uses a dynamic test to determine their resilient modulus after each cycle. Samples are saturated in a vacuum chamber and the conditioning cycles include a period of 6 h at 60°C followed by 2 h at 25°C. Three cycles are done and the modulus is tested after each one using a haversine loading at 10 Hz. A ratio between the modulus values of conditioned samples with respect to non-conditioned ones is calculated and must be superior to 0.7 in order for the material to be acceptable. This methodology intended to respond to the need of a systematic way to determine the resistance to moisture of bituminous mixtures as, at the time, no other existing method had good repeatability (Al-Swailmi & Terrel, 1992; Cooley et al., 2001). Despite the intentions of this procedure to integrate notions of permanent deformation and resilient modulus in the assessing of moisture susceptibility, it is criticized due to the fact that it is very long and complicated to carry out (Mehrara & Khodaii, 2013; Solaimanian et al., 2004).

Despite the efforts to relate moisture damage with other properties of bituminous mixtures, the test procedures currently used are not effective enough and none of the proposed test methodologies provide the needed information for a rational design method of bituminous structures as they do not consider the effects of moisture on the stiffness, fatigue resistance, permanent deformations, amongst others (Gubler, Partl, Canestrari, & Grilli, 2005; Hicks, 1991; Solaimanian et al., 2004). The characteristics of an efficient moisture susceptibility test were detailed by (Solaimanian et al., 2004):

- It must provide information on the in-service performance of the material. This can be done by simulation of the moisture conditions in the field or by accelerating the damage mechanism on the condition that the results are consistent with the observations from the field.
- It must allow distinguishing from good and bad performances regarding moisture damage. The performance of moisture damaged materials needs to be consistent with the field observations.
- It must be repeatable and reproducible.
- It must be easy to carry out, practical and economical. The test methodology has to be easily integrated in the daily practice of pavement structure design.

The importance of obtaining consistent results with the material performance in the field is a recurrent subject in the literature. This means that the achievement of an experimental laboratory method that reproduces the in-situ effects of moisture can only be verified with the return on experience from in-service sites. The test methodology needs then to be calibrated with the real weather and moisture conditions of the considered site and structure type (Aschenbrener, 1995; Solaimanian et al., 1993).

1.4.4.4. Factors affecting the reliability of moisture susceptibility tests

Many authors have highlighted the importance of reproducing the effects of in-situ traffic loading during moisture susceptibility tests. Given the fact that traffic induces a repeated loading on the pavement structure, some of the proposed methods include cyclic loading tests. Static

loading is criticized on the base that it is unable to reproduce the erosive effects on the mastic of the increase in pore pressure caused by repeated loading (Bausano & Williams, 2009). This is the case of the AASTHO T283 and Duriez tests.

In the study by (Kringos et al., 2009), the ITS test is found not to be representative of the effect of traffic on the pavement. This was identified as one of the sources of the feeble correlation of this test results and the materials performance in the field. The authors point out that the AASHTO T283 test is indeed known to be very variable and poorly repeatable. (Kanitpong & Bahia, 2008) also pointed out the feeble correlation of the ITS test with in-situ performances. Indirect tensile tests induce a heterogeneous stress and strain field in the sample, which has also been identified as a possible source of variability of the results. Given the fact that the facture is imposed at the middle part of the sample, the presence of impurities, discontinuities or any default near that area can cause the early failure of the sample which is not induced by moisture damage. Sample compaction becomes then a very important step of the test methodology as the samples should have the most homogeneous void distribution as possible (Kringos et al., 2009).

Even if the simple compression test induces a homogeneous stress and strain field on the samples, the sample fabrication method is also crucial to reduce the variability of the Duriez test results. The samples for both AASHTO T283 and Duriez test are fabricated by compaction of a loose mixture inside of metal cylindrical molds. Voids content is then measured assuming the sample to be a perfect cylinder and not taking into account the air voids at the surface of the sample which can be seen as defaults of the geometry. These external air voids are not representative of the real voids distribution in a compacted bituminous layer. As a consequence, the real voids content of these samples is usually higher than the one measured by a simple geometric method, which alters the homogeneity of the group of tested specimens and therefore increases the variability of the test results (Kringos et al., 2009).

In addition to the miscalculated voids content of the samples, the voids distribution and connectivity are also unknown. The moisture concentration field and the moisture diffusion trend are dependent of these two volumetric characteristics of the samples. Cluster of voids within the sample can generate water accumulation zones with higher pore pressure values than in the rest of the sample, resulting in focused and accelerated damage. All the same, these clusters can also have a draining effect if they are well connected with the exterior, reducing the exposition of the entire zone to pressure build-up. These factors cause heterogeneity within the sample during the test and need to be taken into account (Das, Baaj, Kringos, & Tighe, 2015; Kringos et al., 2009).

The use of freeze-thaw cycles is also subject of discussion in the literature. In the study by (Wong et al., 2004), they treated the effects of different conditioning methods on the resistance to permanent deformation of bituminous mixtures. The increase of the number of freeze-thaw cycles was found to have little effect on the rutting resistance of the materials. Latter, (He & Wong, 2008) decided not to include freeze-thaw cycles at all in their conditioning method after having concluded from a literature review that freezing did not always have a damage accelerating effect, compared to the effect of other techniques such as subjecting the samples to high temperatures. (Kringos et al., 2009) studied the effect of freeze-thaw cycles from a mechanical point of view and concluded that the supplementary stresses caused by the volumetric expansion of water molecules when frozen can cause a certain amount of damage

given the embrittlement of the bituminous binder and mastic at low temperatures. Nevertheless, the nature of this damage is very different from that of the repeated loading caused by traffic on the long term. Freeze-thaw cycles do not accelerate or simulate the real damage mechanisms related to moisture in pavements, which are of an erosive nature on the mastic due to a “pumping action” of the water in the pores when the structure is loaded by traffic.

Vacuum saturation has also been recurrently used as a technique to accelerate the moisture infiltration in bituminous mixtures. This aims to reduce the needed time to attain a certain saturation level of the specimens. Using CT tomography, (Kringos et al., 2009) compared the voids amount that is needed to attain the saturation level dictated by the AASHTO T283 standard with the amount of voids directly connected with the exterior, thus with water. The authors concluded that the amount of voids that could be easily filled with water was not enough to reach the desired saturation level; nonetheless, this did not prevent the sample to be saturated. This was explained by the effect of vacuum on the voids connectivity. Vacuum forces the water inside the sample creating micro-cracks that connect otherwise non-accessible voids. Micro-cracks are indeed a damage in the material but one that is not controllable or predictable. This can generate over connected or over damaged zones in the samples that increase its heterogeneity and the variability of the results. The authors also point that this damage mechanism is not of the same nature as what happens in the field. With respect to vacuum saturation, it is important to note that the (EN 12697-12, 2008) standard suggest that the pressure decrease within the desiccator needs to be done slowly as the sample could be damaged otherwise. Another disadvantage of this technique is that a special equipment for creating vacuum is needed, lowering its practicality.

Exposing the specimens to high temperatures is also a commonly use technique to accelerate moisture damage. Looking at standardized tests, the Lottman test, the modified Lottman test (AASHTO T 283, 2014) and the immersion-compression test (AASHTO T 165, 2002), they all include an immersion period of 24 h in a water bath at 60°C (Hicks, 1991). Complementary freeze-thaw cycles and immersion periods at room or test temperature are also present and difference one test from the other. The fact that a water bath at 60°C is common to all test methodologies highlights the accordance of the authors regarding the effectiveness of this technique for moisture conditioning of bituminous mixtures.

Exposition time to water is also very variable in the different available conditioning methods. According to (Kringos et al., 2009), exposition time has the objective to attain a certain saturation level in most of the conditioning methods, which is why it is commonly reduced by the use of vacuum saturation. However, the necessary time for the reaction between water, bitumen and aggregate at the interfaces is not normally taken into account. Exposition time to water needs then to assure a good saturation of the sample, given its interconnected voids, and also allow the moisture damage mechanisms to act on the binder-aggregate interface (detachment, displacement, spontaneous emulsification (c.f section 1.4.2)).

Duriez test includes a 7 days immersion period in a bath water at 18°C, which seems to be a long enough period to assure the saturation of the accessible voids. However, the bath temperature is rather low compared to the international practices on the subject. The use of water baths at 60°C can have multiple advantages. Such a high temperature softens the bitumen and the mastic, facilitating the action of the damage mechanisms. This also helps increasing the

saturation of the sample in a passive way as new connecting paths between voids can be created by stripping and detachment. Finally, the exposition to high temperatures causes ageing of bitumen and mastic which is a parallel distress to moisture damage that happens over time.

Long periods of submersion in water baths at 60°C can be found in the literature. (Barra et al., 2012) studied the fatigue resistance of moisture conditioned bituminous mixtures. The authors proposed a conditioning method including 5 days in a water bath at 60°C and 3 days in a temperature chamber at the same temperature. In order to simulate the pore pressure build-up in the samples, they vacuum saturated the samples before testing them using the two-point bending test. The results of the study showed a significant reduction in the fatigue life of conditioned samples as well as important evidences of effective stripping (un-coated grains at the fracture plan). These observations are evidence of the effective moisture damage caused by long periods of exposition to water at high temperatures. Nevertheless, the two-points bending tests need the samples to have a perfect geometry for the results to be correctly analyzed. Given the fact that the samples where conditioned after being sawed to their final shape, the long exposition to high temperatures (8 days in total) might have affected their geometry and, therefore, the fatigue test results.

(Arambula, Masad, Martin, et al., 2007) studied the behavior of moisture damaged samples conditioned with the modified Lottman test procedure without the freeze-thaw cycles. The authors carried out dynamic and relaxation tests on conditioned and non-conditioned samples and found that dynamic test results were not statistically different between the two groups of samples. With respect to relaxation tests, they found that tensile relaxation tests allowed differentiating the conditioned samples from the non-conditioned ones, whereas compressive relaxation test did not. These observations are consistent with the literature and with what is expected as the performance to tensile stress depends on the strength of the aggregate-binder interface which is weakened by moisture damage mechanisms. Compressive strength depends more on the inter-granular interaction which relies mostly on the gradation and density of the mixture. They concluded that neither dynamic nor relaxation tests were consistent in evaluating the moisture damage of bituminous mixtures. However, the authors agreed that the used conditioning method is not severe enough to alter the fundamental stiffness properties of the mixtures. Moisture susceptibility has to be assessed through a multi-parameter approach, taking into account mechanical, physical and chemical properties of the material.

The use of the complex modulus test mixed with the AASHTO T283 conditioning protocol was also treated in (Bausano & Williams, 2009) and in (Nadkarni, Kaloush, Zeiada, & Biligiri, 2009). In (Bausano & Williams, 2009) tests were carried out on cores from 21 different field mixtures. The authors compared the results from 5 non-conditioned samples with those from 5 conditioned samples for each mixture. The tests were done at a single temperature and at different frequencies from 0.1 Hz to 10 Hz. As for (Arambula, Masad, Martin, et al., 2007), the complex modulus values of the conditioned samples were not statistically different from those of the non-conditioned ones. Moreover, they carried out conventional ITS tests but these also failed in distinguishing the samples according to their condition. The same outcome was observed by (Gubler et al., 2005). The study by (Gubler et al., 2005) also showed that dense (7% voids content) bituminous mixtures presented no moisture damage using the the CoAxial Shear Test (CAST) while open graded (25% voids content) clearly did. They concluded that compacted specimens could limit the drop of modulus in wet conditions because they present more contact

points between the aggregates, low permeability and mechanical interlocking. These characteristics are specially potentiated in gap-graded mixtures. As for the study by (Nadkarni et al., 2009), the authors conducted modulus tests on the same sample before and after conditioning, highlighting the interest of the non-destructive character of the test. They concluded that the retained stiffness ratio between conditioned and non-conditioned samples was able to systematically identify moisture damage. However, the communication on this study does not specify the complex modulus test loading mode and is confusing on the test temperatures used before and after conditioning. Based on the information given, the complex modulus test is more likely to have been done in constant compression and not in tension-compression since the samples don't seem to have been glued or attached to the hydraulic press. The inconvenient of this kind of tests is that they can cause permanent deformation or damage in the sample due to the constant compressive stress. Assuming that the temperatures of the complex modulus tests were identical for the dry a wet specimens, the conclusions from this study need to be verified since information on the methodology is missing.

All these studies agree though in the fact that testing bituminous mixtures for moisture susceptibility need to be done using mechanical tests that allow accessing fundamental properties of the material and implementing a conditioning procedure that is severe enough to accelerate the moisture damage mechanisms without causing damage of other natures. The conclusion on the good or bad performance with respect to moisture damage has to be done taking into account multiple parameters and not just one performance ratio. These parameters can include performance results from different tests and visual observation of stripping, for example. The test methodology needs to be calibrated with field observations.

Another aspect of importance is the ageing of the material with time. In fact, moisture damage and ageing occur simultaneously during the lifetime of a pavement structure and influence each other. Some of the studies reviewed include ageing periods of the loose or compacted samples within their conditioning procedures. The most common way to accelerate ageing of bituminous materials is by subjecting them to high temperatures during specific periods of time (Barra et al., 2012; He & Wong, 2008; Lottman, 1978). A brief dissection on ageing is presented hereafter.

1.4.5. Ageing of bituminous mixtures

As seen before, ageing refers to the variations of the chemical composition of bitumen in the mixture. Ageing in pavements occurs in two ways:

- Short term ageing: It occurs during heating, mixing and laying of the bituminous mixtures during the construction of a pavement structure.
- Long term ageing: It happens during the service life of the materials in the pavement structure. It is then influenced by the service conditions of the structure.

The main triggers of ageing are the exposition to oxygen and the ultraviolet radiation. Ageing is then presented as a hardening of the bituminous materials due to oxidation and exposition to radiation, reason why there is usually an ageing gradient decreasing with the depth of the bituminous structure. This hardening makes it easier for the moisture damage mechanisms to act and weaken the cohesive and adhesive bonds of mastic and bitumen with the aggregate (Das, 2014; Das et al., 2015). Wearing course materials are highly exposed to UV radiation

whereas base-course mixtures are usually aged by oxidation. In a ballasted railway track configuration, UV radiation of the base-course materials should not be an issue.

Oxygen diffusion in bituminous mixtures is catalogued as a very complex process, the same as moisture diffusion. It depends, amongst other factors, on the voids distribution in the mixture, temperature and pressure. The oxidative process can be described through three phenomena. The first is fragmentation, where bitumen molecules break into smaller fragments generating volatile by-products such as H_2O, CO_2 and CH_4 which eventually leave. The second phenomenon is the oxygen addition that creates carbonyl and sulphinyl groups in the bitumen. The third phenomenon is the formation of larger molecular weight and aromatic molecules, called condensation or carbonization. The association of large molecules creates less soluble hydrocarbons in n-alkane medium. The loss of volatile molecules and the association of large molecules increase the viscosity of bitumen which explains its hardening (Petersen, 1993). Fine filler mineral particles in the mastic can act as a catalyzer of the bitumen ageing process (Das, 2014).

As described in section 1.1.3.5, the RTFO (AASHTO T240, 2013) and the PAV (AASHTO R28, 2012) test procedures are used to simulate short and long term ageing of bitumen, respectively. The PAV procedure is based on the time-temperature superposition principle to accelerate the ageing of bitumen through the exposition to severe high temperatures and pressure conditions. According to (Houston, Mirza, Zapata, & Raghavendra, 2005; Xiaohu, Talon, & Redelius, 2008) the ageing of bitumen by using high temperatures and pressure is fundamentally different from what happens to bitumen in real service conditions. These accelerated ageing procedures do not provide a direct relationship of ageing with time, which is needed as to predict the evolution of the materials performance with time (Das, 2014). Prediction models predict the viscosity of aged binders based on air temperature, initial viscosity, pavement depth and voids content. However, as stablished by (Das, 2014), air voids distribution, connectivity and, in general, the internal structure of bituminous mixtures have an important influence on the material aging.

In the state of the art report on ageing test methods for bituminous materials stablished by (Airey, 2003), different ageing procedures on bituminous mixtures were identified. Many of the test methodologies use extended heating methods based on the ageing through volatilization. Out of 9 identified procedures carried out on compacted samples, 6 of them conserved the samples at 60°C during long periods of time (5 to 10 days) (Airey, 2003; Khalid, 2002; Kim, Bell, Wilson, & Boyle, 1986; Kumar & Goetz, 1977; Von Quintus, Scherocman, & Hughes, 1989).

2

Case study:

The East-European high-speed line test zone with bituminous sub-ballast layer

2.1. Context

In 2004, as part of a research project on track structure improvement, the French National Railway Company (SNCF) built a 3 km long experimental zone with a bituminous mixture sub-ballast layer in the first phase of the East-European High-Speed Line (EE HSL) that connects Paris with eastern France.

Two major advantages of using a bituminous sub-ballast layer in the platform design were identified by the SNCF prior to the construction of the EE HSL test zone.

The first one was the possibility of using this layer as an access way to the construction site. The circulation of engines during the construction phase of a regular HSL, for the installation of catenary poles for example, can damage the platform made only with unbound granular materials (UGM). Moreover, the circulation must be stopped during bad weather. These problems are avoided when the sub-ballast layer is made of bituminous mixture, which facilitates respecting the project planning.

The second one was the reduction of the trackbed height. From an economical point of view, the design solution including a bituminous platform becomes of interest when good quality granular materials lack nearby the construction site. Locations far away from the production sites are associated to very high transportation costs for specific granular materials. In such locations, the reduction of the platform height conferred by the use of a bituminous layer can lead to significant savings. The cost associated to the construction of a track with bituminous mixture sub-ballast layer can be equivalent or sometimes even lower than those associated to the construction of a UGM track structure.

Added to these two advantages, the SNCF expected a better mechanical performance of the test track with respect to conventional ones. To verify this, they instrumented the track with as set of stress and strain sensors. The analysis of the obtained data showed that the bituminous test track presented an excellent mechanical behavior. Moreover, the test zone has presented until now a similar, or even better, behavior in terms of maintenance and security to that of the best behaving conventional zones under similar conditions.

Having confirmed the good performance of the test zone, the SNCF established a technical referent document [IN 8102] that adds the bituminous platform design as an option for HSLs in France. This has encouraged SNCF Réseau, the manager of the French railway network, to further develop the use of bituminous materials in its network. As a result, at this moment, four new major HSL projects are being built, partially or completely, with bituminous mixtures in France and another one in Morocco (Groupement Professionnel des Bitumes, 2014). These projects are:

- The East-European HSL (phase 2) – 55 km (52%) of sub-ballast bituminous layer. In service by mid-2016.
- The Brittany-Loire (BPL) HSL – 105 km (58%) of sub-ballast bituminous layer. In service by 2017.
- The Southern Europe-Atlantic (SEA) HSL – 43 km (14%) of sub- ballast bituminous layer. In service by 2017.
- The Nimes-Montpellier (CNM) HSL bypass – 80 km (100%) of sub- ballast bituminous layer. In service by 2017.

2.1.1. Description of the EE HSL test zone (structure, traffic, materials)

The EE HSL (phase 1) has been in service since June 2007. It consists of a 300 km long ballasted track that goes from Paris to Beaudrecourt, in the Champagne region. By mid-2016, it will be connected to the second phase of the EE HSL project which will cover the remaining 106 km to Strasbourg, at the French-German border. The EE HSL is part of the railway network that connects France with Germany, Luxembourg and Switzerland. French TGV-R, TGV-POS and German ICE3 trains circulate this line at commercial speeds up to 320 km/h. By 2013, its average annual daily traffic (AADT) was estimated at 112 trains per track. Different trains have different spacing between axles and different rolling speeds, as seen before, the geometry and the speed of the train define the excited wavelengths and the loading frequency. Since the bituminous materials behaviour depends on the frequency, it is important to know the characteristics of the circulating trains on the track.

The test zone with sub-ballast bituminous layer, built in the EE HSL (phase 1), is located near the city of Reims. It is 3 km long and comprises straight and curve alignments in cutting and embankment configurations. It is comprised between the kilometric points KP 109,052 and KP 112,052. Four segments of the test zone were instrumented as follows:

- KP 108.705 - Reference zone: Curve alignment (6667 m in radius and 127 mm of cant) in level ground without bituminous material.
- KP 109.205: Curve alignment in cutting with sub-ballast bituminous layer.
- KP 109.755: Curve alignment in embankment with sub-ballast bituminous layer.

- KP 110.605: Straight alignment in level ground with sub-ballast bituminous layer.

The results presented in this chapter correspond to those recovered from the two segments in level ground. The KP 108.705 segment has a conventional track structure with only UGM, which will hereafter be called conventional track. It serves as reference zone. The other segment has a bituminous sub-ballast layer and henceforth will be called bituminous track.

The bituminous mixture layer is 14 cm thick and 10.7 m width. The bituminous mixture was called *grave-bitume plus* (GB+) and it would correspond to a GB3 with and enhanced resistance to fatigue. The mixture has a complex modulus norm value of 10 416 MPa at 15°C and 10 Hz and an ε6 value of at least 110 µm/m at 10°C and 10 Hz at the two-points bending tests on trapezoidal samples. This high fatigue resistance differentiates this mixture from the classical GB3. The maximum nominal aggregate size is of 20 mm. It has a 5% binder content of 35/50 grade bitumen. The layer was compacted with a vibrating roller compactor to a target air void content of 3%. Compared to the conventional track, the height of the bituminous track structure was reduced of 16cm (Marmier, 2005; Robinet & Cuccaroni, 2012) (c.f. Figure 2.1).

The bearing capacity of the granular materials sub-grade under the bituminous mixture is of at least 120 MPa.

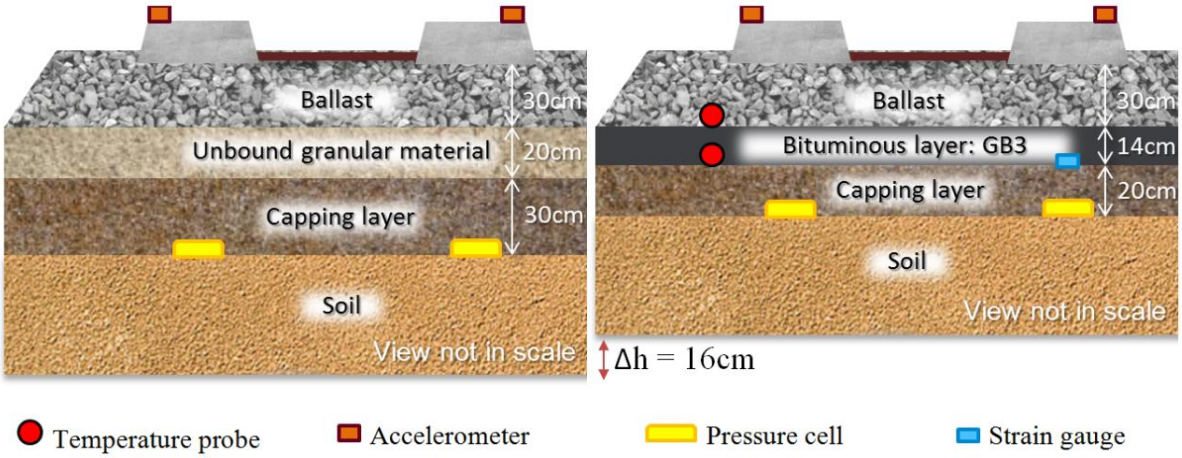

Figure 2.1. Scheme of the instrumentation and structure configuration of the conventional track (left) and of the bituminous track (right) of the EE HSL test zone.

2.1.2. Test zone instrumentation

Figure 2.2 shows the instrumentation plan of the EE HSL test zone, which was made in 2005 during the earthworks construction. The site was instrumented in order to follow the behaviour of the test track and to validate the design hypothesis (calculated efforts at the soil, estimated service life, etc.). Both conventional and bituminous tracks were instrumented with the following sensors:

- Accelerometers on sleepers to measure their vertical acceleration. The speed and the total displacement of the sleepers were calculated from the acceleration data by double integration.
- Stress gauges on the rails to measure the applied load by the passing train.

- Pressure gauges at the top part of the earthworks to validate the design hypothesis of stress transmitted to the soil.

The bituminous track was also equipped with the following sensors:

- Temperature probes to measure the ambient temperature and that of the bituminous layer. Since the behaviour of bituminous mixtures is temperature dependant, temperature is a key parameter when analysing the behaviour of the bituminous layer.
- Strain gauges in the longitudinal and transversal senses at the bottom of the bituminous mixture layer to validate the design hypothesis of strain developed in the bituminous layer. This strain has to be lower than that which causes the fragile fracture of the material or the fatigue failure before the design lifetime is attained.

Figure 2.2 presents a detailed instrumentation plan of the bituminous track, in cross and plan views, at the KP 110.605.

The used accelerometers are piezo-resistive ones with a measurement range of ±50 g. The used load gauges work on the principle of measuring the strain difference between two different points of the rail over time while the train passes. The difference is called “Q Bridge” and it is proportional to the load applied by the passing axle. It is a method commonly used to determine the tonnage of vehicles. The pressure cells at the top of the earthworks operate on the strain gauge measurement principle with a measurement range of 500 KPa. The temperature probes are of type PT100-A, with a measurement range of -20°C to 200°C.

Finally, the strain gauges embedded in the bituminous mixture layer are unidirectional ones of type KM-100HB from the company TML. They have low modulus (400 kgf/cm^2) and a measurement range of ±5000 μm/m. Being waterproof, they are specially designed to be embedded and to assure long term use. The gauges are 10 cm long inside a 2 cm in diameter cylinder. They are mounted on collars at both ends, as shown on Figure 2.3, which are used for fixing the gauge so it doesn’t move during the compactor passing. They were placed in the same vertical axis as the pressure cells.

As seen in Figure 2.3, the disposition of the strain gauges in the bituminous layer does not allow measuring the strain at the bottom part of the layer due to the distance between the axis of the gauge and the bottom (approximatively 2.5 cm). The mounting system also includes rigid steel plates that could alter the local deformation of the material. Moreover, the proximity of the temperature probe to the sensor and the size of the sheath for the connection cables might also alter the materials local response. The strain measurements from this experimentation are to be interpreted taking into consideration these observations.

The presented data in this chapter was taken from the campaign carried out on August 25 of 2009. The data corresponds to the passing of a TGV-R train.

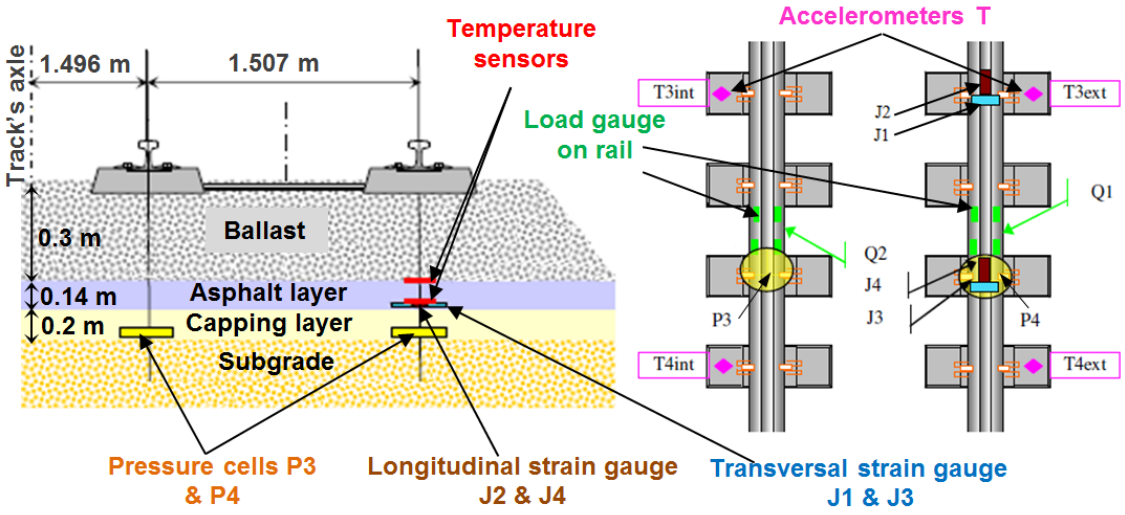

Figure 2.2. Instrumentation of the EE HSL bituminous track: Transversal plan (left) and top plan (right) (Not in scale) (Adapted from an internal document of the SNCF)

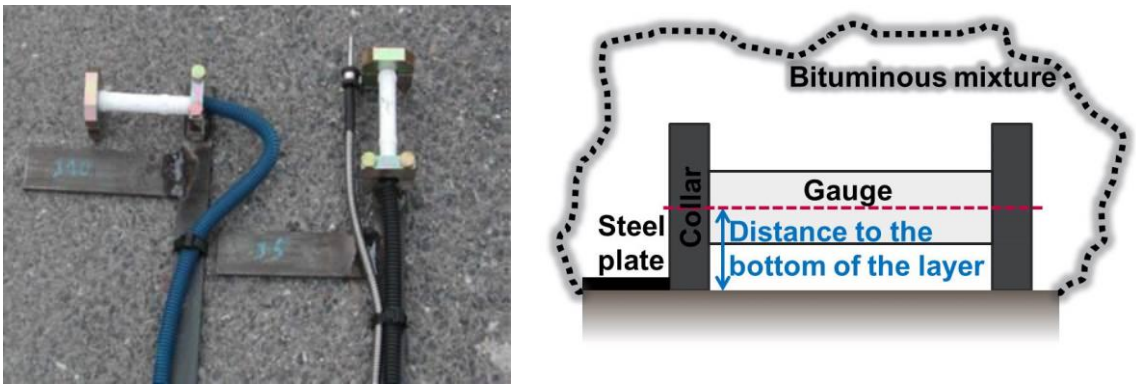

(a) (b)

Figure 2.3. Disposition of the strain gauges at the bottom of the bituminous mixture layer of the EE HSL test zone (a) (source: internal document of the SNCF) and schematic representation of the embedded gauge (b)

2.1.3. Numerical modelling of the EE HSL test zone

The finite element software GEFdyn (Aubry & Modaressi, 1996) was used to simulate the behaviour of the bituminous and conventional tracks. The results from this simulation are presented and compared to the measurements recovered from the EE HSL test zone in section 2.2. This numerical simulation work was carried out in order to validate the strain measurements obtained from the extensometers placed at the bottom of the bituminous layer.

The loading case used for the simulation reproduces the geometry of the loading induced by a French high-speed train (TGV) circulating at 320 km/h. The wheel load used was of 85 kN. The track geometry and loading cases used in the model match those found in real French high-speed lines. Straight alignment was considered for both conventional and bituminous tracks.

A 2.5-dimensional FEM of the track structure with a modified width plane strain condition was used. The calculations were made by the SNCF's Innovation & Research department. The full track system is composed, from top to bottom, of: a rail (beam element), under-rail pads,

concrete sleepers, unconfined ballast between the sleepers, confined ballast under the sleepers, sub-ballast layer, capping layer and the subgrade. The track mesh, whose extract is presented on Figure 2.4, is 72 m long, 4.3 m width and 8m high from the top of the rail to the bottom of the soil. An absorbent material was added at the lateral boundaries to avoid wave reflexion effects (viscous material). The displacements are nil on their normal directions to the boundaries (i.e. u_y=0 at the lateral boundaries, and u_z=0 at the bottom boundary). The mesh is loaded only from the 6th meter to the 66th one in order to avoid boundary effects. A dynamic computation is made in the time domain using the Newmark integration scheme.

Each element of the mesh is 3 cm long with variable height according to the necessary observation points at each layer. The sleepers are 30 cm width and are distanced 60 cm from one another's centre. The periodic cell is then defined as a repeated 60 cm long ensemble including a rail portion with its under-rail pad, a complete sleeper, part of the unconfined ballast and all the track's granular layers. Regarding the constitutive models, elasticity was chosen for all the materials of the track and substructure, including the bituminous mixture. This numerical simulation is then a simplified calculation to estimate the strain levels at the bottom of the bituminous layer taking into account the bituminous mixture properties at 15°C and 10 Hz, the values set by the French design method.

30cm	Ballast	200 MPa
20cm	UGM	200 MPa
30cm	UGM	200 MPa
700cm	Soil	80 MPa

Conventional track

(a)

30cm	Ballast	200 MPa
14cm	**Bituminous mixture**	**9 600 MPa**
20cm	UGM	200 MPa
700cm	Soil	80 MPa

Bituminous track

(b)

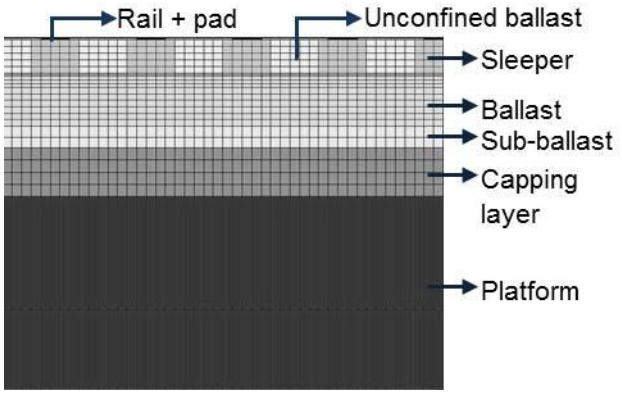

(c)

Figure 2.4. Schematic diagram and parameters of the materials for the simulation of the conventional (a) and bituminous (b) tracks; and extract of the mesh for FEM calculations(c) – (Not in scale)

2.2. Feedback from the EE HSL test zone

The recovered data from the EE HSL instrumented test zone provided interesting feedback on the behaviour of the bituminous sub-ballast layer. The measures from the different sensors are presented as well as the observations regarding maintenance needs of the bituminous track and vertical track stiffness.

The measurements presented in this section correspond to the passing of a French TGV train at 317 km/h. This kind of train is composed of two locomotives, one at the head and one at the rear with two bogies each. There are eight coaches between the locomotives, with one bogie between two coaches. Each bogie is composed of two axles. The locomotive's bogies weight 17 ton, while the coaches' ones weight 16 ton. The wheels axes of a bogie are spaced of 3 m. The coaches are 18.7 m long and the locomotives are 22 m long. The experimental measurements in this section are presented only for the coach bogie located in at the middle of the reference TGV.

All the figures respect the geotechnical conventions for stress and strain (positive values in compression and contraction).

2.2.1. Vertical loads and circulation speed

The load applied by the circulation TGV in both conventional and bituminous instrumented zones is shown in Figure 2.5. These were measured by the load gauges on the rails. The measured load applied to the rail (Qz) was 82.4kN and the train's speed was 317km/h. These values are very similar to the loading case used for FEM simulation.

Both signals present similar load amplitudes as expected since the passing train is the same for both zones. Loading conditions of both zones are then similar and further comparisons of other sensor measurements are then possible.

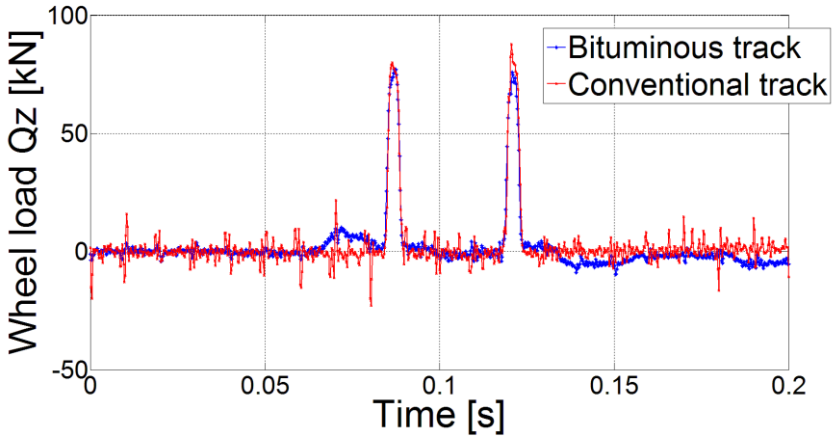

Figure 2.5. Measured wheel load of at the EE HSL test zone – Coach Bogie signal filtered 160Hz (Ramirez Cardona et al., 2014)

2.2.2. Pressure at soil level

The pressure level measured at the top part of the earthworks of the conventional track was 70% higher (22.3kPa) than that of the bituminous track (c.f. Figure 2.6). This could be attributed to the beam-like load transfer mechanism of the bituminous layer compared to compacted soil.

Ballast indentation in the bituminous mixture is also believed to increase load network in the ballast, which leads to a better load distribution to the sub-ballast. These factors contribute to the pressure reduction at the soil level. Thus, the presence of the bituminous sub ballast layer reduces the aggressiveness of the load applied by the circulating trains at the soil. This would increase the lifetime of the subgrade.

The amplitude of the FEM stress simulation results is very similar to that measured by the pressure cells. The FEM reproduces very well the stress signal measured by the pressure cell in the conventional track without bituminous sub-ballast. The differences between the simulation curves and the measurements of the bituminous track may rely on the fact that the bituminous mixture was simulated as an elastic material. This is an evidence of the importance of introducing the viscoelastic model for bituminous mixtures in FEM studies.

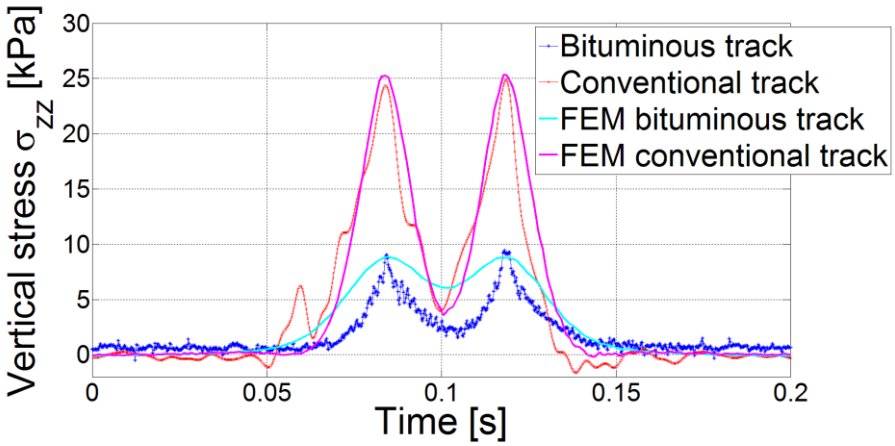

Figure 2.6. Vertical stress at the bottom of the capping layer for both bituminous and conventional tracks – Measurements and FEM simulation - Coach Bogie signal (Ramirez Cardona et al., 2014)

2.2.3. Sleepers vertical acceleration and vertical track stiffness

Figure 2.7 presents the measurements from the external accelerometer in the T4ext position (c.f. Figure 2.2) of both conventional and bituminous tracks. A low-pass elliptic filter at 160Hz was used to treat the raw data. The bituminous track presents lower vertical acceleration peaks of the sleepers than the conventional one. This is a clear evidence of the stabilizing role of the bituminous layer since lower displacements of the sleepers are expected. These results are in accord with the results from (Di Mino et al., 2012).

The FEM simulation results correspond well to the measurements, which validates the use of the simulation results for further calculations, such as vertical rail displacement for the determination of vertical stiffness.

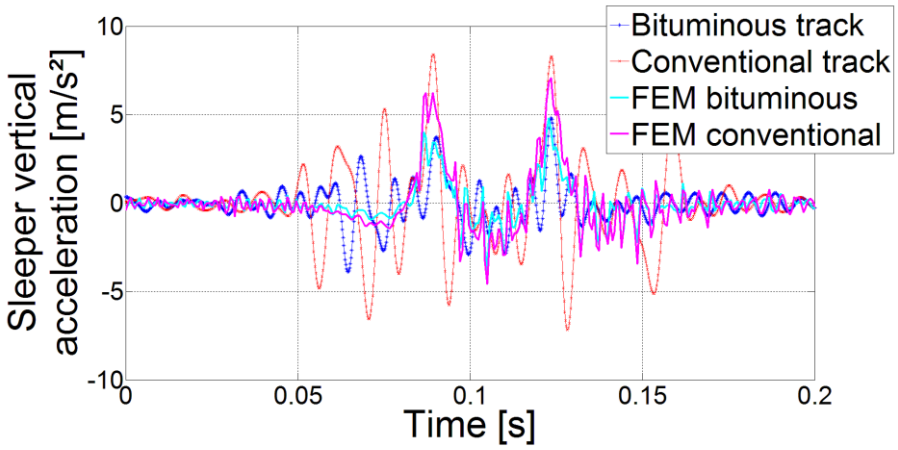

Figure 2.7. Sleeper's vertical acceleration measurements or both bituminous and conventional tracks – Measurements and FEM simulation - Coach Bogie signal filtered 160Hz (Ramirez Cardona et al., 2014)

Vertical track stiffness is an important design parameter for railway tracks. It is defined as the ratio between the vertical force applied by the wheel on the rail and the vertical rail displacement. Vertical stiffness of the bituminous and conventional tracks was calculated by numerical simulation, exposed in section 2.1.3. The bituminous track was found to be only 7.3% stiffer than the conventional one, which is in accord with the observations of a previous study made by the SNCF (Laurens, 2014). This study used the principle of the Swiss EWM measurement wagon to measure the global track stiffness of two French HSLs, including the phase 1 of the EE HSL. The principle of the EWM method is to compare the setting of the loaded track section by the wagon and that of an unloaded section. The wagon axle load is 20 ton and it takes continuous measurements while circulating at 20 km/h to 30 km/h. The study identified a clear correlation between vertical stiffness variations in the track and track degradation.

The setting measurements at the EE HSL test zone don't present a particularly different values or profile from that of adjacent conventional track sections. However, the vertical stiffness standard deviation of the test zone was found to be 40% less compared to the conventional track sections (Laurens, 2014).

Considering the hypothesis of a perfectly elastic track, this stiffness homogeneity would mean a substantial reduction of the differential settings of the bituminous track under dynamic loading. Nevertheless, the behaviour of bituminous mixtures is viscoelastic and dependent on the temperature and loading frequency conditions. Therefore, the observed considerable reduction in stiffness standard deviation can only be associated to the loading conditions at the time of the measurements, especially the loading rate of the wagon circulating at 20 km/h. This is a very low circulation speed compared to the 320 km/h service speed of the EE HSL. Other standard deviation values are expected for higher loading rates of high-speed trains.

Nonetheless, the study highlights the influence of the viscoelastic behaviour of the bituminous material on the global track response.

2.2.4. Temperature

The temperature measurements in the bituminous mixture layer from 2007 to 2013 are condensed in Figure 2.8. The ambient temperatures over the measurement period are rather mild, with no important occurrence of high or low temperatures. The bituminous mixture, however, does not show the same temperature occurrence pattern as the environment. Two occurrence peaks are distinguished: 7°C and 16°C. This means that the bituminous material presents a mild temperature in both winter and summer. It never freezes, as no negative temperature measurement was made in the bituminous layer, and it rarely exceeds 20°C. (Trinh, 2011) had already verified the anti-freeze protection role of the ballast.

The choice of a simplified numerical calculation using the material properties at 15°C is then not far away from the real conditions of the material in the test zone.

The research by (Rose et al., 2002) showed similar temperature measurements for a bituminous sub-ballast layer in Kentucky, USA. The maximum temperature of the bituminous mixture was 24°C during the summer and the minimum was 2°C in winter. The authors concluded that the track configuration creates a very effective protection of the bituminous mixture with respect to temperature as highway pavements can reach extreme temperatures of 50°C to -17°C in the same region.

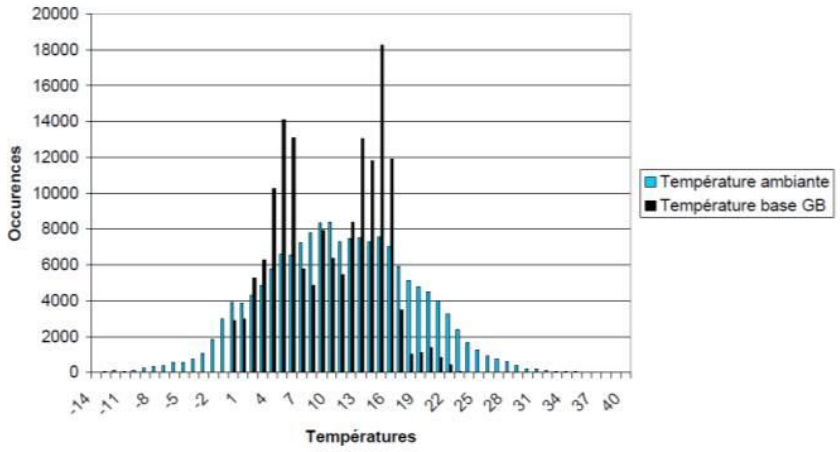

Figure 2.8. Occurrence of ambient temperature and temperature in the bituminous mixture layer of the EE HSL (source: internal document of SNCF)

2.2.5. Strain levels at the bottom of the bituminous layer

Figure 2.9 shows the longitudinal strain measured by the gauges in the J2 and J4 position in the bituminous layer (c.f. Figure 2.2). The FEM calculation results are also exposed. Strain at the bottom of the bituminous layer is a crucial parameter for the design of bituminous structures.

The FEM simulates relatively well the measured strain amplitude at the bituminous layer when loaded by a passing TGV train bogie at 320 km/h. The maximum measured tension strain amplitude is close to 2µm/m. The numerical results show a total relaxation in between axles while the experimental measurements do not. Both the calculations and the experimental measurements show a small compression phase before and after the passing of the train bogie.

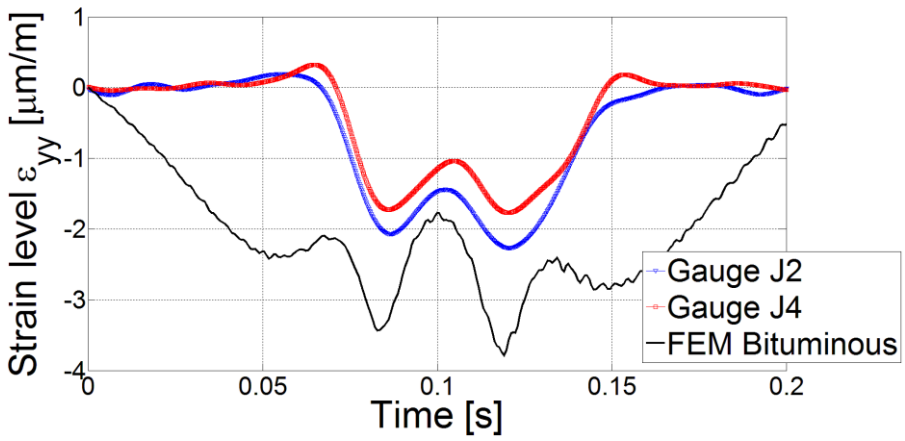

Figure 2.9. Strain levels at the base of the bituminous layer: numerical calculations and measurements from the EE HSL test zone

From the road industry experience, the amplitude of strain signals at the bottom of bituminous pavements is considered between 30µm/m and 40 µm/m for road loading and circulation conditions. The research held by (Gaborit et al., 2014) studied the strain created by a 13 ton/axle truck at different depths of the pavement structure. The truck circulation speed varied from 20 km/h to 90 km/h. The strain gauges used for this project are of type ASG-152 from the company Construction Technologies Laboratories (CTL). These have a rather flat configuration in I form which allows placing them as close as possible to the bottom of the layer while assuring a good anchorage inside the material. These gauges were placed at 19 cm from the road surface in comparison to the gauges used on the EE HSL, placed at 44 cm from the ballast surface. (Gaborit et al., 2014) observed a reduction of the strain with the increase of the circulation speed. They observed strain levels going from 25µm/m, for a circulation speed of 12 km/h, to 9µm/m at 70km/h.

Moreover, (Rose et al., 2002) found that the beam action of the rail, which distributed the wheel loads over several sleepers and then to the well confined stiff ballast layer, effectively reduces the axle loadings effect on the bituminous layer which acts also as a beam when transmitting the load to the subgrade. They concluded that the pressures applied at the sub-ballast bituminous layer are only a fraction in magnitude of the typical pressures applied by road traffic at the surface of a highway pavement. They further concluded that the sub-ballast bituminous layer should have extremely long fatigue life given the low load-induced pressure levels.

These observations, even if they do not correspond to the circulation of a TGV on a HSL, serve as reference to validate the order of magnitude of the experimental measurements at the EE HSL test zone.

2.2.6. Maintenance needs

One of the most interesting observations from the feedback on the EE HSL test section concerns maintenance needs. In service since June 2007, it has needed few maintenance operations compared to neighbouring conventional track sections that are considered as equivalent.

Moreover, the efficiency of the tamping operations in readjusting the track's geometry is also increased with respect to the zones with UGM platforms.

Track geometry can be defined as the difference between the real position of the rail and an average reference position. The parameters that describe this geometry are called vertical, or longitudinal, levelling (VL) and transversal levelling (TL). Vertical levelling defects are a geometrical error in the vertical plane defined as the distance between a point at the top of the rail in the running plane and the ideal average line of the longitudinal profile (Caetano & Teixeira, 2015; Guler, 2014; International Union of Railways, 2008). Poor vertical levelling impacts travel comfort and increases dynamic surcharges. The evolution of the vertical levelling (ΔVL) is expressed in terms of its increase per year. An increase in VL indicates a modification of the track's geometry, usually associated to problems in the mechanical behaviour of the track (Laurens, 2014).

The comparison in terms of maintenance needs between the conventional and the bituminous tracks is based on the standard deviation of the VL, which is considered as the most representative measurement for track quality. Figure 2.10 and Figure 2.11 show the standard deviation of the averaged vertical levelling over time for two sections of 1 km of the EE HSL. In French HSLs, the track-surveillance IRIS 320 TGV train is used to measure the longitudinal profile of the track. The increase of the standard deviation of the vertical levelling measurements is a clear evidence of track degradation.

Figure 2.10 can then be interpreted as the track degradation curve from 2007 to 2016 for the conventional track of the EE HSL test zone. Figure 2.11 presents the same information for the bituminous track structure. In both graphs, grinding and tamping operations are represented by vertical green and red lines, respectively. The kilometric points KP where the operations were carried out are also indicated.

For the following analysis, it is pertinent to remind that traffic and weather conditions have been identical over the service life of both neighbouring sections. The bituminous track section corresponds to the instrumented one in straight levelling and level ground (KP 110.605). The conventional track section is also in straight levelling and level ground but at the KP 112, which is out of the instrumented zone.

Grinding (green solid lines) is done as preventive maintenance operation for long track sections in French HSLs, even if no particular defects are present. It aims to correct the short wavelength defects of the rail surface. Hence, the two adjacent sections were grinded at the same times and for the totality of their length.

Tamping (red dash-dot lines), on the contrary, can be carried out either on singular points or on longer sections presenting particular geometry problems. Tamping operations are launched if the vertical levelling standard deviation reaches a threshold value that indicates dangerous track degradation. This threshold value is set to 0.9 for the French HSL. From Figure 2.10, 10 mechanical tamping operations over more than 100 m of track have been made since 2007 on the conventional track (KP 112). During the same 8 years of service, only 1 mechanical tamping was carried out in the bituminous track (KP 110 – c.f. Figure 2.11).

The slope of the degradation curve can be interpreted as the degradation rate of the track. For comparison purposes, this slope was calculated by linearly fitting the standard deviation values

over the first 3 service years. The degradation rate of the bituminous track is 37.5% lower than the conventional track's.

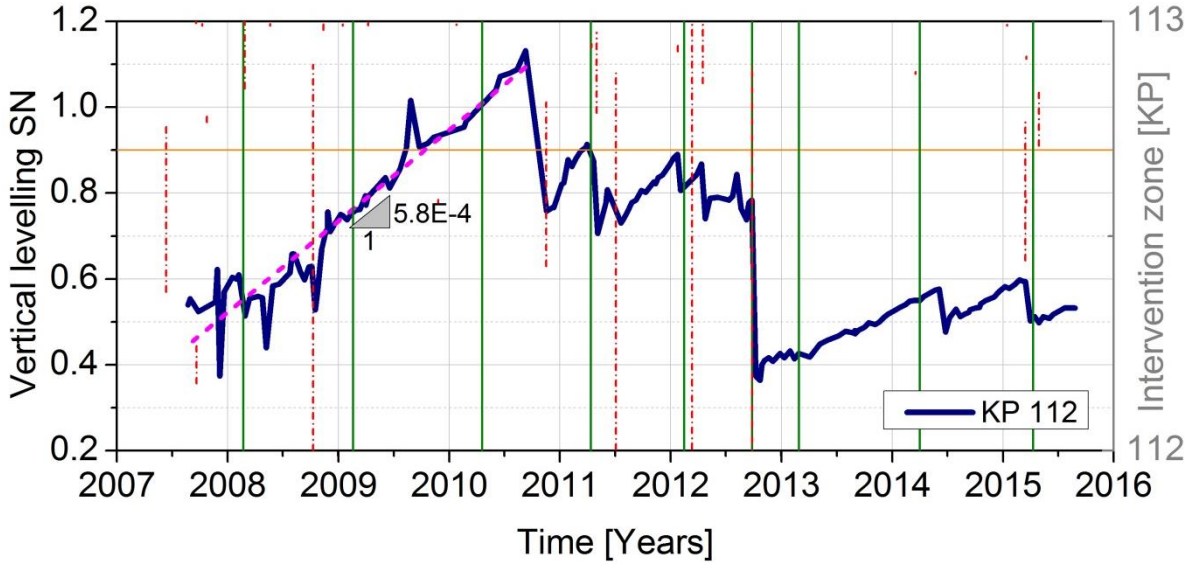

Figure 2.10. Vertical levelling (bold line) variation over time for the conventional track structure and maintenance operations of the KP112: grinding (green vertical solid lines) and tamping (red vertical dash-dot lines) (Ramirez Cardona et al., 2016).

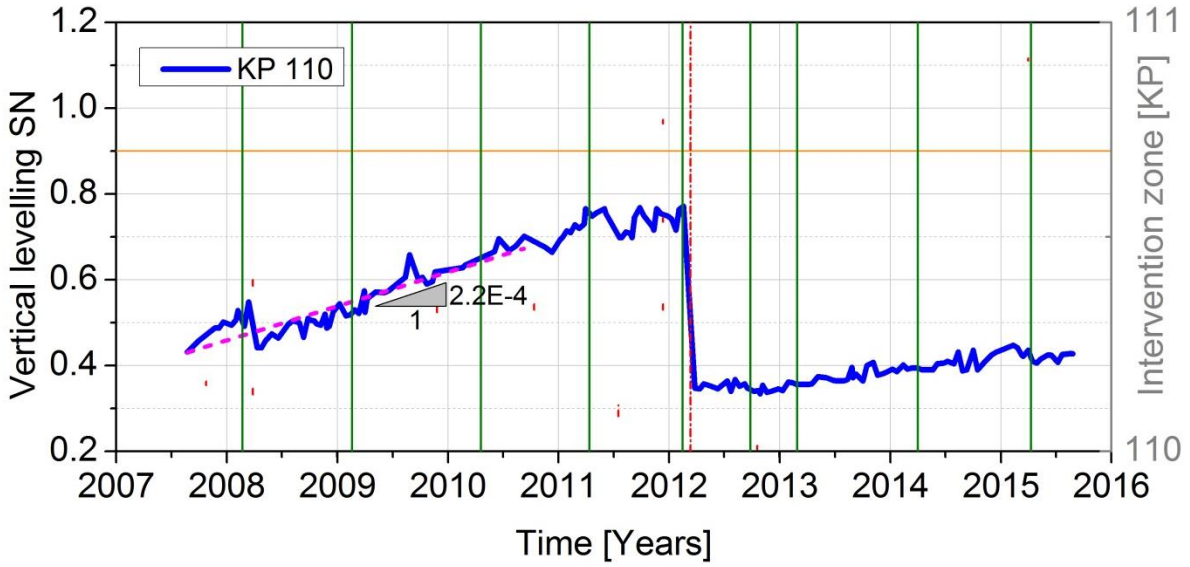

Figure 2.11. Vertical levelling (bold line) variation over time for the bituminous track structure and maintenance operations of the KP110: grinding (green vertical solid lines) and tamping (red vertical dash-dot lines) (Ramirez Cardona et al., 2016).

The lower track degradation rate of the bituminous track is clear evidence that it degrades more slowly than the conventional one. Nevertheless, geometry degradation not only depends on traffic characteristics (load and speed), weather conditions or construction methods and materials but also on the maintenance history of the track (Antoni, 2010; Audley & Andrews, 2013; Selig & Waters, 1994). The multiple tamping operations carried out in the conventional track have to be also considered when analysing the track deterioration as it is an aggressive

operation that leads to the breakage of the ballast grains and, therefore, to a reduction of the internal friction of the ballast.

The influence of tamping on track degradation was studied by (Audley & Andrews, 2013). They analysed maintenance records from the UK railway network and found that tamping accelerates the ballast degradation as well as that of the global track. They also remarked that the chances of achieving a certain track geometry quality after maintenance are lowered after each tamping operation, especially for HSL. Maintenance needs were then observed to increase with time in conventional HSLs. Similar observations were made by (Guler, 2014) who distinguishes three phases of the lifetime of tracks. Many factors were identified as determinants of the duration of each phase, amongst which the number and scale of tamping operations is highlighted. In particular, the "old" phase is characterised by lower efficiency of tamping, increase of deterioration rate and material fatigue and breakage.

The effect of the tamping operations on the track degradation is clearly observed in both Figure 2.10 and Figure 2.11. Lower standard deviation values are observed after each tamping operation, which is expected as tamping attempts to reset the track geometry by rearranging the ballast. However, during the first three and a half years, the conventional track deteriorates fast even after tamping has been done. It presents a more stable behaviour after mid-2011, although with standard deviation values close to the intervention threshold of 0.9. After the tamping operation in late 2012, the standard deviation values decreased and the observed profile is more even. This could indicate that the ballast of the conventional track might have reached its optimum arrangement between 2011 and 2012. The optimal stabilization of the ballast on a compacted UGM layer might take between 6 to 7 years.

The tamping operations made before 2013 might have altered the ballast and reduced its internal friction which would explain the non-negligible deterioration rate of the conventional track after 2013.

As for the bituminous track, its initial quality was almost entirely recovered after the unique tamping operation and, most interesting, with a degradation rate close to zero. The even and low degradation profile of the bituminous track since the HSL opening might indicate that the bituminous layer allows the ballast to rapidly reach its optimal arrangement. The low degradation rate after the tamping operation of 2012 is proof of the integrity of the ballast after 8 years of service.

The viscoelastic properties of the bituminous material and the increased force network in the ballast, due to ballast indentation, might contribute to these improvements.

3

Tested materials and experimental procedures

The objective of the experimental work in this study is to determine whether the available bituminous mixtures present appropriate thermomechanical properties for their use in railway trackbeds. Different parameters are taken into account: bearing capacity, temperature dependence, effect of circulation speed (loading frequency), expected lifetime and moisture susceptibility. Three different bituminous mixtures were studied. Two of them, the GB3 and GB4 formulations, correspond to commonly used road base-course materials in France. In the formulation of the third studied mixture, the GB PMB, polymer-modified bitumen replaces the base bitumen of the GB3 formulation. A moisture conditioning procedure is proposed based on the results from the literature review. This procedure was used to condition the samples in order to assess the moisture susceptibility of each material through complex modulus and fatigue tests.

This chapter includes a description of the tested materials and a presentation of the experimental procedures carried out on these materials to characterize their linear viscoelastic behaviour and fatigue resistance properties. The used experimental devices allow studying the behaviour of bituminous mixtures in the small strain domain at different loading frequencies and temperatures.

3.1. Tested materials

A detailed description of the used materials is presented in this section. Three different bituminous mixtures were studied: GB3, GB4 and GB PMB.

3.1.1. Aggregate selection

The used coarse and fine aggregates come from the Baglione rhyolite quarry in the Mayenne department located in north-western France. Rhyolite is a silica-rich rock with an acidic nature.

Aggregates with this nature were chosen as they are commonly used in France for the formulation of high-quality bituminous mixtures. Aggregates from this quarry were also used in the formulation of the bituminous mixture used as sub-ballast layer of the Brittany-Loire HSL. All mixtures have a maximum nominal grain size of 14 mm (0/14).

The used filler comes from the Haut Lieu quarry in the Nord department located in Northern France. This filler is calcareous, as it is common in French bituminous mixtures formulations. Figure 3.1 shows the grading curves of the three studied mixtures. Table 3-1 summarizes the composition of the aggregate structure of the bituminous mixtures. The GB3 and GB PMB formulations have the same exact aggregate structure (same aggregates and grading curve). The GB4 mixture has a discontinuity of the 2/6 fraction which is intended to improve the density of the mixture and to increase the inter-aggregate contact of the coarse fraction. The fine particles content of each of the two different aggregate natures present in the mixtures (acidic from the rhyolite and basic from the limestone) is shown in Table 3-2. The higher fine content of the GB4 also helps in its densification. GB4 mixture has more limestone filler content than the GB3 and GB PMB ones. Given the higher affinity of water for acidic aggregates, this is to be taken into account for the analysis of moisture susceptibility.

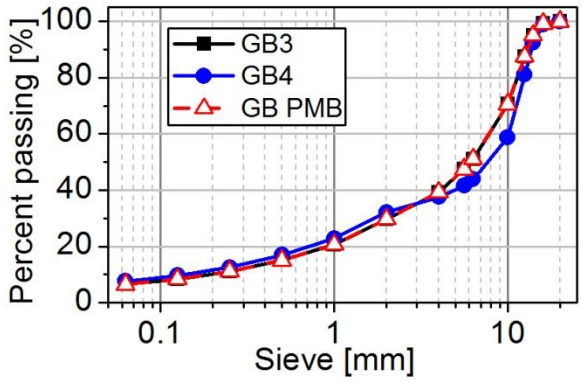

Figure 3.1. Grading curves of the three tested mixtures

Table 3-1. Aggregates of the three tested bituminous mixtures

Element	Type	Fraction [mm]	Percentage of total mass [%]		
			GB3	GB4	GB PMB
Coarse/fine aggregates (0/14)	Rhyolite – Baglione quarry (53 Mayenne) – Acidic nature	0-2	26.3	28.1	26.3
		2-6	21.2	10.0	21.2
		6-10	18.4	12.0	18.4
		10-14	27.2	41.7	27.2
Added filler	Limestone – Haut Lieu quarry (59 Nord) – Basic nature	<0.063	2.5	3.4	2.5

Table 3-2. Fine particles content of the three tested bituminous mixtures

Fine particle nature	Type	Percentage of total mass [%]			Percentage of filler mass [%]		
		GB3	GB4	GB PMB	GB3	GB4	GB PMB
Acidic	Rhyolite	4	4.3	4	61.5	55.8	61.5
Basic	Limestone (added filler)	2.5	3.4	2.5	38.5	44.2	38.5
Total		6.5	7.7	6.5			

3.1.2. Bitumen selection

The three studied mixtures have the same base bitumen. It consists of a 35/50 penetration grade bitumen from the Total Donges refinery in the Loire-Atlantique department in western France. This bitumen is considered as a hard one, intended to confer high bearing capacity properties to the materials. The bitumen used in the GB PMB mixture was modified with 2.5% of SBS cross-linked polymers. The polymer-modified bitumen was produced in the PRBG plant of the company Total and it is a Biprène® 41R formula by EIFFAGE. Table 3-3 presents the binder content of the studied mixtures. The maximum density of the mixtures, measured with the pycnometer method (EN 12697-5, 2009), is also presented.

Table 3-3. Bitume nature and content of the three studied mixtures

Formulation	Bitumen	Percentage of total mass [%]	Maximum density [Mg/m^3]
GB3	Total Donges 35/50	4.4	2.486
GB4	Total Donges 35/50	4.8	2.476
GB PMB	Total Donges 35/50 with 2.5% cross-linked SBS	4.4	2.486

3.1.1. The GB3, GB4 and GB PMB mixtures

The mixtures were fabricated by the French company EIFFAGE Infrastructures at the Research and Innovation Centre in Corbas, Rhone department. All of the components of the studied mixtures are commonly used in France in the road industry.

The GB3 mixture is considered as a basic base-course road material. It is normally used in road projects without special traffic characteristics. It is the reference material for this study as it is very common and it is the most basic available base-course mixture in the French market for railway infrastructure.

According to the European standards, GB4 mixtures present better performances than GB3 ones (c.f. section 1.1.5.2). They are usually intended for pavement structures subjected to high traffic such as highways. The used GB4 formulation is an improved version of a common GB4 mixture. It was chosen since it is proposed as a material suitable to railway structures. It is indeed the

same material as the one used to build the sub-ballast layer of the Brittany-Loire HSL. The improvement relies on the optimized aggregate packing made by the 2/6 fraction discontinuity. For this study, this material is considered as an improved alternative to the reference GB3 without the use of additives.

The GB PMB mixture was specially designed for this study since PMBs are not used in GB3 type mixtures. The interest of the GB PMB formulation is to assess the contribution of the polymer-modification of the bitumen to the thermomechanical properties of the reference material (i.e. the GB3).

There is also a difference between the GB3 and GB4 formulations in terms of compaction effort. The results of the PCG test (c.f. section 1.1.4.2) show that the GB4 mixture is much easier to compact than the GB3 one (c.f. Figure 3.2). The voids content at 100 gyrations, specified as reference value by the European Standard (NF P98-231-2, 1992), is of 5.2% for the GB4 compared to 9.9% for the GB3. For GB3 mixtures, this value is rather common which ratifies the reference character of the used GB3 formulation. However, the PCG value for the studied GB4 mixture is rather low for a material of this type. This means that the used mixture reaches a higher density for the same compaction effort than other materials of its type. This is a clear advantage of the GB4 mixture from a constructive point of view. Since the GB3 and GB PMB have the same binder content and aggregate structure, their PCG values are similar.

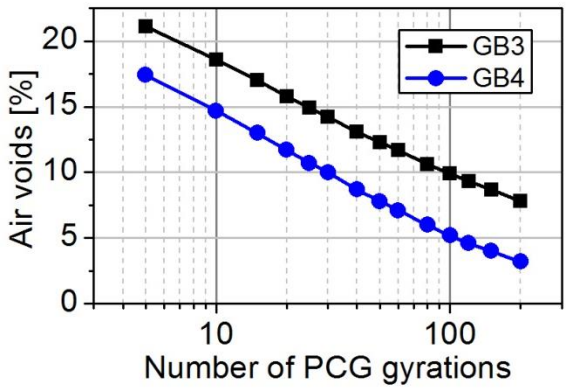

Figure 3.2. PCG results for the GB3 and GB4 mixtures (NF P98-231-2, 1992)

3.1.2. Samples preparation: confection and naming

As to produce the studied mixtures, aggregates were preheated for at least 12 h and bitumen for 4 h. Preheating the aggregates not only facilitates the coating by bitumen but also eliminates water films present at the surface. After mixing, the materials were compacted into slabs of 600 mm x 400 mm x 150 mm using a LPC roller compactor (EN 12697-33+A1, 2007). The same compaction effort and plan was applied to all slabs. Four slabs of each material were fabricated in the Research and Innovation Centre of EIFFAGE Infrastructures in Corbas (69). The slabs were cored at least two weeks after fabrication. Before coring, the slabs were cut into three parts as shown in Figure 3.3.

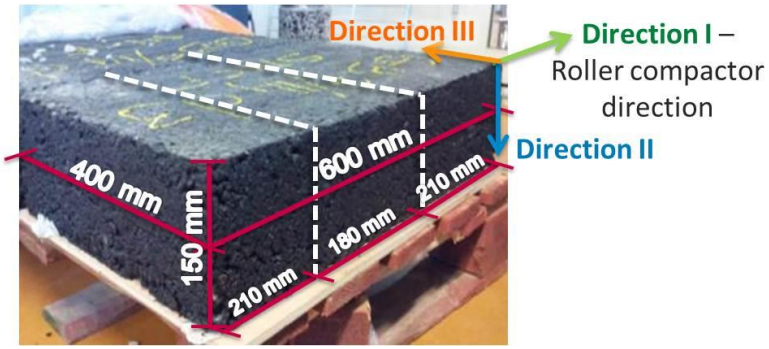

Figure 3.3. Bituminous mixture slab dimensions and cutting plan

The center part of the slab is narrower than the other two as the cutting and coring plan was intended to extract the cores from the most central part of the slabs as possible. Figure 3.4 shows how the cores from the external parts (named Part I and Part D) where extracted leaving a margin of 4 cm from the edges of the slab. The interest is to avoid the voids heterogeneities associated to the borders of the slabs. Due to friction between the mold and the material during compaction, the borders usually present higher void content and voids of bigger size. They are less compacted and are not representative of the material.

Twelve cores were extracted by slab, four out of each part. The coring direction is the same as the moving direction of the roller compactor. Therefore, the axial direction of the sample corresponds to main loading direction when the bituminous layer reacts as a beam in a pavement structure. The cores were then trimmed using a diamond blade. The final specimen dimensions are close to 75 mm in diameter and 140 mm in height. The diameter of the specimens does not vary significantly between specimens as they were all cored with the same diamond core drill. The samples were identified depending on their position in the slab by a letter (I, C or D) and a number. The different positions are schematized in Figure 3.4.

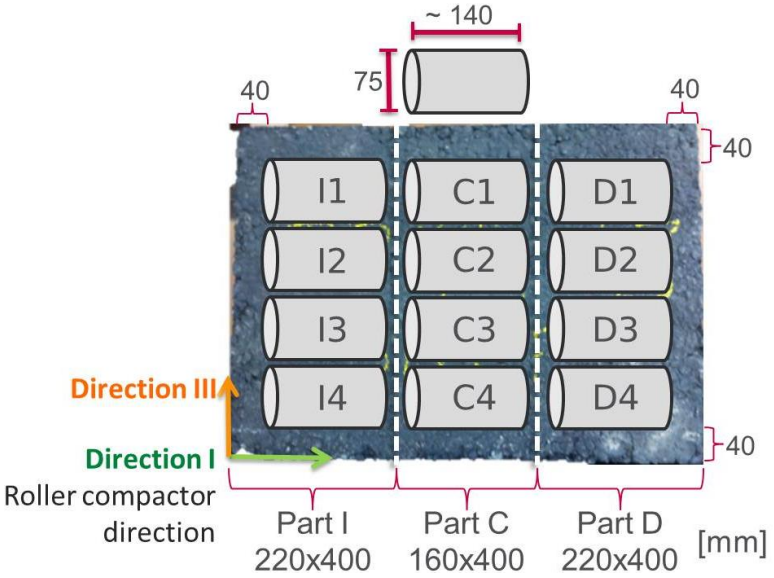

Figure 3.4. Coring plan of the bituminous mixture slabs and core positions (dimensions in mm)

Water is used to cool down the cutting tools used to fabricate the samples. After a period of two weeks, the samples were considered as dry and the bulk density of each sample was determined by volumetric measurements. This allowed calculating their air voids content. Each sample is named after the mixture, the slab where it comes from, its position in the slab and its voids content. The nomenclature system is presented in Figure 3.5. Eventually, the suffix "w" or "d" can be added to differentiate moisture conditioned samples from non-conditioned ones.

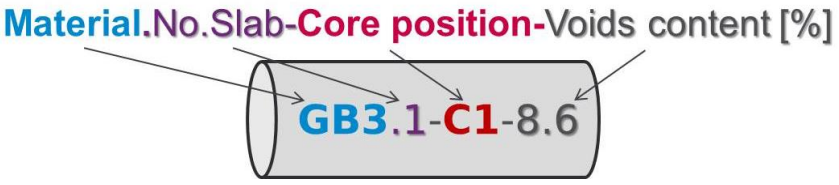

Figure 3.5. Nomenclature system for bituminous mixtures samples

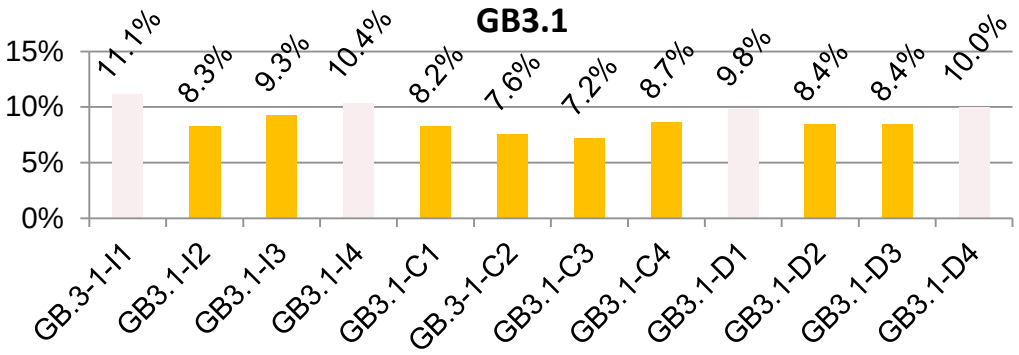

Figure 3.6. Voids content of the samples from the slab GB3.1

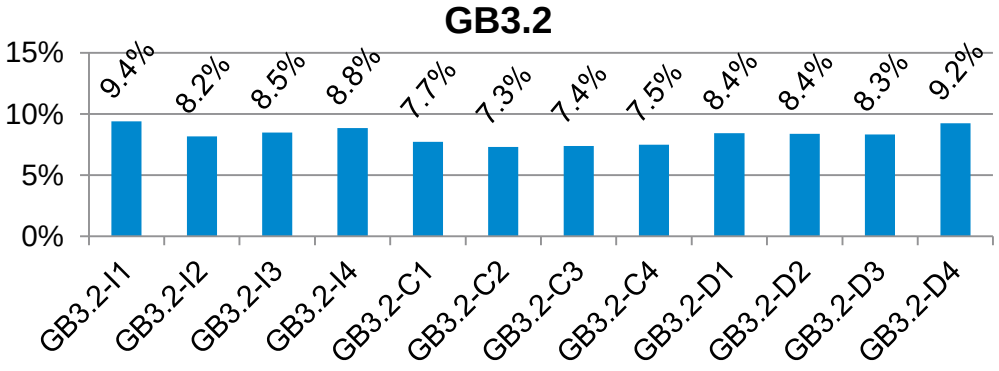

Figure 3.7. Voids content of the samples from the slab GB3.2

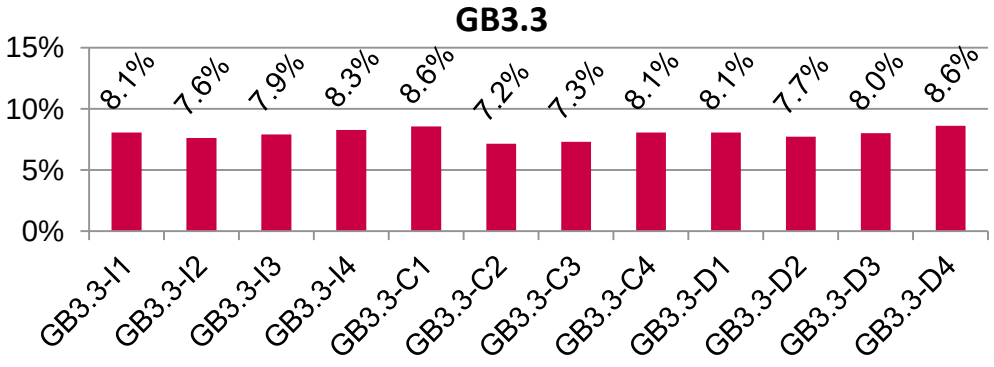

Figure 3.8. Voids content of the samples from the slab GB3.3

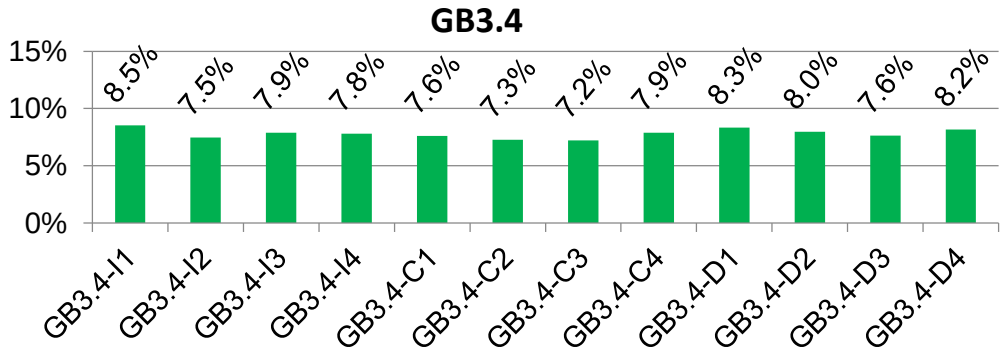

Figure 3.9. Voids content of the samples from the slab GB3.4

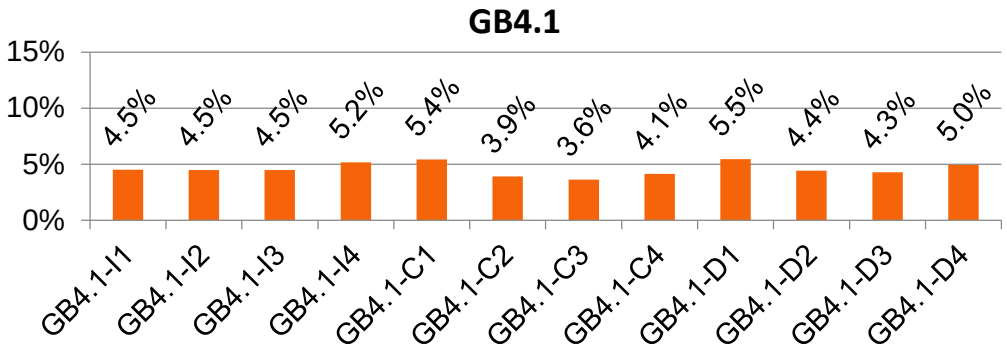

Figure 3.10. Voids content of the samples from the slab GB4.1

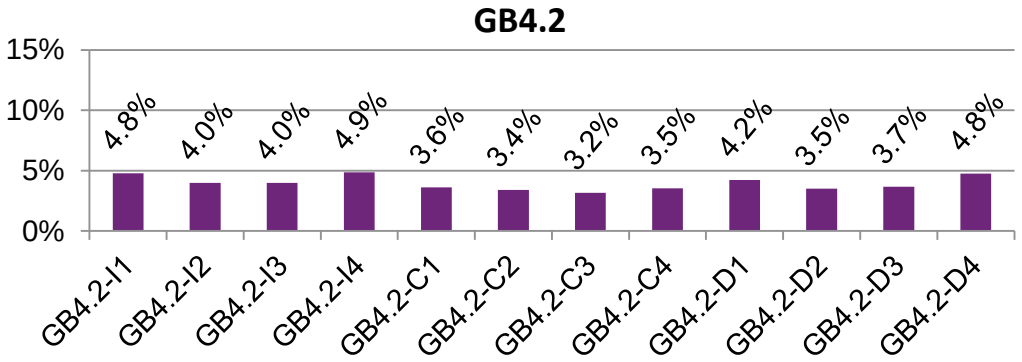

Figure 3.11. Voids content of the samples from the slab GB4.2

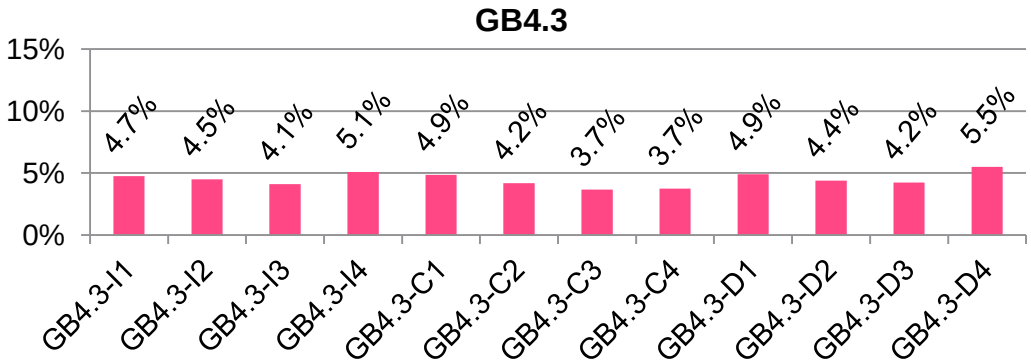

Figure 3.12. Voids content of the samples from the slab GB4.3

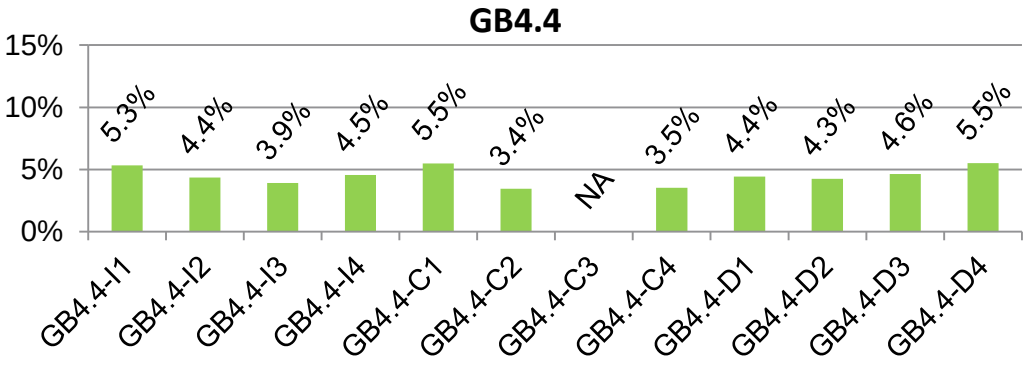

Figure 3.13. Voids content of the samples from the slab GB4.4

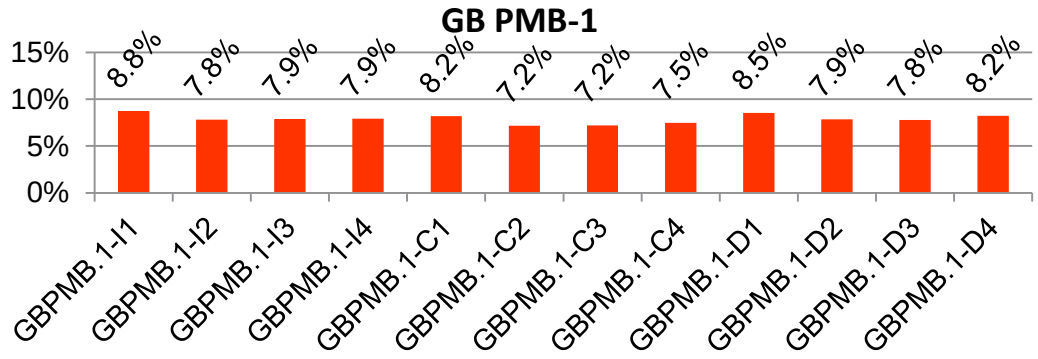

Figure 3.14. Voids content of the samples from the slab GB PMB.1

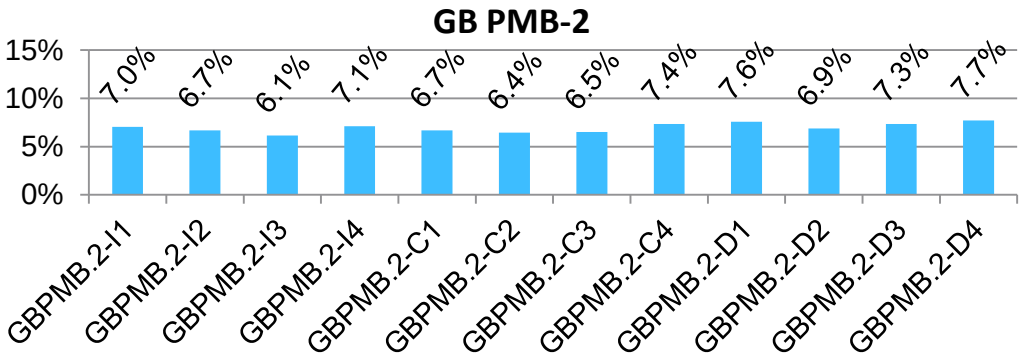

Figure 3.15. Voids content of the samples from the slab GB PMB.2

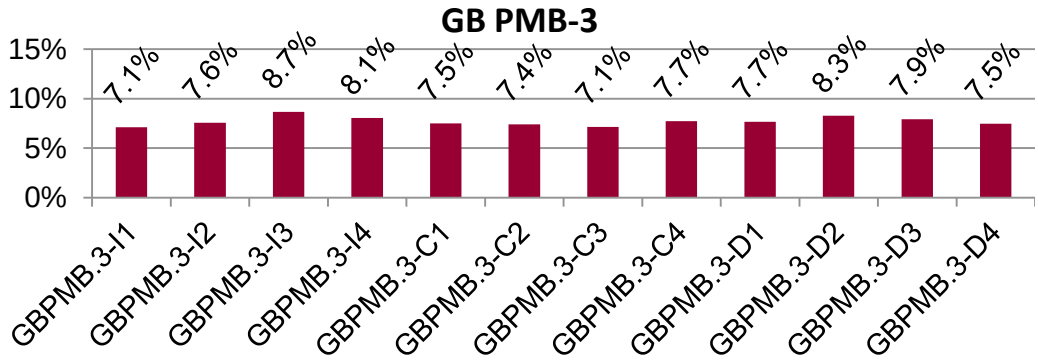

Figure 3.16. Voids content of the samples from the slab GB PMB.3

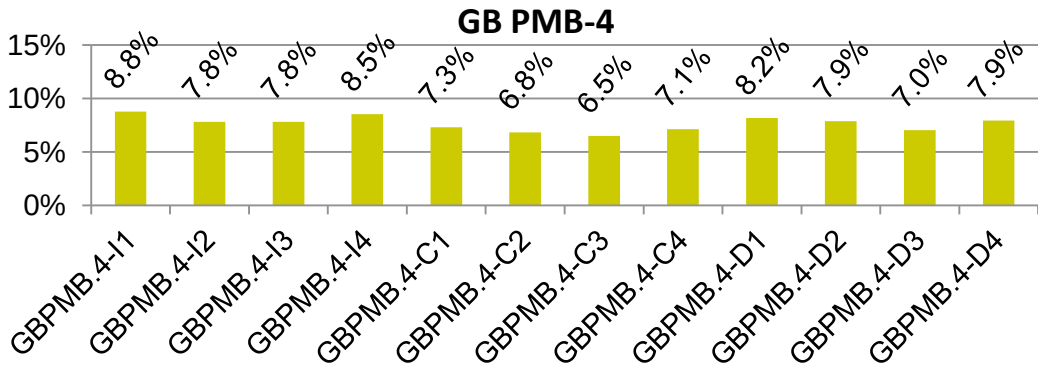

Figure 3.17. Voids content of the samples from the slab GB PMB.4

Figure 3.6 to Figure 3.9 show the air void contents of all the GB3 specimens. In slab GB3.1, the samples I1, I4, D1 and D4 present higher voids content than the average for the GB3 mixture due to the fact that they are 16 cm in height, including more of the slab border. These were the first samples to be cored. Due the high variability in voids content of theses samples the sample height was lowered to 14 cm in order to trim the most of the slab border. Figure 3.10 to Figure 3.13 present the voids content of the GB4 samples and Figure 3.14 to Figure 3.17 of the GB PMB.

Table 3-4. Average air voids content for GB3, GB4 and GB PMB mixtures

Mixture	Slab	Average voids content [%]	Standard deviation – S [%]
GB3	GB3.1	8.3*	0.7*
	GB3.2	8.3	0.7
	GB3.3	8.0	0.4
	GB3.4	7.8	0.4
	All samples*	8.1	0.6
GB4	GB4.1	4.6	0.6
	GB4.2	4.0	0.6
	GB4.3	4.5	0.6
	GB4.4	4.5	0.7
	All samples	4.4	0.6
GB PMB	GB PMB.1	8.1	0.4
	GB PMB.2	7.0	0.5
	GB PMB.3	7.7	0.5
	GB PMB.4	7.7	0.7
	All samples	7.6	0.6
*Without samples GB3.1-I1, GB3.1-D1 and GB3.1-D4			

The aimed voids content of the GB3 and GB PMB mixtures was the same. Therefore, the samples of both materials have similar voids contents. GB4 samples have almost half the air void content than the two other mixtures.

3.2. Moisture conditioning procedure

Based on the literature review on moisture damage (c.f. section 1.4) a moisture conditioning procedure is proposed. The complete fabrication and conditioning procedure is detailed hereafter (Figure 3.18):

1. Coring and trimming of the sample.
2. Cure and drying of the sample at ambient temperature and hygrometry for at least 2 weeks.
3. Bulk density measurement with the geometric procedure. At least 6 measures of height and diameter have to be taken at 6 different points of the sample.
4. Calculation of the voids content of the sample. The sample is rejected if its voids content differs in 1.5% or more from the average value for the material.
5. Immersion in a water bath at 60±1°C for 7 days ±1 h. The samples are laid horizontally on a sand bed during the immersion time.
6. Measurement of the mass of the sample after having dried its surface. The samples are taken out of the bath and immediately rolled over a 40 cm long absorbing paper from one end to the other. The sample is rolled five times over this distance: back and forth two times in two different papers and one time in a third paper. Then, the top and bottom ends of the sample are dried by placing it upwards on a new dry paper for 5 seconds on each end. The sample is immediately placed on a balance to measure its mass.
7. The sample is then placed inside a hermetic plastic bag containing 10 cl of water. The plastic is squeezed around the sample as to spread the water evenly on the surface of the sample. The bag is sealed so that the most air is expulsed from it.
8. Freeze-thaw cycle. The sample is placed horizontally on a sand bed inside a freezer at -18±1°C for 24±1 h. A temperature probe is placed near the sample as to monitor the temperature.
9. The sample is taken out of the plastic bag and its mass is measured.
10. The sample is placed on a sand bed in a temperature chamber at 40±1°C for 30±1 h. This step will be referred to as “drying”.
11. The sample is taken out of the temperature chamber at 40±1°C and left on a sand bed for at least 4 h before testing.

During storage, all of the samples were kept at room temperature and laid horizontally on a sand bed with an absorbing paper or plastic sheet between the sand and the sample.

Saturation of the sample is calculated as in equation [1-42]. The circulating bath Thermo-Fisher Scientific® SC100-A5B was used during the conditioning procedure. It was able to maintain the 60°C water temperature with fluctuations of ±0.1°C. Two devices were used for the freeze-thaw cycles: a freezer LIEBHERR® MedLine LGT 4752-41A/001 and the temperature chamber B.I.A Climatic® MTH6-140SP. In both cases the desired freezing temperature of the air surrounding the sample was attained after 1 h of having introduced the sample inside the chamber. The mass

of the frozen sample, before placing it in the temperature chamber at 40±1°C, was not systematically taken as ice blocks were sometimes attached to the sample. The temperature chamber B.I.A Climatic® MTH6-140SP was used for the thawing (drying) at 40±1°C.

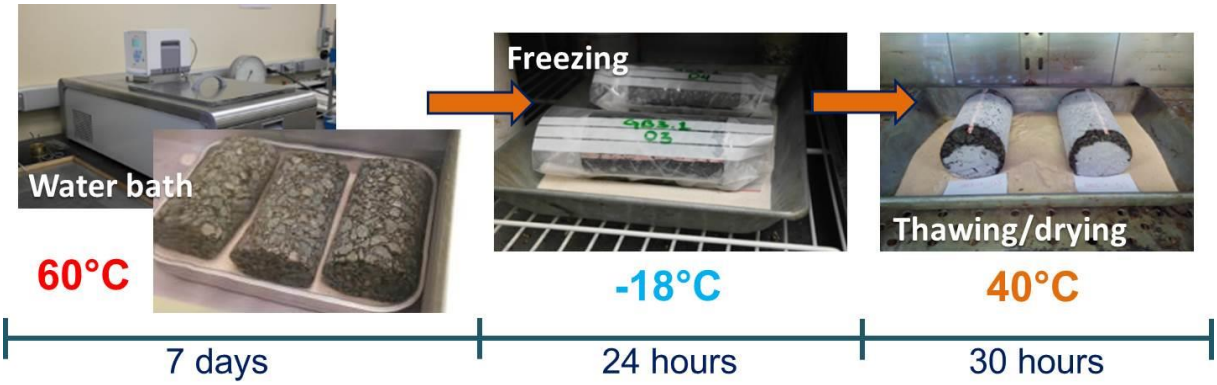

Figure 3.18. Used moisture conditioning procedure

The proposed procedure takes into account the exposition time to water of the French Duriez test (7 immersion days) combined with the damage accelerating effect of high temperature water baths as used in the AASHTO T283 test. This should allow enough exposition time to obtain the saturation of the accessible voids in the samples and for the moisture damage mechanisms to act on the binder-aggregate interfaces. No vacuum saturation was included as it was seen in the literature review that it causes damage of a different nature than moisture induced damage. The freezing procedure included is the same as the one considered by the AASHTO T283 procedure. The final step of the conditioning procedure, the conservation at 40±1°C for 30±1 h, has the main objective to dry the sample for gluing. Indeed water at the surface would be noxious for the gluing of the sample to the metallic heads needed for tension-compression testing. Accessorily, this long exposition to a relatively high temperature should slightly accelerate bitumen ageing.

Table 3-5 shows the saturation level after the immersion period for all conditioned samples. The mass of some samples was also measured after the drying period to observe the retained saturation. An average retained saturation after drying of 11.8% was observed for all mixtures. The GB PMB mixture presents lower retained saturation than the GB3 and GB4 mixtures. The bulk density of the conditioned samples was not systematically measured as the dimensions after conditioning were not measured for all samples. Conditioned samples that were not tested served as witnesses of the volumetric variation induced in the samples by the conditioning procedure. The geometry of these samples was accessed by taking 5 height measurements and 6 diameter ones, as for the first determination of the bulk density for all samples. The precision of the measurements is of 0.01 mm. No considerable modification of the samples diameter was observed though. The samples remained cylindrical after conditioning (c.f. Table 3-6).

Table 3-5. Moisture conditioned samples and saturation levels after water bath and after conservation at 40±1°C

Mixture	Sample	Saturation after water bath – S_{sd} [%]	Saturation after drying – S [%]	Test
GB3	GB3.1-C1-8.2%	38.0		Fatigue
	GB3.1-C4-8.7%	40.8	9.0	Complex modulus
	GB3.1-D3-8.4%	57.5	9.6	Complex modulus
	GB3.1-D4-10.0%	77.0	29.6	Complex modulus
	GB3.2-I1-9.4%	42.5		Complex modulus
	GB3.2-I2-8.2%	39.3		Fatigue
	GB3.2-I4-8.8%	31.2		Complex modulus
	GB3.2-C1-7.7%	31.5		-
	GB3.2-C2-7.3%	13.6		Fatigue
	GB3.2-C4-7.5%	30.5		Fatigue
	GB3.3-I1-8.1%	40.5		Fatigue
	GB3.3-I2-7.6%	30.2		Fatigue
	GB3.3-C2-7.2%	54.2	15.8	Fatigue
	GB3.3-C4-8.1%	41.3		Fatigue
	GB3.3-D1-8.1%	47.7		Fatigue
	GB3.3-D2-7.7%	50.82	12.5	Fatigue
	GB3.4-I1-8.5%	35.6		-
	GB3.4-I3-7.9%	26.9		Fatigue
GB4	GB4.1-I1-4.5%	23.8		Fatigue
	GB4.1-I3-4.5%	29.0		Fatigue
	GB4.1-C1-5.4%	25.8		Complex modulus
	GB4.1-D1-5.5%	23.3		Complex modulus
	GB4.1-D2-4.4%	47.8	17.6	Fatigue
	GB4.1-D3-4.3%	32.1		Fatigue
	GB4.2-I1-4.8%	32.4		Complex modulus
	GB4.2-I2-4.0%	29.8		Fatigue
	GB4.2-C1-3.6%	28.0		Fatigue
	GB4.2-C4-3.5%	30.2	13.8	Fatigue
	GB4.2-D3-3.7%	27.9		Fatigue
	GB4.2-D4-4.8%	28.2	19.1	Fatigue

	GB4.3-I1-4.7%	25.4		Fatigue
	GB4.3-C2-4.2%	25.5	6.9	Fatigue
	GB4.3-C4-3.7%	16.9		-
	GB4.3-D2-4.4%	25.5	11.2	Fatigue
	GB4.4-I3-3.9%	27.0	10.2	Fatigue
	GB4.4-D2-4.3%	25.6	14.6	Fatigue
GB PMB	GBPMB.1-I1-8.8%	28.8	8.1	-
	GBPMB.1-I4-7.9%	25.6		Complex modulus
	GBPMB.1-C1-8.2%	24.9	8.6	Fatigue
	GBPMB.1-D3-7.8%	25.9	8.3	Fatigue
	GBPMB.2-I1-7.0%	21.7	5.3	-
	GBPMB.2-I4-7.1%	20.8	4.4	-
	GBPMB.2-C4-7.4%	20.4		Fatigue
	GBPMB.2-D3-7.3%	22.3		Fatigue
	GBPMB.2-D4-7.7%	23.2		Fatigue
	GBPMB.3-D3-7.9%	24.3		Fatigue
	GBPMB.4-I2-7.8%	22.8		Fatigue
	GBPMB.4-C1-7.3%	32.4		Fatigue
	GBPMB.4-D3-7.0%	17.0	5.3	-

Table 3-6. Volumetric variation of witness samples after conditioning - measurements precision of 0.01 mm

Sample	Void difference after conditioning [%]	Average height variation [mm]	Height standard deviation (mm)	Average diameter variation [mm]	Diameter standard deviation [mm]
GB3.2-C1-7.7%	0.21	0.32	0.53	0	0.01
GB3.4-I1-8.5%	0.48	0.74	0.46	0.1	0.02
GB4.3-C4-3.7%	0.21	0.29	0.51	0	0.01
GBPMB.1-I1-8.8%	0.13	0.14	0.47	0.1	0.01
GBPMB.2-I1-7.0%	0.13	0.14	0.43	0.2	0.02
GBPMB.2-I4-7.1%	0.18	0.19	0.12	0.2	0.03
GBPMB.4-D3-7.0%	0.06	0.04	0.30	0.1	0.02

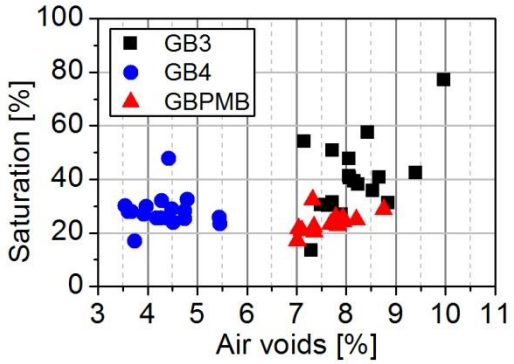

Figure 3.19. Saturation after having dried the surface of the sample with respect to the air voids content of all moisture-conditioned samples

The saturation of the moisture conditioned samples is presented in function of their air voids content in Figure 3.19. Using the same moisture conditioning procedure, most of the samples reach a saturation level between 20% and 40%. The dispersion in saturation is very high for the GB3 mixture, which could indicate that this mixture presents a rather heterogeneous voids content distribution or connectivity. For the GB PMB mixture, the samples describe a tendency indicating that saturation increases with the voids content. Due to the dispersion, this is not very clear for the GB3 mixture. The GB4 mixture shows rather stable values of saturation.

3.3. Experimental devices

All tests were carried out at the LGCB / LTDS laboratory of the ENTPE at Vaulx-en-Velin, France. The experimental devices used for the thermomechanical tests are described in this section.

During this study, two hydraulic presses were used: one from the company Instron® and another form the company MTS®. Most of the mechanical tests were performed by means of an Instron® 8874 hydraulic press with a maximum actuator travel of ±52.5 mm. A Dynacell® load cell with a ±25 kN maximum load capacity was associated with the Instron® press to measure axial force. The precision of the load cell is of 25 N. Given the fact that the geometry of the samples is known, the axial stress σ_1 is calculated as:

$$\sigma_1 = \frac{F}{\pi\left(\frac{D}{2}\right)^2} \qquad [3\text{-}1]$$

Where F is the force measured by the load cell and D is the diameter of the sample

For the tests carried out with the Instron® press, the axial strain was measured by three Instron® 2620-603 extensometers placed at 120° from each other as shown on Figure 3.20. These extensometers have a span of 72.5 mm, with a travel of ±1 mm, and a precision of 0.5 µm. They were positioned in the central part of the specimen leaving 3.4 cm between the extensometer

and the metallic cap to which the specimens were glued. The directions in Figure 3.20 correspond to those indicated in the cutting plan (Figure 3.3 and Figure 3.4).

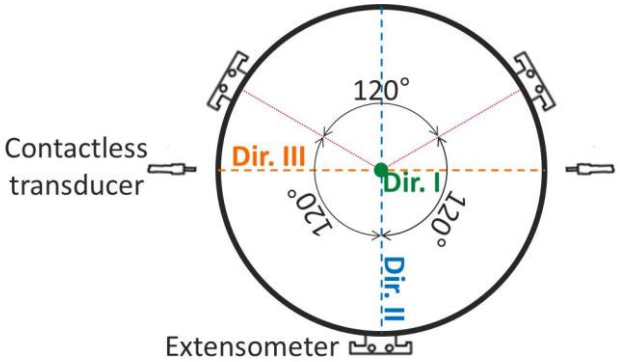

Figure 3.20. Schematic top view of the instrumented sample with the directions represented in Figure 3.3

The axial strain (ε_{1_i}) measured by each extensometer (i=[1,2,3]) is obtained as:

$$\varepsilon_{1\_i} = \frac{\Delta L_i}{L} \qquad [3\text{-}2]$$

Where ΔL_i is the displacement measured by the extensometer i and L the span of the extensometer

All tests were controlled based on the average value (ε_1) of the measures from the three extensometers:

$$\varepsilon_1 = \frac{\varepsilon_{1\_1} + \varepsilon_{1\_2} + \varepsilon_{1\_3}}{3} \qquad [3\text{-}3]$$

Radial strain was obtained by means of two non-contact transducers placed at opposite sides of the sample in direction 3 as shown in Figure 3.20. Alternating current circulation in the transducer head coil generates an alternating magnetic field which induces eddy currents in an aluminum target tape glued to the surface of the sample. The aluminum target generates then a resisting magnetic field and the interaction between both fields depends on the distance between the target and the head of the transducer. During cyclic loading, the magnetic field sensed by the electronics in the transducer varies as the sample deforms radially. These variations are then translated into variations of the distance between the sensor head and the sample. Radial strain (ε_3) was calculated from the two displacement measures (Δl_{3_i} with i=[1,2]) as:

$$\varepsilon_3 = \frac{\Delta l_{3\_1} + \Delta l_{3\_2}}{D} \qquad [3\text{-}4]$$

Two brands of non-contact transducers were used: Microepsilon® and Lion Precision®. Both have a measure range of ±500 µm with a resolution of 0.05 µm. Microepsilon® sensors were of type U05(09) and connected to a DT3010-A controller for non-ferromagnetic targets. Lion Precision® ones were of type U3B connected to an ECL202-U3-SAM-3.0 controller.

Associated to the Instron® press, a B.I.A. Climatic® MTH6-74 temperature chamber was used to condition the samples to the test temperatures. This chamber has a range from -40°C to 150°C with ±0.3°C stability. The temperature at the surface of the sample was measured with a PT100 temperature probe attached to the sample with tape. The precision of the probe is of 0.1°C. The temperature control of the chamber is carried out by an independent sensor. The autonomous control system and the thermal dispersions of the chamber explain the slight differences between target test temperatures and the effective measured ones.

Sampling frequency was set in order to acquire a minimum of 250 point per cycle. Data signal processing was carried out by combining data from consecutive cycles. For every cycle i, a least square regression was carried out for the combined data of cycles i and i+1. A sinusoidal function was used for axial stress and strain and for radial strain. Based on this, the LVE parameters were calculated as described in section 1.3.

(a) (b)

Figure 3.21. Instron® hydraulic press and B.I.A. Climatic® temperature chamber (a) and instrumented sample for a complex modulus test with the Instron® hydraulic press (b)

The second press used, the MTS® hydraulic press, was equipped with a MTS® 244.21 actuator and a MTS® 661.21B-02 load cell used to measure axial force (±50 kN range and 50 N precision). A second load cell with a ±200 N range and a precision of 0.2 N was used during test stages at high temperatures. This load cell was connected to the press assembly by a bypass system as seen in Figure 3.22(b). MTS® 632-11F-30 extensometers with 100 mm span and a measurement range of ±1 mm were used with this press. The temperature chamber associated to the MTS® press was a B.I.A. Climatic® MTH6-140SP model with the same temperature range and precision as the one used with the Instron® press.

(a) (b) (c)

Figure 3.22. MTS® hydraulic press and B.I.A. Climatic temperature chamber (a), bypass system for the 200 N load cell to be used at high temperature stages and instrumented sample for a test (c)

3.3.1. Sample setting

Prior to testing, the cylindrical samples were cleaned of any remaining sand grains from the sand beds were they reposed during storage. They were then glued to two metallic caps at each bottom of the sample. These metallic caps had the appropriate thread to attach the samples to the press assembly. The caps were first scrubbed with sandpaper to remove all impurities and glue residues from previous uses, and then cleaned with an acetone soaked tissue to remove bitumen and grease residues. The cap was then positioned on a bench, as seen in Figure 3.23, so as the sample was centred and in a vertical position. The bench is needed as the sawing could not assure the perfect horizontality of the surfaces at the ends of the samples. An epoxy Huntsman® Adralite® 2000 Plus glue was used. Tape was used to create a barrier for the glue not to pour out of the cap. After pouring the glue on the cap, the sample was quickly placed on the cap in a way so that the sample was always in touch with the four vertical guides of the bench. A weight of 2 kg was placed on top of the sample to increase the pressure during gluing. The sample was manually kept in touch with the vertical guides until the glue acquired enough strength (hardened) to keep the sample in place. The 2 kg weight was then removed and a cure time of at least 2 hours was allowed before gluing the second cap to the other end of the sample.

The second cap was glued directly at the hydraulic press (c.f. Figure 3.21 and Figure 3.22). The sample was attached to the upper part of the press assembly by means of a bolt fitting into the hole and thread of the already glued cap. After gripping the bolt, the force cell value was set to zero. The second cap was screwed to the lower part of the press assembly and tape was used to form a barrier for the glue not to pour out of it, as for the first cap. After pouring the glue, the actuator was carefully lowered in position control mode until the sample touched the second cap which happened when the load cell showed values of around 20 N in compression. Then, the actuator was set to force control mode and a target constant force of 25 N in compression was

set. The glue was then leaved to cure at ambient temperature for at least 2 hours before instrumenting the sample.

(a) (b)

Figure 3.23. Gluing of a cylindrical sample using a bench

Once the glue had hardened enough, the sample was instrumented with the three extensometers, the non-contact transducers and the temperature probe. The extensometers were placed according to the following procedure:

- With the help of a rubber band around the sample, the extensometers were positioned at their approximate positions.
- Springs were placed to attach the hooks of successive springs at their top part.
- Springs were placed to attach the hooks of successive springs at their lower part.
- The elastic band was removed.
- Using a ruler, the extensometers were placed so that its upper ends were at a distance of 3.4 cm from the closest edge of the metallic cap.
- The verticality of the extensometers was visually verified.
- The security pin was removed from the extensometers and verticality was verified anew.

Once the extensometers were in place, the non-contact transducers were positioned. The sensors heads were mounted on a metallic device with a spring allowing the adjustment of the distance between the head and the aluminium tape serving as target. With the target in place, the mounting devices of the two non-contact sensors were attached to a metallic ring as shown in Figure 3.21. Once gripped, the distance between the sensor head and the target was set so that the sensor showed a measurement close to the middle of the linear range of the sensor. In this way, all measurements during the test would be within the linear range making it easy to convert the measured voltage change into displacement variations. Finally, the PT 100 temperature probe was spread with a silicone based heat transfer compound and attached to the surface of the sample with tape.

A minimum cure time of 12 hours at 15°C was allowed for the epoxy glue to harden before the start of the mechanic tests.

All samples were then kept at the test temperature for 4 hours prior to loading. During the stabilization of the sample temperature, a small compression force of 10 N was applied to the samples.

3.4. The complex modulus test

Complex modulus tests were performed at 10 different temperatures from -25°C to 65°C. At each temperature, a sinusoidal tension-compression loading was applied at different frequencies. A sinusoidal loading under strain control was used. The sinus amplitude ε_{01} was set at 50 µm/m. Considering the experience from previous works carried out at the laboratory, it is assumed that the materials present LVE behaviour for this strain level.

The ensemble of tested frequencies at a single temperature is referred to as a test stage in this thesis. Figure 3.24 shows the different stages of the complex modulus test. The first step is the cure time for the epoxy glue to harden at 25°C. Then a first stage at 15°C starts. Each stage comprises a temperature stabilization time and a set of loadings at different frequencies. In between loadings, there is a rest period of 5 min. The experience from previous works at the laboratory shows that a minimum of 4 h is needed for the temperature of the sample to be homogeneous.

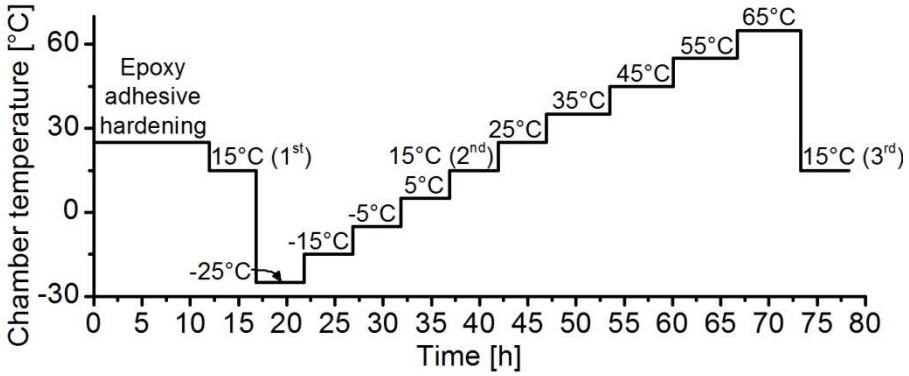

Figure 3.24. Tested temperatures during the complex modulus test

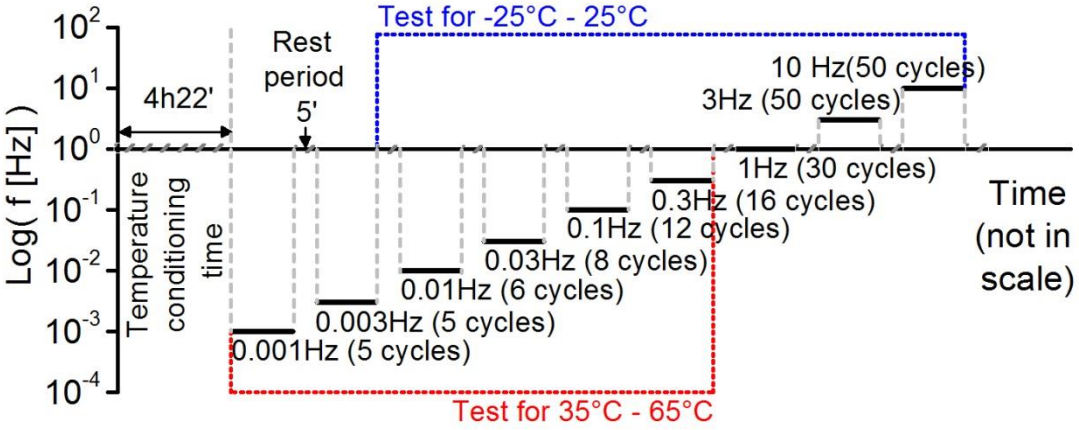

Figure 3.25. Tested frequencies for each temperature of the complex modulus test

Not all frequencies were tested for all temperature stages. At low temperatures (-25°C to 25°C), the samples were loaded at 0.01 Hz to 10 Hz. At high temperatures (35°C to 65°C), the samples were loaded at 0.001 Hz to 0.3 Hz (c.f. Figure 3.25). A certain number of cycles were applied at each frequency as to obtain at least two complete cycles at the correct strain amplitude (c.f Figure 3.25).

The stages at very low frequencies (0.001 Hz and 0.003 Hz) were not carried out at low temperatures since this would have extended the test time unnecessarily as the tested frequencies already allowed having enough points to build master curves. For the high temperature stages, as will be developed in section 4, the measured forces were low and a 200 N load cell was used instead of the 50 kN one. Therefore, to guarantee that the loadings at these temperatures were not over 200 N, only lower frequencies than 0.3 Hz were used. Indeed, the modulus of the material increases with the increase in loading frequency as will be exposed in section 4.

The test stage at 15°C was repeated 3 times: at the beginning, at the middle and at the end of the test. This was done in order to verify whether the sample suffered damage during the test or not. The results in section 4 show that no sample presented damage. The values presented as results in this thesis correspond to all frequency/temperature combinations. These are the average value of all the complete cycles of each loading at the correct strain amplitude. The cycles at the beginning of a loading are not taken into account since they are carried out during the stabilization time of the actuator. There are also transitory effects during the first loading cycles that alter the results (Gayte, Di Benedetto, Sauzéat, & Nguyen, 2016).

3.4.1. Calculation of mechanical parameters

Figure 3.26 presents typical stress and strain measurements from a sinusoidal tension-compression test. This example applies for both fatigue and complex modulus tests.

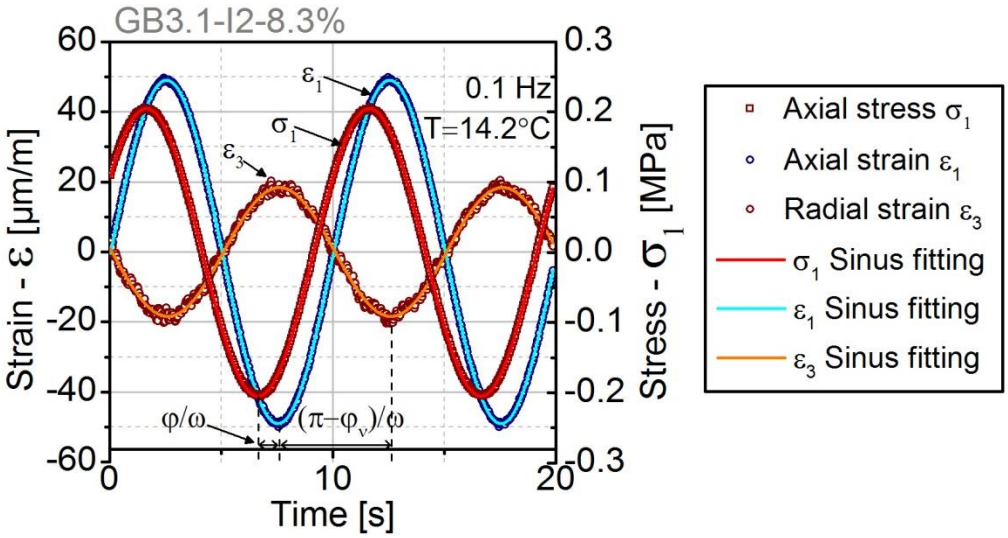

Figure 3.26. Example of measurements from a tension-compression test

Strain and strain signals are centred by subtracting from all the points of a cycle their average value. Since the tests were designed to be centred on zero stress, the average value of the stress signal is controlled. For this example the $\sigma_{average1}$ value is -0.013 kPa, which is very small compared to σ_{01}.

Given equations [1-13] and [1-14] that describe the strain and stress signals, the norm of the complex modulus ($|E^*|$) and its phase angle are calculated as:

$$|E^*| = \frac{\sigma_{01}}{\varepsilon_{01}} \quad [3\text{-}5]$$

$$\varphi = \omega\Delta t = 2\pi f\Delta t \quad [3\text{-}6]$$

Where Δt is the delay in time between the strain and stress signals

As inferable from equation [1-19], the real and imaginary components of the complex modulus are calculated as:

$$E_1 = |E^*| \cos\varphi \quad [3\text{-}7]$$

$$E_2 = |E^*| \sin\varphi \quad [3\text{-}8]$$

The norm of the complex Poisson's ratio and its phase angle are calculated as:

$$|\nu^*| = \frac{\varepsilon_{03}}{\varepsilon_{01}} \quad [3\text{-}9]$$

$$\varphi_\nu = \pi - 2\pi f\Delta t_{1\to3} \quad [3\text{-}10]$$

Where $\Delta t_{1\to3}$ is the delay in time between the axial strain and radial strain signals

In the same way as for the complex modulus, the real and imaginary components of the complex Poisson's ratio are calculated as:

$$\nu_1 = |\nu^*| \cos\varphi_\nu \quad [3\text{-}11]$$

$$\nu_2 = |\nu^*| \sin\varphi_\nu \quad [3\text{-}12]$$

Table 3-7. Parameters monitored during sinusoidal tension-compression cyclic tests on cylindrical bituminous samples

Parameter	Symbol	Measure unit
Frequency	f	Hz
Axial stress amplitude	σ_{01}	MPa
Axial stress average value	$\sigma_{average1}$	MPa
Axial strain amplitude	ε_{01}	µm/m
Axial strain average value	$\varepsilon_{average1}$	µm/m
Axial strain amplitude of the extensometer i	ε_{01_i}	µm/m
Phase angle of the extensometer i	φ_i	°
Radial strain amplitude	ε_{03}	µm/m
Radial strain average value	$\varepsilon_{average3}$	µm/m
Surface temperature	T	°C
Complex modulus norm	|E*|	MPa
Complex modulus phase angle	φ	°
Real component of the complex modulus	E_1	MPa
Imaginary component of the complex modulus	E_2	MPa
Complex Poisson's ratio norm	|ν*|	-
Complex Poisson's ratio phase angle	φ_ν	°
Real component of the complex Poisson's ratio	ν_1	-
Imaginary component of the complex Poisson's ratio	ν_2	-
Dissipated energy per cycle	W	J m^{-3}

3.5. The fatigue test

Fatigue tests were performed by applying a tension-compression sinusoidal loading centred on zero stress and in strain control mode. The target temperature for all tests was 10°C and all tests were loaded at 10 Hz. After the temperature stabilization time of 4 h, the same as for the complex modulus test, the loading was repeated until the end of the test. The test was considered as ended when the sample presented physical rupture, when one extensometer exceeded its travel length (1 mm) or when the stress amplitude at the cycle N was only 10% of the force measured at cycle 1. For the GB3 and GB4 mixtures, four strain levels were applied: 60 µm/m, 70 µm/m, 90 µm/m and 110 µm/m. For the GB PMB mixture, only the 70 µm/m, 90 µm/m and 110 µm/m strain levels were tested. The use of different strain amplitudes allows representing the fatigue life (number of cycles before failure) with respect to the strain endured by the material. This kind of representation is called a Wöhler curve (c.f. Figure 1.34).

Because of the great number of loading cycles that could be done for each sample, not all cycles were recorded. According to the theory of fatigue testing in laboratory, the fastest |E*| loss

occurs during the first loadings before attaining the stabilisation phase (phase II) (c.f. section 1.3.6). This is why the number of recorded cycles is greater at the beginning of the test. The cycles were recorded as follows:

- All cycles recorded from cycle 1 to 1 000.
- Two consecutive cycles recorded every 20 cycles from cycles 1 000 to 10 000 (starting with cycles 1 000 and 1 001).
- Two consecutive cycles recorded every 200 cycles from cycles 10 000 to 100 000 (starting with cycles 10 000 and 10 001).
- Two consecutive cycles recorded every 2 000 cycles from cycles 100 000 to 1'000 000 (starting with cycles 100 000 and 100 001).
- Two consecutive cycles recorded every 5 000 cycles from cycle 1'000 000 on (starting with cycles 1'000 000 and 1'000 001).

Figure 3.27 presents a schematic representation of the data acquisition during a fatigue test. Two consecutive cycles are needed as the data is analysed in the same way described for the complex modulus test. For example, the data from cycle 1 001 is used to analyse the cycle 1 000. A total of 500 points are then used to analyse each cycle (250 points form the cycle n and 250 points from the cycle n+1).

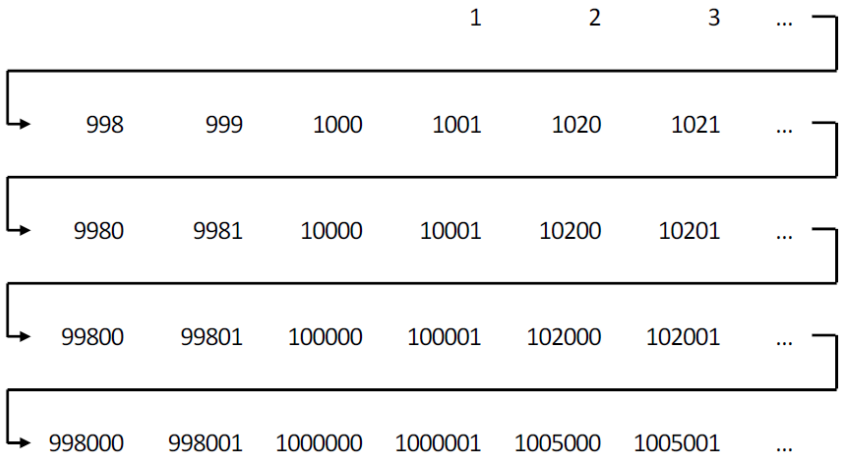

Figure 3.27. Scheme of recorded cycles during a tension-compression fatigue test (Mangiafico, 2014)

The same parameters as for the complex modulus test are calculated for the fatigue test. The evolution of $|E^*|$ and φ are of particular importance since fatigue failure criteria are based on them. Besides these parameters, the energy dissipation per loading cycle is calculated as in equation [1-23] (c.f. section 1.3.3). Dissipated energy can be used as a failure criterion since part of the energy dissipates in form of crack propagation. The higher the energy dissipated per cycle, the higher the probability of cracks developing within the material. Table 3-8 presents a summary of the used failure criterion for the analysis of the fatigue test results in this thesis. For more information and for graphic examples, refer to section 1.3.7. As a reminder, the initial values, such as the initial modulus $|E^*|_0$, were taken as the value at the 60^{th} cycle.

Table 3-8. Considered fatigue criteria and plots to be used

Fatigue criterion	Symbol	Condition	Plot
Classical approach	$N_{f\text{-}50\%}$	$\lvert E^* \rvert_n = 0.5 \lvert E^* \rvert_0$	$\lvert E^* \rvert$ vs N
Energetic Approach	$N_{f\text{-}Wn}$	$\left(\frac{DER}{DER_{Linear\ fit}}\right)_n = 0.5$	DER vs N
Loss of homogeneity with respect to average strain amplitude	$N_{f\text{-}\Delta\varepsilon}$	$(\Delta\varepsilon_{01\_i})_n = \left\lvert \left(\frac{\varepsilon_{01\_i}}{\varepsilon_{01}}\right)_n \right\rvert = 0.25$	$\Delta\varepsilon_{01\_i}$ vs N
Loss of homogeneity with respect to the initial amplitude strain value of the extensometer	$N_{f\text{-}\Delta\varepsilon\_extenso}$	$(\Delta\varepsilon_{01\_i\_ext})_n = \left\lvert \left(\frac{\varepsilon_{01\_i}}{\varepsilon_{01\_i_0}}\right)_n \right\rvert = 0.3$	$\Delta\varepsilon_{01\_i\_ext}$ vs N
Loss of homogeneity with respect to the phase angle of the average strain signal	$N_{f\text{-}\Delta\varphi}$	$(\Delta\varphi_i)_n = \lvert(\varphi_i - \varphi)_n\rvert = 5°$	$\Delta\varphi_i$ vs N
Concavity change	$N_{f\text{-concavity}}$	$\Delta b_i = \left\lvert \frac{b_i}{b_{i-1}} \right\rvert = 0.2$ with b the slope of the cycles interval i	$\lvert E^* \rvert$ vs N

For the concavity change criteria, the size of the intervals for this failure criterion depends on the length of the second phase of the fatigue tests. For long second phases, bigger intervals have to be taken into account and vice-versa. The interval sizes of the tests analysed in this thesis are comprised between 2 000 and 50 000 cycles depending on the test.

4

Linear viscoelastic behaviour of the tested bituminous mixtures

The complex modulus tests results for the three studied bituminous mixtures are presented in this section. The results from the sample GB3.1-I2-8.3% are used in section 4.1 as an example to illustrate the analysis procedure. This part of the study aims to characterize the linear viscoelastic (LVE) behaviour of the studied bituminous mixtures. The influence of the materials volumetric characteristics and of the exposure to moisture on LVE properties is highlighted.

4.1. Test results

An important number of complex modulus tests were carried out on the GB3 mixture. Being the reference material, it was the first material to be tested and the test protocol was adjusted using GB3 samples. The first tests did not comprise the stage at 65°C (c.f. section 3.4) and were carried out with the Instron® hydraulic press. The high variability of the results at high temperature (45°C and 55°C) observed for the first GB3 samples was, at first, associated to the fact that the measured forces at these conditions were at the lower limit of the load cell precision. This is why the complex modulus tests were henceforth carried out with the MTS® hydraulic press using a 200 N load cell during the high temperatures stages. This also allowed including the stage at 65°C in order to better identify the static modulus of the material. In this section, the tested samples are presented for all materials and an example of test results is given with the GB3.1-I2-8.3% sample.

4.1.1. Tested samples

Table 4-1 presents the tested samples for complex modulus for all materials. The press used and the moisture condition of the samples are specified.

Table 4-1. Complex modulus tests for all materials

Mixture	Sample	Press used	Moisture condition
GB3	GB3.1-I1-11.1%	Instron®	Non-conditioned
	GB3.1-I2-8.3%	Instron®	Non-conditioned
	GB3.1-I3-9.3%	Instron®	Non-conditioned
	GB3.1-C4-8.7%	Instron®	Conditioned – No freeze-thaw cycle
	GB3.1-D1-9.8%	Instron®	Non-conditioned
	GB3.1-D3-8.4%	Instron®	Conditioned
	GB3.2-I1-9.4%	MTS®	Conditioned
	GB3.2-I3-8.5%	MTS®	Conditioned
	GB3.2-I4-8.8%	Instron®	Conditioned
	GB3.2-D2-8.4%	MTS®	Non-Conditioned
	GB3.2-D4-9.2%	Instron®	Non-Conditioned
	GB3.3-C1-8.6%	MTS®	Non-Conditioned
	GB3.3-D4-8.6%	MTS®	Non-Conditioned
GB4	GB4.1-I4-5.2%	MTS®	Non-Conditioned
	GB4.1-C1-5.4%	MTS®	Conditioned
	GB4.1-D1-5.5%	MTS®	Conditioned
	GB4.1-D4-5.0%	MTS®	Non-Conditioned
	GB4.2-I1-4.8%	MTS®	Conditioned
	GB4.2-I4-4.9%	MTS®	Non-Conditioned
GB PMB	GBPMB.1-I2-7.8%	MTS®	Non-Conditioned
	GBPMB.1-I4-7.9%	MTS®	Conditioned

The tested GB3 samples served to define the definitive complex modulus test protocol. The tests on the GB4 and GB PMB samples were performed on the MTS® press and the 200 N load cell for the 45°C, 55°C and 65°C stages. Six GB4 samples were tested under this protocol; three of them were moisture conditioned. The same amount of GB PMB samples was to be tested but, due to unexpected events, the MTS® press became out of service before finishing the experimental work. Two GB PMB samples were nonetheless tested and, given the high repeatability of the complex modulus test for other materials, no further tests were considered necessary.

4.1.1. Temperature of the samples

The measured temperature at the surface of the samples was slightly different from the target temperature for each test stage. During a temperature stage, small temperature variations of the order of 0.1°C were observed. The presented temperature values are the average values from all the points of each stage.

The temperature chamber presented problems during the tests with samples GB3.1-D3-8.4%, GB3.2-I4-8.8%, GB4.1-D4-5.0% and GB4.2-I4-4.9% (c.f. Appendix II). The test stages at negative temperatures were not taken into account for these tests. The stage at 5°C for the GB4.2-I4-4.9% test was also not taken into account. Not all tests included the stage at 65°C since it was not part of the initial test protocol. Table 4-2 presents the average value and the standard deviation of the measured surface temperature of the samples taking into account all complex modulus tests. It is observed that stages at extreme low temperatures (-25°C and -15°C) present higher temperature variability. This highlights the necessity to measure the real temperature of the sample during all tests.

Table 4-2. Average value, per test stage, of the measured surface temperature of the samples taking into account all complex modulus tests

Test stage	-25°C	-15°C	-5°C	5°C	15°C	25°C	35°C	45°C	55°C	65°C
Average temperature [°C]	-20.4	-12.5	-4.9	4.8	14.4	24.1	33.6	43.3	52.6	61.8
Standard deviation [°C]	4.7	5.4	0.6	0.3	0.2	0.2	0.4	0.2	0.3	0.5

4.1.2. Validation of the time temperature equivalence principle

Different plots can be used to present the complex modulus test results. The two most intuitive ones are the isotherm and isochrone curves. Figure 4.1 presents the |E*| isotherms and isochrones for the sample GB3.1-I2-8.3%. The effect of temperature and of loading frequency on the stiffness of the sample is clearly observed.

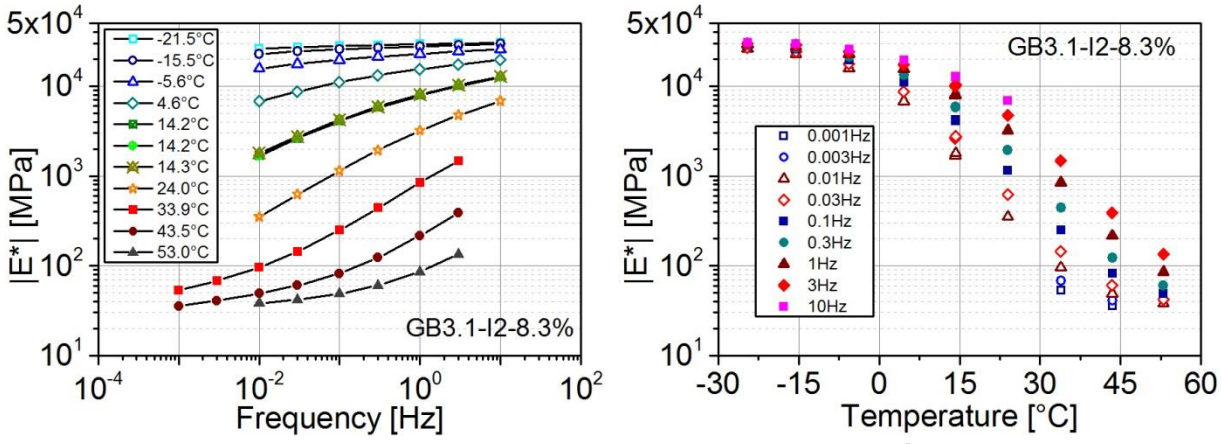

Figure 4.1. Isotherms (a) and isochrones (b) of the norm of the complex modulus: influence of the temperature and of the loading frequency on stiffness

The norm of the complex modulus increases with the increase of the loading frequency and with the decrease of the temperature. Coupling these two conditions leads to high modulus values that tend to an asymptotic value. Low modulus values can be achieved by coupling the effect of low frequencies and high temperatures. The material also presents an asymptotic behaviour for extreme low frequencies and high temperatures. For this thesis, isotherm curves are selected for the presentation of complex modulus test results over isochrones.

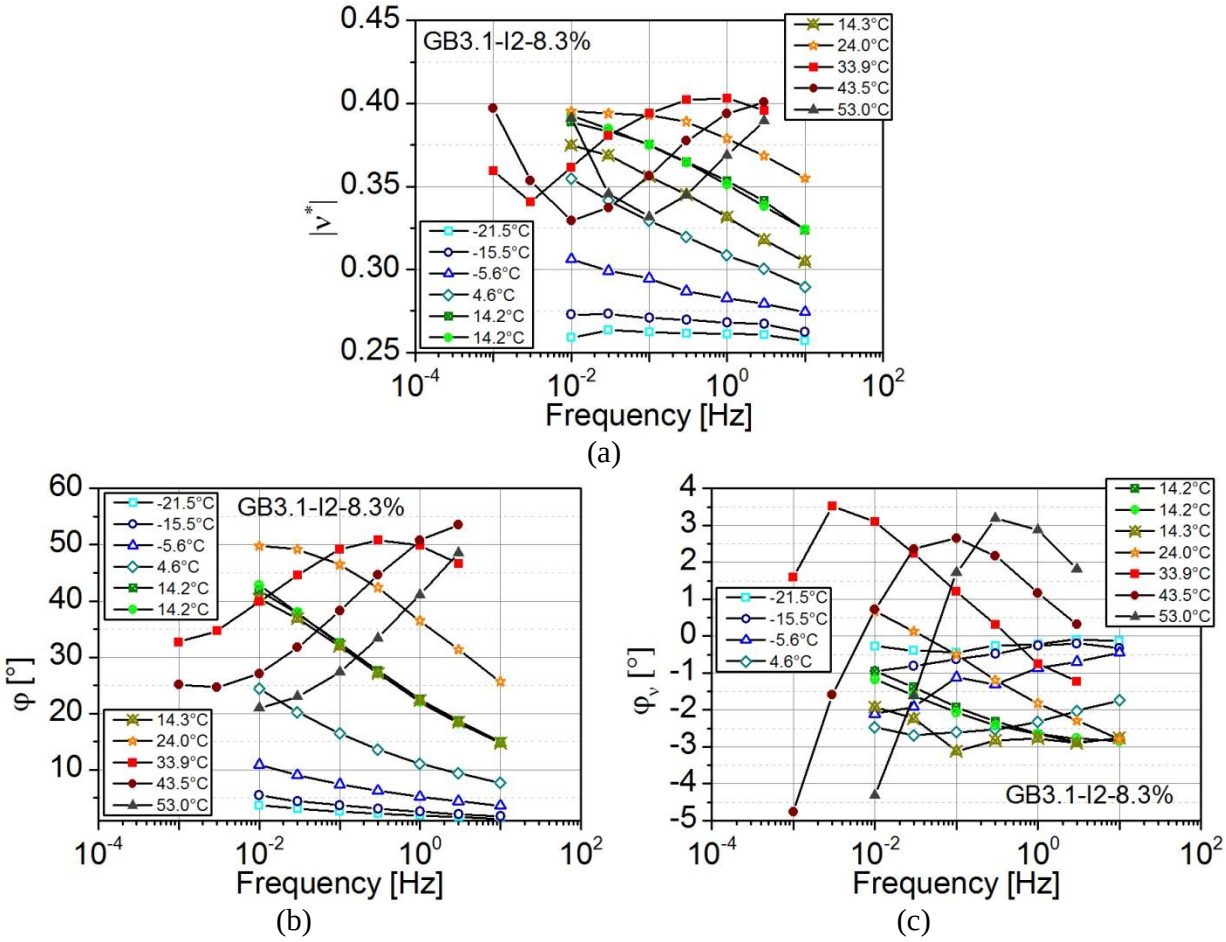

Figure 4.2. Isotherms of the complex Poisson's ratio (a) and of the E* (b) and ν* (c) phase angles: influence of the temperature and of the loading frequency on the 3-dimensional LVE behaviour

Figure 4.2 presents the isotherm curves of the complex Poisson's ratio and of the phase angles of E* and ν* respectively. It is evident that temperature and frequency also condition the complex Poisson's ratio of bituminous mixtures and that it is not correct to consider its value as a constant. As for the phase angle of the complex modulus, it decreases with the increase in the loading frequency for low temperature conditions (-25°C to 25°C). The isotherm at 35°C clearly shows an inflexion point indicating the presence of a maximum phase angle value. Isotherms at higher temperatures than 35°C present the opposite tendency compared to isotherms at low temperatures with an increase of the phase angle with the frequency. However, these curves seem to present an asymptotic behaviour at a value different from 0 when high temperatures and low frequencies are coupled. This deserves detailed analysis and specific experimental works. The complex Poisson's ratio phase angle isotherms also present opposite tendencies depending on the test temperature. The phase angle φ_ν decreases with the increase in

frequency for temperatures above 5°C, whereas it increases for temperatures below 5°C. High Poisson's ratio phase angle (φ_v) values at high temperatures (35°C, 45°C and 55°C) are evidence of the difficulties encountered to measure the radial strain at such conditions during the test.

The test results can also be presented in the Cole-Cole and Black plots (c.f. section 1.3.2.4) as in Figure 4.3 and Figure 4.4.

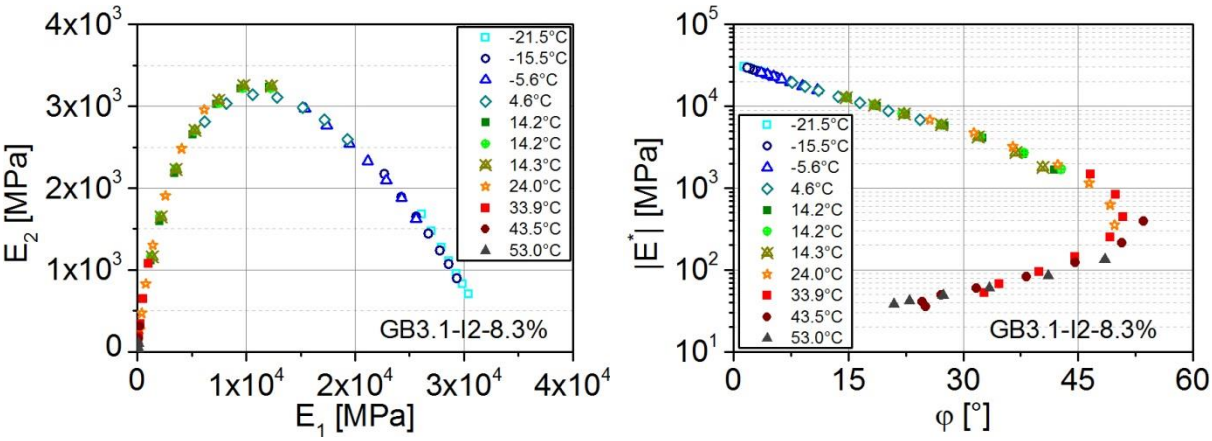

Figure 4.3. Complex modulus in Cole-Cole (a) and Black (b) plots

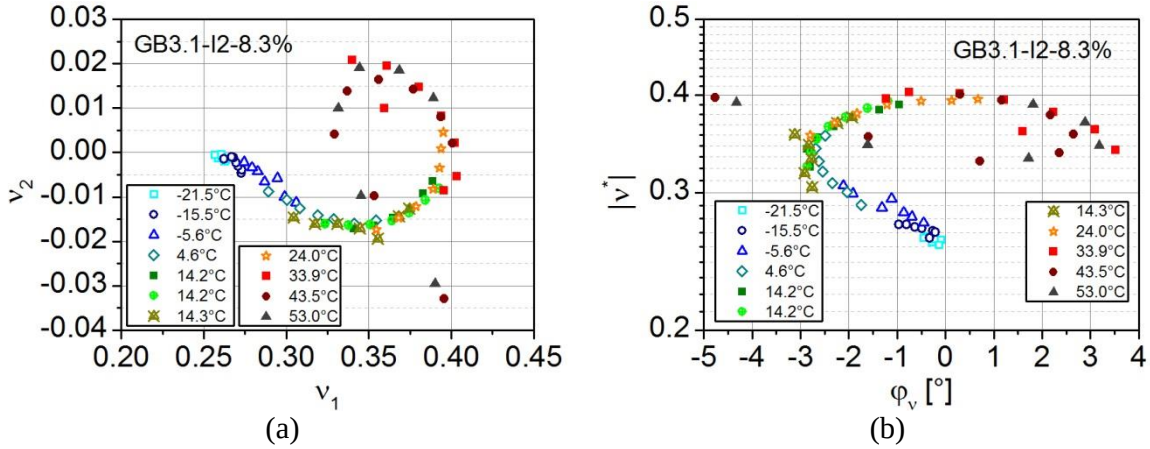

Figure 4.4. Complex Poisson's ratio in Cole-Cole (a) and Black (b) plots

Analysing Figure 4.3 it is clear that the Cole-Cole plot allows observing the LVE behaviour of the material at low temperatures, whereas the Black plot is more suitable for the analysis at high temperatures. These plots can be seen as the footprint of the LVE behaviour of bituminous mixtures as the test results at any temperature/frequency combination will be placed on this unique line. These plots are then the base to calibrate any rheological model of the LVE behaviour of the materials. The problems in the radial strain measurements during the test stages at high temperatures are evident in the complex Poisson's ratio Cole-Cole and Black plots since the points are scattered and do not form part of the unique line described by the rest of the points. This is particularly true for the points at the lowest frequencies tested which are the most extreme conditions to which the sample was subjected. The negative values of the imaginary part of the Complex Poisson's ratio indicate that radial strain happens slightly after axial strain.

When represented in Cole-Cole and Black plots, the complex modulus test results describe a single and unique continuous line which allows validating the Time-Temperature Superposition Principle for the mixtures. Complex Poisson's ratio results also describe a single line and this validates the TTSP for the 3-dimensional case. The shifting procedure explained in section 1.3.4 can then be applied to build |E*|, φ, |ν*| and φ_ν master curves.

Figure 4.5 shows the construction of the master curves. The used a_T shift factors were first established by building a |E*| master curve at a reference temperature equal to the real temperature of the sample at the second stage at 15°C. The same a_T factor values were used to build the φ master curve. Moreover, it was found that the same a_T factor values could be used to build the |ν*| and φ_ν master curves, as seen in Figure 4.5(c, d). This validates the use of the same a_T shift factor for the characterisation of the 3-dimensional LVE behaviour of the studied bituminous mixtures over a large range of frequencies and/or temperatures. The same observations have been made by previous studies on other bituminous mixtures (Di Benedetto et al., 2007b; Q. T. Nguyen et al., 2013).

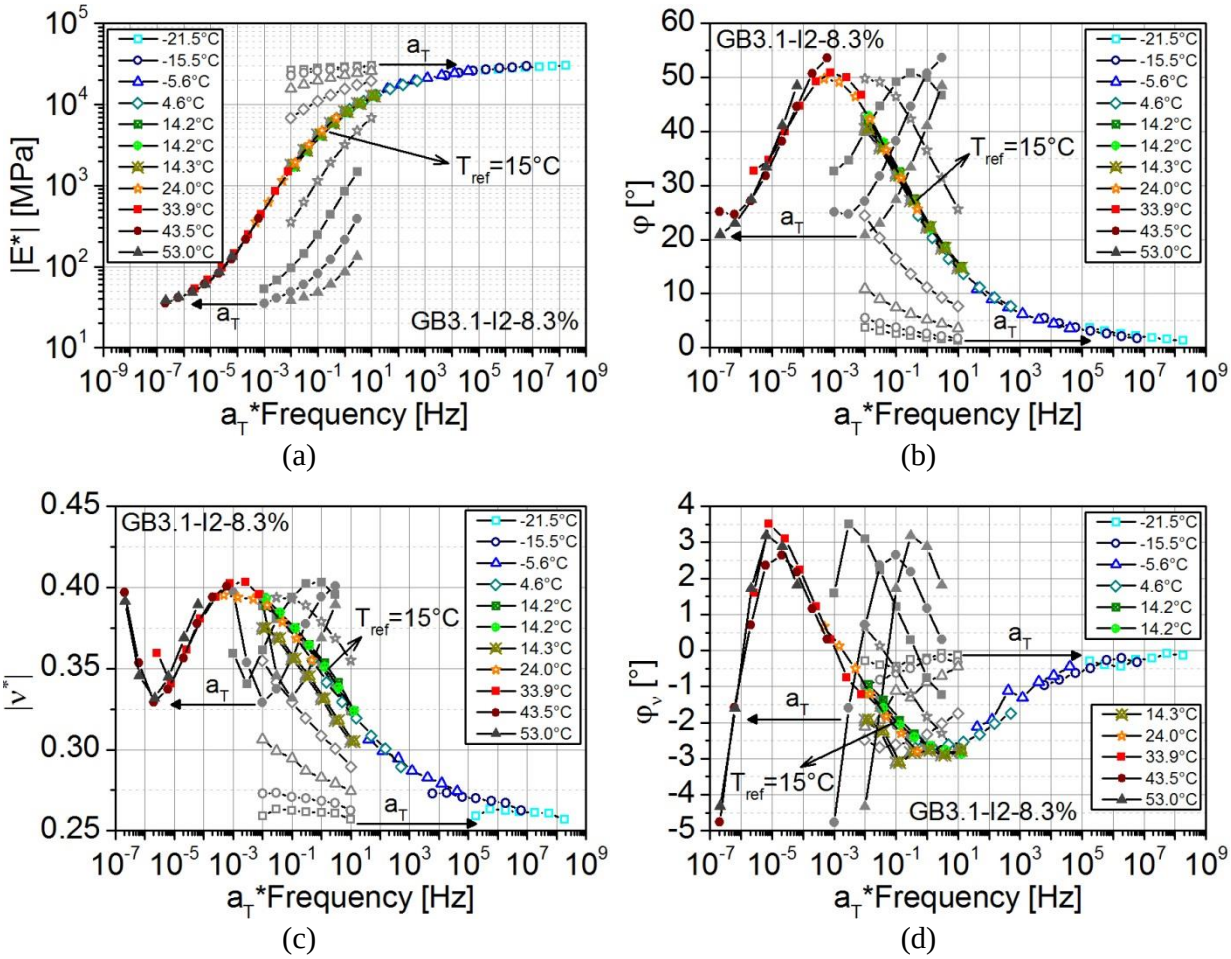

Figure 4.5. Construction of the complex modulus (a, b) and complex Poisson's ratio (c, d) master curves

The a_T shifting factors used for all tested samples are presented in Figure 4.6 to Figure 4.9. The experimental points are presented for the reference temperature of the test which is the real measured surface temperature at the second stage at 15°C. The presented WLF fit is at a

reference temperature of 15°C for all samples to allow direct comparison of the results coming from different tests. The reference temperature of 15°C was chosen based on the Frecnh pavement design method and on the temperature measurements of the EE HSL test zone (c.f. section 2.2.4). The suffix “w” or “d” is added to the name of each sample to differentiate moisture conditioned samples from non-conditioned ones.

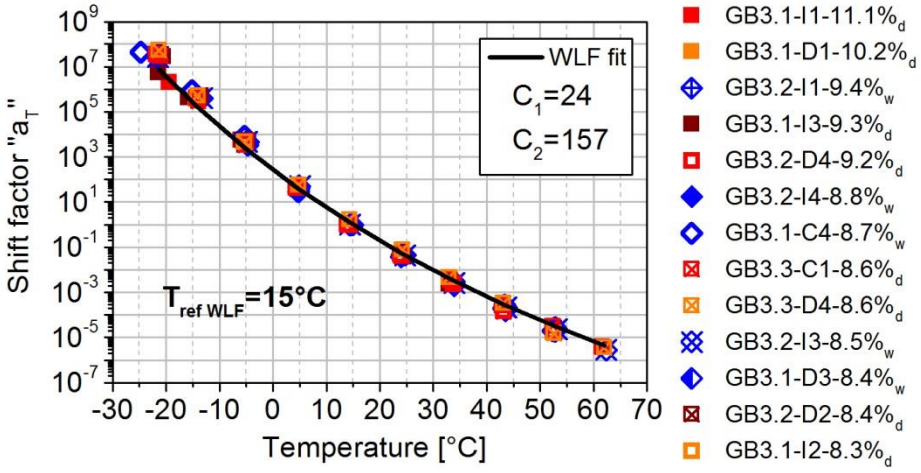

Figure 4.6. Shit factor a_T and WLF fitting for the GB3 complex modulus tests –Blue diamond icons correspond to moisture conditioned samples, also marked with the suffix “w”; the suffix d stands for non-conditioned “dry” samples

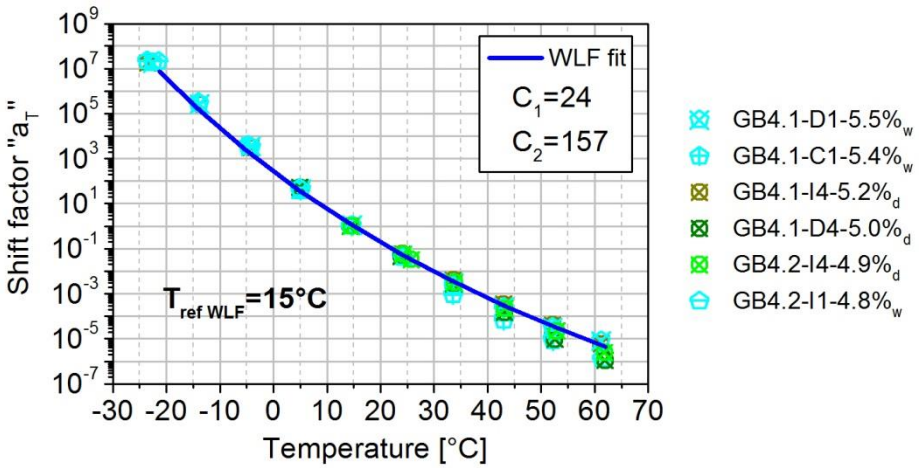

Figure 4.7. Shit factor a_T and WLF fitting for the GB4 complex modulus tests –Light blue pentagon icons correspond to moisture conditioned samples

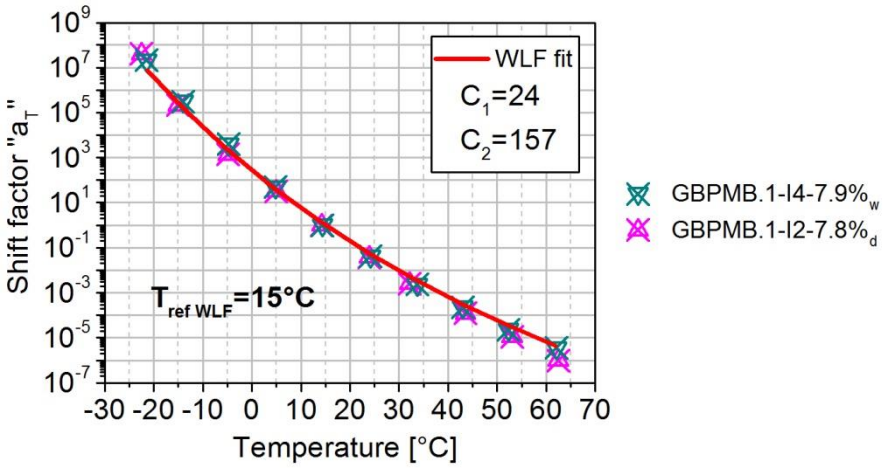

Figure 4.8. Shit factor a_T and WLF fitting for the GBPMB complex modulus tests –dark cyan up-side-down triangle icons correspond to moisture conditioned samples

The icons on the figures indicate the conditioning state and the hydraulic press used for each test (c.f. Figure 4.6 to Figure 4.9). Icons comprising a cross or a line in them (either in form of x, + or -) indicate that the test was done with the MTS® hydraulic press. Other icons indicate the use of the Instron® hydraulic press.

Analysing each mixture separately, the values of the a_T factor of all tests describe the same line. The a_T factor of each material can then be described by a single couple of C_1 and C_2 coefficients of the WLF equation (c.f. equation [1-26]). Moisture conditioning does not seem to alter the shift factor equation for any of the studied materials.

Moreover, Figure 4.9 shows that the a_T shift factor trend does not depend on the mixture. This is in accordance with the findings of previous studies reporting that the a_T factor is inherent of the bitumen nature and independent of the mixtures design (Di Benedetto et al., 2007b; Olard & Di Benedetto, 2003; Olard et al., 2005). This is evidence that the binder nature was not significantly altered by the used conditioning procedure. The retained values for the WLF equation constants are C_1= 24 and C_2= 157 at 15°C.

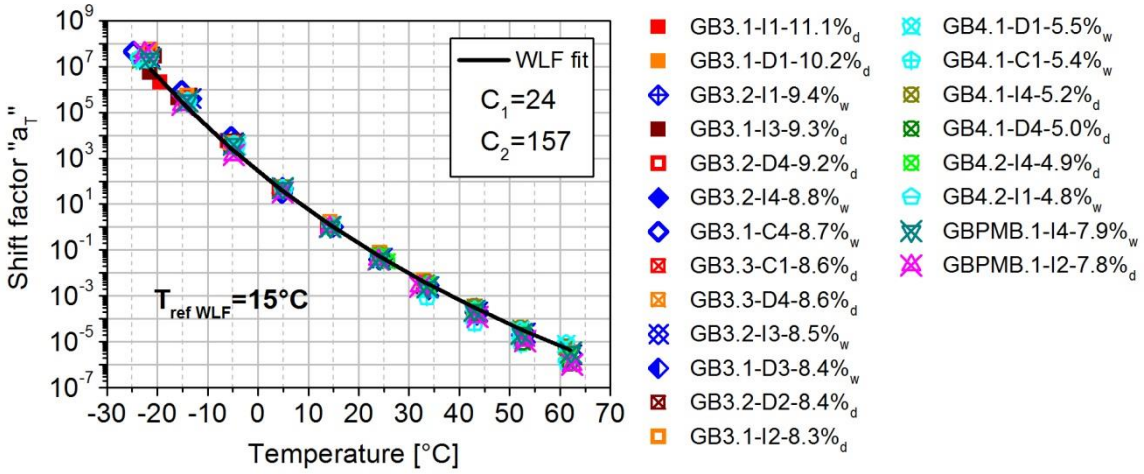

Figure 4.9. Shit factor a_T for all complex modulus tests and WLF fitting

4.1.3. 2S2P1D model parameters

The 2S2P1D model parameters (c.f. section 1.3.5) are calibrated on the Cole-Cole and Black plots as schematized in Figure 1.33. The calibration of the model parameters on the test results from the GB3.1-I2-8.3% sample is presented in Figure 4.10, Figure 4.11 and Figure 4.12. The model parameters used for the presented example are provided in Table 4-3.

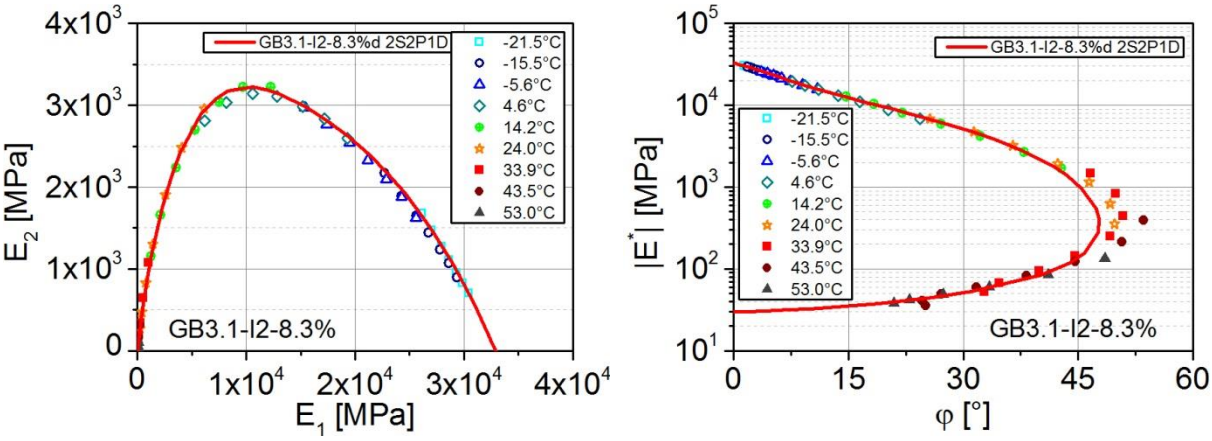

(a) (b)

Figure 4.10. 2S2P1D simulation of the complex modulus in Cole-Cole (a) and Black (b) plots

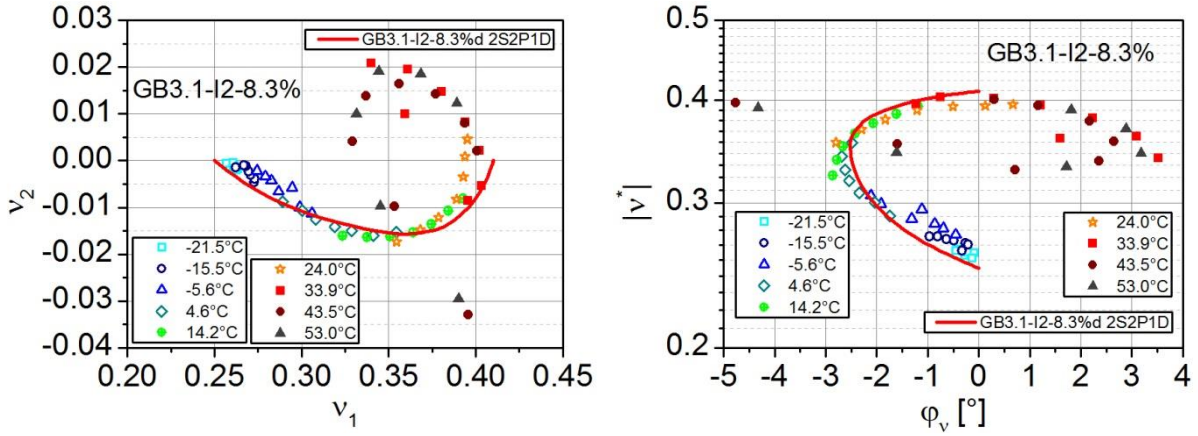

(a) (b)

Figure 4.11. 2S2P1D simulation results of the complex Poisson's ratio in Cole-Cole (a) and Black (b) plots

Table 4-3. 2S2P1D model parameters for GB3.1-I2-8.3% complex modulus test

2S2P1D model parameters for simulation of GB3.1-I2-8.3% sample results at T_{ref}=15°C									
E_{00} [MPa]	**E_0 [MPa]**	**k**	**h**	**δ**	**τ [s]**	**β**	**ν_{00}**	**ν_0**	**τ_ν [s]**
30	32 900	0.19	0.59	2.05	0.18	350	0.41	0.25	0.91

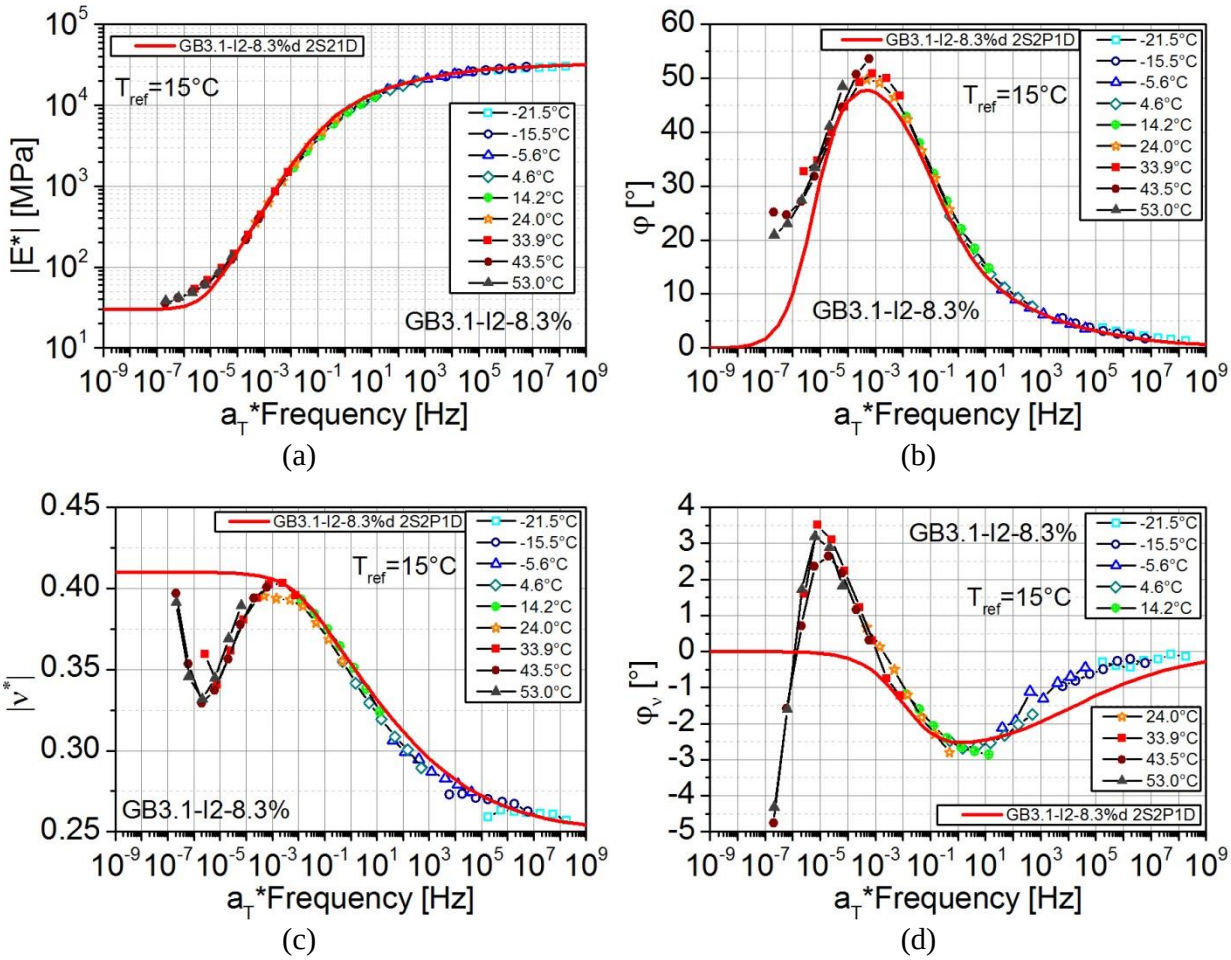

Figure 4.12. 2S2P1D simulation results of the complex modulus (a, b) and complex Poisson's ratio (c, d) mater curves

The same shape parameters (k, h, δ and β) of the 2S2P1D model were found to correctly describe the LVE behaviour of the three studied mixtures (c.f. section 4.2). The retained shape parameters for all complex modulus tests are provided in Table 4-4. These parameters remained unchanged for moisture conditioned samples with respect to non-conditioned ones (c.f. section 4.3). The temperature dependent parameter τ, and the static and glassy moduli and Poisson's ratios (E_{00}, E_0, ν_{00}, ν_0) will be further analysed in sections 4.3 and 4.4.

Table 4-4. 2S2P1D model shape parameters retained for all complex modulus tests

2S2P1D model shape parameters			
k	**h**	**δ**	**β**
0.19	0.59	2.05	350

4.2. Analysis of the complex modulus test results

Figure 4.13 and Figure 4.14 show the complex modulus test results of the GB3 samples in a Cole-Cole plot. The legend of the figures is organised by decreasing voids content in order to highlight the fact that the E_0 value increases with the decrease of the voids content. This is evident in the

figures since the plot from more compact samples reaches further on the abscissa axis (E_1). There is then a correlation between the glassy modulus values (E_0) and the air voids content for the GB3 mixture.

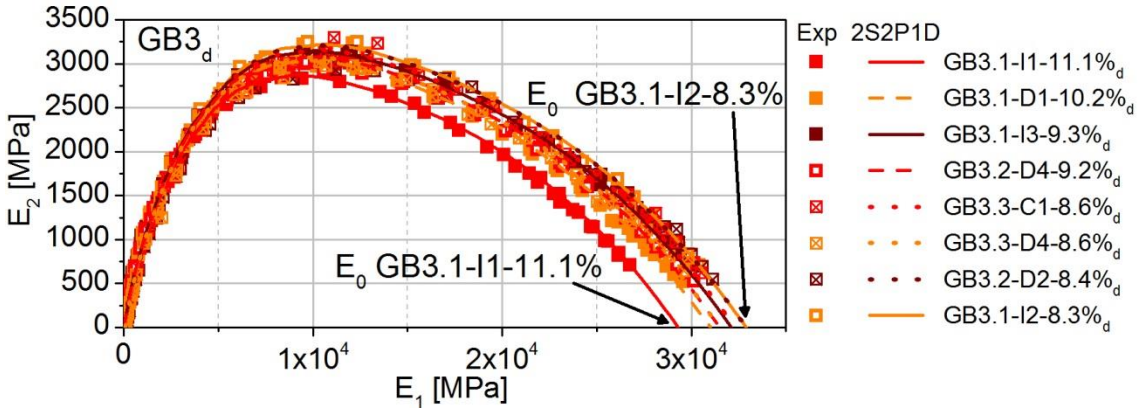

Figure 4.13. Complex modulus test results in Cole-Cole plot for non-conditioned GB3 samples and 2S2P1D simulations for each test

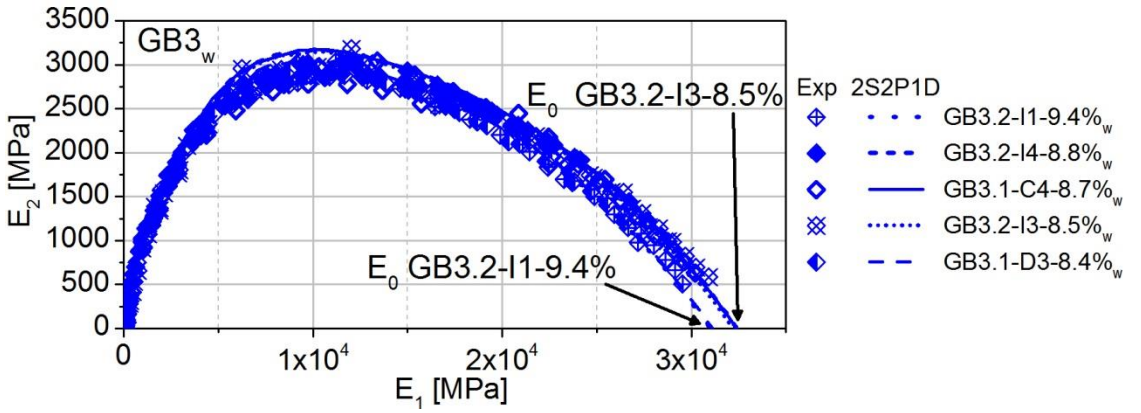

Figure 4.14. Complex modulus test results in Cole-Cole plot for moisture-conditioned GB3 samples and 2S2P1D simulations for each test

Figure 4.15 shows the results for the non-conditioned GB4 samples in a Cole-Cole plane. The glassy modulus E_0 increases with the decrease of the voids content of the samples.

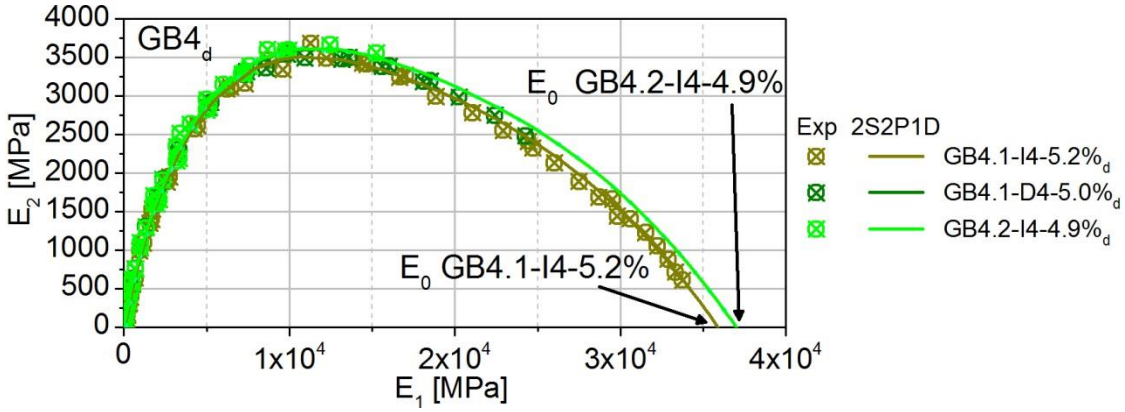

Figure 4.15. Complex modulus test results in Cole-Cole plot for non-conditioned GB4 samples and 2S2P1D simulations for each test

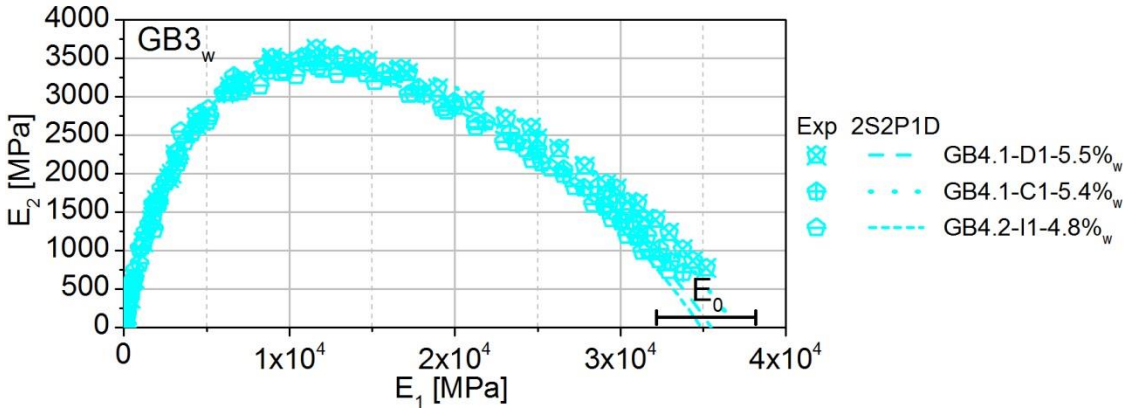

Figure 4.16. Complex modulus test results in Cole-Cole plot for moisture-conditioned GB4 samples and 2S2P1D simulations for each test

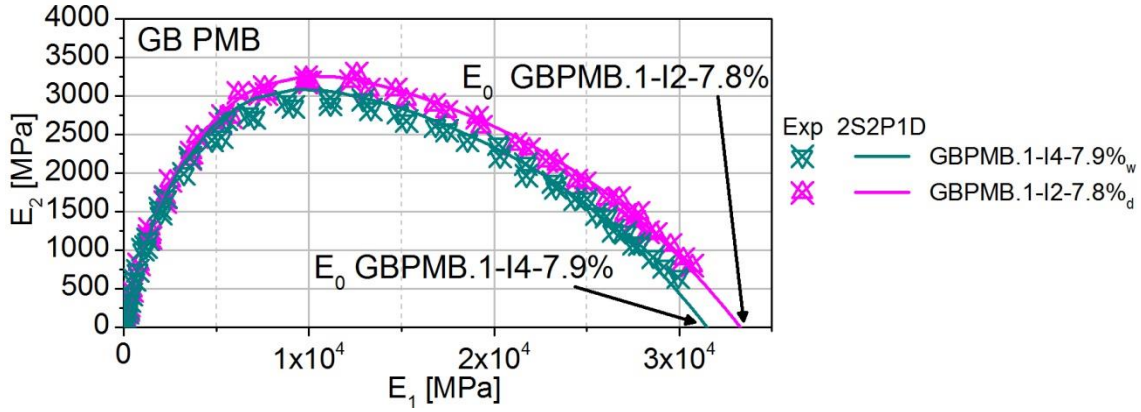

Figure 4.17. Complex modulus test results in Cole-Cole plot for all GB PMB samples and 2S2P1D simulations for each test

Glassy modulus values were plotted against air void content in Figure 4.18. The good linear fit carried out considering all points from all tests, regardless of the conditioning state, indicates that E_{00} is a parameter directly dependent of the voids content of the sample. Nor binder content or polymer-modification seems to affect the glassy modulus value more than voids content.

Moisture conditioned samples show a less direct correlation with void content than non-conditioned ones. In the case of the conditioned GB4 samples, the E_0 trend even appears inversed. High dispersion of E_0 with respect to the voids content could be an indicator of moisture damage of the material.

The τ parameter of the 2S2P1D model was also found to correlate with void content. Figure 4.19 shows that there is a very good linear fit of τ against void content considering all GB3 and GB4 mixtures. The moisture-conditioned GB3.1-C4-8.7% sample constitutes the only point that does not fit into the linear regression and lowers the coefficient of determination. A direct correlation between τ and void content could mean that the effects of compactness could be related to the effects of temperature since τ is the only 2S2P1D model parameter dependent on the temperature. It is important to highlight that the results from the GB PMB mixture do not fit into the linear regression. This is clearly an effect of the polymer-modification of the binder.

With respect to the static modulus (E_{00}), no correlation was found with voids content or moisture conditioning (c.f. Figure 4.20 to Figure 4.25). The fact that the E_{00} values are measured at the "accuracy" limits of the load cell used for the complex modulus tests does not allow further conclusions on this parameter.

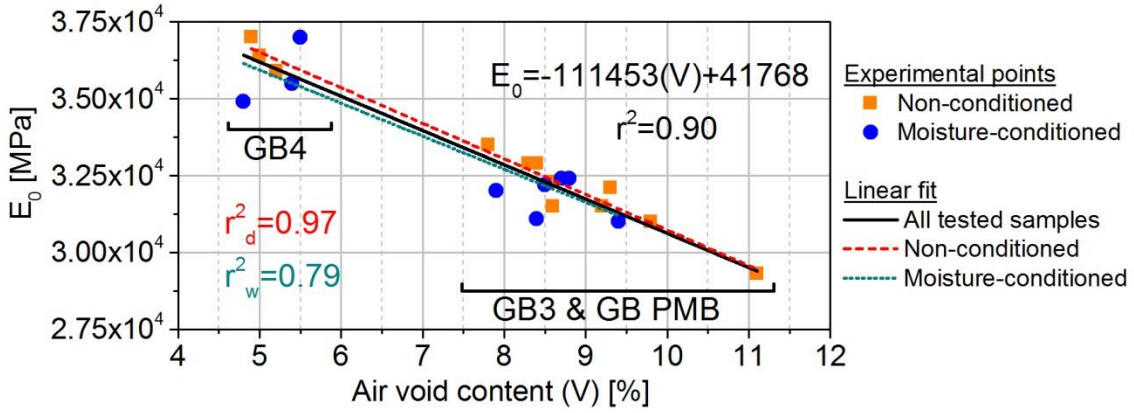

Figure 4.18. Glassy modulus (E_0) against voids content for all tested samples

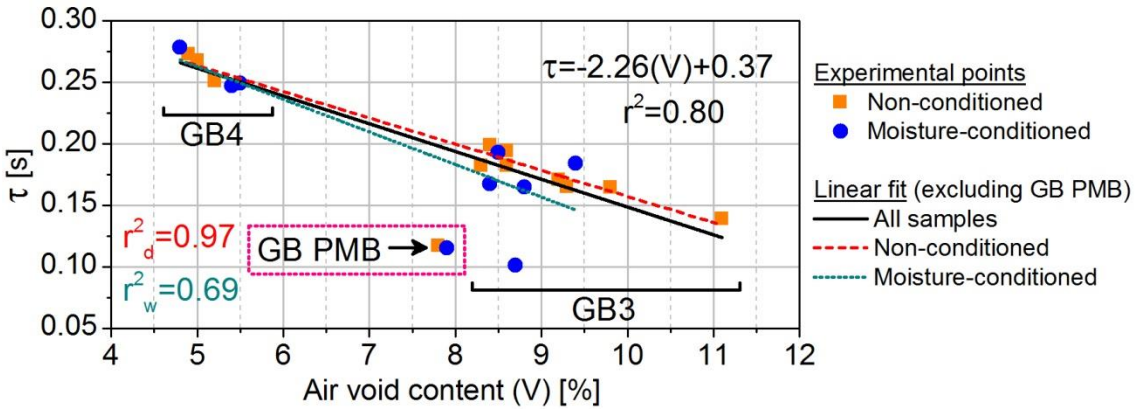

Figure 4.19. Characteristic time (τ) against voids content for all tested samples

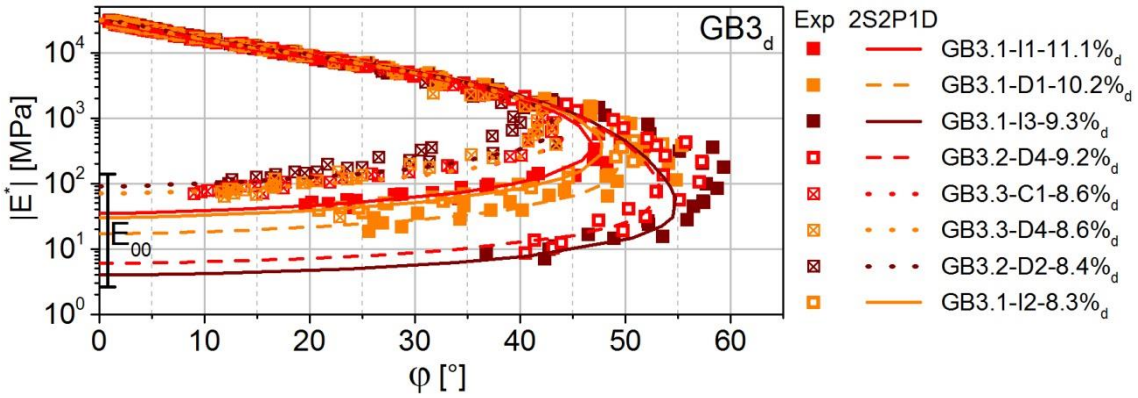

Figure 4.20. Complex modulus test results in Black plot for non-conditioned GB3 samples and 2S2P1D simulations for each test

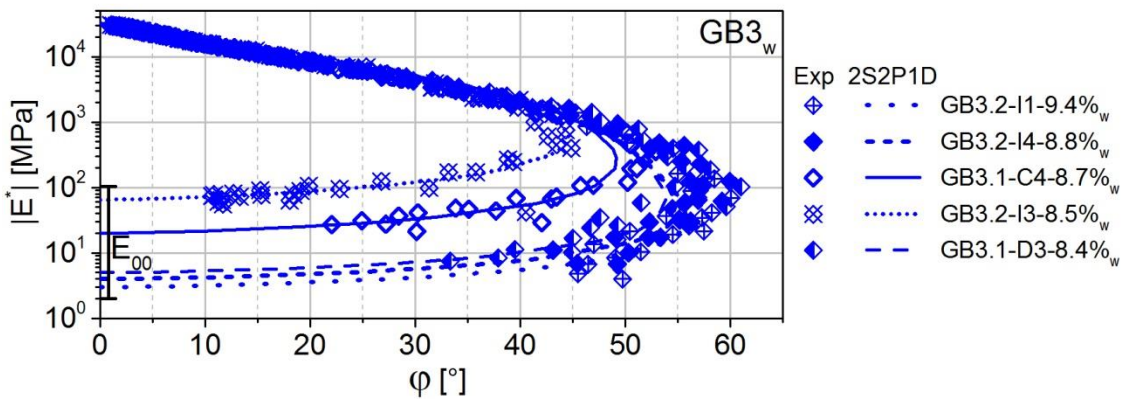

Figure 4.21. Complex modulus test results in Black plot for moisture-conditioned GB3 samples and 2S2P1D simulations for each test

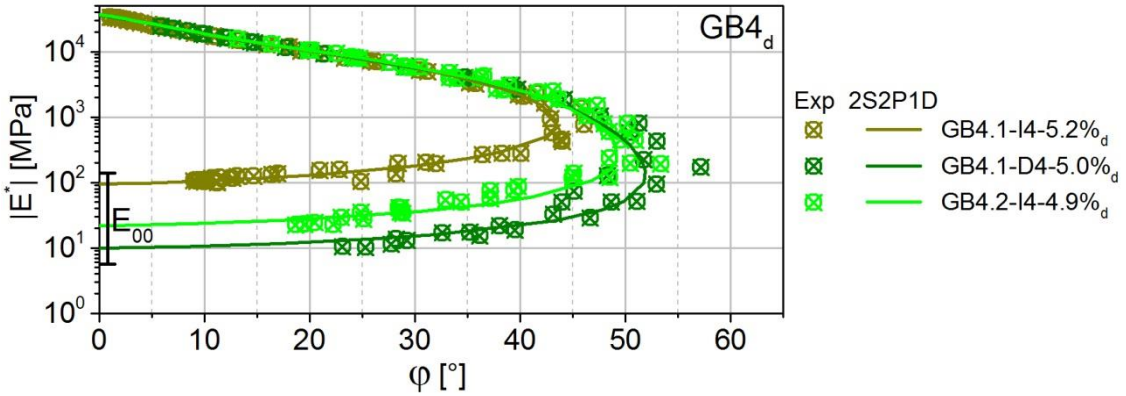

Figure 4.22. Complex modulus test results in Black plot for non-conditioned GB4 samples and 2S2P1D simulations for each test

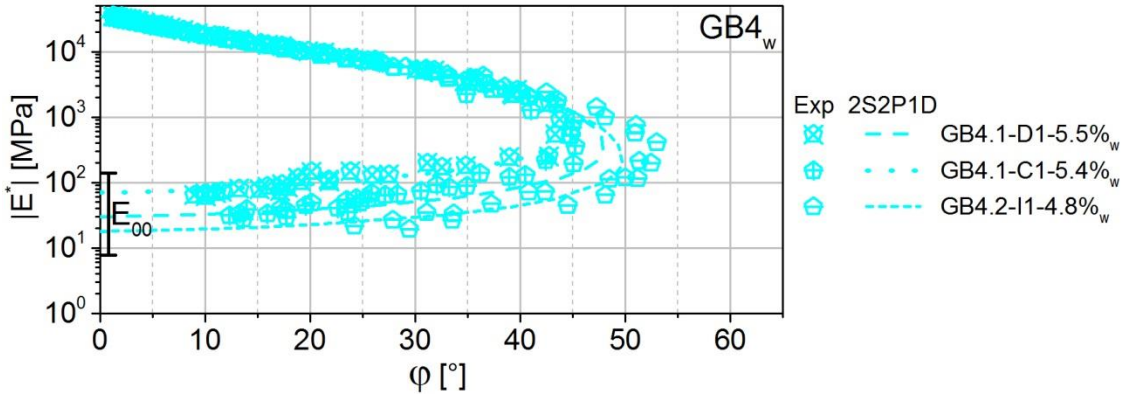

Figure 4.23. Complex modulus test results in Black plot for moisture-conditioned GB4 samples and 2S2P1D simulations for each test

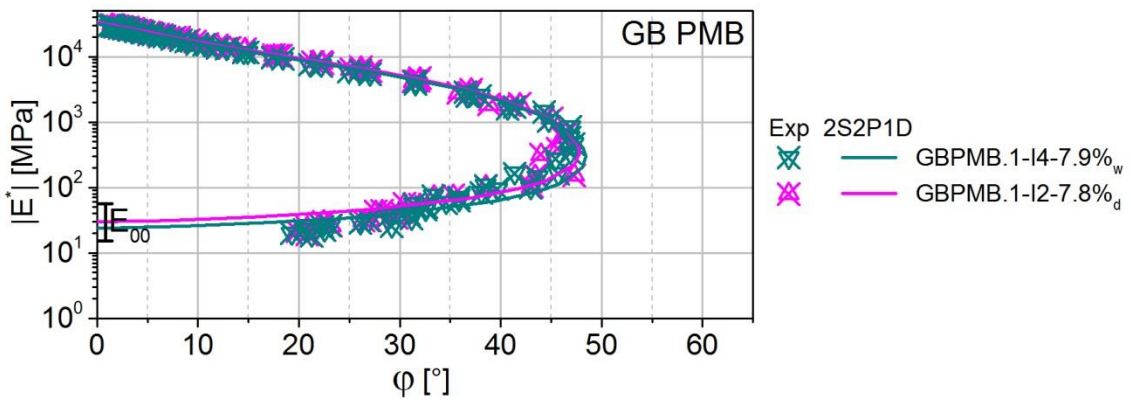

Figure 4.24. Complex modulus test results in Black plot for all GB PMB samples and 2S2P1D simulations for each test

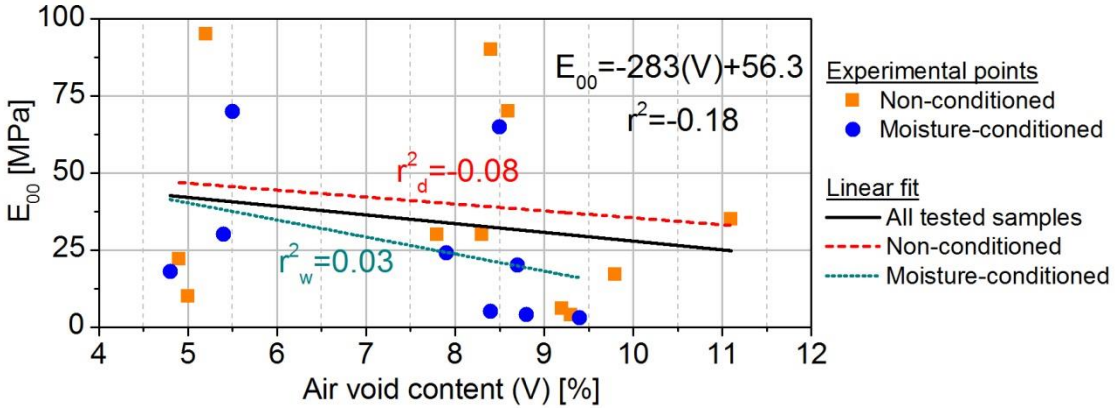

Figure 4.25. Static modulus (E_{00}) against voids content for all tested samples

The equations of the linear regressions for E_0 and τ presented in Figure 4.18 and Figure 4.19 were used to calculate the E_0 and τ values associated to the average void content (c.f. Table 3-4) of the GB3, GB4 and GB PMB samples. These values, together with the average E_0 value, were used to provide an average 2S2P1D simulation for each material (c.f. Table 4-6). This average 2S2P1D simulation serves to compare the three mixtures between them and is represented with thick continuous lines in Figure 4.26 to Figure 4.30. In these figures, the average void content of each material is specified in the legend.

Table 4-5. E_{00}, E_0 and τ values for average 2S2P1D simulation of each material

Mixture	Average voids content [%]	E_0 [MPa]	τ [s]	E_{00} [MPa]	E_{00} standard deviation [MPa]	ν_{00}	ν_0	τ_v [s]
GB3	8.1	32 740	0.19	32	31	0.37	0.17	2.5
GB4	4.4	36 864	0.28	41	34	0.35	0.21	3.1
GB PMB	7.6	33 297	0.20	27	4*	-	-	-

* Based on only 2 GB PMB samples

Figure 4.26 to Figure 4.29 show the LVE behaviour comparison of the studied mixtures using the 2S2P1D average simulations.

GB4 mixture presents higher E_0 values than the other two mixtures due to its lower air void content. The optimized aggregate packing of the GB4 allows it to present higher stiffness values at low temperature and/or high frequency loading conditions. GB4 mixture also presents higher loss modulus (E_2) values than the GB3 and GB PMB mixtures. Higher energy dissipation properties are expected from the GB4 mixture.

From the analysis of the master curves, it is observed that GB4 presents higher stiffness values for the whole equivalent frequency range (c.f. Figure 4.27). This is also due to its optimized aggregate packing and low void content. In terms of Poisson's ratio, the GB3 mixture seems to be less susceptible to frequency changes than the GB4. However, both mixtures present a non-negligible variation of |v*| with frequency and/or temperature that needs to be taken into account.

The polymer-modification of the GB PMB binder does not seem to significantly affect the stiffness of the mixture with respect to the reference GB3 mixture. Both GB PMB and GB3 mixtures present similar E_2 and E_1 values. They present therefore the same stiffness for the studied equivalent frequency range. All mixtures present similar E* phase angle values.

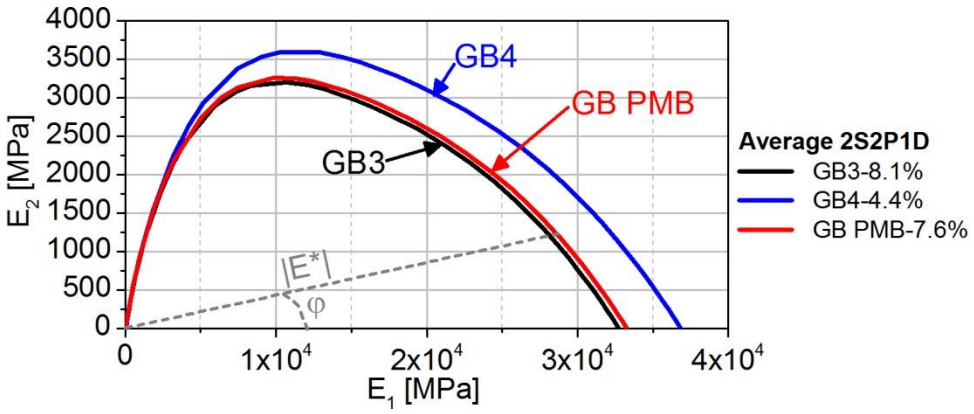

Figure 4.26. Comparison of the GB3, GB4 and GB PMB mixtures in Cole-Cole plot - |E*| at same φ and highlight on the behaviour at low temperature and/or high frequency

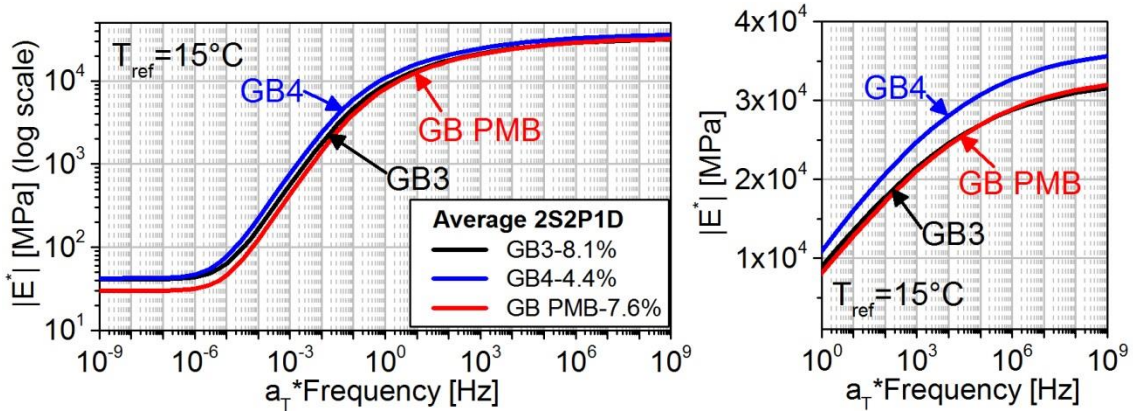

Figure 4.27. Comparison of the GB3, GB4 and GB PMB |E*| master curves (left) with zoom at the high equivalent frequencies range in a semi-logarithmic plot (right)

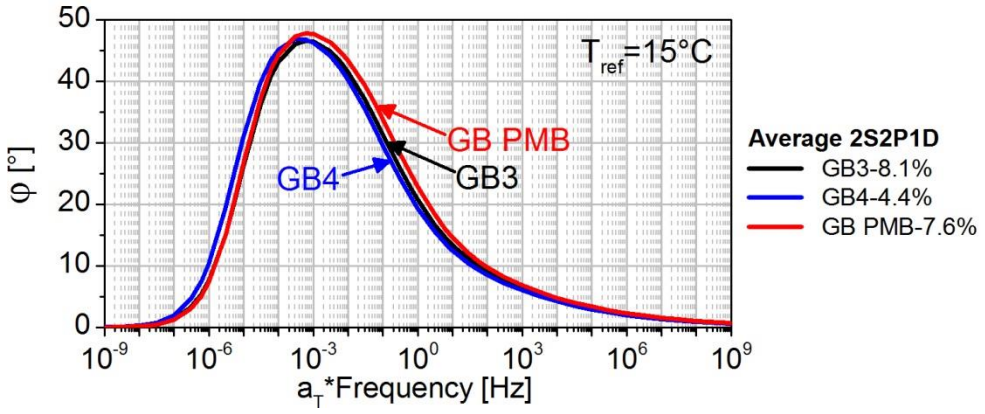

Figure 4.28. Comparison of the GB3, GB4 and GB PMB E* phase angle master curves

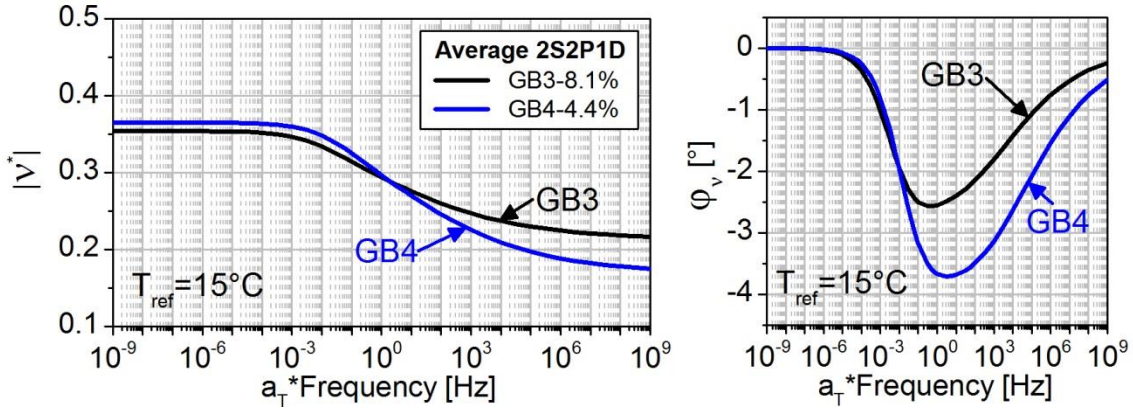

Figure 4.29. Comparison of the GB3 and GB4 |v*| master curve (left) and v* phase angle master curve (right)

Figure 4.30 presents the dissipated energy (W) calculations for the three studied mixtures at both stress and strain control modes. The calculations were made with the average 2S2P1D simulation with strain amplitude of 50 µm/m and stress amplitude of 35 kPa. The stress amplitude value was arbitrarily chosen as to obtain W values of the same order of magnitude as the ones calculated for the strain control mode.

For a strain control mode, such as the one used during the tests carried out during this study, the GB4 mixture presents a higher peak of energy dissipation per loading cycle than the GB3 and GB PMB ones. This is in accordance with the higher E_2 values of the GB4 mixture. In this loading case, the polymer-modification of the GB PMB binder does not significantly alter the energy dissipation properties of the GB3 reference mixture. However, for a stress control mode, the calculations show that the energy dissipation peak of the GB PMB is much higher than the other two mixtures'. It is important to note that the energy dissipation peak for a stress control mode is attained at very low frequencies (around 10^{-5} Hz) while it appears at around 1 Hz for a strain control mode.

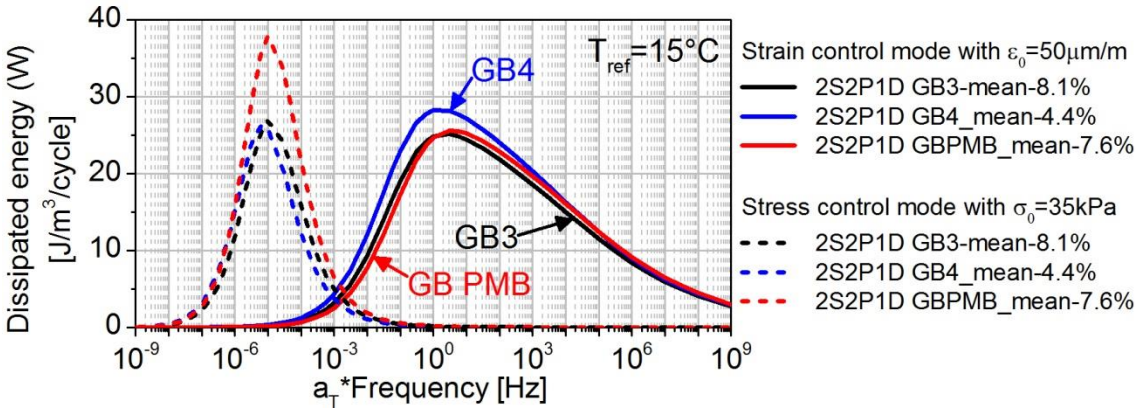

Figure 4.30. Comparison of the GB3, GB4 and GB PMB energy dissipation master curves for both stress and strain control modes

In order to analyse the test results without taking into account the influence of the air voids content of the samples, the results can be plotted in normalised Cole-Cole plots. In such plots, the real and imaginary parts of the complex modulus are normalized by the E_{00} and E_0 moduli as shown in equations [4-1] and [4-2]:

$$E_{1\_norm} = \frac{E_1 - E_{00}}{E_0 - E_{00}} \quad [4\text{-}1]$$

$$E_{2\_norm} = \frac{E_2}{E_0 - E_{00}} \quad [4\text{-}2]$$

$$\tan(\varphi_{norm}) = \frac{E_{2\_norm}}{E_{1\_norm}} \quad [4\text{-}3]$$

$$|E^*|_{norm} = \sqrt{{E_{1\_norm}}^2 + {E_{2\_norm}}^2} \quad [4\text{-}4]$$

Likewise, the same normalisation process can be done for the complex Poisson's ratio. Normalising eliminates then the influence of E_0 and E_{00} in the Cole-Cole plot and the parameter τ does not alter its form. Figure 4.31 and Figure 4.32 show the normalised Cole-Cole plot for the complex modulus of the GB3 samples. Both figures show a very good superposition of the complex modulus tests results for both conditioned and non-conditioned samples, respectively. A single calibration of the shape parameters of the 2S2P1D model can then be used for each conditioning state. The repeatability of the tests can also be verified with the normalised Black plot and with the normalised master curves (c.f. Figure 4.33 to Figure 4.39).

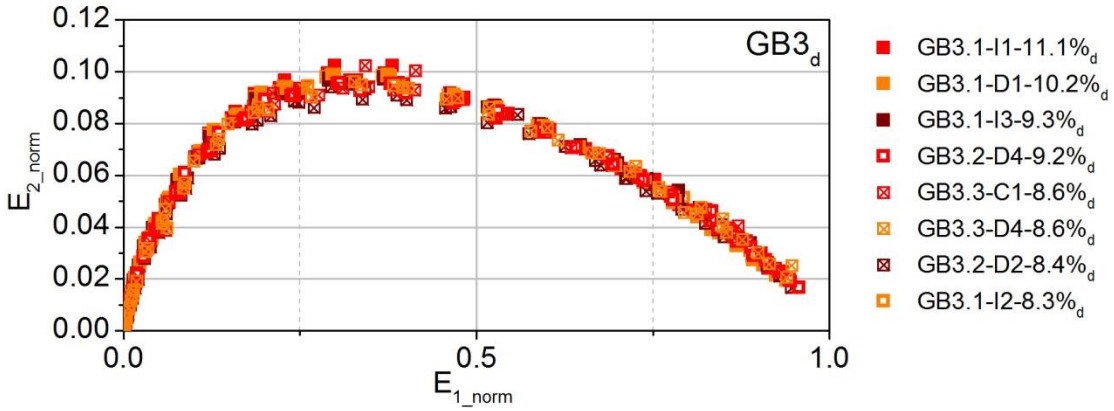

Figure 4.31. Complex modulus test results of non-conditioned GB3 samples in normalised Cole-Cole plot

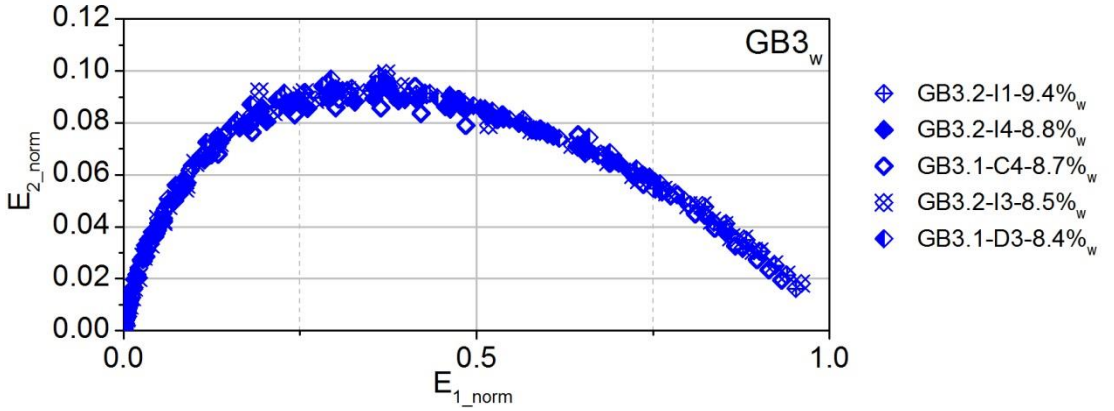

Figure 4.32. Complex modulus test results of moisture-conditioned GB3 samples in normalised Cole-Cole plot

Black plots highlight the behaviour at high temperatures and/or low frequencies. The normalised Black plots in Figure 4.33 and Figure 4.34 show a high dispersion of the |E*| data corresponding to normalised phase angle values over 45°. These points correspond to the test conditions at high temperatures, mainly 55°C and 65°C. At these temperatures, the accuracy limit of the sensors is reached since the measured force is very low. As a reminder, the icons comprising a cross or a line in them indicate that the test was done with the MTS® hydraulic press. Despite the evident dispersion at high temperatures, most of the experimental points correspond to normalised phase angle values lower than 40° and they superpose very well for both conditioning states of the GB3 mixture.

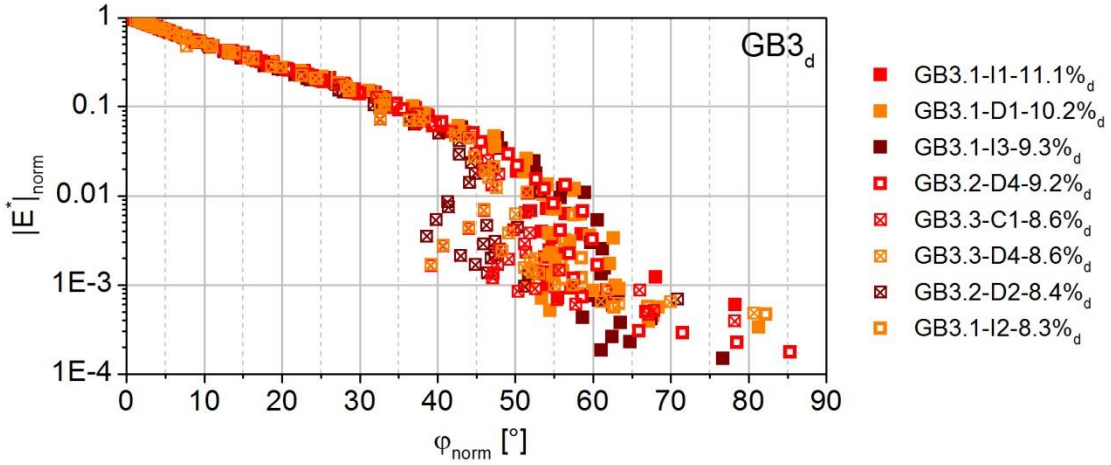

Figure 4.33. Complex modulus test results of non-conditioned GB3 samples in normalised Black plot

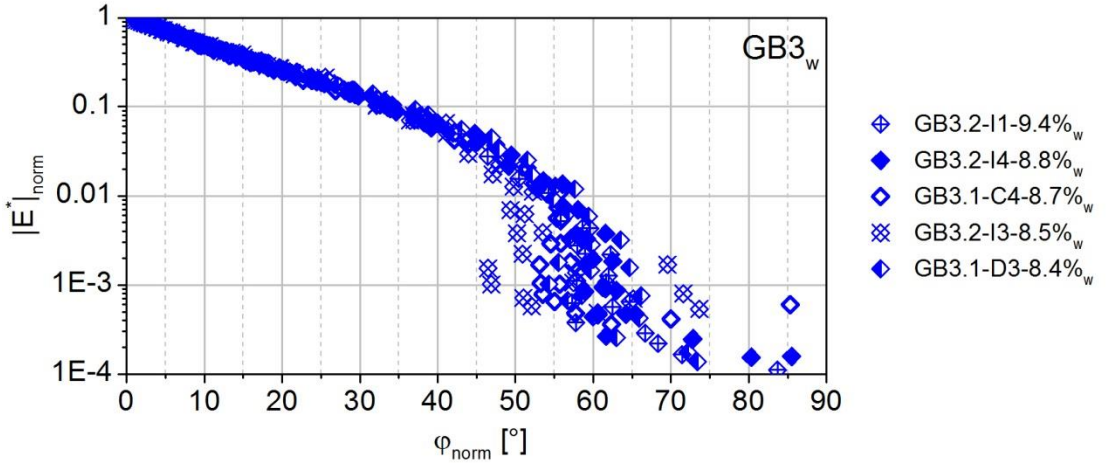

Figure 4.34. Complex modulus test results of moisture-conditioned GB3 samples in normalised Black plot

Normalised |E*|master curves, plotted in semi-logarithmic axes (log(a_T*f), $|E^*|_{norm}$), allowed observing a superposition of the experimental data at high equivalent frequencies (c.f. Figure 4.35 and Figure 4.36). This is in accordance with the good superposition of the results in the normalised Cole-Cole plots. With both logarithmic axes, the same dispersion as seen in the normalised Black plots would be seen at low equivalent frequencies. Normalised phase angle values shown in Figure 4.37 show a good superposition of the test results for equivalent frequencies above 10^{-3} Hz. The normalised curves of complex Poisson's ratio norm and phase angle are presented in Figure 4.38 and Figure 4.39. The results in both figures show a good repeatability and a clear trend of the Poisson's ratio measurements also for equivalent frequencies above 10^{-3} Hz. This allows the calibration of the 2S2P1D model for the 3-dimensional case. Radial strain measurements were nonetheless imprecise at high temperature test stages, which could be due to an excessive softening of the mastic. For the GB3 unconditioned state, samples GB3.1-I3-9.3%, GB3.2-D4-9.2% and GB3.1-I2-8.3% present repeatable enough v* results. The complex Poisson's ratio results from the moisture conditioned sample GB3.1-C4-8.7% do not

seem to be representative of the LVE behaviour of the material given the uncertain trend they describe.

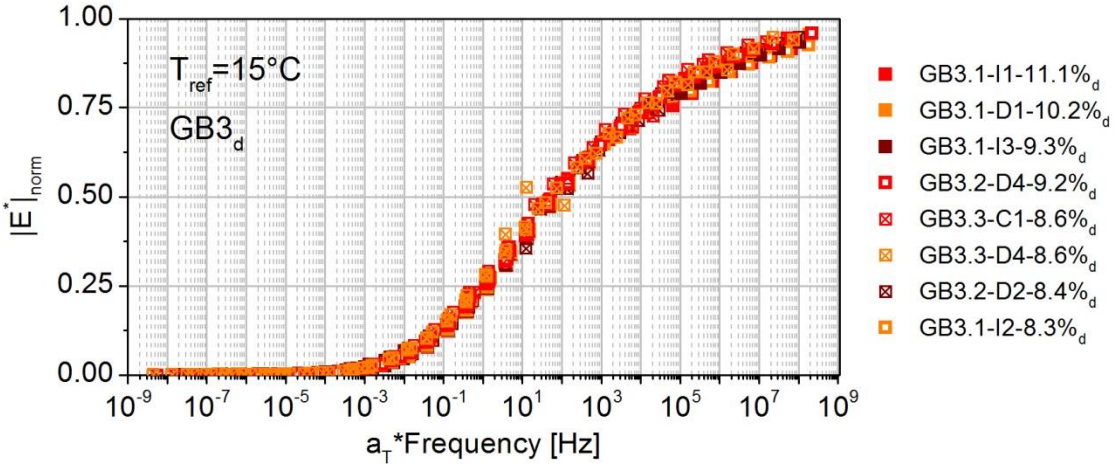

Figure 4.35. Normalised master curve of the norm of the complex modulus of non-conditioned GB3 samples

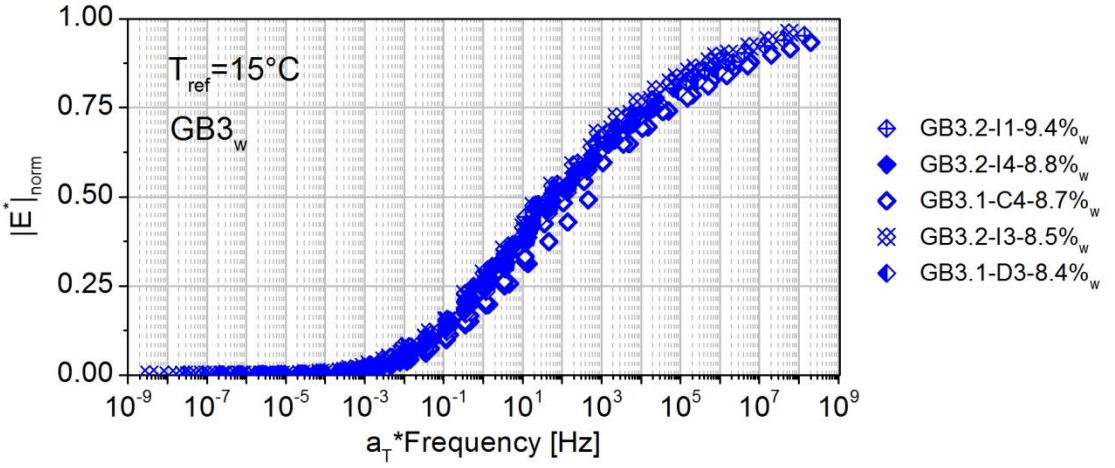

Figure 4.36. Normalised master curve of the norm of the complex modulus of moisture-conditioned GB3 samples

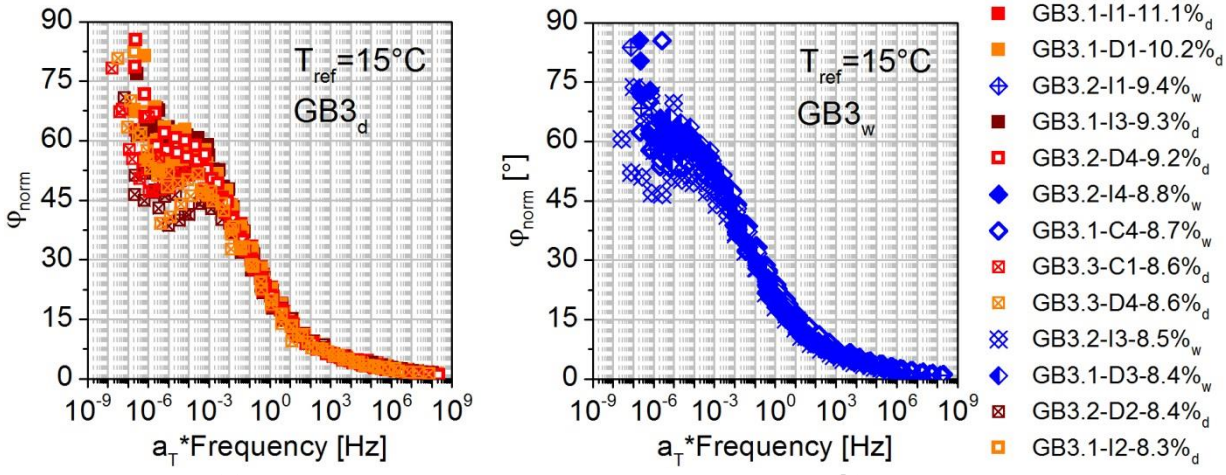

(a) (b)

Figure 4.37. Normalised master curve of the E* phase angle of non-conditioned (a) and moisture-conditioned (b) GB3 samples

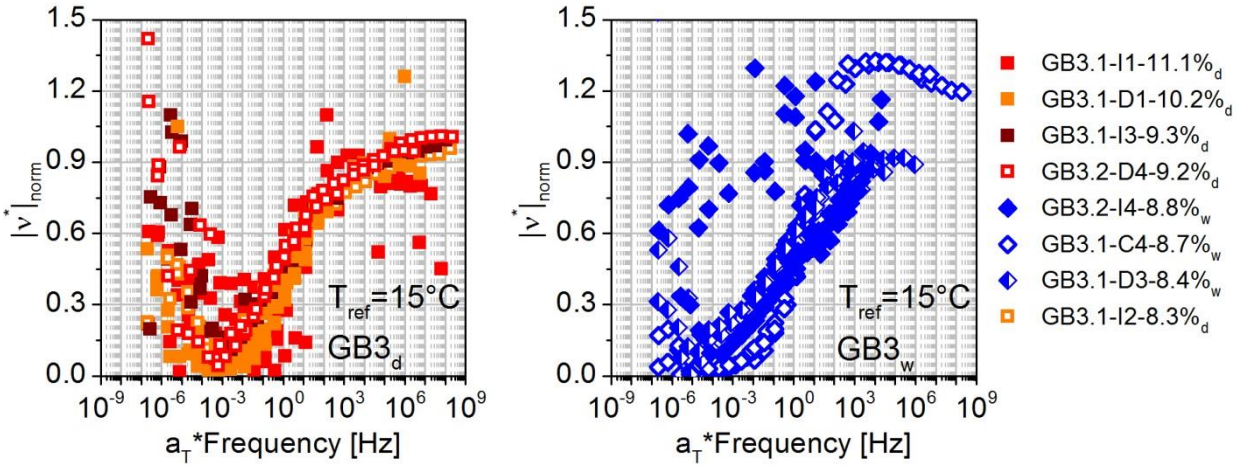

(a) (b)

Figure 4.38. Normalised master curve of the complex Poisson's ratio of non-conditioned (a) and moisture-conditioned (b) GB3 samples

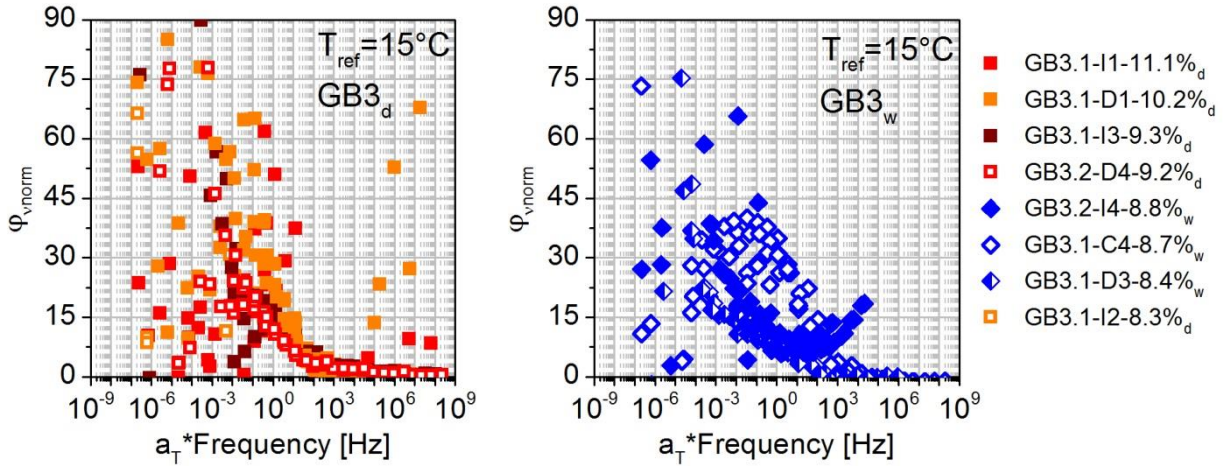

(a) (b)

Figure 4.39. Normalised master curve of the v* phase angle of non-conditioned (a) and moisture-conditioned (b) GB3 samples

In conclusion, a good repeatability of the GB3 complex modulus tests was observed for both conditioning states in the tri-dimensional case. Closer analysis must be done for the test conditions at high temperatures and low frequencies since the results are less repeatable. Section 4.4 presents a specific experimental work carried out to explain the low repeatability for such extreme loading conditions. The same conclusions on repeatability were made for the GB4 mixture as seen in Figure 4.40 to Figure 4.43. A single 2S2P1D calibration can then be used for each conditioning state of the GB4 samples. Poisson's ratio results were obtained from only one sample of GB4 at each conditioning state.

The good repeatability of the complex modulus tests observed for the GB3 mixture allowed reducing the number of tests carried out on the GB4 and GB PMB mixtures.

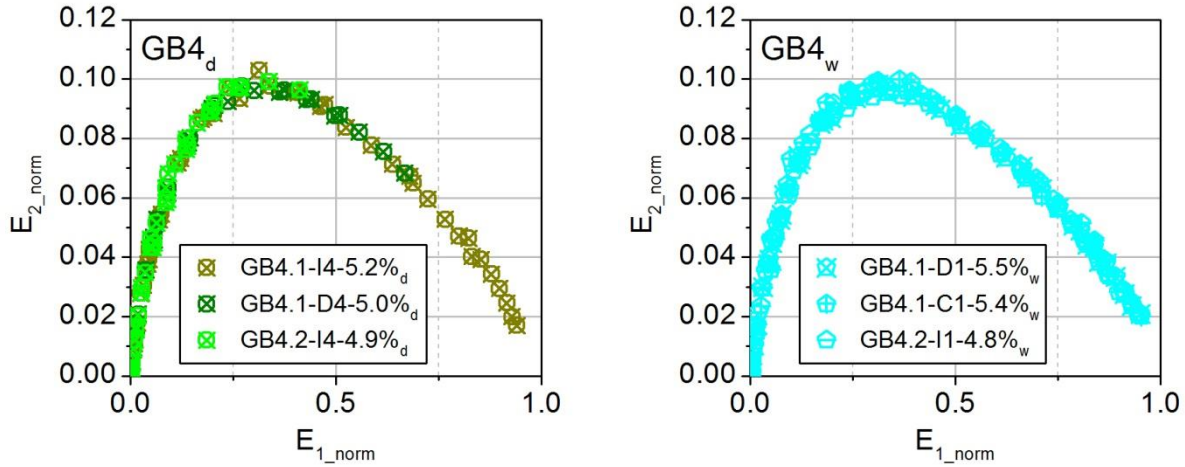

(a) (b)

Figure 4.40. Complex modulus test results of non-conditioned (a) and moisture-conditioned (b) GB4 samples in Cole-Cole plot

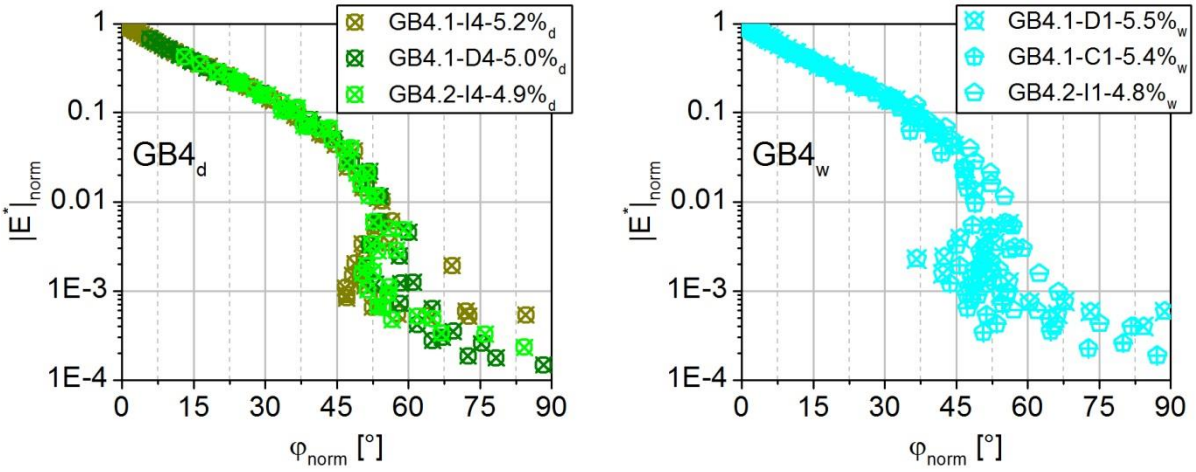

(a) (b)

Figure 4.41. Complex modulus test results of non-conditioned (a) and moisture-conditioned (b) GB4 samples in Cole-Cole plot

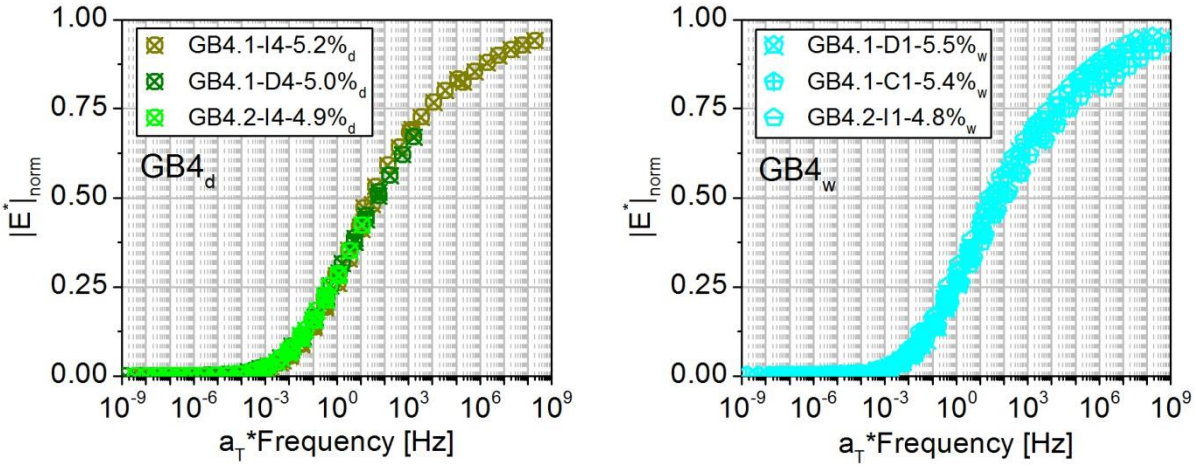

(a) (b)

Figure 4.42. Normalised |E*| master curves of non-conditioned (a) and moisture-conditioned (b) GB4 samples

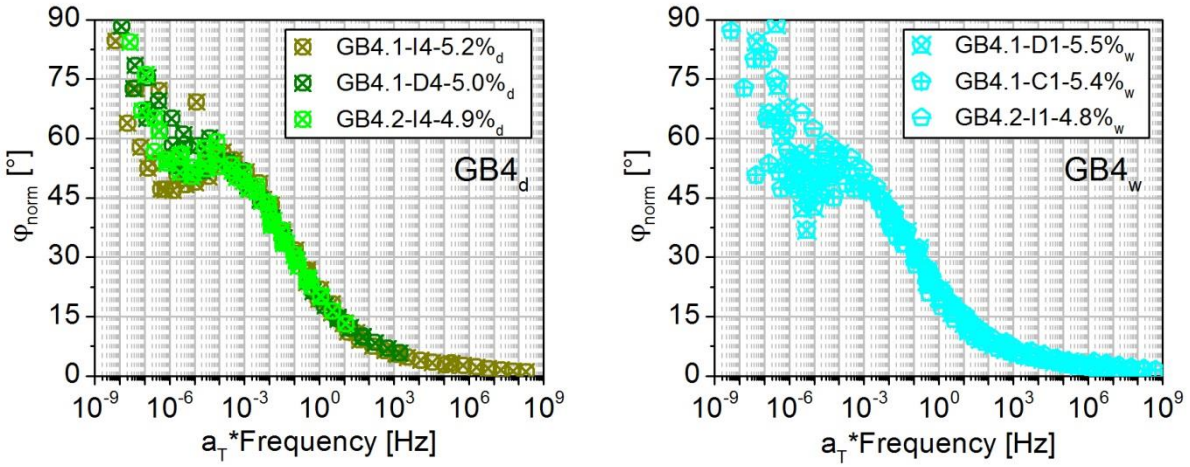

(a) (b)

Figure 4.43. Normalised E* phase angle master curves of non-conditioned (a) and moisture-conditioned (b) GB4 samples

4.3. Influence of moisture conditioning on LVE behaviour

In order to determinate the influence of moisture conditioning on the LVE properties of the studied mixtures, the complex modulus tests results are compared in normalised plots. A significantly different shape of the normalised plots might indicate considerable changes in the LVE behaviour of the material due to moisture conditioning.

Figure 4.44 shows the complex modulus test results of all tested GB3 samples in a normalised Cole-Cole plot. In Figure 4.44, the results from the moisture conditioned samples describe the same curve as those from the non-conditioned ones. This is also the case when plotted in a normalised Black plot as seen in Figure 4.45. Even the data dispersion at high temperature conditions is similar between conditioned and non-conditioned samples. This allows concluding that a single 2S2P1D calibration can be used for all GB3 tests regardless of their moisture-conditioning state.

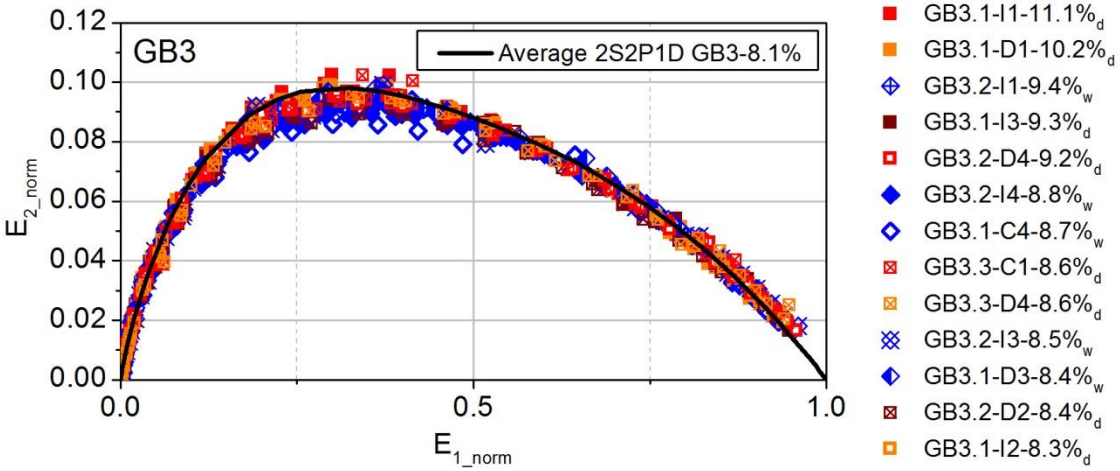

Figure 4.44. Normalised complex modulus test results of all tested GB3 samples in Cole-Cole plot and normalised 2S2P1D simulation for a sample with average voids content of 8.1%

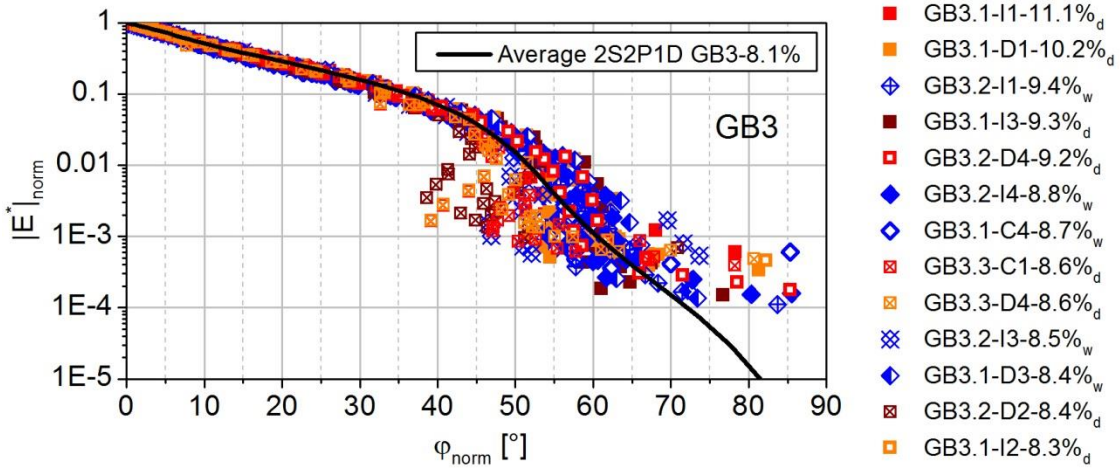

Figure 4.45. Normalised complex modulus test results of all tested GB3 samples in Black plot and normalised 2S2P1D simulation for a sample with average voids content of 8.1%

The 2S2P1D simulation presented in both Figure 4.44 and Figure 4.45 used the shape parameters (k, h, δ and β) that are provided in Table 4-4. The E_{00}, E_0 and τ values correspond to that of a sample with voids content of 8.1% which is the average of all GB3 tested samples (c.f. Table 4-5).These parameters depend on the voids content as shown previously.

The same observations as for the GB3 mixture were found for the GB4 mixture. In Figure 4.46 and Figure 4.47, the normalised Cole-Cole and Black plots of all GB4 samples do not show significant differences between the results from moisture-conditioned and non-conditioned samples.

Figure 4.48 and Figure 4.49 present the complex modulus test results for the GB PMB moisture-conditioned and non-conditioned samples in normalised Cole-Cole and Black plots, respectively. For the GB PMB mixture no evident differences in the shape of the normalised plots was found indicating no significant changes of the LVE behaviour of the mixture due to moisture conditioning. The 2S2P1D simulation presented in the figures corresponds to that of the GBPMB.1-I2-8.7% sample.

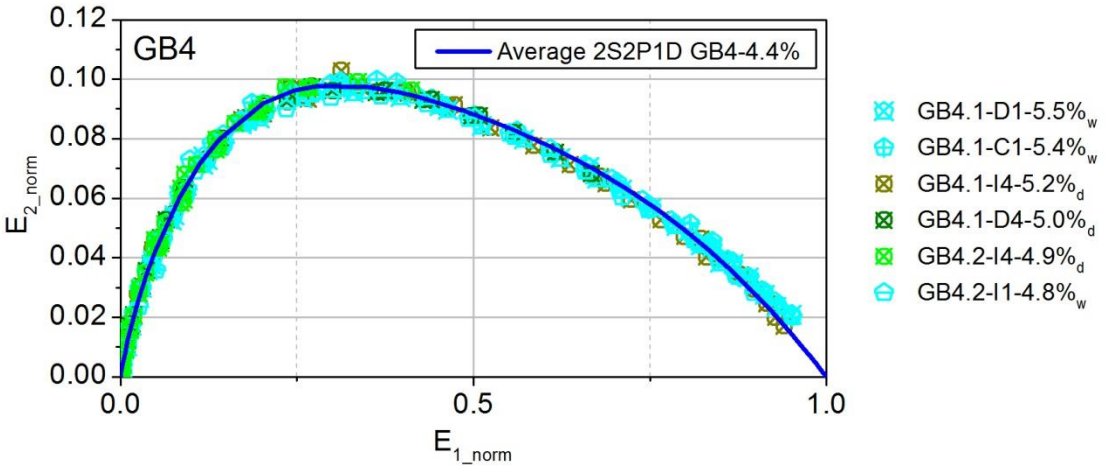

Figure 4.46. Normalised complex modulus test results of all tested GB4 samples in Cole-Cole plot and normalised 2S2P1D simulation for a sample with average voids content of 4.4%

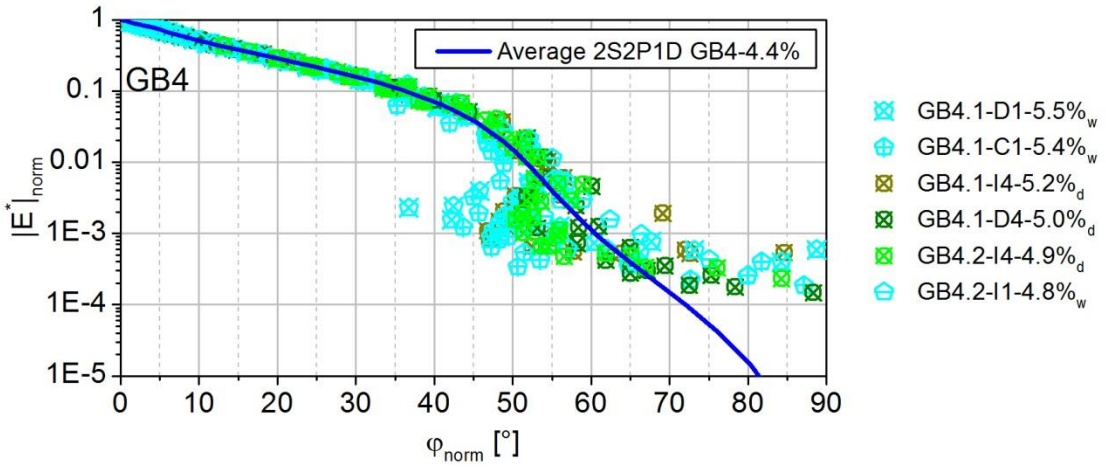

Figure 4.47. Normalised complex modulus test results of all tested GB4 samples in Cole-Cole plot and normalised 2S2P1D simulation for a sample with average voids content of 4.4%

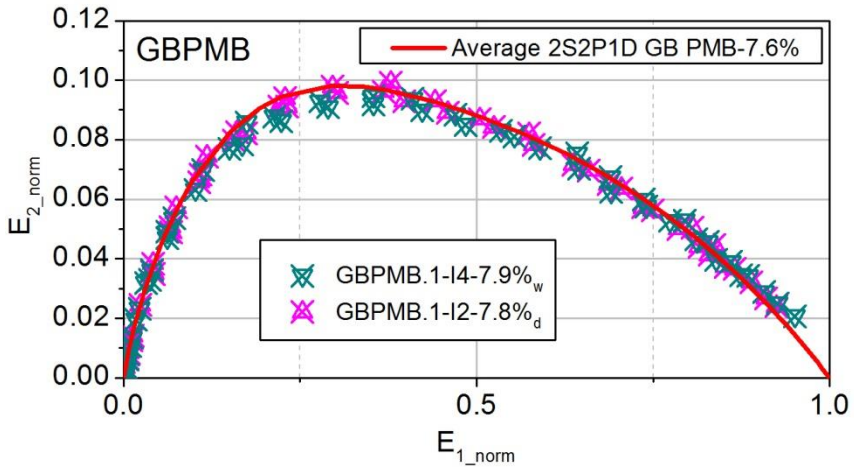

Figure 4.48. Normalised complex modulus test results of all tested GB PMB samples in Cole-Cole plot and normalised 2S2P1D simulation for a sample with average voids content of 7.6%

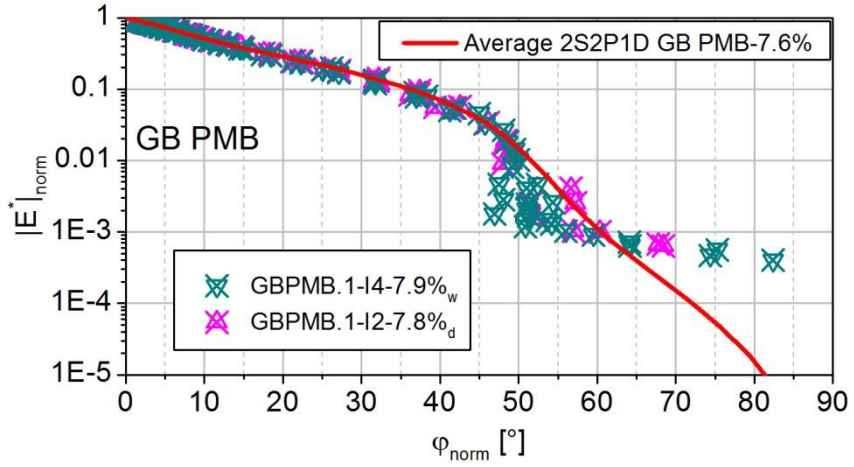

Figure 4.49. Normalised complex modulus test results of all tested GB PMB samples in Black plot and normalised 2S2P1D simulation for a sample with average voids content of 7.6%.

The used moisture conditioning procedure does not seem to significantly alter the LVE properties of any of the materials. This is interesting since, at negative temperatures, the water trapped in the interstices of the bituminous mixtures freezes and should cause a different behaviour of the partially saturated samples with respect to the non-conditioned ones. The presence of ice in the pores should add stiffness to the mixture since ice would act as a filling stiff material reducing the effective void content at low temperatures. The saturation levels of the conditioned samples are then very low to cause a real modification of the LVE behaviour of the tested materials at negative temperatures. Moreover, Figure 4.50 and Figure 4.51 show that all test results from all samples at both moisture-conditioning states describe the same curves in normalised Cole-Cole and Black plots. This is why a single 2S2P1D calibration (shape parameters presented in Table 4-4) is used for all samples. The feeble impact of moisture conditioning on the LVE behaviour of the materials might lay on the fact that saturation levels of the moisture-conditioned samples are very low and the damage caused is so small that it does not affect the materials performance for short duration loadings at very low strain levels.

The values of the E_{00}, E_0 and τ values for the 2S2P1D simulation of all tested samples are provided in Table 4-6. No clear relation between moisture-conditioning state and those parameters was observed. The same observation is made for the 3-dimensional case after analysis of the model parameters for the Poisson's ratio.

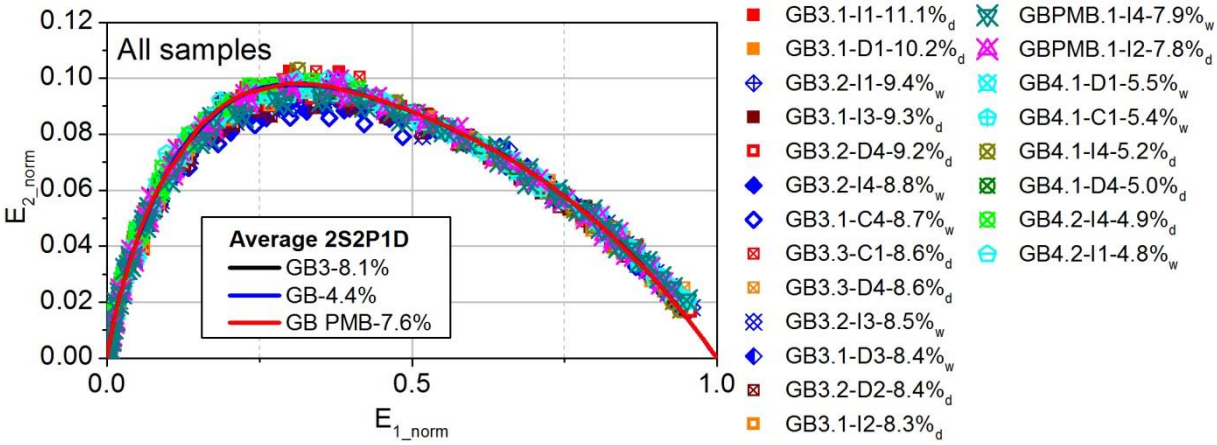

Figure 4.50. Normalised complex modulus test results of all tested samples in Cole-Cole plot and normalised 2S2P1D simulations

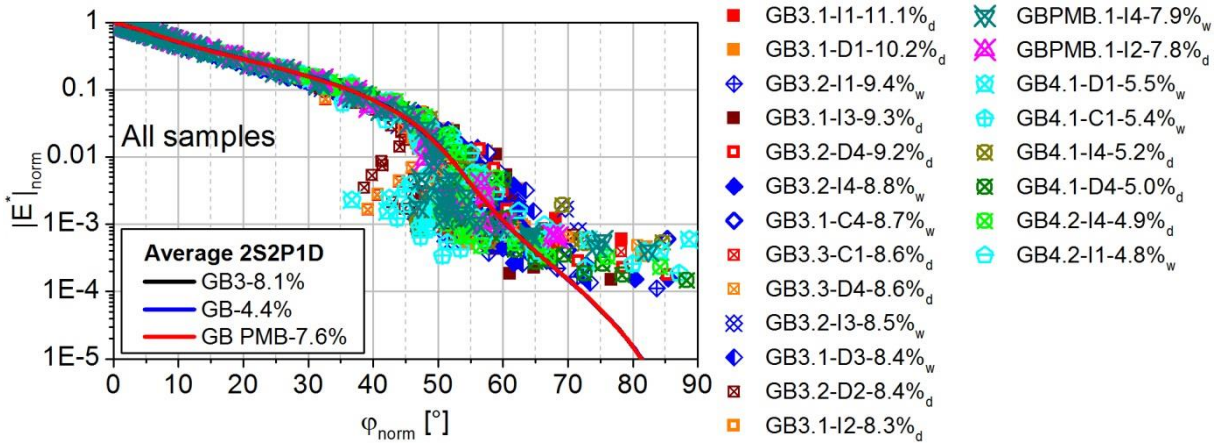

Figure 4.51. Normalised complex modulus test results of all tested samples in Black plot and normalised 2S2P1D simulations

Table 4-6. 2S2P1D model constants for all samples tested for a reference temperature of 15°C (blue filling indicates a moisture-conditioned sample)

Mixture	Sample	E_{00} [MPa]	E_0 [MPa]	τ [s]	k	h	δ	β	C_1	C_2
GB3	GB3.1-I1-11.1%$_d$	35	29 300	0.14	0.19	0.59	2.05	350	24	157
	GB3.1-D1-9.8%$_d$	17	31 000	0.16						
	GB3.2-I1-9.4%$_w$	3	31 000	0.18						
	GB3.1-I3-9.3%$_d$	4	32 100	0.17						
	GB3.2-D4-9.2%$_d$	6	31 500	0.17						
	GB3.2-I4-8.8%$_w$	4	32 400	0.16						
	GB3.1-C4-8.7%$_w$	20	32 400	0.10						
	GB3.3-C1-8.6%$_d$	70	32 300	0.20						
	GB3.3-D4-8.6%$_d$	70	31 500	0.18						
	GB3.2-I3-8.5%$_w$	65	32 200	0.19						
	GB3.1-D3-8.4%$_w$	5	31 100	0.17						
	GB3.2-D2-8.4%$_d$	90	32 900	0.20						
	GB3.1-I2-8.3%$_d$	30	32 900	0.18						
GB4	GB4.1-C1-5.4%$_w$	30	35 500	0.25						
	GB4.1-D1-5.5%$_w$	70	37 000	0.25						
	GB4.1-I4-5.2%$_d$	95	35 900	0.25						
	GB4.1-D4-5.0%$_d$	10	36 400	0.27						
	GB4.2-I4-4.9%$_d$	22	37 000	0.27						
	GB4.2-I1-4.8%$_w$	18	34 900	0.28						
GB PMB	GBPMB.1-I4-7.9%$_w$	24	32 000	0.12						
	GBPMB.1-I2-7.8%$_d$	30	33 200	0.12						

Table 4-7. Poisson's ratio 2S2P1D model constants for a reference temperature of 15°C (blue filling indicates a moisture-conditioned sample)

Mixture	Sample	ν_{00}	ν_0	τ_ν [s]
GB3	GB3.1-I1-11.1%$_d$	0.15	0.30	3.9
	GB3.1-D1-9.8%$_d$	0.24	0.33	1.0
	GB3.1-I3-9.3%	0.21	0.32	0.83
	GB3.2-D4-9.2%	0.22	0.41	1.2
	GB3.2-I4-8.8%	0.15	0.39	4.1
	GB3.1-C4-8.7%	0.03	0.40	0.51
	GB3.1-D3-8.4%	0.21	0.40	12.6
	GB3.1-I2-8.3%	0.25	0.41	0.84
GB4	GB4.1-D4-5.0%	0.17	0.37	0.06
	GB4.2-I1-4.8%	0.10	0.41	8.2

4.4. Study on the quasi static modulus of bituminous mixtures

This section presents the analysis and work carried out in order to understand the high variability of the static modulus E_{00}.

It is possible for the samples to have been extended or contracted during the complex modulus tests. It is reminded that during temperature stabilisation period after each change of temperature a constant load is applied to the specimen. This load is fixed at zero but very small fluctuation from monitoring system, especially at high temperature, may induce contraction or extension of the sample following sign of applied load. Contraction or extension of the sample could alter the measure of E_{00} which is measured at the end of the test. To verify if the sample suffered any kind of extension or contraction during the test, the central strain values of the loading stages at 15°C can be compared with each other. The central strain value is referred to as $\varepsilon_{average1}$ (c.f. Equation [1-13]). The initial $\varepsilon_{average1}$ value ($\varepsilon_{average1\_0}$) is the central strain value of the loading at 0.01 Hz of the first stage at 15°C. The variation of $\varepsilon_{average1}$ during the test ($\Delta\varepsilon_{average1}$) is calculated as:

$$\Delta\varepsilon_{average1} = \varepsilon_{average1} - \varepsilon_{average1\_0} \quad [4\text{-}5]$$

where $\varepsilon_{average1}$ is the central strain value of a loading at 15°C

Only the values at 15°C can be compared with each other since this allows neglecting the influence of temperature on the extensometers.

As an example, Figure 4.52 shows the variation of $\varepsilon_{average1}$ during the GB3.1-I2-8.3% test for which the sample suffered contraction (negative $\Delta\varepsilon_{average1}$ values). It is observed that there is almost no variation of the central value of the strain signal between the two first stages at 15°C.

However, between the first and the third stages at 15°C, the $\varepsilon_{average1}$ value decreased of 850 µm/m. This means that the sample suffered contraction during the high temperature stages.

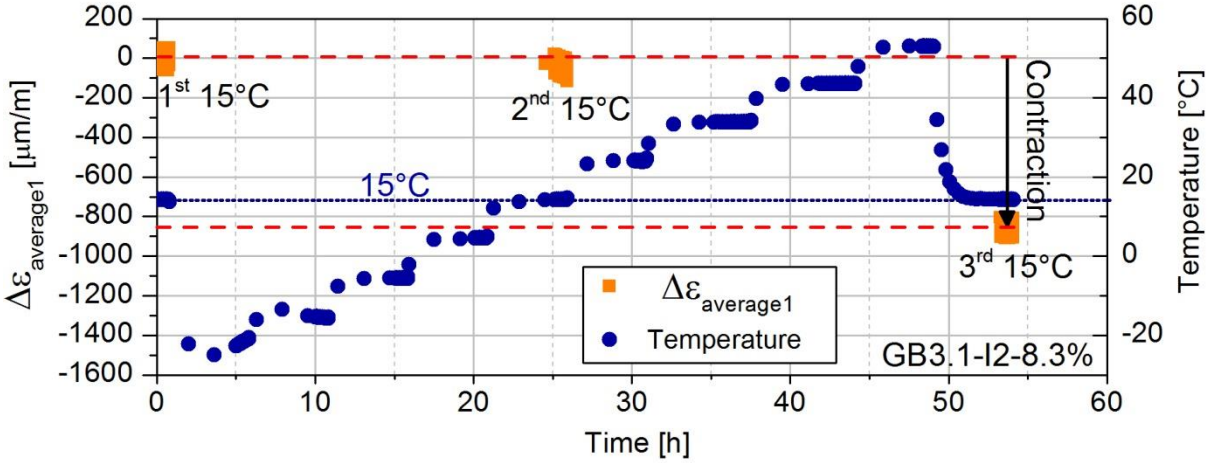

Figure 4.52. Evolution of the $\varepsilon_{average1}$ during a complex modulus test presenting sample contraction GB3.1-I2-8.3%

Figure 4.53 shows the variation of $\varepsilon_{average1}$ for the GB3.1-I3-9.3% test for which the sample suffered extension (positive $\Delta\varepsilon_{average1}$ values). As for the GB3.1-I2-8.3% test, there is almost no variation of $\varepsilon_{average1}$ between the first and second stages at 15°C. However, between the first stage and third stage at 15°C, the $\varepsilon_{average1}$ value increased of almost 1000 µm/m. This means that the sample suffered extension during the high temperature stages.

As a reminder, the hydraulic press control is set to maintain a nil force during the temperature change and stabilization periods. This means that the force values oscillate around zero during these periods since maintaining a force value equal to zero is impossible. Due to the relaxation properties of bituminous mixtures, the application of very small stresses, perceived as nil by the load cell, might lead to strain development over time. The effect of these small stresses on the sample deformation is amplified as the modulus decreases due to the rise in temperature. At high temperatures, for a sample in contraction, these stresses are bore by the aggregate structure which opposes to the contraction and develops forces perceived by the load cell. This helps regulating the stress and strain levels during the temperature stabilization periods. However, the aggregate structure does not bear the traction efforts developed in a sample in extension. At high temperatures, the mastic is soft and opposes weakly to traction, developing forces that are not perceived by the load cell. The small tractions are then not regulated and are applied during long periods of time causing the extension of the sample.

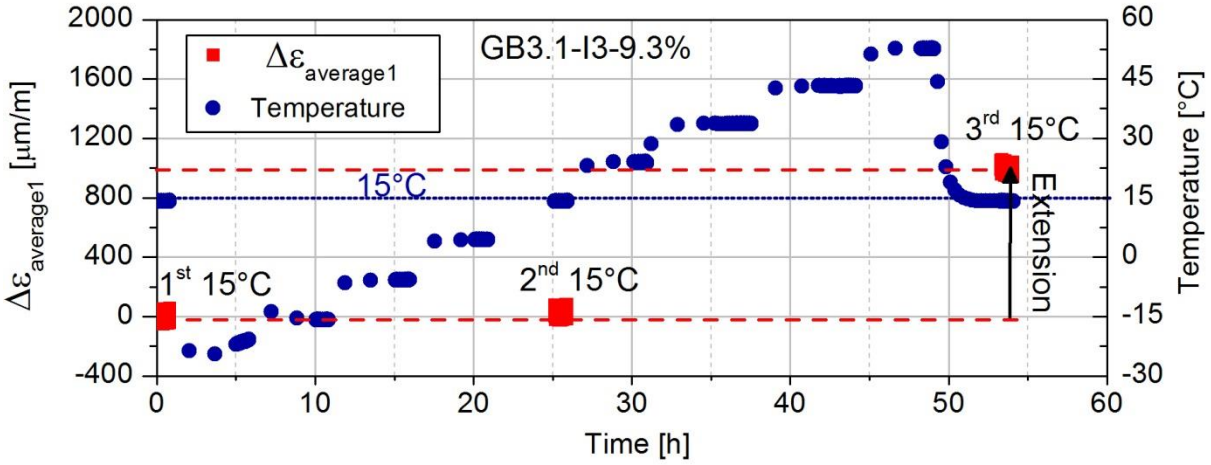

Figure 4.53. Evolution of the $\varepsilon_{average1}$ during a complex modulus test presenting sample extension GB3.1-I3-9.3%

Figure 4.54 shows the variation of the central value of the strain signal between the first and second stages at 15°C for the tests on GB3 samples. Positive $\Delta_{\varepsilon average1}$ values express extension and negative ones contraction. Figure 4.55 presents the variation calculated between the first and the third stages at 15°C. It is important to remind that the third stage at 15°C could not be carried out for all tests. Comparing Figure 4.54 and Figure 4.55 it is clear that the extension or contraction suffered by the samples during the stages at low temperatures is much lesser than that suffered during the high temperature stages. As an example, the extension suffered by sample GB3.1-I3-9.3% between stages 1 and 2 at 15°C was of about 50 µm/m, which makes only 5% of the total extension of the sample (between stages 1 and 3 at 15°C). However, all samples that presented extension between stages 15°C(1) and 15°C(2) also presented extension at the end of the test. The same observation is made for those samples in contraction. It is possible to assume that the extension or contraction of the samples during the stages before 15°C(2) increases during the stages that follow.

Both Figure 4.54 and Figure 4.55 also present the static modulus value of each sample. It is clear that the samples presenting extension have lower E_{00} values than samples in contraction. Given this, two test procedures were conceived as to confirm and quantify the dependence of the static modulus on the extension of the sample. The test procedures and results are presented in sections 4.4.1 and 4.4.2.

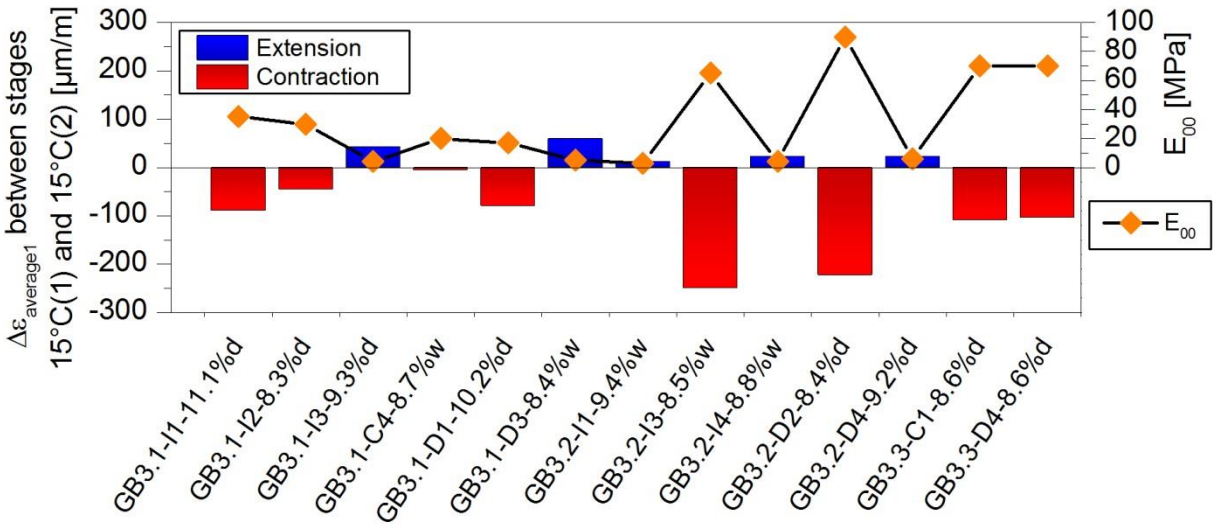

Figure 4.54. $\Delta\varepsilon_{average1}$ between the first and second stages at 15°C of the complex modulus tests carried out on GB3 samples

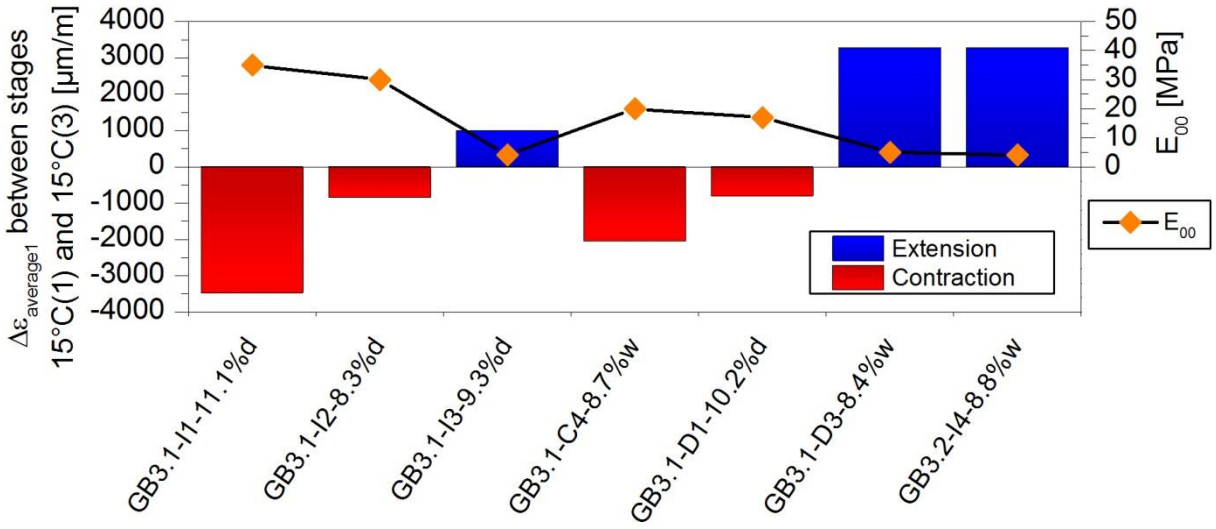

Figure 4.55. $\Delta\varepsilon_{average1}$ between the first and third stages at 15°C of the complex modulus tests carried out on GB3 samples

4.4.1. Cyclic loading test at different average strain levels and fixed temperature – *The ladder test*

The *ladder test* was conceived to observe the possible variation of the complex modulus with the extension of the sample. It consists in applying a sinusoidal strain of 50 µm/m in amplitude centred on different strain values $\varepsilon_{average1}$ (c.f. Figure 4.56). The value $\varepsilon_{average1}$ is defined in section 1.3.2. The test temperature is fixed at 35°C. Each average strain value is considered as a test stage. Each stage starts with a variation of the strain level of the sample at a rate of 50 µm/m per minute. After attaining the desired strain level, the sample is left to relax for a period of 1 hour. Then, seven cyclic loadings at different frequencies are applied with a 5 minute rest period between each one. This loading part of the test stage is the same as for a complex modulus test

(c.f. Figure 4.56). During this test the complex modulus E* is considered as function of the loading frequency and of the central value of the strain signal ($E^*(\omega, \varepsilon_{average1})$).

The first 3 stages (0 µm/m, 200 µm/m and 600 µm/m) are repeated after the stage at 1 000 µm/m in a decreasing way. This is done in order to determine whether the complex modulus measurements are the same after having attained the maximum extension level. The test was conceived to be carried out with the MTS® hydraulic press using the 200 N load cell in order to accurately measure the low forces at such a high temperature and low loading frequencies.

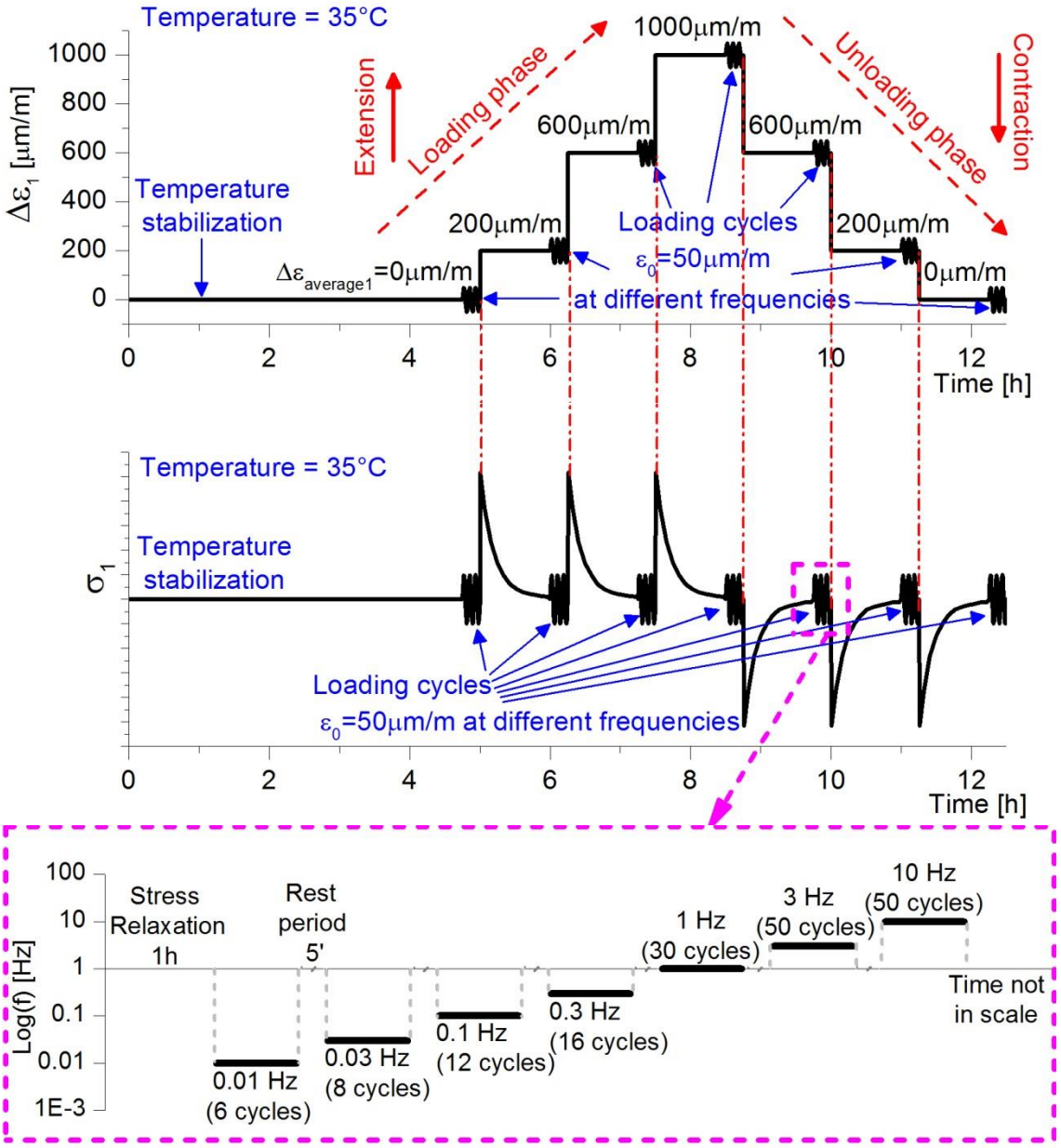

Figure 4.56. Ladder test protocol indicating the different test stages at different average strain value, schematic representation of the stress developed during the test and zoom on the loading frequencies at each test stage

Figure 4.57 presents some of the test results. The values of the complex modulus norm at three different frequencies are presented for all of the average strain levels of the test. The symbols used allow distinguishing the results from the loading phase from those from the unloading phase. Slightly higher |E*| values (of the order of 3%) are observed at the first stage at 0 µm/m with respect to those from the stage at 1 000 µm/m. However, these results are not evidence of a significant variation of |E*| due to the increase of the average strain value. This was observed for all of the tested frequencies. Moreover, the |E*| variation during the unloading phase is even smaller (less than 1% between the stage at 1 000 µm/m and the final stage at 0 µm/m). Table **4-8** and Table **4-9** present the complete test results (|E*| and ϕ respectively). The low standard deviation values for both |E*| and ϕ at a single frequency are evidence of the observed low variation of the complex modulus with the variation of the average strain level.

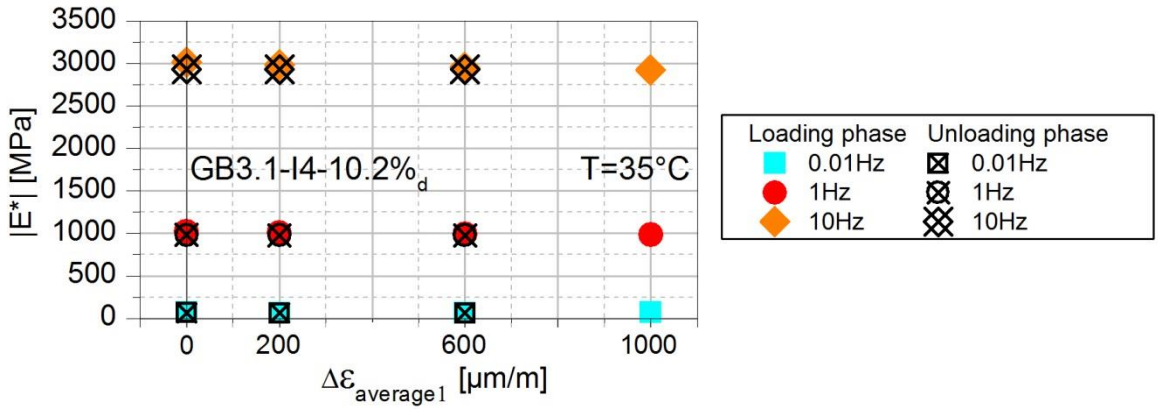

Figure 4.57. Complex modulus norm values at different average strain levels and frequencies – Ladder test results for the loading and unloading phases GB3.1-I4-10.2%$_d$ sample

Table 4-8. Test results from the ladder test performed on the GB3.1-I4-10.2%$_d$ sample – Complex modulus norm

Frequency [Hz]	Complex modulus norm |E*| [MPa]							Average |E*| [MPa]	|E*| Standard deviation [MPa]
	Loading phase $\Delta\varepsilon_{average1}$ [µm/m]				Unloading phase $\Delta\varepsilon_{average1}$ [µm/m]				
	0	200	600	1000	600	200	0		
0.01	68.6	67.2	67.4	69.4	61.5	63.0	64.9	66.0	2.9
0.03	134.6	131.4	119.4	129.7	124.3	125.1	126.2	127.3	5.0
0.1	276.5	270.4	267.2	265.0	259.3	260.2	261.3	265.7	6.2
0.3	527.7	517.1	510.1	505.4	499.4	499.7	500.7	508.6	10.6
1	1024.0	1007.7	995.2	984.9	980.3	979.9	981.2	993.3	16.9
3	1778.0	1754.6	1734.1	1718.0	1714.5	1715.9	1716.7	1733.1	24.6
10	3016.1	2984.4	2954.6	2928.8	2932.3	2932.6	2936.7	2955.1	33.3

Table 4-9. Test results from the ladder test performed on the GB3.1-I4-10.2%$_d$ sample – Complex modulus phase angle

Frequency [Hz]	Complex modulus phase angle φ [°]							Average φ [°]	φ Standard deviation [°]
	Loading phase $\Delta\varepsilon_{average1}$ [µm/m]				Unloading phase $\Delta\varepsilon_{average1}$ [µm/m]				
	0	200	600	1000	600	200	0		
0.01	55.1	55.5	54.2	53.6	56.3	54.7	52.9	54.6	1.2
0.03	57.5	57.5	56.9	56.3	58.1	57.5	57.0	57.3	0.6
0.1	56.0	55.9	55.9	55.7	56.4	56.4	56.1	56.0	0.3
0.3	53.4	53.5	53.5	53.4	53.9	53.9	53.8	53.6	0.2
1	49.1	49.3	49.4	49.4	49.6	49.7	49.6	49.4	0.2
3	44.0	44.2	44.4	44.4	44.5	44.6	44.7	44.4	0.2
10	37.9	38.1	38.2	38.3	38.3	38.4	38.4	38.2	0.2

The results presented in Table 4-8 and Table 4-9 are plotted in Figure 4.58 and compared to the complex modulus test results from the non-conditioned GB3 samples. It is observed that the ladder test results are superposed to the complex modulus test results regardless of the $\varepsilon_{average1}$ value. Moreover, the ladder test results match the test results of samples GB3.2-D4-9.2%$_d$ and GB3.1-I3-9.3%$_d$ which are the non-conditioned samples presenting the lowest E_{00} values. These two samples are also the only GB3$_d$ ones in extension (c.f. Figure 4.54).

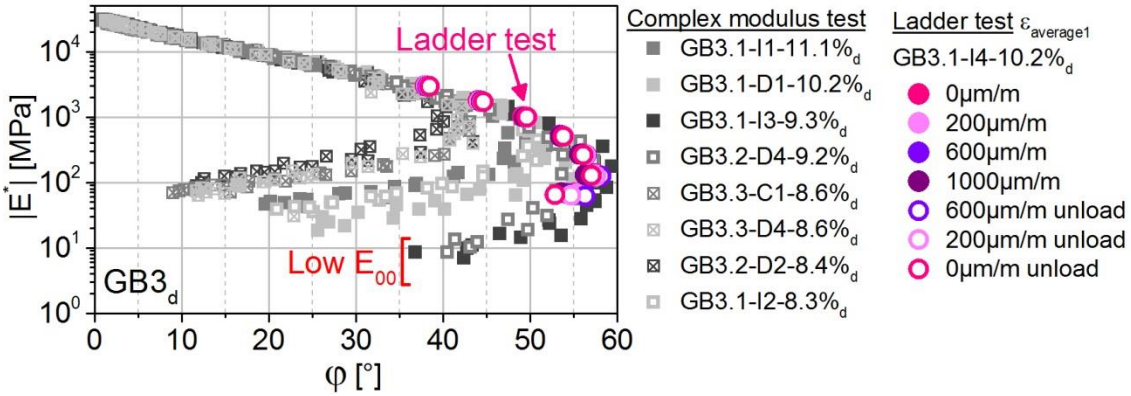

Figure 4.58. Comparison between the ladder test results from sample GB3.1-I4-10.2%$_d$ and the GB3$_d$ complex modulus test results

Special attention must be given to the first stage of the ladder test at 0 µm/m. During the first stage of the conception of the ladder test, its objective was to determine if the relative increase of the extension of the sample would cause a modification of the complex modulus. For this, the initial state of the sample was considered of low importance and the initial 0 µm/m centre value was defined by setting to zero the measurements from the three extensometers right before the beginning of the cyclic loading, after the relaxation period of 1 hour (stress level close to zero).

At this state, the sample might have already suffered some extension which would explain the match between the ladder test results and the complex modulus test results from samples in extension. Under this hypothesis, the GB3.1-I4-10.4% test effectively allowed determining that extension causes a decrease in E_{00}. However, it did not allow quantifying the amount of the decrease since the results from the first test stage do not really correspond to a zero strain condition. Unfortunately, the MTS® hydraulic press became out of service before finishing the experimental work and no further tests cyclic were carried out.

These results suggest that there is a strong diminution of the static modulus caused by the extension of the sample, regardless of the magnitude of the extension. This also means that the E_{00} loss is not recoverable by lowering the extension level.

Further investigation using relaxation tests is presented in section 4.4.2.

4.4.2. The relaxation test

The relaxation test was conceived to identify the value of the static modulus with a different method than cyclic loading. The test consists in imposing different strain levels to the sample and maintaining each one for 24 hours before changing to another (c.f. Figure 4.59). Each strain level corresponds to a test stage (i) as shown in Figure 4.59 and Figure 4.60. There are 8 test stages. The variation of the strain level is done at a rate of 50 µm/m per minute.

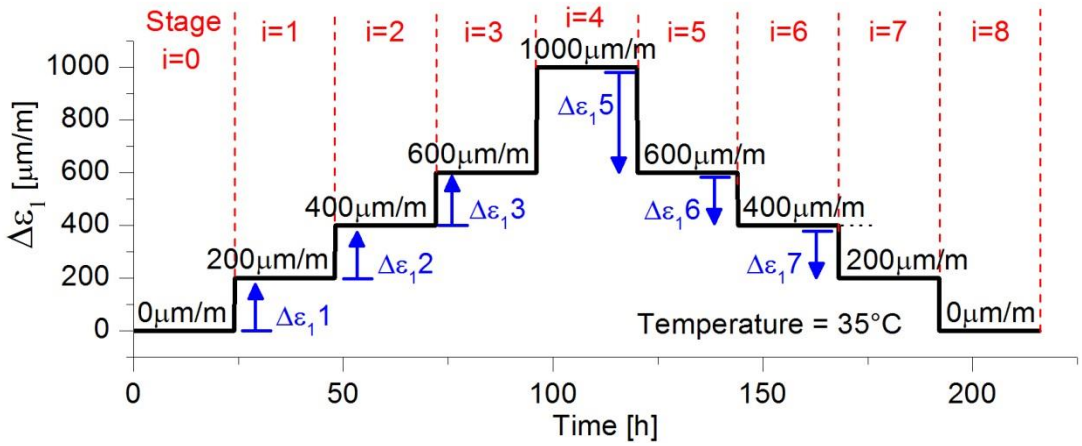

Figure 4.59. Stress relaxation test ε_1 protocol

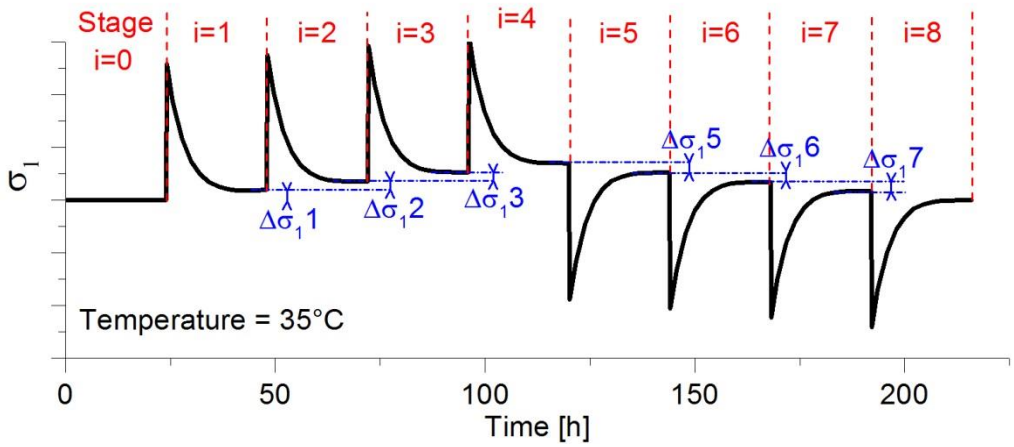

Figure 4.60. Schematic representation of the stress evolution during the relaxation test

Due to viscoelastic properties of the material, stress is relaxed over time when the strain level is maintained constant as shown in Figure 4.60. However, as seen in Figure 4.61(b), the stress does not completely relax after an increase in the strain level. The residual stress serves to calculate the static modulus of the material (E_{00R}). The subscript R is used to indicate the modulus E_{00} is obtained from the relaxation test. The static modulus is calculated as the ratio between the residual stress between two test stages ($\Delta\sigma_1 i$) and the strain difference between them ($\Delta\varepsilon_1 i$).

$$E_{00R(i)} = \frac{\Delta\sigma_1 i}{\Delta\varepsilon_1 i} \quad [4\text{-}6]$$

The static modulus loss is calculated as the relative difference between the E_{00R} value at each stage (E_{00Ri}) and the E_{00R} calculated at the first stage (i=1) ($E_{00R(1)}$).

$$E_{00R(1)} = \frac{\Delta\sigma_1 1}{\Delta\varepsilon_1 1} \quad [4\text{-}7]$$

$$E_{00R}loss = 1 - \frac{E_{00R(i)}}{E_{00R(1)}} \quad [4\text{-}8]$$

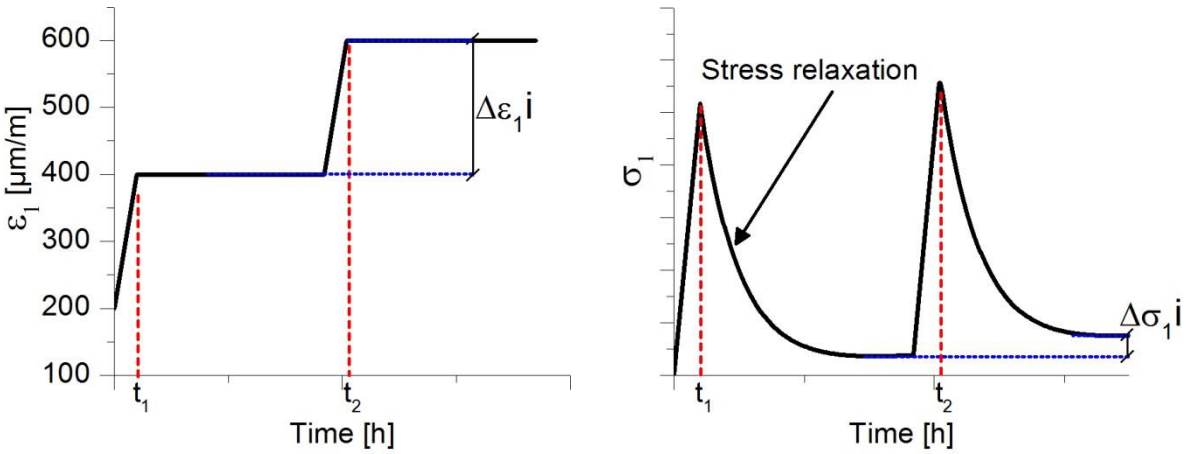

(a) (b)

Figure 4.61. Scheme of the imposed strain (a) and developed stress (b) in the sample during two stages of the stress relaxation test

Two samples were tested: the GB3.4-D1-8.3% and the GB3.2-I3-8.5%. The E_{00R} values found for each of the approaches for the two samples are shown in Figure 4.62 and Figure 4.63 in semi logarithmic plots. It is observed that the static modulus calculated from the first extension of the sample ($E_{00R(1)}$) is considerably higher than the values obtained from the subsequent test stages. Most interesting is the fact that the static modulus values are not entirely recoverable during the unloading phase, indicating a permanent alteration of the sample after the first extension. The calculated values during the unloading phase are rather stable. In Figure 4.62 to Figure 4.64, the presented static modulus value for the unloading phase corresponds to the average value of stages 5 to 8 (E_{00R_unload}).

$$E_{00R\_unload} = \frac{E_{00R(5)} + E_{00R(6)} + E_{00R(7)} + E_{00R(8)}}{4} \quad [4\text{-}9]$$

The average static modulus during the unloading phase is 3.5 MPa taking into account both tests. This corresponds to an E_{00R} loss of around 40% to 45%. Finally, results from both discrete and cumulative interpretations of the test are well described by exponential fitting.

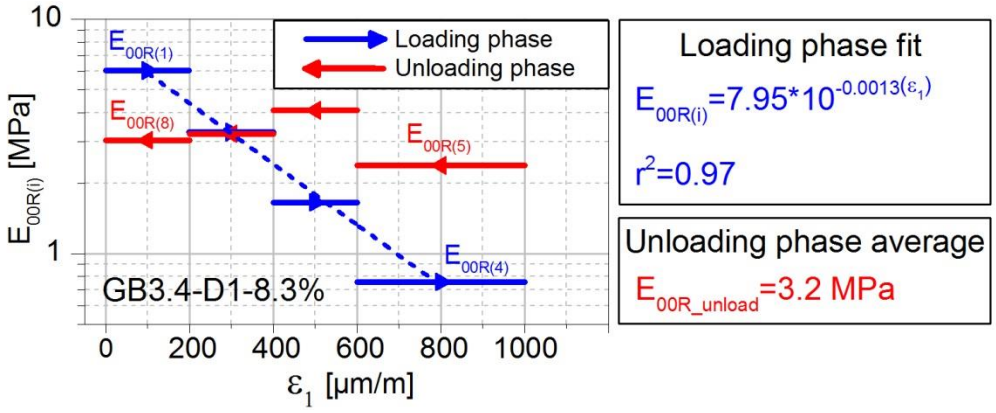

Figure 4.62. Static modulus $E_{00R(i)}$ for the GB3.4-D1-8.3% sample

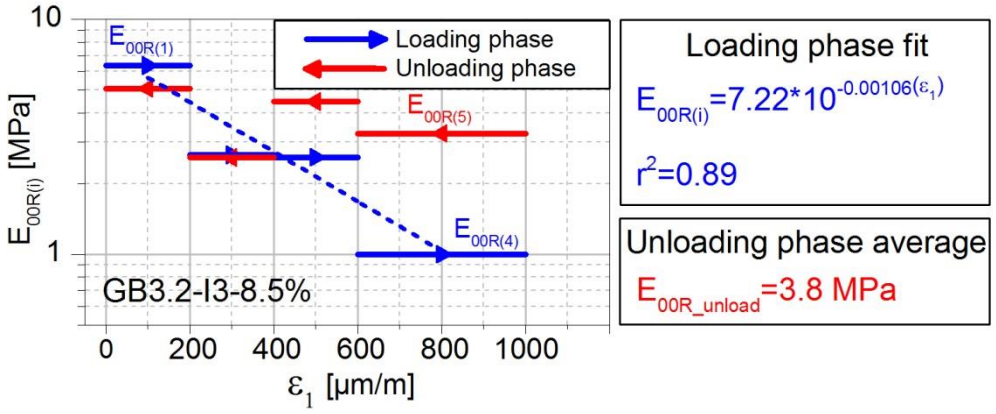

Figure 4.63. Static modulus $E_{00R(i)}$ for the GB3.2-I3-8.5% sample

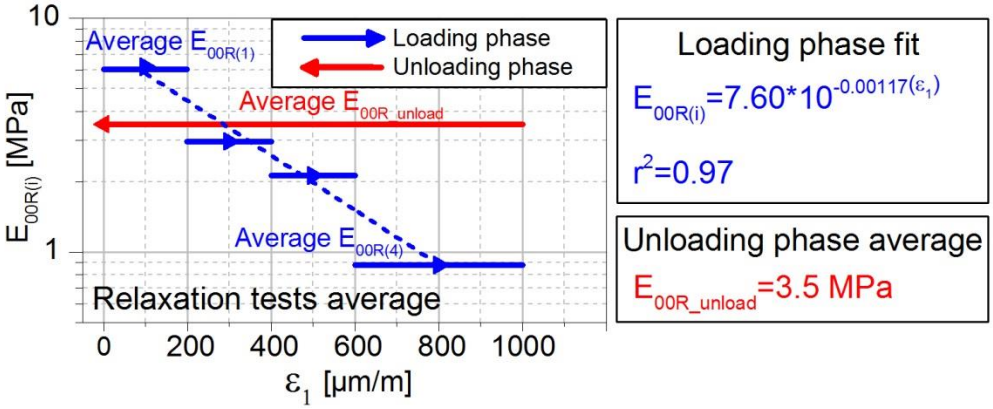

Figure 4.64. Average static modulus $E_{00R(i)}$ from the relaxation tests

Figure 4.65 presents the comparison between the static modulus (E_{00}) from the complex modulus tests on GB3 samples and the E_{00R} resulting from the relaxation tests. The E_{00R} values represented correspond to the $E_{00R(1)}$, E_{00R_unload} and $E_{00R(4\_8)}$ values of each relaxation test. The static modulus values are presented in decreasing order.

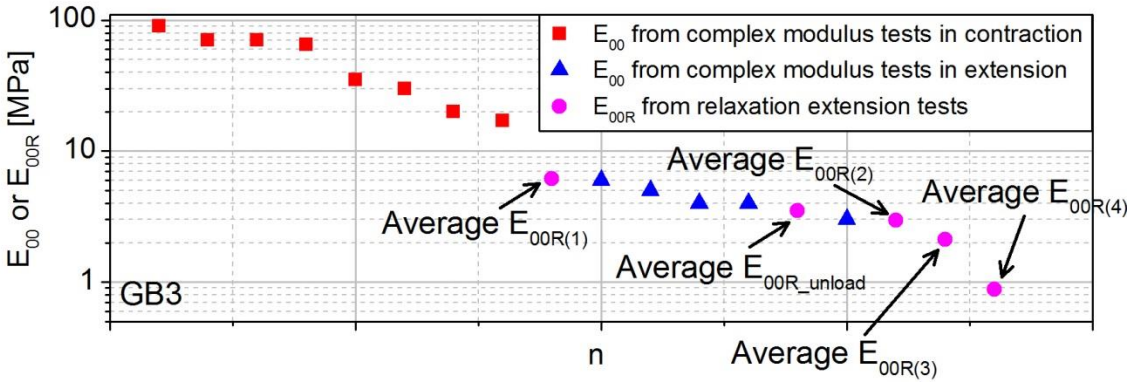

Figure 4.65. E_{00} values from the complex modulus tests on GB3 samples and E_{00R} values from the relaxation tests

The results from the relaxation tests are very similar to those from the five GB3 samples that suffered extension during the complex modulus test. The tendency described by these results is clear evidence that the extension suffered by the sample causes a significant reduction of the static modulus.

During complex modulus tests, the |E*| results at low equivalent frequencies (f_{eq} ~ 10^{-7} Hz at T_{ref}=15°C) allow the estimation of E_{00}. These results are obtained from the high temperature stages (55°C and 65°C) performed at the end of the test. The analysis presented in this section shows that the extension suffered by the sample during the test causes a reduction of the E_{00} value. However, when comparing the results at 15°C from the samples presenting extension, there is no significant reduction of the |E*| values obtained from the 3rd stage at 15°C with respect to the 1st one. As a reminder, this 3rd stage at 15°C was carried out after the stage at 55°C, when the sample has suffered its maximum extension. This means that a certain extension of the sample causes a clear reduction of |E*| at high temperatures while is does not affect |E*| at 15°C. For T_{ref}=15°C, this indicates that the effect of the extension state of the sample on E* is higher at low equivalent frequencies. The different strain states of the samples might explain the high dispersion of the static modulus values from the complex modulus test results.

It is important to remind that the initial strain state of the sample before beginning the complex modulus tests is unknown. The samples might have suffered extension or contraction during the gluing phase or during the first temperature stabilisation period. Though, the effects of this initial strain state of the sample would not affect E* during the stages at low temperature. More specifically, it would not affect the glassy modulus E_0, which is associated with high equivalent frequencies. This might explain why there is no glassy modulus dispersion despite of the different strain states of the samples.

The study by (Q. T. Nguyen, Di Benedetto, & Sauzéat, 2015) showed that the effects of non-linearity, which causes a modulus loss, are higher at high temperature and low loading frequency. These test conditions correspond to those of low equivalent frequencies. The authors found a relationship between the reduction of |E*| and a variation of the strain amplitude. They observed that in order to cause a reduction of 5% of |E*|, the necessary ε_0 variation is much lower at low equivalent frequencies than at high ones. As an example, for the same test conditions as in (Q. T. Nguyen et al., 2015), to cause a 5% |E*| loss at f_{eq}=10^{-9} Hz an amplitude

variation of 9 µm/m is needed. In order to cause the same |E*| loss at $f_{eq}=10^9$ Hz the needed amplitude variation is of 785 µm/m. The lower the equivalent frequency is, the lower the needed amplitude variation is to cause a certain modulus loss.

Taking into account the respective strain state of the samples (extension or contraction), the static modulus E_{00} values from the complex modulus tests were compared to the results from the relaxation tests. In Figure 4.66, the E_{00} values from the complex modulus tests in contraction and the average $E_{00R(i)}$ exponential fit from the relaxation tests are plotted. The complex modulus test results were located, along the abscissas axis, at a distance equal to the contraction $\Delta\varepsilon_{average1}$ from the abscise of the $E_{00R(4)}$ point. The relative zero strain value was set at the abscissa of the E_{00} value equal to 65 MPa from the GB3.2-I3-8.5% sample. The value $\Delta\varepsilon_{average1}$ corresponds to the maximum contraction of the sample during the complex modulus test. During a complex modulus test, especially for the high temperature stages, the average value of the strain signal was observed to vary during the cyclic loading. This means that, at a same temperature, the sample suffers contraction or extension during the cyclic loading. The maximum contraction of the sample was estimated by adding these variations of the average strain value over the different loading cycles of the complex modulus test.

Figure 4.66 shows that the E_{00} values are compatible with the exponential fit from the relaxation test. Moreover, the study by (Nguyen, 2010) revealed that the complex modulus norm of bituminous mixtures increase with the contraction of the sample for average strain values below 1% (in contraction). Since the maximum contraction suffered by the samples is of the order of 2 000 µm/m, the results are compatible with the conclusions from the cited study.

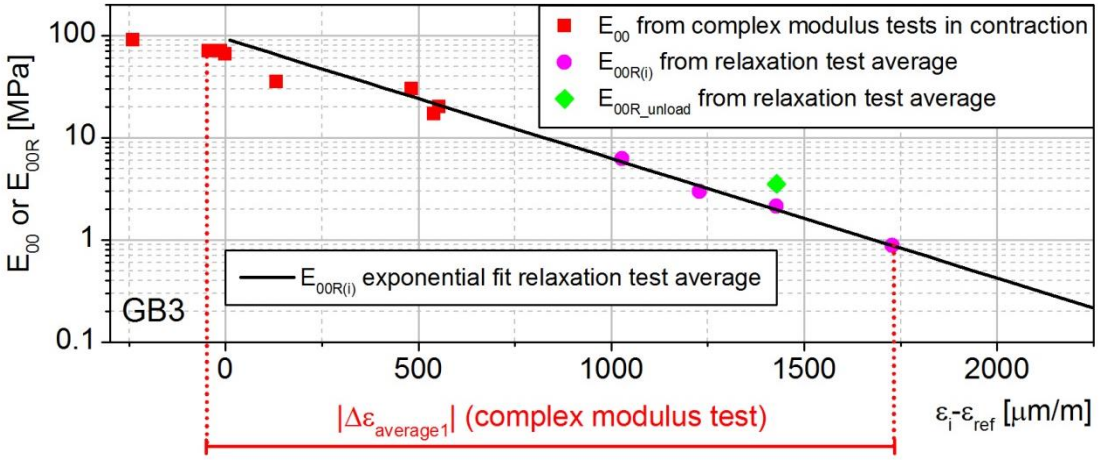

Figure 4.66. Comparison of the E_{00} values from the complex modulus tests on GB3 samples and the E_{00R} values from the relaxation tests in function of the strain state

The relaxation test results show a relationship between the strain state of the samples and the static modulus that is compatible with the order of magnitude of the complex modulus test results. Even if this might explain the dispersion of the E00 values from the complex modulus test, more experimental work is needed to provide a suitable correction of the static modulus in function of the maximum contraction or extension of the sample.

5

Fatigue behaviour of the tested bituminous mixtures

The fatigue test results for the three studied bituminous mixtures are presented in this section. This part of the study aims to characterise the fatigue resistance properties of the materials. The effect of strain amplitude on the fatigue life of the samples is explained using the GB4 mixture as example. Then, the test analysis using the different failure criteria is presented, followed by the construction of a Wöhler curve using the non-conditioned GB4 mixture as example. The Wöhler curves are used to compare the three materials between them.

As for moisture damage, a comparison between the test results of a conditioned and not-conditioned GB4 sample at single strain amplitude is presented. The influence of moisture conditioning on the fatigue life of each material is assessed through comparison of the Wöhler curves at each conditioning state. Conclusions are drawn on the moisture susceptibility of each material.

As a reminder, fatigue tests were carried out applying a tension-compression sinusoidal loading at 10 Hz and 10°C on cylindrical samples without resting periods. The test results obtained with these tests are indicators of the fatigue resistance properties of the materials under these specific loading conditions. Therefore; the ε_6 values cannot be interpreted as the number of loading cycles that the materials withstand on a pavement structure. Correlations between laboratory ε_6 values and in-situ fatigue life can be made through the analysis of the return on experience from in-service pavement structures. Since the existing railway tracks with bituminous sub-ballast layers in France have been in service for a very short time and since they have not yet presented fatigue associated distresses, not enough information is available at the moment for making such correlations. The presented results serve only to compare the fatigue resistance properties of the studied materials between them and not to predict the fatigue life of bituminous layers in railway track structures.

5.1. Test results

An important number of tension-compression fatigue tests were carried out on cylindrical samples of each of the three studied bituminous mixtures. Four strain amplitudes were tested for the GB3 and GB4 mixtures: 60 µm/m, 70 µm/m, 90 µm/m and 110 µm/m. The GB PMB mixture was tested at three strain amplitudes: 70 µm/m, 90 µm/m and 110 µm/m. All tests were done at 10°C and at a loading frequency of 10 Hz using the Instron® hydraulic press.

The samples were chosen in a way that all samples of a material tested at the same strain amplitude had similar voids content. Table 5-1 presents the average voids content of the samples of each material per strain level.

Table 5-1. Average voids content of the samples tested at same strain amplitude per material

Mixture	Strain level [µm/m]	Number of samples	Average voids content [%]			Standard deviation [%]
			All samples	Non-conditioned samples	Moisture conditioned samples	
GB3	60	3	8.1	8.1	8.0	0.17
	70	6	8.1	8.1	8.1	0.10
	90	5	7.6	7.5	7.6	0.10
	110	5	7.3	7.3	7.3	0.12
GB4	60	3	4.7	4.6	4.7	0.10
	70	8	4.3	4.3	4.3	0.09
	90	6	4.0	4.0	4.1	0.08
	110	8	3.6	3.6	3.6	0.12
GB PMB	70	4	8.0	8.0	8.0	0.17
	90	6	7.8	7.8	7.8	0.05
	110	6	7.2	7.2	7.3	0.10

The $|E^*|$ evolution during the test can be expressed in terms of its normalised value which is calculated as the ratio between $|E^*|$ at a cycle n divided by the $|E^*|_0$ value. $|E^*|_0$ is defined as the intercept with the ordinates axis of the linear regression made for the cycles 60 to 110 of the $|E^*|$ vs N plot, being N the number of cycles (c.f. section 1.3.6).

5.1.1. Study for a single strain amplitude

Figure 5.1 presents the results for three fatigue tests carried out at different strain amplitudes. It is clear that the fatigue life of the samples decreases with the increase in the strain amplitude. The number of cycles for which the failure is attained (N_f) is marked by a dashed line. The N_f value shown on Figure 5.1 corresponds to the average value of the different N_f determined with each of the considered failure criteria (c.f. section 1.3.7).

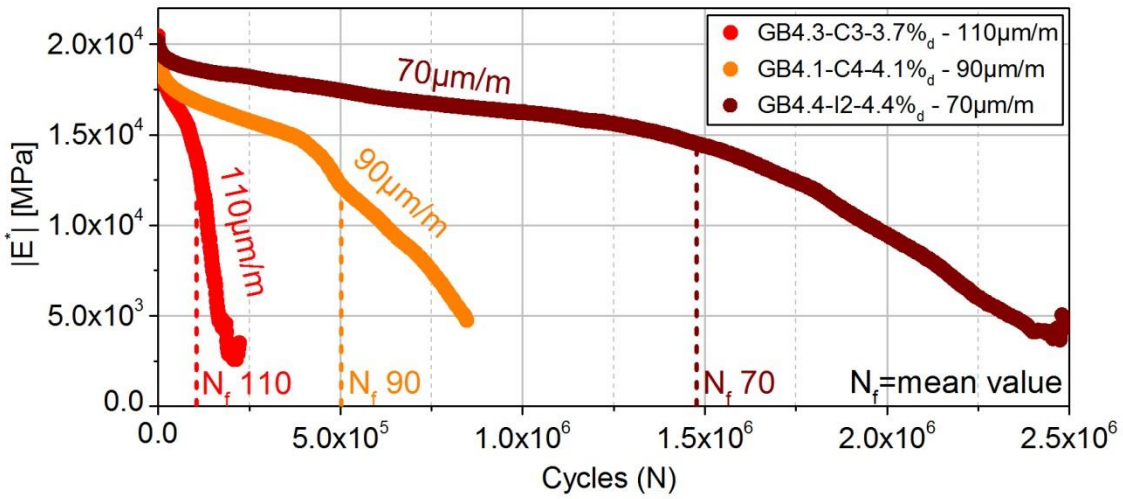

Figure 5.1. Fatigue tests results at different strain levels

The different failure criteria considered for this thesis are described section 1.3.7. The analysis of the GB4.3-C3-3.7% fatigue test at 110 µm/m is presented as example in Figure 5.2 to Figure 5.5. It is important to note that some tests did not allow the application of all eight fatigue criteria due to the unsuitable shape of the curves described by the experimental measurements. Tests ending because of physical rupture are the most common case of this, especially because the |E*| against N plot does not present a clear third phase.

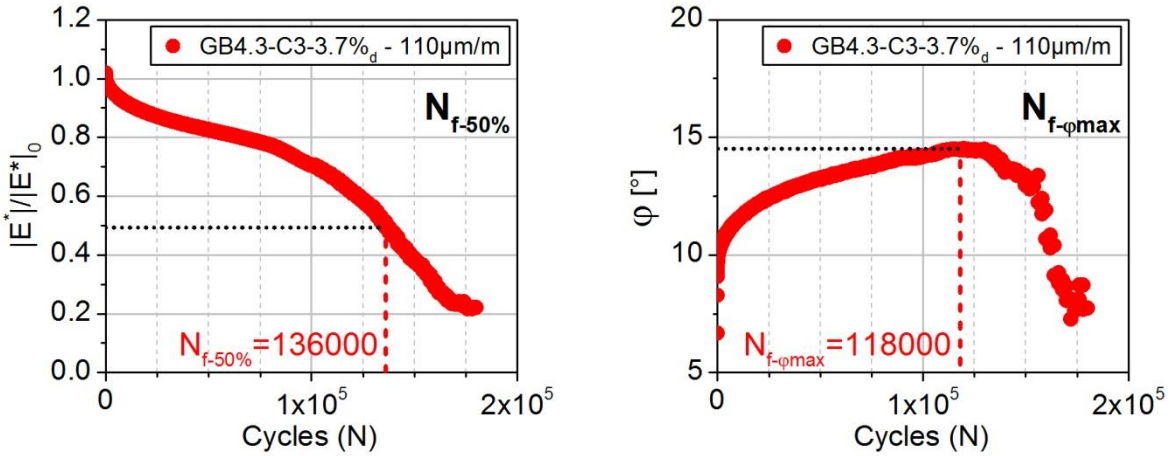

(a) (b)

Figure 5.2. Classical approach (a) and phase angle peak (b) failure criteria applied to the GB4.3-C3-3.7% fatigue test

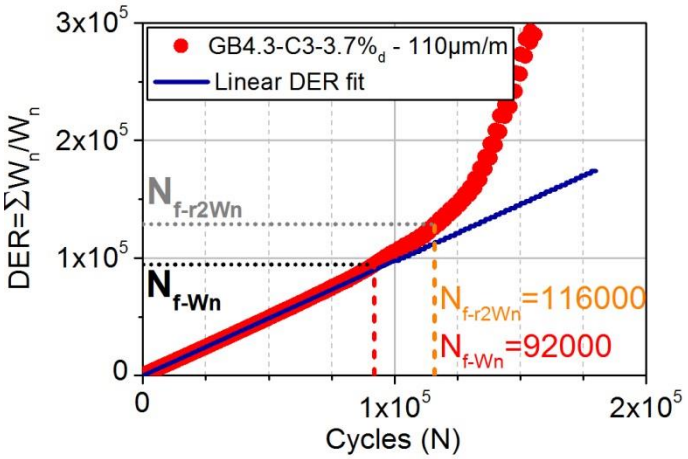

Figure 5.3. Energetic approach to define failure of the GB4.3-C3-3.7% fatigue test – DER deviation from the linear fit at the beginning of the test (black/red dashed line) and variation of the coefficient of determination (r^2)of the DER experimental points (grey/orange dashed line)

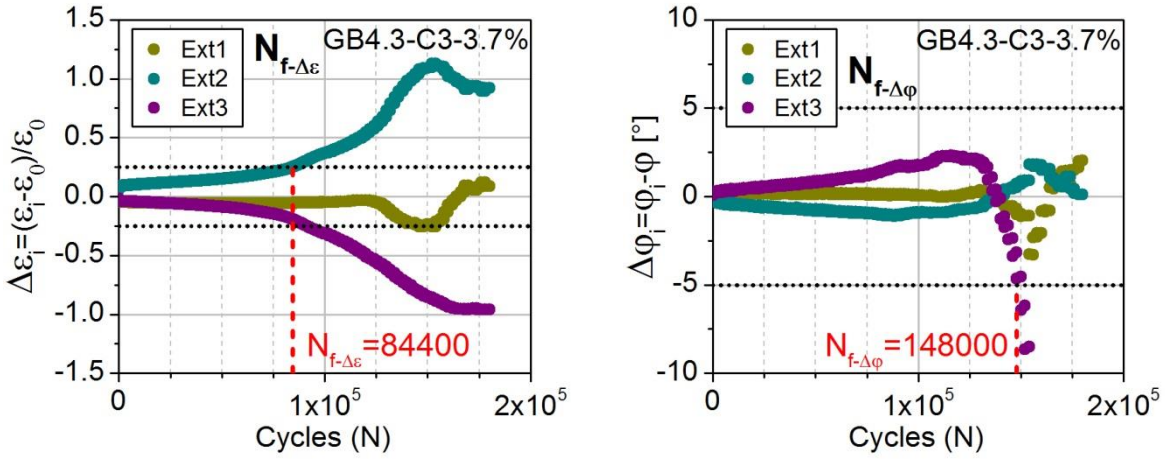

(a) (b)

Figure 5.4. Failure criteria based on the divergence of the measures from each extensometer with respect to the average strain signal's amplitude (a) and of the phase angle (b)

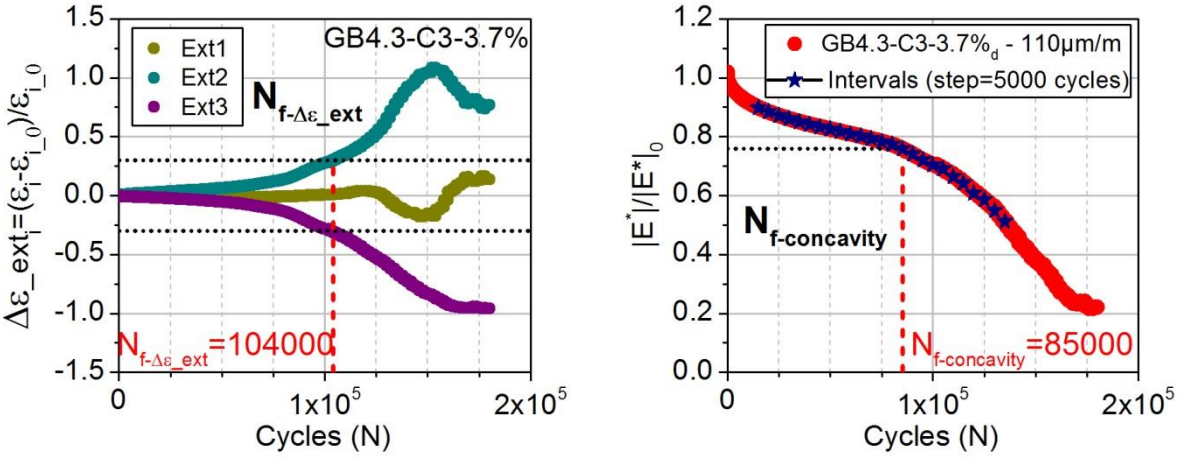

(a) (b)

Figure 5.5. Failure criteria based on the divergence of the measures from each extensometer with respect to their initial strain amplitude (a) and on the concavity change of the |E*| against N plot criterion (normalised |E*|) (b)

The differences between N_f values found with each failure criterion are non-negligible and each one has to be analysed to verify its coherency with the theory of fatigue resistance. As an example, the classical approach and the phase angle divergence criteria identify the failure at a very late stage of the test as seen in Figure 5.6. The end of the second phase of the fatigue test is indicated by the $N_{f\_concavity}$ criterion which has high sensibility to changes in the slope of the |E*| vs N curve. For the GB4.3.C3-3.7% test, the $N_{f\_\Delta\varepsilon}$, N_{f_Wn} and $N_{f\_\Delta\varepsilon\_ext}$ correlate well to the end of the second phase of the test. Since the slope change of the curve is not very pronounced for this test, it is not strange for the $N_{f\_\varphi Max}$ and N_{f_r2Wn} criteria to indicate the failure latter than the $N_{f\_concavity}$ criterion. The phase angle evolves at a different rate than |E*| during the tests and it presents a slight discontinuity around 90 000 cycles as seen in Figure 5.2(b) which is not perceived as failure by the criteria. From the analysis of all criteria, it is correct to affirm that the sample presents a behaviour change between the cycles 85 000 and 118 000 which indicates that the failure happens within this interval of cycles. The $N_{f\_\Delta\varphi}$ and the $N_{f\_50\%}$ criteria are then not representative of the failure of the GB4.3-C3-3.7% sample. In fact, the classical approach criterion was found not to be representative of the failure of most of the fatigue tests carried out during this study. It was taken into account mainly for the analysis of tests for which the end of the second phase was not perceived, which are characterised by a physical failure (macro-crack) outside of the span of the extensometers.

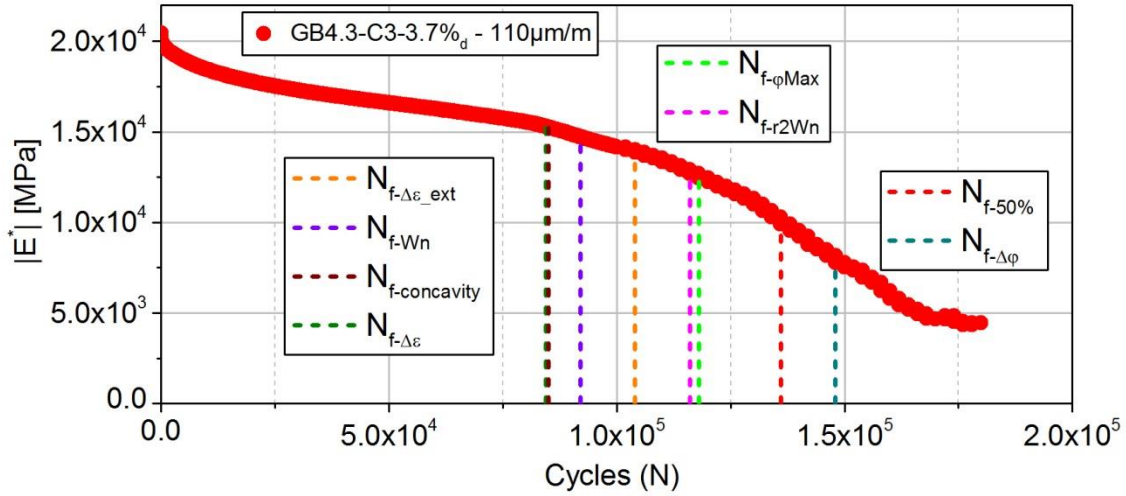

Figure 5.6. Representation of the different N_f values of the GB4.3C3-3.7% fatigue test according to each failure criterion

Two N_f values were retained for the fatigue tests of this study. The first one is $N_{f\_concavity}$ since it is considered as very sensible to the behaviour changes of the sample. The second one is the average of the N_f from the criteria considered as representative of the failure each fatigue test, issued from an analysis as the one previously exposed for the GB4.3-C3-3.7% test. It is called $N_{f\_average}$ and takes into account for the most part of the tests the N_{f_Wn}, N_{f_r2Wn}, $N_{f\_\Delta\varepsilon\_ext}$, $N_{f\_\varphi Max}$ and $N_{f\_concavity}$.

Figure 5.7 to Figure 5.10 present the correlation of the different failure criteria with respect to the $N_{f\_concavity}$ for all fatigue tests carried out on the three studied mixtures. Values from tests carried out on moisture-conditioned samples are presented in blue, cyan and dark cyan. The

black continuous line in the plots represents the perfect correlation with $N_{f\_concavity}$. Values below the line indicate that the analysed criterion declares the failure earlier than $N_{f\_concavity}$. The criteria that consistently correlate well with $N_{f\_concavity}$ are the energetic approaches (N_{f_Wn} and N_{f_r2Wn}) and the divergence of the extensometers with respect to their initial amplitude ($N_{f\_\Delta\varepsilon\_ext}$). Table 5-2 shows the occurrence of the different failure criteria. Since not all criteria occurs for all tests, it is important to base the determination of the samples failure in several criteria.

Since most of the points in Figure 5.7 to Figure 5.10 are above the perfect correlation line, the change of concavity criterion announces then the start of a quick degradation of the sample. The use of this criterion is seen as a preventive measure since it sets strain threshold values above which the degradation is amplified and not for which the material fails. Since the criterion $N_{f\_\Delta\varepsilon}$ is the one that correlates the least with $N_{f\_concavity}$, it is not taken into account for the fatigue life estimation.

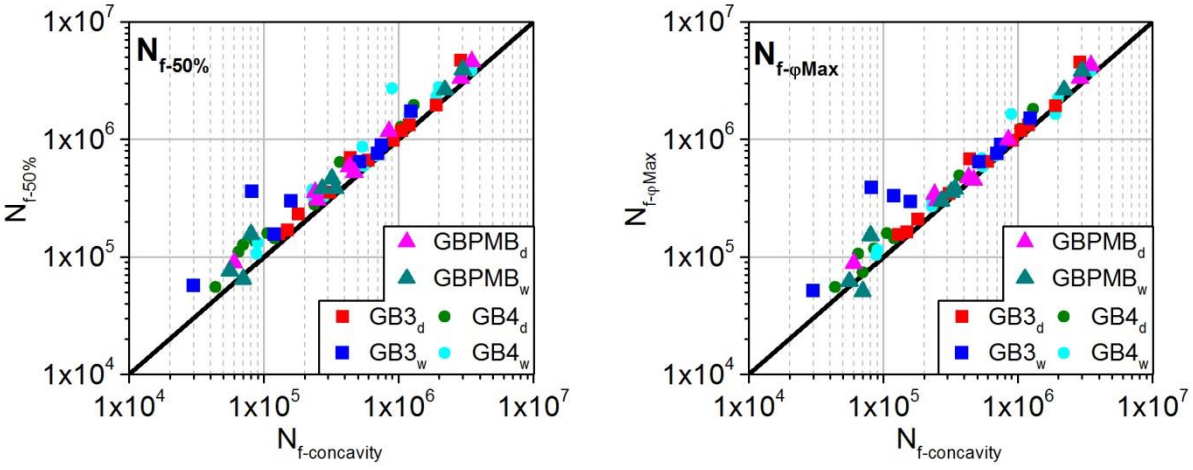

(a) (b)

Figure 5.7. Correlation of $N_{f\_50\%}$ (a) and $N_{f\_\varphi Max}$ (b) with respect to $N_{f\_concavity}$

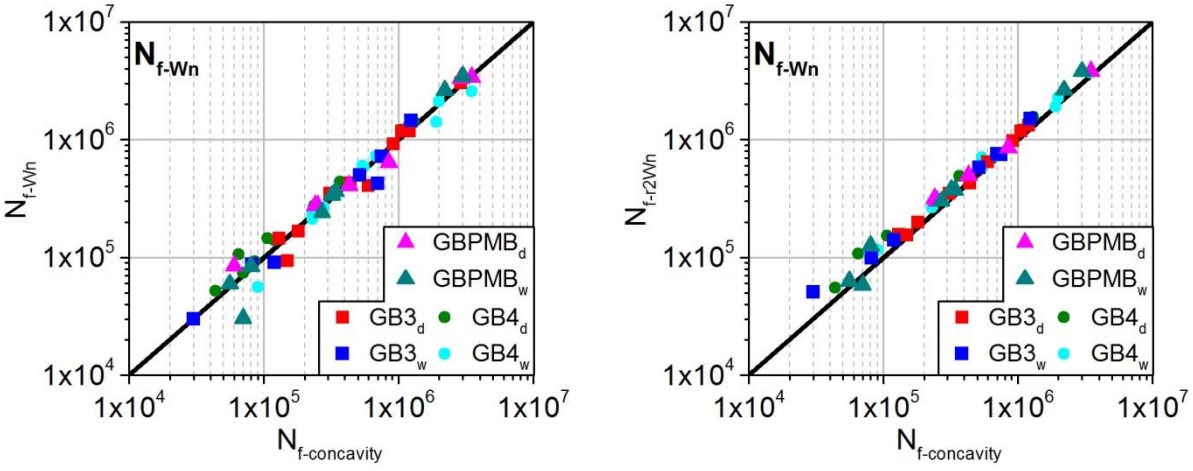

(a) (b)

Figure 5.8. Correlation of N_{f_Wn} (a) and N_{f_r2Wn} (b) with respect to $N_{f\_concavity}$

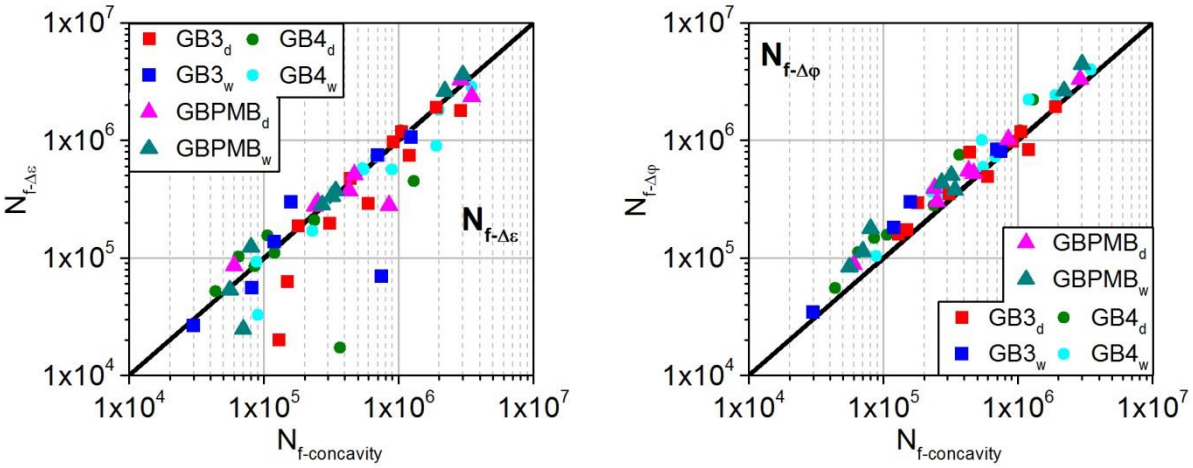

Figure 5.9. Correlation of $N_{f\_\Delta\varepsilon}$ (a) and $N_{f\_\Delta\varphi}$ (b) with respect to $N_{f\_concavity}$

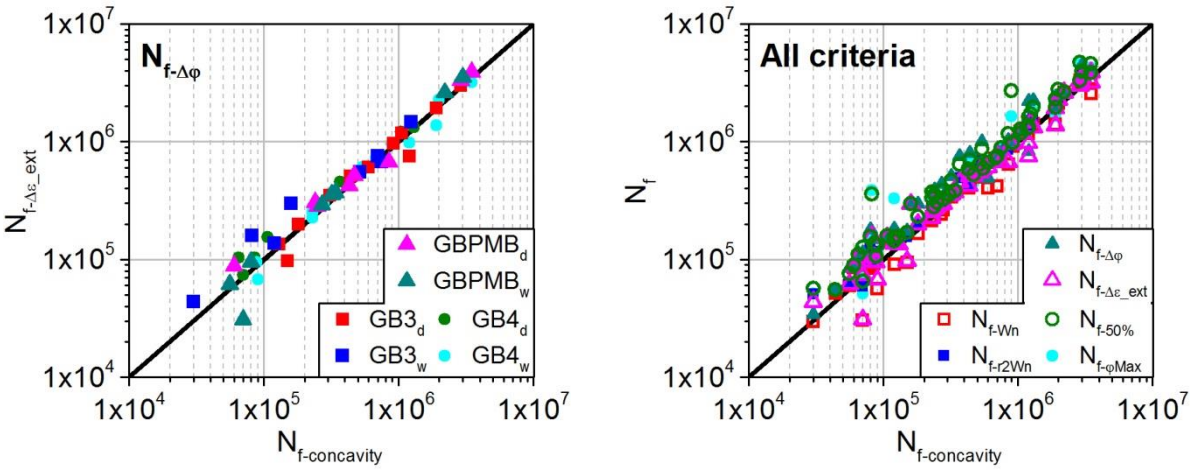

Figure 5.10. Correlation of $N_{f\_\Delta\varepsilon\_ext}$ with respect to $N_{f\_concavity}$ (a) and correlation of all criteria (excluding $N_{f\_\Delta\varepsilon}$) with respect to $N_{f\_concavity}$ (b)

Table 5-2. Occurrence of the different failure criteria during the fatigue resistance study

Criteria	Number of occurrences	Percentage of occurrence [%]
$N_{f\_50\%}$*	60	100
$N_{f\_\varphi Max}$	60	100
N_{f_Wn}	55	92
N_{f_r2Wn}	49	82
$N_{f\_\Delta\varepsilon}$	59	98
$N_{f\_\Delta\varphi}$	48	80
$N_{f\_\Delta\varepsilon\_ext}$	58	97
$N_{f\_Concavity}$**	60	100

* Taken as the last cycle of the test when the sample presented physical rupture before attaining a reduction of 50% of the initial |E*| value

** Taken as the beginning of the last interval for tests not presenting a 3rd fatigue test phase

5.1.2. The Wöhler curve and determination of the ε_6 value

The couple of N_f and strain amplitude of each test is used to plot a Wöhler curve for each material and moisture-conditioning state. Table 5-3 shows the cycles to failure for each of the tests carried out on the non-conditioned GB4 mixture. Figure 5.11 and Figure 5.12 show the Wöhler curves plotted in logarithmic axis using the data in Table 5-3. Based on the linear fitting of each plot, the strain amplitude causing the failure of the sample after 10^6 cycles (ε_6) is estimated as in equation [5-1].

$$\varepsilon_6 = 10^{(a-6b)} \quad [5\text{-}1]$$

where b is the slope of the linear fit and a its intercept with the ordinates axis

The coefficient of determination of the linear fit (r^2) is also calculated. The ε_6 and 1/b values are used in common practice to characterize the fatigue resistance of bituminous mixtures. Due to the data scatter in Wöhler curves, the uncertainty of ε_6 ($\Delta\varepsilon_6$) is also required during the design process of bituminous layers (c.f. equations [5-2], [5-3] and [5-4]).

$$\Delta\varepsilon_6 = 0.5\varepsilon_6(10^{-2bS_0} - 10^{2bS_0}) \quad [5\text{-}2]$$

$$S_0 = S_N\sqrt{\frac{1}{n} + \frac{\left(\log\varepsilon_6 - \overline{\log\varepsilon}\right)^2}{(n+1)S_{\log\varepsilon}{}^2}} \quad [5\text{-}3]$$

$$S_N = S_{logN}\sqrt{\frac{(1-R^2)(n-1)}{n-2}} \quad [5\text{-}4]$$

where n is the number of points for the linear fit, $\overline{\log\varepsilon}$ is the average of all $\log\varepsilon$ values of the tested samples, $S_{log\varepsilon}$ is the standard deviation of the $\log\varepsilon$ values, R the coefficient of determination r^2 and S_{logN} is the the standard deviation of the $\log N$ values

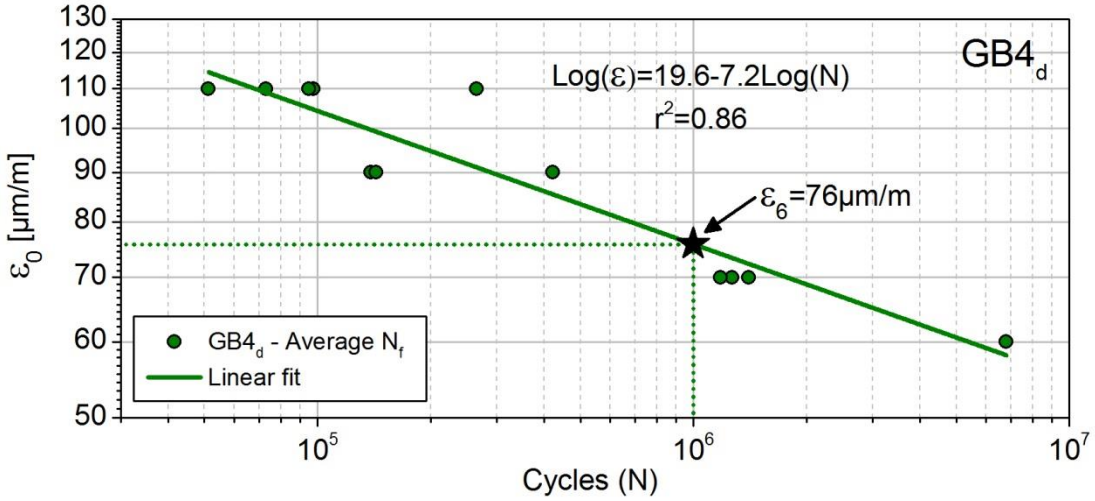

Figure 5.11. Wöhler curve for the non-conditioned GB4 mixture using the average N_f

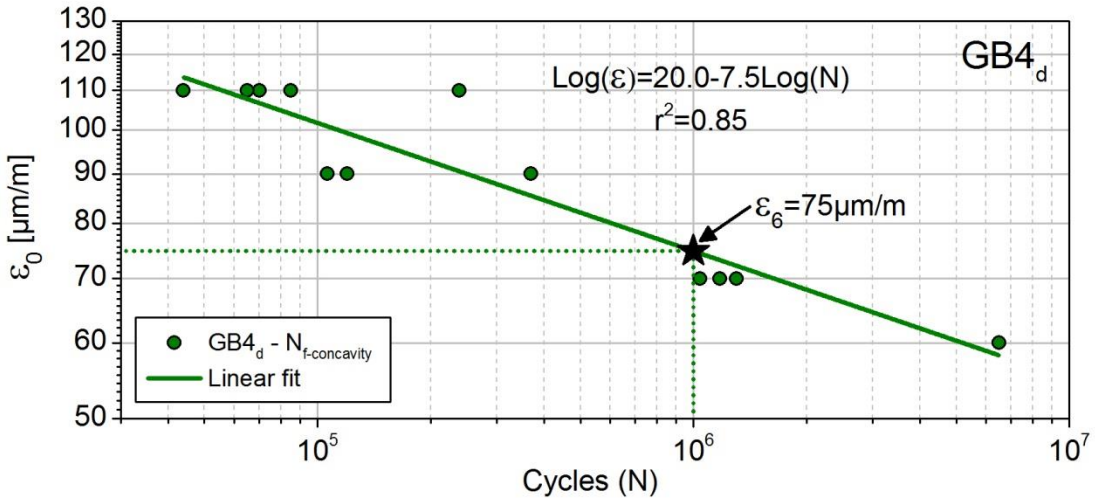

Figure 5.12. Wöhler curve for the non-conditioned GB4 mixture using $N_{f\_concavity}$

As expected, the use of the change of concavity criterion provides a lower ε_6 value than the other failure criteria. However, standard deviation and ε_6 uncertainty of both data sets are not very different which is related to the good correlation of the averaged N_f values with $N_{f\text{-}concavity}$. Defining the thickness of a bituminous layer with both data sets is then possible. The use of the highest ε_6 value with the lowest uncertainty will produce a thinner layer.

Table 5-3. N_f values for the non-conditioned GB4 according to the change in concavity criterion and to the average of the representative criteria of each test

Sample	Strain ε_0 [µm/m]	$N_{f\_average}$	$N_{f\_concavity}$
GB4-4-D3-4.6%	60	6 801 667	6 500 000
GB4-1-I2-4.3%	70	1 253 334	1 175 000
GB4-2-D1-4.2%	70	1 180 000	1 040 000
GB4-4-I2-4.3%	70	1 485 000	1 300 001
GB4-1-C4-3.9%	90	447 200	370 000
GB4-3-I3-4.1%	90	143 200	106 000
GB4-2-I3-4.0%	90	136 800	120 000
GB4-1-C2-3.7%	110	51 550	44 000
GB4-1-C3-3.4%	110	72 800	70 001
GB4-2-C2-3.7%	110	97 800	65 000
GB4-2-D2-3.5%	110	266 800	238 000
GB4-3-C3-3.7%	110	103 000	85 000
S_N		0.34	0.36
S_0		0.13	0.14
r^2		0.85	0.85
ε_6 [µm/m]		76	75
$\Delta\varepsilon_6$ [µm/m]		7.1	7.4

5.2. Influence of materials characteristics on fatigue resistance

In this section, the three studied mixtures are compared in terms of their fatigue resistance properties. An example is presented comparing the |E*| against N curves of one test of each material at a same strain amplitude. Further analysis is made based on the comparison of the Wöhler curves of the non-conditioned materials. Since the difference in air voids content of the samples of a same material tested at a same strain level is not significant, no comparison in this aspect was made.

Figure 5.13 presents three |E*| against N curves from tests at 70 µm/m, one from each of the studied bituminous mixtures. Its serves as example to illustrate the influence of the mixtures characteristics on the modulus loss during a fatigue test. GB4 mixture presents higher initial modulus values than the GB3 and GBPMB mixtures. In general, GB4 mixture is stiffer than the other two mixtures during the first and second phases of the fatigue tests. This is in accordance with the complex modulus test results, where the GB4 was found to be stiffer due to the optimized granular packing. However, its higher stiffness does not give the GB4 higher fatigue resistance than the other two mixtures.

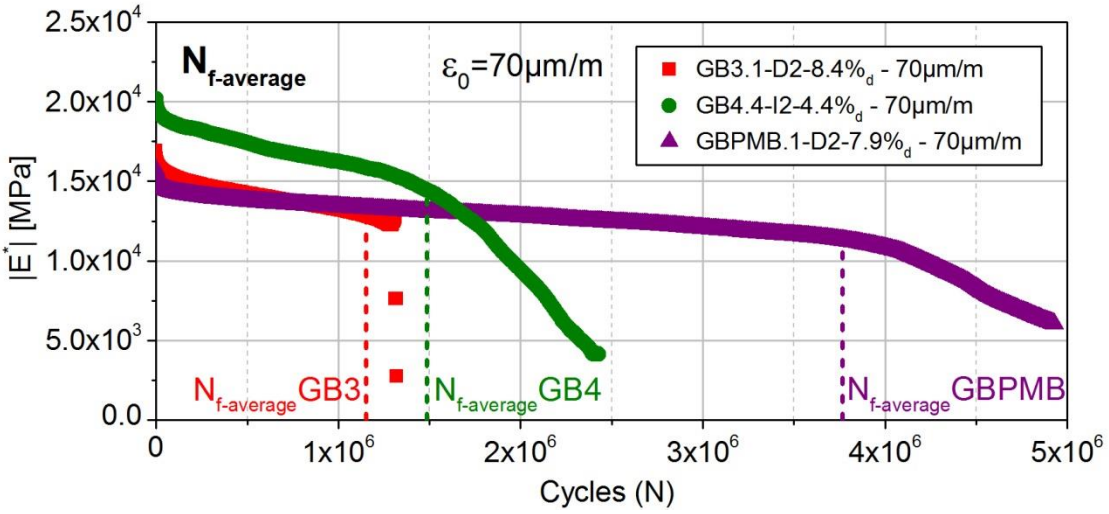

Figure 5.13. |E*| vs N plots of a test at 70 µm/m of each of the three studied mixtures

Figure 5.14 to Figure 5.16 present the Wöhler curves for each material at the non-conditioned state. The non-conditioned GB4 and GB3 mixtures presents very similar a ε_6 values (c.f. Figure 5.14). The GB3, however, presents a higher 1/b value than the GB4 which indicates a lower sensibility to strain amplitude changes, i.e., a small increment or decrease in the strain amplitude does not affect much the fatigue life of the GB3 as it does the GB4's. The GB4 presents higher ε_6 uncertainty than the GB3 (c.f. Table 5-4) which would penalise the layer thickness design. Optimizing the aggregate packing of bituminous mixtures does not seem to significantly affect fatigue resistance properties. The lower slope of the GB4 with respect to the GB3's could be explained by its higher binder content.

Figure 5.15 presents the comparison of the Wöhler curves form the GB3 and GB PMB mixtures. The influence of the PMB on fatigue resistance is clearly observed. The GB PMB presents a much higher ε_6 value and a lower 1/b value than the GB3. This is an evidence of the improvement in

fatigue life conferred by the PMB. Fatigue life of the GB PMB is higher than the GB3's for all strain amplitudes below 110 µm/m. Due to the lower 1/b value of the GB PMB, its fatigue life is expected to be much higher than the GB3's at low strain amplitudes. The ε_6 uncertainty of the GB PMB results is higher than the GB3's.

Figure 5.16 presents the comparison of the GB4 and GB PMB Wöhler curves. Both linear fits have similar slopes; therefore the materials present the same susceptibility to changes in strain amplitude. The GB PMB presents higher fatigue life at all strain amplitudes than the GB4. This means that the use of PMB is more effective to enhance fatigue resistance of bituminous mixtures than optimizing the aggregate packing.

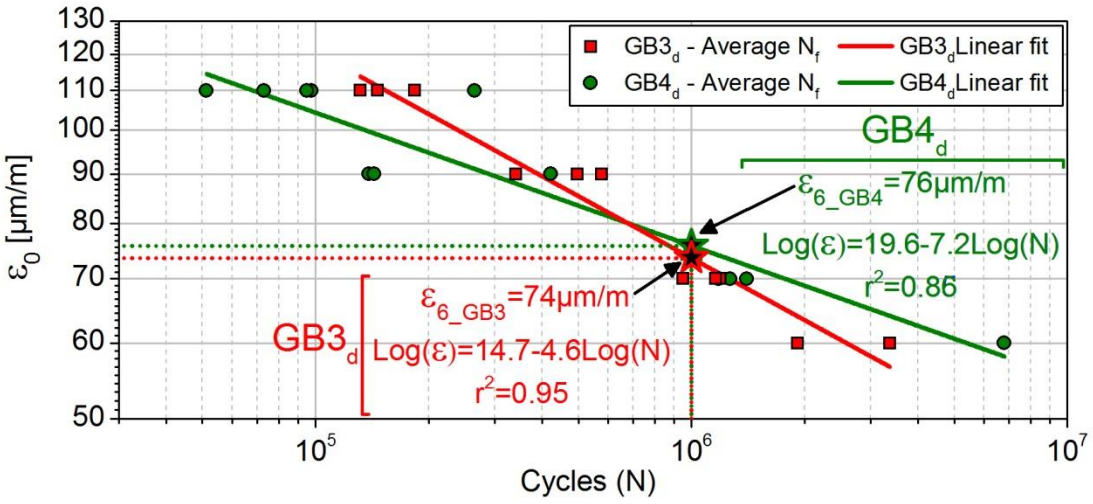

Figure 5.14. Non-conditioned GB3 (red) and GB4 (green) Wöhler curves

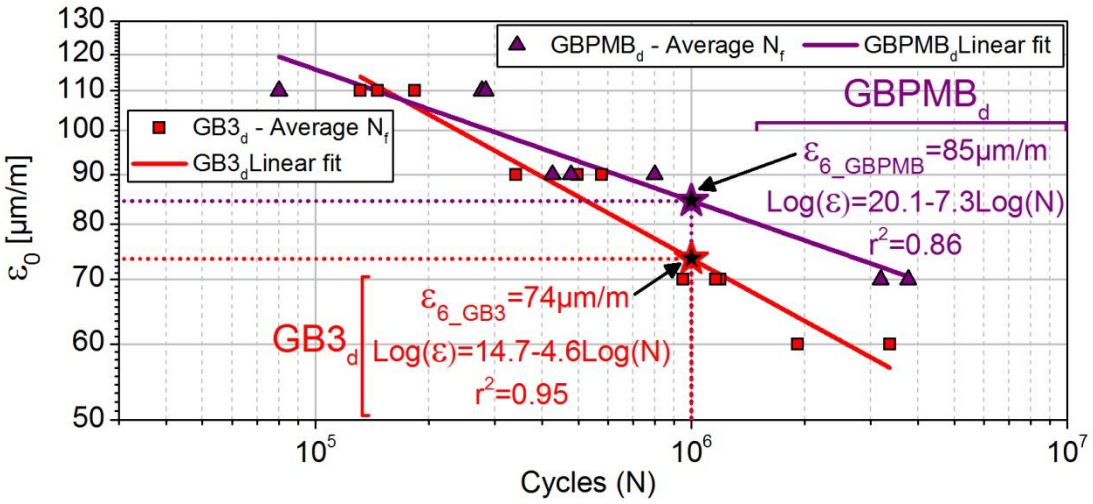

Figure 5.15. Non-conditioned GB3 (red) and GB PMB (purple) Wöhler curves

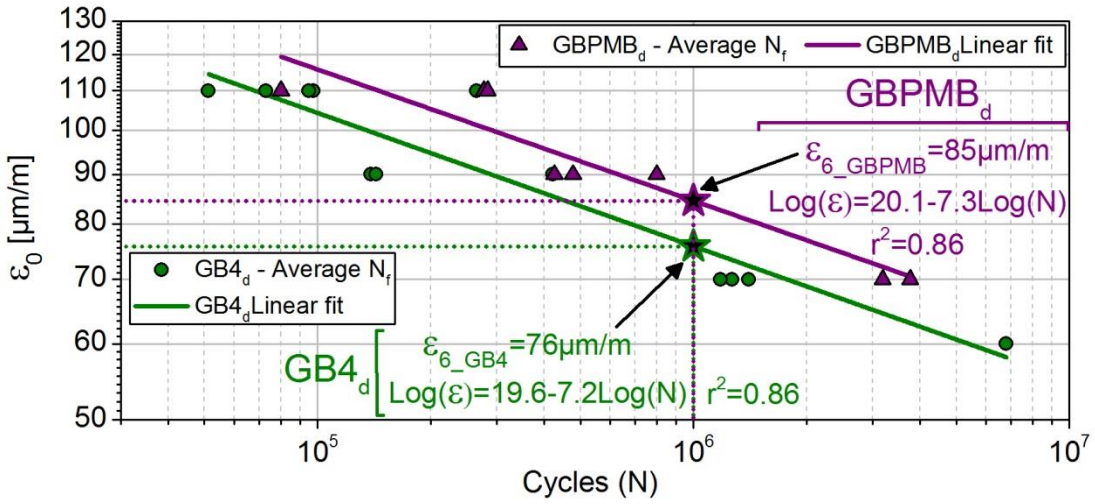

Figure 5.16. Non-conditioned GB4 (green) and GB PMB (purple) Wöhler curves

5.3. Influence of moisture conditioning on fatigue resistance

In this section, the moisture susceptibility the three studied mixtures is assessed with respect to fatigue resistance. An example is presented comparing the |E*| against N curves conditioned and non-conditioned GB4 samples at same strain amplitude. Further analysis is made by comparing the Wöhler curves of each material for the moisture conditioned and not-conditioned states.

5.3.1. Study for a single strain amplitude

Figure 5.17 to Figure 5.19 compare the evolution of |E*| during a fatigue test between two samples of each material, one moisture-conditioned and one not. They serve as example of the effect of moisture conditioning on the behaviour of the samples during the fatigue tests. Results presented in Figure 5.17 to Figure 5.19 correspond to tests presenting the three phases of the fatigue behaviour, but for the non-conditioned GB3 sample. These figures present the results at 70 µm/m and are not representative of the behaviour of the mixtures at other strain levels.

Figure 5.17 is a perfect example of the effect of moisture conditioning on the GB3 mixture. The conditioned sample presented a rapid degradation during the fatigue test compared to the non-conditioned one. This is seen in the increase of the slope of the second phase of the fatigue curve. The example presented for the GB4 mixture shows how moisture conditioning might reduce the fatigue life of the sample, however, the variability of the GB4 results was very high and some conditioned samples resisted more loading cycles than the non-conditioned ones. Figure 5.19 shows an example of the low impact of moisture conditioning of the GB PMB mixture at 70 µm/m.

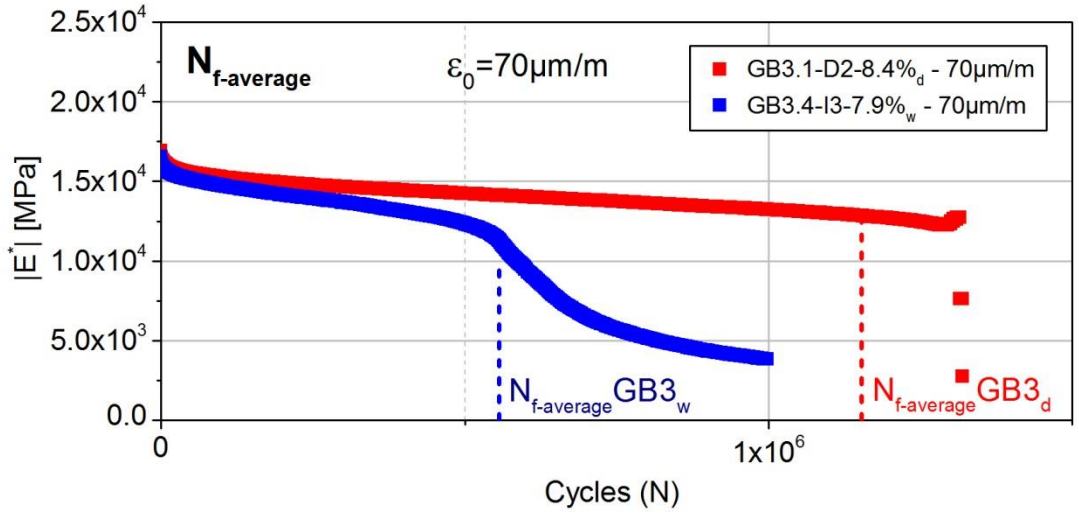

Figure 5.17. |E*| vs N plots of a test at 70 µm/m of a moisture-conditioned (blue) and a non-conditioned (red) GB3 samples

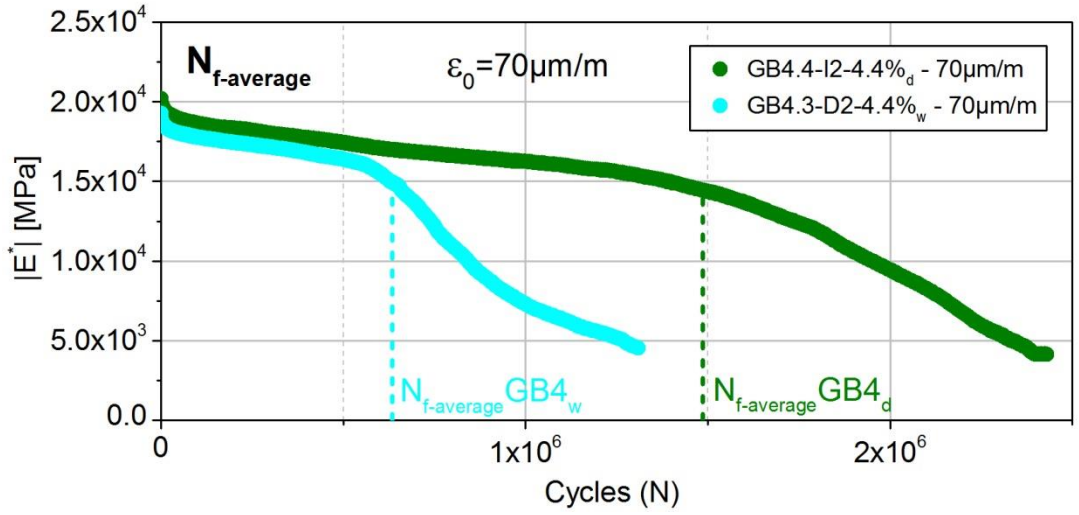

Figure 5.18. |E*| vs N plots of a test at 70 µm/m of a moisture-conditioned (cyan) and a non-conditioned (green) GB4 samples

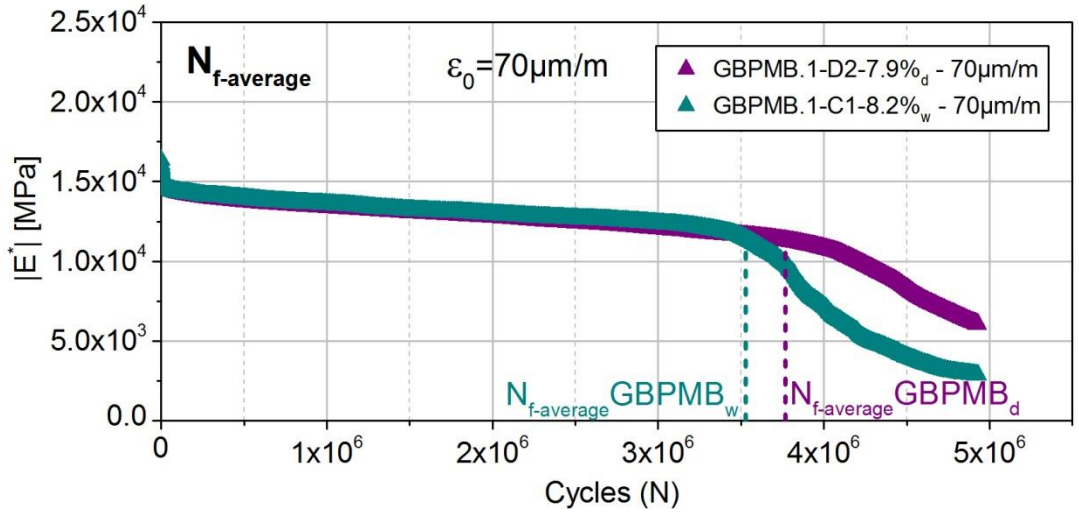

Figure 5.19. |E*| vs N plots of a test at 70 µm/m of a moisture-conditioned (dark cyan) and a non-conditioned (purple) GB PMB samples

5.3.2. Moisture influence on ε_6

The influence of moisture conditioning on the Wöhler curves of each material is presented in Figure 5.20 to Figure 5.22. Figure 5.20 compares the Wöhler curves of the GB3 for both conditioning states. The non-conditioned GB3 presents a ε_6 of 74 µm/m. After conditioning, the ε_6 decreases to 66 µm/m. An increase of the Wöhler curve slope is also observed after conditioning. The uncertainty of ε_6 is also higher for the conditioned state than for the non-conditioned one (c.f. Table 5-4). This shows a clear degradation of the fatigue resistance properties of the GB3 due to moisture conditioning.

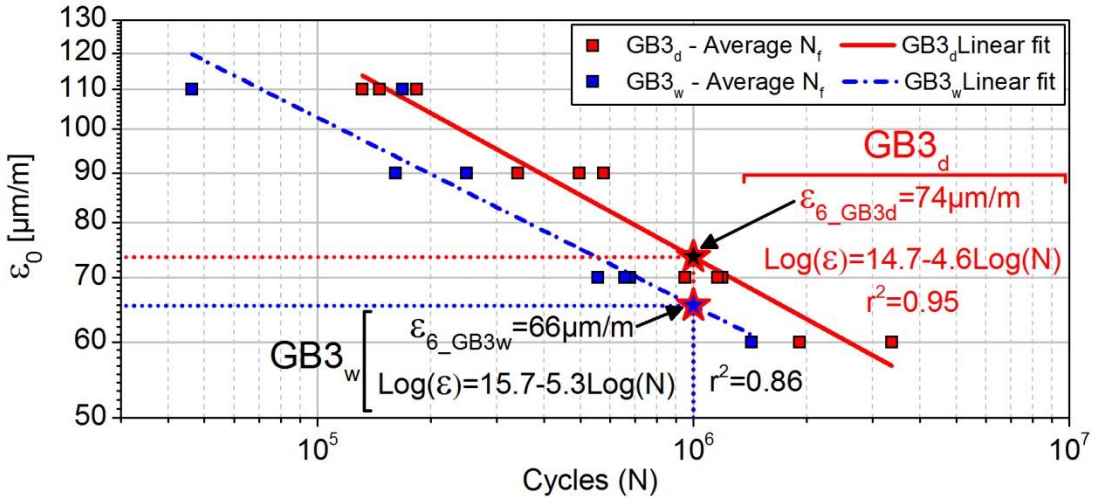

Figure 5.20. Non-conditioned (red) and moisture conditioned (blue) Wöhler curves for the GB3 mixture

The influence of moisture conditioning on the GB4 is presented in Figure 5.21. No evident signs of degradation are shown by the results from the moisture-conditioned samples when compared to those from non-conditioned ones. In fact, the dispersion of the points conforming both conditioned and non-conditioned Wöhler curves is high and there is no clear tendency of reduced N_f for either state at all tested strain amplitudes but 60 µm/m. The GB4 samples subjected to the moisture conditioning procedure seem to have been affected very differently one from the other by water. This could be due to the presence of zones of privileged contact with water in some samples. The fact that the GB4 presents such dispersion, reflected in high $\Delta\varepsilon_6$ values, is penalizing for the design of structural layers with this material. The optimized aggregate packing of the GB4 evidently increases its compactness but it might also favour the creation of void clusters. The real distribution of air voids within the compacted samples needs to be investigated.

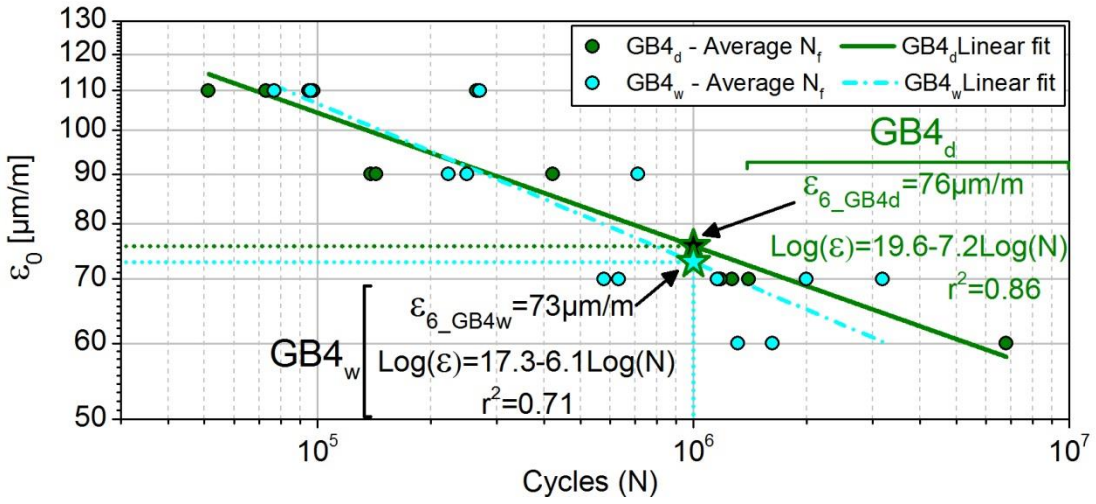

Figure 5.21. Non-conditioned (green) and moisture conditioned (cyan) Wöhler curves for the GB4 mixture

The GB PMB Wöhler curves are presented in Figure 5.22. As for the GB3, the ε_6 value decreases and the slope increases slightly after conditioning. However, the degradation of the GB PMB caused by moisture is lesser than the GB3's (decrease of 5 μm/m in ε_6 compared to 8 μm/m). Most interesting is to note that the conditioned GB PMB ε_6 is higher than those from the GB3 and GB4 in both states. This clearly indicates that the GB PMB performs better to fatigue than the other two studied mixtures, even after moisture damage.

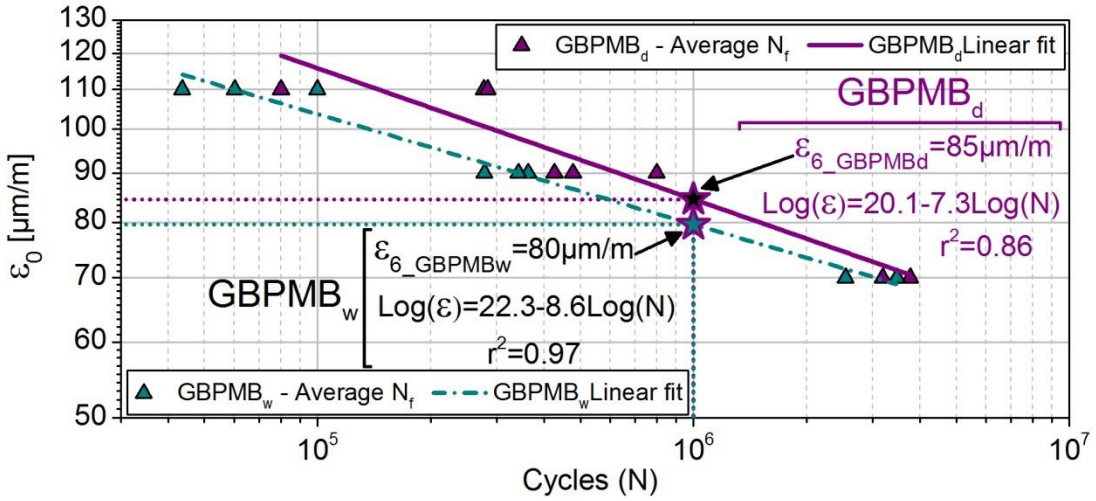

Figure 5.22. Non-conditioned (purple) and moisture conditioned (dark cyan) Wöhler curves for the GB PMB mixture

Table 5-4. Wöhler curves parameters for each material and conditioning state with $N_{f\_average}$

Material	Conditioning state	ε_6 [µm/m]	1/b	$\Delta\varepsilon_6$ [µm/m]	r^2	Average air void content [%]
GB3	Non-conditioned	73.6	-0.21	3.8	0.95	7.7
	Moisture-conditioned	66.1	-0.19	8.6	0.86	7.7
GB4	Non-conditioned	76.0	-0.14	7.1	0.85	4.0
	Moisture-conditioned	73.4	-0.17	10.2	0.70	4.2
GB PMB	Non-conditioned	84.7	-0.14	6.8	0.86	7.6
	Moisture-conditioned	79.7	-0.12	3.3	0.96	7.7

Figure 5.23 resumes the effect of moisture on the fatigue resistance properties of the studied mixtures. Figure 5.23(a) presents the ratio between ε_6 values from moisture-conditioned and non-conditioned samples. The uncertainty of the ratio (Δ) was calculated taking into account the $\Delta\varepsilon_6$ values of each ε_6, following the basic rules of error propagation as shown in equation [5-5].

$$\Delta = \frac{\varepsilon_{6w}}{\varepsilon_{6d}}\left(\frac{\Delta\varepsilon_{6w}}{\varepsilon_{6w}} + \frac{\Delta\varepsilon_{6d}}{\varepsilon_{6d}}\right) \quad [5\text{-}5]$$

It is clear that the GB3 mixture presents the highest moisture susceptibility of the three studied mixtures, even if the ε_6 loss is merely above 10%. The GB4 results presented high dispersion which is reflected in its ε_6 loss uncertainty. Therefore, in the most pessimistic situation, the GB4 would present higher moisture susceptibility than the GB PMB. Hence, the GB PMB mixture can be rated as the best fatigue resistant and least susceptible to moisture of the studied mixtures. Regarding the effect of moisture conditioning on the Wöhler curve slope, GB3 and GB PMB mixtures present similar 1/b reduction and the high dispersion of the GB4 results might explain the slope increase after conditioning.

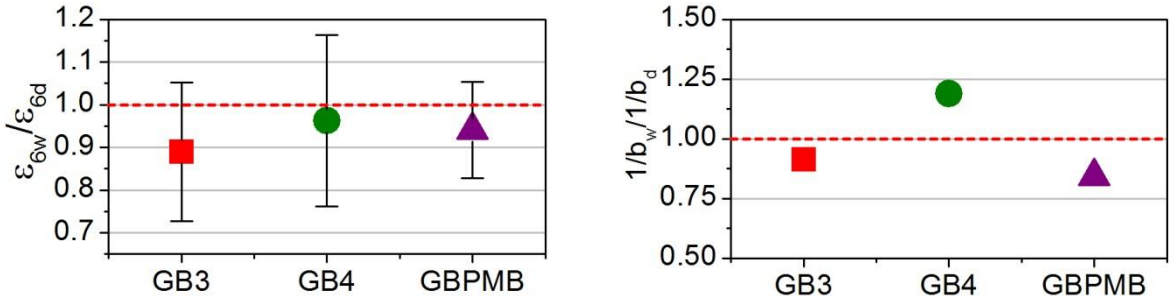

Figure 5.23. Moisture susceptibility ratios based on fatigue resistance for the three studied mixtures: $\varepsilon_{6w}/\varepsilon_{6d}$ taking into account each $\Delta\varepsilon_6$ value (a) and $^1/_{b_w}/^1/_{b_d}$ (b)

No direct correlation between the dry surface saturation level of the samples and the N_f was found. The corrected damage level of each sample for which the failure is attained is calculated as presented in section 1.3.10. Figure 5.24 to Figure 5.26 show the D_{IIIc} values for the GB3, GB4 and GB PMB mixtures respectively. The grey points in Figure 5.24(a), Figure 5.25(a) and Figure 5.26(a) are from samples that presented an unsuitable |E*| against N plot for the application of the damage correction procedure and weren't taken into account for the statistical analysis (box charts). Mostly, these tests presented an increase of the norm of the complex modulus before

attaining the physical rupture distorting the value of |E*| at the failure. The third phase of the fatigue curve was also not attained in these cases.

For each material, all samples present a similar damage value at the failure, regardless of the strain level of the fatigue test. This is in accordance with the work from (Tapsoba, 2012; Tapsoba et al., 2013) indicating that the damage level at failure is independent from the strain amplitude. Moreover, this damage level is very similar for the moisture-conditioned and non-conditioned samples. Moisture conditioning does not seem to alter the damage level at failure of the tested materials. Since moisture conditioning caused a decrease of the fatigue resistance properties of the mixtures, it is presumed that moisture accelerates their damaging rate.

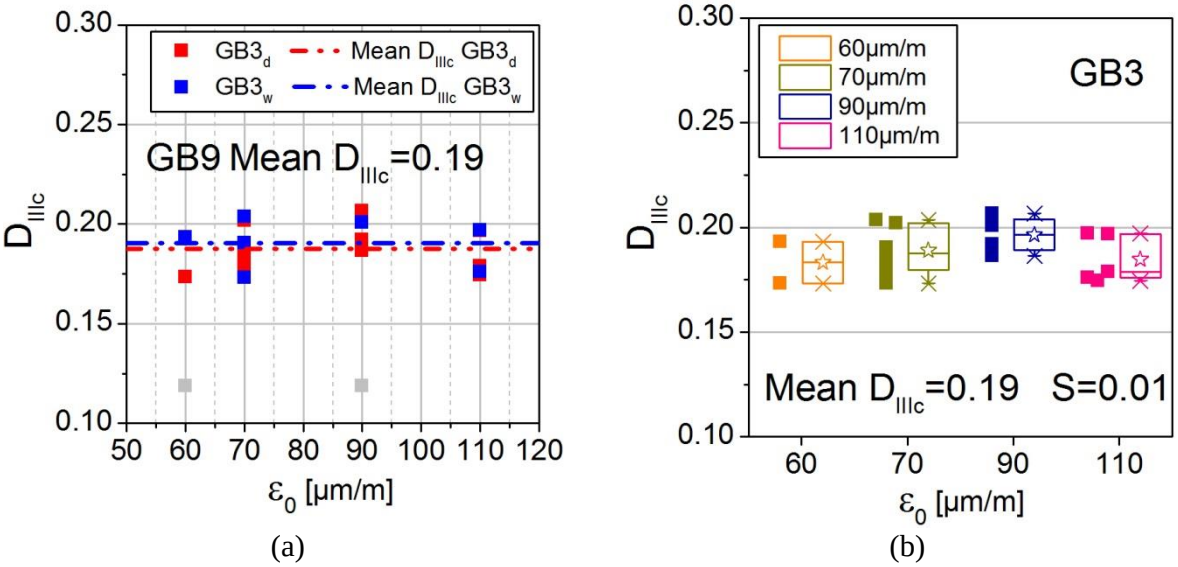

(a) (b)

Figure 5.24. Corrected damage at failure (D_{IIIc}) of the GB3 moisture-conditioned and non-conditioned samples (a) and box chart of the GB3 D_{IIIc} values per strain level (b)

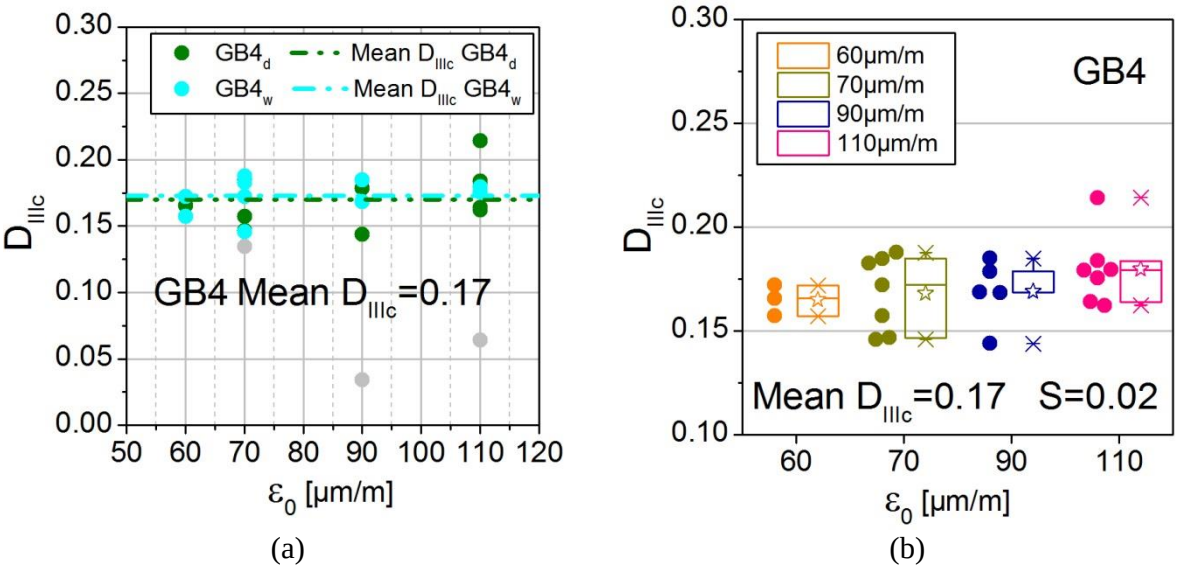

(a) (b)

Figure 5.25. Corrected damage at failure (D_{IIIc}) of the GB4 moisture-conditioned and non-conditioned samples (a) and box chart of the GB4 D_{IIIc} values per strain level (b)

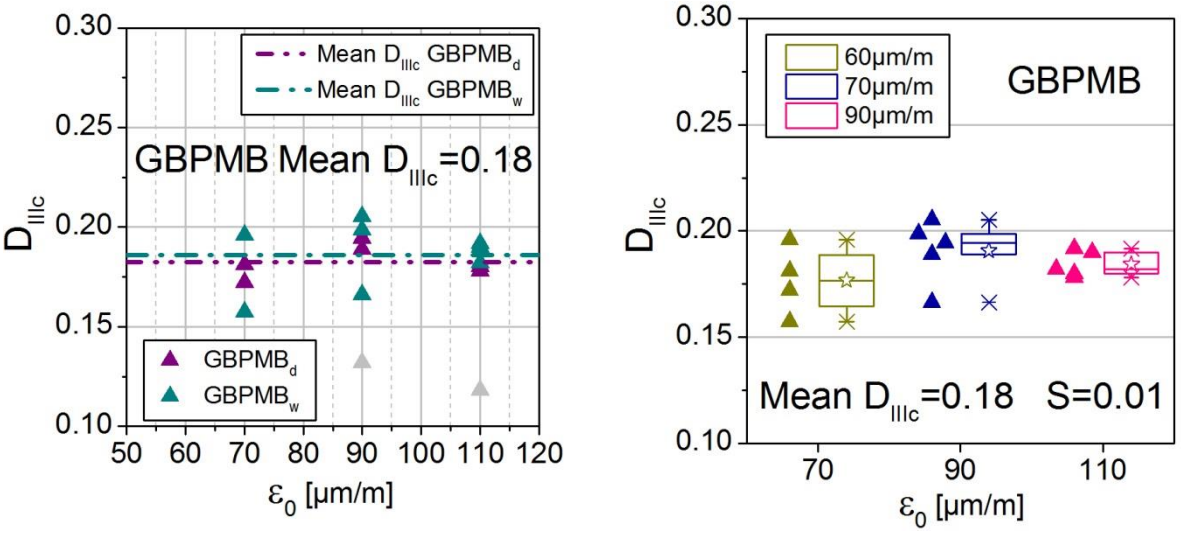

(a) (b)

Figure 5.26. Corrected damage at failure (D_{IIIc}) of the GB PMB moisture-conditioned and non-conditioned samples (a) and box chart of the GB PMB D_{IIIc} values per strain level (b)

Comparing the three mixtures, the damage level at failure is very similar for the three of them. Given the superior fatigue resistance properties of the GB PMB, this indicates that the polymer modified binder helps slowing the damaging rate due to cyclic loading. However, it does not grant the mixture the ability to take on more damage before failure.

Table 5-5. Corrected damage at failure (D_{IIIc}) for all tested materials at moisture conditioned and non-conditioned states

Material	Conditioning state	D_{IIIc}	D_{IIIc} Standard deviation
GB3	Non-conditioned	0.19	0.01
	Moisture-conditioned	0.19	0.01
GB4	Non-conditioned	0.17	0.02
	Moisture-conditioned	0.17	0.01
GB PMB	Non-conditioned	0.18	0.01
	Moisture-conditioned	0.18	0.01

6

Conclusions and recommendations for future works

The objective of this study was to characterise the thermomechanical properties of bituminous mixtures to be used for railway trackbeds. Linear viscoelastic (LVE) behaviour and fatigue resistance properties have been investigated. Road base-course mixtures were tested in order to assess whether commonly available mixtures present suitable properties for railway applications or not. Given the design life of railway tracks and the disposition of the bituminous mixtures in the track structure, the perennity of the materials properties was of special concern. Moisture damage was identified as a potential trigger for premature damaging of the bituminous mixtures in railway structures. A new protocol for moisture conditioning was proposed to evaluate performance of the mixtures after being exposed to humidity. This protocol is based on standard test procedures and on the observations from the literature review on the subject.

Sinusoidal tension-compression tests on cylindrical cored samples were carried out for this study. The LVE behaviour was characterised by means of the complex modulus test at different temperatures and loading frequencies. The fatigue resistance properties were obtained by means of continuous fatigue tests at 10°C and 10 Hz for different strain amplitudes. The materials were tested at conditioned and non-conditioned states in order to characterise their susceptibility to moisture damage.

In this section, conclusions drawn from this investigation are presented.

a. Regarding the analysis of the feedback from the EE HSL test zone

The feedback from 8 service years of the East-European high-speed line (EE HSL) test zone has put in evidence several advantages of using a bituminous sub-ballast layer in high-speed tracks.

Compared to the surrounding conventional track zones made with unbound granular materials (UGM), the test zone presents:

- Higher and more homogeneous vertical stiffness values.
- Lower vertical stress transmitted to the supporting soil.
- Lower vertical acceleration of the superstructure components.
- Slower degradation rate of the track geometry.
- Higher efficiency of the tamping operations in resetting the track geometry.

From an industrial point of view, the most interesting observation from the EE HSL feedback is the important reduction of the degradation rate of the bituminous track with respect to the conventional one. At average temperature conditions (around 15°C) and for typical loading frequencies from train traffic, the higher stiffness of the bituminous mixture compared to compacted soil might provide increased support and confinement to the ballast layer. This leads to an enhancement of the force network between ballast grains and to high internal shear. As a consequence, the ballast layer is less prone to disaggregation. The low degradation rate of the bituminous track after tamping also implies that the damaging effects of tamping on ballast are minimized by the presence of the bituminous sub-ballast.

The EE HSL test section presents an overall good behaviour similar, or even better, than that of the best behaving conventional track sections.

b. Regarding the LVE properties of the tested bituminous mixtures

Complex modulus tests at different temperatures and loading frequencies were carried out on the three studied mixtures. Moisture conditioned and non-conditioned samples were tested.

The Time-Temperature Superposition Principle (TTSP) was validated for all of the studied materials, even when moisture conditioned. For the moisture-conditioned samples, the water present in the pores freezes during the test stages at negative temperatures. This was expected to overly increase the stiffness of the samples at those test conditions, causing a discontinuity of the Cole-Cole plot. However, the saturation level of the moisture-conditioned samples seems to have been insufficient in order to cause this.

The a_T shift factor was observed to remain unchanged by moisture conditioning. This implies that the bitumen is not significantly altered by the used moisture conditioning protocol. It is important to recall that the conditioning protocol is based on the most severe conditions contemplated in the European and American standard moisture susceptibility tests.

All of the studied mixtures were found to present high modulus values for the frequencies excited by French train traffic and for the average temperature range of sub-ballast layers in France. It is important to clarify that the temperature reference was taken from the EE HSL test zone. This zone is located in an area presenting a continental climate with important air temperature changes between summer and winter. These temperature changes were not reflected in the bituminous sub-ballast layer temperature measures.

In general, the used moisture conditioning protocol did not alter the LVE behaviour of the studied bituminous mixtures. The representation on a normalized Cole-Cole plan permitted to

observe this. The results from moisture-conditioned and from non-conditioned samples could be modelled using the same 2S2P1D model shape parameters (h, k, β and δ).

Moreover, the same 2S2P1D model shape parameters could be used to model the complex modulus test results for the three mixtures. This indicates that these parameters depend only of the bitumen properties. The 2.5% cross-liked SBS modification of the base 35/50 bitumen did not alter the shape parameters of the model either.

The glassy modulus E_0 and the parameter τ were found to be dependent of the void content of the samples. Both parameters values decrease with the increase of the air void content. The parameter τ was though altered by the polymer modification of the GB PMB bitumen.

As for the static modulus E_{00}, no direct correlation was found with other parameters or characteristics of the samples. It does not seem to depend on the moisture conditioning state of the sample either. The difficulties to identify E_{00} were due to the limit conditions of the used equipment for the mechanical tests. Samples which suffered traction during the test were found to present low E_{00} values compared to those samples in compression. The results from the cyclic loading test at different average strain levels and from the relaxation test permitted confirming the fact that the static modulus depends on the extension of the sample.

c. Regarding fatigue resistance properties

Fatigue test results from moisture-conditioned samples presented higher dispersion than those from non-conditioned ones. This could be related to the different voids distribution of the samples which could cause different degrees of moisture damage between the conditioned samples.

The GB3 mixture presents the most moisture susceptibility regarding fatigue resistance, followed by the GB PMB. The GB4 fatigue resistance properties did not seem to be altered by the used moisture conditioning protocol. This implies that the increase of air void content probably increases the susceptibility to moisture of the fatigue resistance properties of this kind of bituminous mixtures. However, the GB4 also presented the highest ε_6 uncertainty of the three mixtures.

The GB PMB mixture presents, however, the highest fatigue resistance properties of the three studied mixtures, even after moisture conditioning. This is a clear evidence of the positive effect of polymer modification on the fatigue life of bituminous mixtures.

Based on the French road design method, given the observed low strain levels at the bottom of the EE HSL test zone bituminous layer, the fatigue resistance properties of the three studied mixtures, even after moisture damage, seem suitable for their use as sub-ballast layers. However, the EE HSL strain measurements need to be rectified and confirmed by other in-situ measurement campaigns.

d. Contributions of the study

This thesis was carried out in collaboration with the French National Railway Company (SNCF). The results from the study provide the industry with valuable information on the thermomechanical behaviour of bituminous mixtures to be used in railway applications. This information will serve to amend the technical referent documents concerning the use of bituminous materials for sub-ballast layers. Useful insights on the formulation requirements for bituminous mixtures, such as voids content, binder content and binder type, are provided. The results from the characterisation of the thermomechanical behaviour of the materials were also added to the data base of the company to be used in future track simulation projects.

The conclusions of the study allowed corroborating that the available bituminous mixtures in the French market present adequate thermomechanical properties for their use in railway infrastructure. More specifically, the GB4 mixture, already used for the construction of the Brittany-Loire (BPL) high-speed line, was found to be a well performing material. The information provided on the GB4 will be of utility for the interpretation of the return on experience from the mentioned HSL.

New test methods for bituminous mixtures were also proposed by this study. A new moisture conditioning procedure for compacted mixtures was developed taking into account the French and American standard test procedures as well as the insights from the literature review on the subject. This new moisture conditioning method is considered as aggressive and respectful of the specimens' characteristics while being simple to carry out. Since saturation levels are not imposed, in order to estimate the exposition to moisture of each sample, it is recommended to thoroughly characterise their voids content and internal disposition.

Moreover, two test procedures were proposed to access the static modulus value of bituminous mixtures and to evaluate its dependence on the strain state of the samples. The results from these tests show the reduction of the static modulus value with the extension of the sample. More experimental work should be carried out on the subject, including performing the tests in contraction.

The conclusions from this study also give way to other research questions such as the viability of using bituminous mixtures with high Recycled Asphalt Pavement (RAP) contents for railway applications, the use of bituminous mixtures in ballast-less tracks, or even their use in sleeper-less tracks for tunnels.

e. Recommendations for future works

Several points of the study are worth further investigation, in particular the following ones:

- Creating and monitoring instrumented zones in railway tracks with bituminous sub-ballast layers in different geographical locations. This will provide more insight on how bituminous mixture layers improve the mechanical behaviour of the tracks and on the lifetime and evolution of the material in such conditions. This is necessary in order to identify the stress and stress levels at the bituminous layers as sub-ballast.
- Further development of the mechanical tests to identify the real value of the static modulus E_{00}. These tests have to take into account the fact that this parameter depends

largely on whether the samples suffer extension or not. The complex modulus test protocol needs to be adapted in order to avoid small traction efforts during the rest periods.

- The use of ant-stripping agents in bituminous mixtures for railway applications. Their pertinence need to be assessed through various thermomechanical properties such as fatigue and permanent deformation resistance.
- Characterising voids content by CT tomography. This would be particularly helpful for the analysis of moisture susceptibility regarding fatigue resistance. Fatigue test results from moisture-conditioned samples present higher dispersion which could be explained by an heterogeneous exposure to water.
- Characterising the bitumen properties of moisture-conditioned samples. This could be used to verify whether the proposed conditioning protocol ages the bitumen or not.
- Coupling the fatigue test results to image analysis of the fracture surfaces of the samples to determine weather stripping is observable or not. Visual observation could help refining the analysis of fatigue tests on moisture-conditioned sample as it does for non-conditioned samples when defects are evident on a sample.

7

References

AASHTO M320. Standard Specification for Performance-Graded Asphalt Binder (2010). American Association of State Highway and Transportation Officials.

AASHTO R28. Standard Practice for Accelerated Aging of Asphalt Binder Using a Pressurized Aging Vessel (PAV) (2012). American Association of State Highway and Transportation Officials.

AASHTO T240. Standard Method of Test for Effect of Heat and Air on a Moving Film of Asphalt Binder (Rolling Thin-Film Oven Test) (2013). American Association of State Highway and Transportation Officials.

AASHTO T313. Standard Method of Test for Determining the Flexural Creep Stiffness of Asphalt Binder Using the Bending Beam Rheometer (BBR) (2012). American Association of State Highway and Transportation Officials.

AASHTO T314. Standard Method of Test for Determining the Fracture Properties of Asphalt Binder in Direct Tension (2012). American Association of State Highway and Transportation Officials.

AASHTO T315. Standard Method of Test for Determining the Rheological Properties of Asphalt Binder Using a Dynamic Shear Rheometer (DSR) (2012). American Association of State Highway and Transportation Officials.

AASHTO T316. Standard Method of Test for Viscosity Determination of Asphalt Binder Using Rotational Viscometer (2013). American Association of State Highway and Transportation Officials.

AASHTO T 165. Standard Method of Test for Effect of Water on Cohesion of Compacted Bituminous Mixtures (2002). American Association of State and Highway Transportation Officials.

AASHTO T 283. Standard Method of Test for Resistance of Compacted Asphalt Mixtures to Moisture-Induced Damage (2014). American Association of State and Highway Transportation Officials.

AASHTO TP70. Standard Method of Test for Multiple Stress Creep Recovery (MSCR) Test of Asphalt Binder Using a Dynamic Shear Rheometer (DSR) (2013). American Association

of State Highway and Transportation Officials.

Airey, G. D. (1999). Dynamic shear rheometry, fluorescent microscopy, physical and chemical evaluation of polymer modified bitumens. *Proceedings of Che 7lh Conference on Asphalt*. Retrieved from http://ntl.bts.gov/lib/55000/55700/55745/CAPSA-99.PDF

Airey, G. D. (2003). State of the Art Report on Ageing Test Methods for Bituminous Pavement Materials, *4*(September), 165–176. http://doi.org/10.10850/1029843042000198568

Airey, G. D. (2010). Construction Materials: Their Nature and Behaviour, Fourth Edition. In P. Domone & J. Illston (Eds.), *Construction Materials: Their Nature and Behaviour* (4th ed., pp. 218–223). book, Abingdon: Spon Press.

Airey, G. D., Collop, A. C., Zoorob, S. E., & Elliott, R. C. (2008). The influence of aggregate , filler and bitumen on asphalt mixture moisture damage. *Construction and Building Materials*, *22*, 2015–2024. http://doi.org/10.1016/j.conbuildmat.2007.07.009

Airey, G. D., Rahimzadeh, B., & Collop, A. C. (2003). Viscoelastic linearity limits for bituminous materials. *Materials and Structures*, *36*(10), 643–647. http://doi.org/10.1007/BF02479495

Alfaro Albalat, S., Montalban Domingo, L., Villalba Sanchis, I., Real Herraiz, J., & Villanueva Segarra, A. (2011). Crumb Rubber Modified Bitumen for sub-ballast layer. In *9th World Congress on Railway Research* (pp. 1–9). Lille, France.

Al-Swailmi, S., & Terrel, R. L. (1992). Evaluation of Water Damage of Asphalt Concrete Mixtures Using the Environmental Conditioning System (ECS). *Journal of the Association of Asphalt Paving Technologists (AAPT)*, *61*, 405–445.

Alvarez-Lugo, A. E., & Carvajal-Munoz, J. S. (2014). Practical lessons learnt from the application of X-ray computed tomography to evaluate the internal structure of asphalt mixtures. *DYNA*, *81*(188), 52–59. http://doi.org/10.15446/dyna.v81n188.40042

Anderson, D. A., Christensen, D. W., Bahia, H. U., Dongre, R., Sharma, M. G., Antle, C. E., & Button, J. (1994). *Binder characterization and evaluation* (Vol. 3: Physica). Washington DC, Etats Unis: National Academy of Sciences.

Anderson, M. (2014). Understanding the MSCR Test and its Use in the PG Asphalt Binder Specification Recording. Asphalt Institute & Federal Highway Administration. Retrieved from http://www.asphaltinstitute.org/understanding-the-mscr-test-and-its-use-in-the-pg-asphalt-binder-specification-recording/

Anderson, M., D'Angelo, J., & Walker, D. (2010). MSCR: A Better Tool for Characterizing High Temperature Performance Properties. *Asphalt*, *25*(2), 15–23.

Antoni, M. (2010). Degradation laws of railway ballasted track. In *3rd International Conference on Accelerated Life Testing - Estimation of the need of maintenance*. Clermont-Ferrand, France.

Arambula, E. (2007). *Influence of fundamental material properties and air void structure on moisture damage of asphalt mixes*. PhD Thesis, Texas A&M University. Retrieved from http://oaktrust.library.tamu.edu/bitstream/handle/1969.1/ETD-TAMU-1276/ARAMBULA-MERCADO-DISSERTATION.pdf?sequence=1

Arambula, E., Masad, E., Martin, A. E., & Lytton, R. (2007). Suitability of dynamic and

relaxation tests for the evaluation of moisture susceptibility of asphalt mixtures. *Journal of Testing and Evaluation*, *36*(2).

Arambula, E., Masad, & Martin, A. E. (2007). Influence of Air Void Distribution on the Moisture Susceptibility of Asphalt Mixes. *Journal of Materials in Civil Engineering*, *19*, 655–665.

Aschenbrener, T. (1995). *Evaluation of Hamburg Wheel-Tracking Device to Predict Moisture Damage in Hot Mix Asphalt*. *Transportation Research Record*. Washington, DC: Transportation Research Board.

Asphalt Institute. (1995). *Performance Graded Asphalt Binder, Specification and Testing* (Report SP-). Lexington, KY.

ASTM D1559-89. Test Method for Resistance of Plastic Flow of Bituminous Mixtures Using Marshall Apparatus (Withdrawn 1998) (1989). http://www.astm.org/Standards/D1559. http://doi.org/10.1520/D1559-89

ASTM D4867. Standard Test Method for Effect of Moisture on Asphalt Concrete Paving Mixtures (2014). American Society for Testing Materials.

ASTM D6925-15. Standard Test Method for Preparation and Determination of the Relative Density of Asphalt Mix Specimens by Means of the Superpave Gyratory Compactor (2015). http://www.astm.org/Standards/D6925.htm.

Aubry, D., & Modaressi, A. (1996). GEFDyn Version X.X. Paris, France: Manuel scientifique, École Centrale Paris, LMSS-Mat.

Audley, M., & Andrews, J. (2013). The effects of tamping on railway track geometry degradation. *Proceedings of the Institution of Mechanical Engineers, Part F: Journal of Rail and Rapid Transit*, *227*(4), 376–391. http://doi.org/10.1177/0954409713480439

Baaj, H. (2002). *Comportement à la fatigue des matériaux granulaires traités aux liants hydrocarbonés [Fatigue behaviour of granular materials treated with hydrocarbon binders]*. PhD Thesis, ENTPE/University of Lyon.

Baaj, H. (2003). Fatigue of mixes: an intrinsic damage approach. In *Sixth International RILEM Symposium on Performance Testing and Evaluation of Bituminous Materials* (pp. 394–400). RILEM Publications SARL. http://doi.org/10.1617/2912143772.049

Bagampadde, U., Isacsson, U., & Kiggundu, B. . (2005). Influence of aggregate chemical and mineralogical composition on stripping in bituminous mixtures. *International Journal of Pavement Engineering*, *6*(4), 12.

Bagampadde, U., & Karlsson, R. (2007). Laboratory studies on stripping at bitumen/substrate interfaces using FTIR-ATR. *Journal of Materials Science*, *42*(9), 3197–3206. http://doi.org/10.1007/s10853-006-0181-x

Bari, J., & Witczak, M. (2005). Evaluation of the Effect of Lime Modification on the Dynamic Modulus Stiffness of Hot-Mix Asphalt: Use with the New Mechanistic-Empirical Pavement Design Guide. *Transportation Research Record: Journal of the Transportation Research Board*, *1929*, 10–19. http://doi.org/10.3141/1929-02

Barnes, C. L., & Trottier, J.-F. (2010). Evaluating laboratory-induced asphalt concrete moisture damage using surface waves. *International Journal of Pavement Engineering*, *11*(6), 489–497. http://doi.org/10.1080/10298430903578929

Barra, B., Momm, L., Guerrero, Y., & Bernucci, L. (2012). Fatigue behavior of dense asphalt mixes in dry and environmental-conditioning states. *Construction and Building Materials*, *29*, 128–134. http://doi.org/10.1016/j.conbuildmat.2011.10.003

Bausano, J., & Williams, R. C. (2009). Transitioning from AASHTO T283 to the simple performance test using moisture conditioning. *Journal of Materials in Civil Engineering*, (21), 73–82.

Bazin, P., & Saunier, J. (1967). Deformability, fatigue and healing properties of asphalt mixes. In *Proceedings of the 2nd International Conference on the Structural Design of Asphalt Pavements* (pp. 438–451). Ann Arbor, MI.

Birgisson, B., Roque, R., & Page, G. C. (2003). Evaluation of Water Damage Using Hot Mix Asphalt Fracture Mechanics. *Journal of the Association of Asphalt Paving Technologists*, *72*, 424–462.

Bocci, M., Cardone, F., Cerni, G., & Santagata, E. (2006). Rheological Characterization of the Fatigue Resistance of Asphalt Binders. In *Proceedings of the 10th International Conference on Asphalt Pavements 2006 (ISAP Quebec 2006)*. Quebec City, Canada.

Bodin, D., Soenen, H., & De la Roche, C. (2004). Temperature effects in binder fatigue and healing tests. In *Proceedings of the 3rd Eurasphalt and Eurobitume Congress* (Vol. 2). Vienna, Austria.

Bolton, M. D., & Wilson, J. M. R. (1989). An experimental and theoretical comparison between static and dynamic torsional soil tests. *Géotechnique*, *39*(4), 585–599. http://doi.org/10.1680/geot.1989.39.4.585

Buchanan, M. S. (2000). Evaluation of the effect of flat and elongated particles on the performance of hot mix asphalt mixtures. Auburn, AL: National Center for Asphalt Technology, Auburn University.

Buonanno, A., & Mele, R. (2000). The use of bituminous mix sub-ballast in the Italian State Railways . In *2nd Eurasphalt & Eurobitume congress*. Barcelona.

Caetano, L. F., & Teixeira, P. F. (2015). Optimisation model to schedule railway track renewal operations: a life-cycle cost approach. *Structure and Infrastructure Engineering*, *11*(11), 1524–1536. JOUR. http://doi.org/10.1080/15732479.2014.982133

Canestrari, F., Cardone, F., Graziani, A., Santagata, F. A., & Bahia, H. U. (2010). Adhesive and cohesive properties of asphalt-aggregate systems subjected to moisture damage. *Road Materials and Pavement Design*, *11*(sup1), 11–32. http://doi.org/10.1080/14680629.2010.9690325

Caro, S., Beltrán, D. P., Alvarez, A. E., & Estakhri, C. (2012). Analysis of moisture damage susceptibility of warm mix asphalt (WMA) mixtures based on Dynamic Mechanical Analyzer (DMA) testing and a fracture mechanics model. *Construction and Building Materials*, *35*, 460–467. http://doi.org/10.1016/j.conbuildmat.2012.04.035

Caro, S., Masad, E., Bhasin, A., & Little, D. (2010). Coupled Micromechanical Model of Moisture-Induced Damage in Asphalt Mixtures. *Journal of Materials in Civil Engineering*, *22*(4), 380–389.

Caro, S., Masad, E., Bhasin, A., & Little, D. . (2007). Moisture susceptibility of asphalt mixtures Part 2 : characterisation and modelling. *International Journal of Pavement*

Engineering, *9*(2), 99–114.

Caro, S., Masad, E., Bhasin, A., & Little, D. . (2008). Moisture susceptibility of asphalt mixtures Part 1 : mechanisms. *International Journal of Pavement Engineering*, *9*(2), 81–98.

Carpenter, S., Ghuzlan, K., & Shen, S. (2003). Fatigue endurance limit for highway and airport pavements. *Transportation Research Record: Journal of the Transportation Research Board*, *1832*, 131–138. http://doi.org/10.3141/1832-16

Carret, J.-C., Falchetto, A. C., Marasteanu, M. O., Di Benedetto, H., Wistuba, M. P., & Sauzeat, C. (2015). Comparison of rheological parameters of asphalt binders obtained from bending beam rheometer and dynamic shear rheometer at low temperatures. *Road Materials and Pavement Design*, *16*(sup1), 211–227. http://doi.org/10.1080/14680629.2015.1029696

Castelblanco Torres, A. (2004). *Probabilistic analysis of air void structure and its relationship to permeability and moisture damage of hot mix asphalt*. Master's thesis, Texas A&M University. Retrieved from http://hdl.handle.net/1969.1/3114

Chen, J.-S., Lin, K.-Y., & Young, S.-Y. (2004). Effects of Crack Width and Permeability on Moisture-Induced Damage of Pavements. *Journal of Materials in Civil Engineering*, *16*(3), 276–282. http://doi.org/10.1061/(ASCE)0899-1561(2004)16:3(276)

Chen, J.-S., & Peng, C.-H. (1998). Analyses of Tensile Failure Properties of Asphalt-Mineral Filler Mastics. *Journal of Materials in Civil Engineering*, *10*(4), 256–262. http://doi.org/10.1061/(ASCE)0899-1561(1998)10:4(256)

Cheng, D., Little, D., Lytton, R., & Holste, J. (2002). Surface Energy Measurement of Asphalt and Its Application to Predicting Fatigue and Healing in Asphalt Mixtures. *Transportation Research Record: Journal of the Transportation Research Board*, *1810*, 44–53. http://doi.org/10.3141/1810-06

Cheng, D., Little, D. N., Lytton, R. L., & Holste, J. C. (2003). Moisture Damage Evaluation of Asphalt Mixtures by Considering Both Moisture Diffusion and Repeated-Load Conditions. *Transportation Research Record*, (1832), 42–49.

Cheng, J., Shen, J., & Xiao, F. (2011). Moisture Susceptibility of Warm-Mix Asphalt Mixtures Containing Nanosized Hydrated Lime. *Journal of Materials in Civil Engineering*, *23*(11), 1552–1559. http://doi.org/10.1061/(ASCE)MT.1943-5533

Chevassu, G. (1969). Influence des caractéristiques pétrographiques de quelques roches sur leur résistance à l'attrition [Influence of the petrographic characteristics of some rocks on their resistance to fragmentation]. *Bulletin de Liaison Des Laboratoires Des Ponts et Chaussés*, (39), 65–72.

Collop, A. C., Choi, Y., & Airey, G. D. (2008). Effects of Pressure and Aging in SATS Test, *133*(11), 618–625.

Cooley, L. A., Brown, E. R., & Maghsoodloo, S. (2001). Development of critical field premeability and pavement density values for coarse-graded superpave pavements. NCAT Report 01-03, Auburn, AL: National Center for Asphalt Technology, Auburn University.

Copeland, A., Youtcheff, J., & Shenoy, A. (2007). Moisture Sensitivity of Modified Asphalt

Binders: Factors Influencing Bond Strength. *Transportation Research Record: Journal of the Transportation Research Board*, *1998*, 18–28. http://doi.org/10.3141/1998-03

Corté, J.-F., & Di Benedetto, H. (2004). *Matériaux routiers bitumineux 1 : description et propriétés des constituants*. (Hermes-Lavoisier, Ed.). Paris.

CP-L 5116. Colorado Procedure – Laboratory 5116-10 Linear Kneading Compaction of Bituminous Mixtures (2014). Colorado Department of Transportation. Retrieved from https://www.codot.gov/

Cundall, P. A., Drescher, A., & Strack, O. D. (1982). Numerical experiments on granular assemblies; measurements and observations. In P. A. Vermeer & H. J. Luger (Eds.), *Deformation and failure of granular materials: Proceedings of IUTAM Symposium* (pp. 355–370). Rotterdam, The Netherlands: A. A. Balkema.

Das, P. K. (2014). *Ageing of asphalt mixtures: micro-scale and mixture morphology investigation*. PhD Thesis, KTH Royal Institute of Technology.

Das, P. K., Baaj, H., Kringos, N., & Tighe, S. (2015). Coupling of oxidative ageing and moisture damage in asphalt mixtures. *Road Materials and Pavement Design*, *16*(sup1), 265–279. http://doi.org/10.1080/14680629.2015.1030835

De la Roche, C. (1996). *Module de rigidité et comportement en fatigue des enrobés bitumineux. Expérimentations et nouvelles perspectives d'analyse [Stiffness modulus and fatigue behaviour of bituminous mixtures: Experimentation and new perspectives for analysis"*. PhD Thesis, Ecole Centrale de Paris.

De la Roche, C., Corté, J.-F., Gramsammer, J.-C., Odéon, H., Tiret, L., & Caroff, G. (1994). Étude de la fatigue des enrobés bitumineux à l'aide du manège de fatigue du LCPC [Study of bituminous mixture fatigue using the LCPC fatigue carousel]. *Revue Générale Des Routes et Aérodromes*, *716*, 62–74.

Delaporte, B., Van Rompu, J., Di Benedetto, H., Chaverot, P., & Gauthier, G. (2008). New procedure to evaluate fatigue of bituminous mastics using an annular shear rheometer prototype. In *Pavement Cracking*. CRC Press. http://doi.org/10.1201/9780203882191.ch45

Di Benedetto, H. (1998). Modélisation: écart entre état des connaissances et applications [Modelling: Difference between the state of the art and the applications]. In *Journée technique LAVOC: Dimensionner les chaussées*. Lausanne, Switzerland.

Di Benedetto, H., Ashayer Soltani, A., & Chaverot, P. (1996). Fatigue damage for bituminous mixtures: a pertinent approach. *Journal of the Association of Asphalt Paving Technologists*, *65*.

Di Benedetto, H., & Corté, J.-F. (2004). *Matériaux routiers bitumineux 2 : constitution et propriétés thermomécaniques des mélanges*. (Hermes-Lavoisier, Ed.). Paris.

Di Benedetto, H., & De la Roche, C. (1998). State of the art on stiffness modulus and fatigue of bituminous mixtures. In L. Francken & RILEM Report 17 (Eds.), *Bituminous Binders and Mixes: State of the art and interlaboratory tests on mechanical behaviour and mix design* (pp. 137–180). London, UK: E & FN Spon.

Di Benedetto, H., de La Roche, C., Baaj, H., Pronk, A., & Lundström, R. (2004). Fatigue of bituminous mixtures. *Materials and Structures*, *37*(3), 202–216.

http://doi.org/10.1007/BF02481620

Di Benedetto, H., Delaporte, B., & Sauzéat, C. (2007a). Three-Dimensional Linear Behavior of Bituminous Materials : Experiments and Modeling, (April), 149–158.

Di Benedetto, H., Delaporte, B., & Sauzéat, C. (2007b). Three-Dimensional Linear Behavior of Bituminous Materials: Experiments and Modeling. *International Journal of Geomechanics*, *7*(2), 149–157. http://doi.org/10.1061/(ASCE)1532-3641(2007)7:2(149)

Di Benedetto, H., Gabet, T., Grenfell, J., Perraton, D., Sauzéat, C., & Bodin, D. (2013). Mechanical Testing of Bituminous Mixtures (pp. 143–256). Springer Netherlands. http://doi.org/10.1007/978-94-007-5104-0_4

Di Benedetto, H., Nguyen, Q. T., & Sauzéat, C. (2011). Nonlinearity, Heating, Fatigue and Thixotropy during Cyclic Loading of Asphalt Mixtures. *Road Materials and Pavement Design*, *12*(1), 129–158. http://doi.org/10.1080/14680629.2011.9690356

Di Benedetto, H., Olard, F., Sauzéat, C., & Delaporte, B. (2004). Linear viscoelastic behaviour of bituminous materials: From binders to mixes. *Road Materials and Pavement Design*, *5*(sup1), 163–202. http://doi.org/10.1080/14680629.2004.9689992

Di Mino, G., Di Liberto, M., Maggiore, C., & Noto, S. (2012). A Dynamic Model of Ballasted Rail Track with Bituminous Sub-Ballast Layer. *Procedia - Social and Behavioral Sciences - 5th International Congress - Sustainability of Road Infrastructures*, *53*(S), 366–378. http://doi.org/10.1016/j.sbspro.2012.09.888

Doan, T. H. (1976). *Les études de fatigue des enrobés bitumineux au LCPC [Bituminous material fatigue studies at LCPC]*. *Bulletin de liaison des Laboratoires des Ponts et Chaussés*. Marne la Vallée.

Doubbaneh, E. (1995). *Comportement mécanique des enrobés bitumineux des "petites" aux "grandes" déformations*. INSA Lyon.

Dubois, V., De la Roche, C., & Burban, O. (2010). Influence of the compaction process on the air void homogeneity of asphalt mixtures samples. *Construction and Building Materials*, *24*(6), 885–897. http://doi.org/10.1016/j.conbuildmat.2009.12.004

EAPA, E. A. P. A. (2014). *Asphalt in Railway Tracks*. Breukelen, Pays Bas.

EN 1097-1. Tests for mechanical and physical properties of aggregates - Part 1 : determination of the resistance to wear (micro-Deval) (2011). European Standard.

EN 1097-2. Tests for mechanical and physical properties of aggregates - Part 2 : methods for the determination of resistance to fragmentation (2010). European Standard.

EN 1097-8. Tests for mechanical and physical properties of aggregates - Part 8 : determination of the polished stone value (2009). European Standard.

EN 12591. Bitumen and bituminous binders - Specifications for paving grade bitumens (2009). European Standard.

EN 12593. Bitumen and bituminous binders - Determination of the Fraass breaking point (2015). European Standard.

EN 12697-12. Bituminous mixtures - Test methods for hot mix asphalt - Part 12 : determination of the water sensitivity of bituminous specimens - Mélanges bitumineux (2008). European Standard.

EN 12697-24. Bituminous mixtures - Test methods for hot mix asphalt - Part 24 : resistance to fatigue - Mélanges bitumineux (2012). European Standard.

EN 12697-33+A1. Bituminous mixtures - Test methods for hot mix asphalt - Part 33 : specimen prepared by roller compactor (2007). European Standard.

EN 12697-5. Bituminous mixtures - Test methods for hot mix asphalt: Determination of the maximum density (2009). European Standard.

EN 12697-6. Bituminous mixtures - Test methods for hot mix asphalt: Determination of bulk density of bituminous specimens (2012). European Standard.

EN 12697-7. Bituminous mixtures - Test methods for hot mix asphalt: Determination of the bulk density of bituminous specimens by gamma rays (2002). European Standard.

EN 13043. Aggregates for bituminous mixtures and surface treatments for roads, airfields and other trafficked areas (2003). European Standard.

EN 13108-1. Bituminous mixtures - Material specifications - Part 1 : asphalt concrete (2007). European Standard.

EN 13924-1. Bitumen and bituminous binders - Specification framework for special paving grade bitumen - Part 1 : hard paving grade bitumens (2016). European Standard.

EN 13924-2. Bitumen and bituminous binders - Specification framework for special paving grade bitemen - Part 2 : multigrade paving grade bitumens (2014). European Standard.

EN 1426. Bitumen and bituminous binders - Determination of needle penetration (2007). European Standard.

EN 1427. Bitumen and bituminous binders - Determination of softening point - Ring and Ball method (2007). European Standard.

Eurobitume. (2016). Bitumen. Retrieved March 7, 2016, from http://www.eurobitume.eu/bitumen/production/?L=0

European Asphalt Pavement Association, & National Asphalt Pavement Association. (2011). The Asphalt Paving Industry A Global Perspective - 2nd edition. Global Series 101. Retrieved from http://www.asphaltpavement.org/images/stories/GL_101_Edition_3.pdf

Fang, M., Fernández Cerdas, S., & Qiu, Y. (2013). Numerical determination for optimal location of sub-track asphalt layer in high-speed rails. *Journal of Modern Transportation*, *21*(2), 103–110. http://doi.org/10.1007/s40534-013-0012-0

Ferry, J. D. (1980). *Viscoelastic properties of polymers* (3rd ed.). New York, NY: Wiley & Sons.

Gaborit, P., Sauzéat, C., Di Benedetto, H., Pouget, S., Olard, F., & Claude, A. (2014). Investigation of highway pavements using in-situ strain sensors. In Massimo Losa and Tom Papagiannakis (Ed.), *Sustainability, Eco-efficiency, and Conservation in Transportation Infrastructure Asset Management* (pp. 331–337). London, UK: CRC Press. Retrieved from http://www.crcnetbase.com/doi/abs/10.1201/b16730-49

Gallegos, C., & Martinez Boza, F. J. (2010). Linear viscoelasticity. In C. Gallegos (Ed.), *Rheology: Encyclopedia of life support systems (Vol. 1)* (pp. 120–143). Oxford, UK: EOLSS.

Gauthier, G., Bodin, D., Chailleux, E., & Gallet, T. (2010). Non Linearity in Bituminous Materials during Cyclic Tests. *Road Materials and Pavement Design*, *11*(sup1), 379–410. http://doi.org/10.1080/14680629.2010.9690339

Gayte, P., Di Benedetto, H., Sauzéat, C., & Nguyen, Q. T. (2016). Influence of transient effects for analysis of complex modulus tests on bituminous mixtures. *Road Materials and Pavement Design*, *17*(2), 271–289. http://doi.org/10.1080/14680629.2015.1067246

Goode, J. F., & Lufsey, L. A. (1962). A new graphical chart for evaluating aggreagte gradation. *Proceedings of the Association of Asphalt Paving Technologists*, (31), 176–207.

Groupement Professionnel des Bitumes. (2013). BitumeINFO_No.Special3.pdf. *Bitume.Info, Special Edition No.3*, 22–24. Retrieved from http://www.bitume.info/

Groupement Professionnel des Bitumes. (2014). *Bitume.info: Sous les rails, le bitume [Bitume.info: Under the rails, the bitumen]*. Puteaux, france. Retrieved from http://www.bitume.info/pdf/BI-TAP-GEORAIL.pdf

Gubler, R., Partl, M. N., Canestrari, F., & Grilli, A. (2005). Influence of water and temperature on mechanical properties of selected asphalt pavements. *Materials and Structures*, *38*(5), 523–532. http://doi.org/10.1007/BF02479543

Gudmarsson, A., Ryden, N., Di Benedetto, H., & Sauzéat, C. (2015). Complex modulus and complex Poisson's ratio from cyclic and dynamic modal testing of asphalt concrete. *Construction and Building Materials*, *88*, 20–31. http://doi.org/10.1016/j.conbuildmat.2015.04.007

Guler, H. (2014). Prediction of railway track geometry deterioration using artificial neural networks: a case study for Turkish state railways. *Structure and Infrastructure Engineering : Maintenance , Management , Life-Cycle Design and Performance*, *10*(5), 614–626. JOUR. http://doi.org/10.1080/15732479.2012.757791

Harman, T., Bukowski, J., Moutier, F., Huber, G., & McGennis, R. (2002). History and Future Challenges of Gyratory Compaction: 1939 to 2001. *Transportation Research Record: Journal of the Transportation Research Board*, *1789*, 200–207. http://doi.org/10.3141/1789-22

Hartman, A. M., Gilchrist, M. D., & Walsh, G. (2001). Effect of Mixture Compaction on Indirect Tensile Stiffness and Fatigue. *Journal of Transportation Engineering*, *127*(5), 370–378. http://doi.org/10.1061/(ASCE)0733-947X(2001)127:5(370)

Harvey, J. T., Deacon, J. A., Tsai, B.-W., & Monismith, C. L. (1995). *Fatigue performance of asphalt concrete mixes and its relationship to asphalt concrete pavement performance in California*. Berkeley, CA. Retrieved from http://trid.trb.org/view.aspx?id=636498

He, G.-P., & Wong, W.-G. (2008). Effects of moisture on strength and permanent deformation of foamed asphalt mix incorporating RAP materials. *Construction and Building Materials*, *22*(1), 30–40. http://doi.org/10.1016/j.conbuildmat.2006.06.033

Hefer, A. W., Bhasin, A., & Little, D. N. (2006). Bitumen Surface Energy Characterization Using a Contact Angle Approach. *Journal of Materials in Civil Engineering*, *18*(6), 759–767.

Hicks, R. G. (1991). *Moisture Damage in Asphalt Concrete: Synthesis of Highway Practice* (NCHRP Repo). Washington, DC: Transportation Research Board, National Research Council.

Holzfeind, J., & Hummitsch, R. (2008). Qualitätsverhalten von Gleisen [Quality behaviour of the track]. *ZEV Rail Glasers Annalen*, *132*(6–7), 212–224.

Homsi, F. (2011). *Endommagement des enrobés bitumineux sous chargements multiessieux [Damaging of bituminous mixtures under multi-axle loading]*. PhD Thesis, Ecole Centrale de Nantes.

Hopman, P. C., Kunst, P. A. J., & Pronk, A. (1989). A renewed intepretation method for fatigue measurements: verification of Miner's rule. In *Proceedings of the 4th Eurobitume Symposium* (pp. 557–561). Madrid, Spain.

Houston, W. N., Mirza, M. W., Zapata, C. E., & Raghavendra, S. (2005). *Environmental Effects in Pavement Mix and Structural Design Systems*. (N. C. H. R. Program, Ed.) (Part 1 of). Washington, DC: Transportation Research Board.

Huang, Y., Lin, C., & Rose, J. G. (1984). Huang et al - 1984 - Asphalt pavement Design Highway Vs Railroad.pdf. *Journal of Transportation Engineering*, *110*(2), 276–282.

Huang, Y., Rose, J. G., & Khoury, C. J. (1987). Thickness design for hot mix asphalt railroad trackbeds. *Proceedings of the Association of Asphalt Paving Technologists*, *56*(87), 427–453.

Huet, C. (1963). *Étude par une méthode d'impédance du comportement viscoélastique des matériaux hydrocarbonés [Study of viscoelastic behavior of hydrocarbon-treated materials by means of an impedance method]*. University of Paris.

Hughes, C. S. (1989). *Compaction of asphalt pavement*. (N. R. C. (U. S.). T. Research, Ed.)*NCHRP Synthesis of Highway Practice*. Transportation Research Board, National Research Council.

Hunter, A. E., McGreavy, L., & Airey, G. D. (2009). Effect of Compaction Mode on the Mechanical Performance and Variability of Asphalt Mixtures. *Journal of Transportation Engineering*, *135*(11), 839–851. http://doi.org/10.1061/(ASCE)0733-947X(2009)135:11(839)

IFSTTAR. (2016a). Catalogue des matériels MLPC® de laboratoire pour enrobés - BBPAC [Materials catalogue MLPC pour laboratory of bituminous mixtures]. Retrieved April 1, 2016, from http://www.ifsttar.fr/partenariat-innovation/nos-technologies-industrielles/materiels/catalogue-des-materiels-mlpcr-de-laboratoire-pour-enrobes/produit/bbpac/

IFSTTAR. (2016b). Catalogue des matériels MLPC® de laboratoire pour enrobés - PCG3 [Materials catalogue MLPC pour laboratory of bituminous mixtures]. Retrieved April 1, 2016, from http://www.ifsttar.fr/partenariat-innovation/nos-technologies-industrielles/materiels/catalogue-des-materiels-mlpcr-de-laboratoire-pour-enrobes/produit/pcg_3/

International Union of Railways. (2008). *Best practice guide for optimum track geometry durability*. (Editions Techniques Ferroviaires, Ed.). Paris, France.

Jaeger, H. M., & Nagel, S. R. (1992). Physics of the Granular State. *Science*, *255*(5051), 1523–1531. http://doi.org/10.1126/science.255.5051.1523

Jasso, M., Hampl, R., Vacin, O., Bakos, D., Stastna, J., & Zanzotto, L. (2015). Rheology of conventional asphalt modified with SBS, Elvaloy and polyphosphoric acid. *Fuel*

Processing Technology, *140*, 172–179. http://doi.org/10.1016/j.fuproc.2015.09.002

Jimenez, R. A. (1974). *Testing for Debonding of Asphalt from Aggregates*. *Transportation Research Record*. Washington, DC: Transportation Research Board.

Kanitpong, K., & Bahia, H. U. (2008). Evaluation of HMA moisture damage in Wisconsin as it relates to pavement performance. *International Journal of Pavement Engineering*, *9*(1), 9–17. http://doi.org/10.1080/10298430600965122

Kassem, E. A.-R. A. (2008). *Compaction Effects on Uniformity, Moisture Diffusion, and Mechanical Properties of Asphalt Pavements*. PhD Thesis, Texas A&M University. Retrieved from http://oaktrust.library.tamu.edu/handle/1969.1/ETD-TAMU-2008-12-242

Khalid, H. A. (2002). A new approach for the accelerated ageing of porous asphalt mixtures. *Proceedings of the ICE - Transport*, *153*(3), 171–181. http://doi.org/10.1680/tran.2002.153.3.171

Khan, R., Grenfell, J., Collop, A., Airey, G. D., & Gregory, H. (2013). Moisture damage in asphalt mixtures using the modified SATS test and image analysis. *Construction and Building Materials*, *43*, 165–173.

Kiggundu, B. M., & Roberts, F. L. (1988). *Stripping in HMA Mixtures: State-of-the-art and critical review of test methods*. Auburn, AL.

Kim, D., & Park, S. (2011). Relationship between the subgrade reaction modulus and the strain modulus obtained using a plate loading test. In *9th World Congress on Railway Research* (p. 11). Lille, France.

Kim, O. K., Bell, C. A., Wilson, J. E., & Boyle, G. (1986). Effect of moisture and aging on asphalt pavement life - Part 2: Effect of aging. Washington, DC: Oregon Department of Transportation - Federal Highway Administration.

Kim, Y.-R., Lee, H. J., & Little, D. N. (1997). Fatigue Characterization of Asphalt Concrete Using Viscoelasticity and Continuum Damage Theory. *Journal of the Association of Asphalt Paving Technologists*, *66*.

Kim, Y.-R., Little, D. N., & Lytton, R. L. (2003). Fatigue and Healing Characterization of Asphalt Mixtures. *Journal of Materials in Civil Engineering*, *15*(1), 75–83. http://doi.org/10.1061/(ASCE)0899-1561(2003)15:1(75)

Kim, Y.-R., Little, D., & Song, I. (2003). Effect of Mineral Fillers on Fatigue Resistance and Fundamental Material Characteristics: Mechanistic Evaluation. *Transportation Research Record: Journal of the Transportation Research Board*, *1832*, 1–8. http://doi.org/10.3141/1832-01

Kose, S., Guler, M., Bahia, H., & Masad, E. (2000). Distribution of Strains Within Hot-Mix Asphalt Binders: Applying Imaging and Finite-Element Techniques. *Transportation Research Record: Journal of the Transportation Research Board*, *1728*, 21–27. http://doi.org/10.3141/1728-04

Kringos, N., Azari, H., & Scarpas, A. (2009). Identification of parameters related to moisture conditioning that cause variability in Modified Lottman Test. *Transportation Research Record : Journal of the Transportation Research Board*, (2127), 1–11.

Krishnan, J. M., & Lakshmana Rao, C. (2001). Permeability and bleeding of asphalt concrete

using mixture theory. *International Journal of Engineering Science*, (39), 611–627. http://doi.org/10.1016/S0020-7225(00)00064-1

Kumar, A., & Goetz, W. H. (1977). Asphalt hardening as affected by film thickness, voids and permeability in asphaltic mixtures. In *Proceedings of the Association of Asphalt Paving Technologists* (Vol. 46, pp. 571–605). San Antonio, TX.

Labout, J. W. (1950). *The properties of asphaltic bitumen: with reference to its technical applications*. (J. P. Pfeiffer, Ed.). book, New York: Elsevier.

Lackner, R., Spiegl, M., Blab, R., & Eberhardsteiner, J. (2005). Is Low-Temperature Creep of Asphalt Mastic Independent of Filler Shape and Mineralogy?—Arguments from Multiscale Analysis. *Journal of Materials in Civil Engineering*, *17*(5), 485–491. http://doi.org/10.1061/(ASCE)0899-1561(2005)17:5(485)

Lakes, R. (2009). *Viscoelastic Materials*. Cambridge: Cambridge University Press. http://doi.org/10.1017/CBO9780511626722

Lamas-Lopez, F. (2016). *Etude 'in-situ' et en laboratoire sur le comportement dynamique des matériaux constitutifs des plateformes ferroviaires classiques dans le contexte d'augmentation du trafic [Field and laboratory investigation on the dynamic behaviour of conventional railw*. PhD thesis, Paris Est University - Ecole Nationale des Ponts et Chaussées.

Lamas-Lopez, F., Alves Fernandes, V., Cui, Y. J., Aguiar, S. C. D., Calon, N., Canou, J., … Robinet, A. (2014). Assessment of the double integration method using accelerometers data for conventional railway platforms. In *The Second International Conference on Railway Technology: Research, Development and Maintenance* (p. 19). Ajaccio, France: Civil-Comp Press.

Lamas-Lopez, F., Cui, Y. J., Dupla, J. C., Canou, J., Tang, A. M., Costa d'Aguiar, S., … Robinet, A. (2014). Effect of increasing the load frequency on materials from conventional railways platforms. In *International Conference on Railway Technology : Research, Development and Maintenance* (p. 20). Ajaccio, France: Civil-Comp Press.

Lamothe, S. (2014). *Endommagement d'un enrobé bitumineux partiellement saturé en eau ou en saumure soumis à des sollicitations cycliques de gel-dégel et mécaniques*. PhD Thesis, ENTPE/University of Lyon.

Laurens, P. E. (2014). Prise en compte de la raideur de la voie dans la compréhension des mécanismes de dégradation du nivellement [Taking into account the track stiffness in the understanding of the vertical level degradation mechanisms]. In *Proceedings of the 2nd international symposium on railway geotechnical engineering - Georail 2014* (pp. 99–108). Marne la Vallée, France: IFSTTAR.

LC 25-005. Recouvrance d'élasticité (2004). Ministère des Transports du Québec.

LC 25-009. Evaluation de la résistance d'un liant bitumineux au désenrobage en focntion d'une source granulaire donnée (2009). Ministère des Transports du Québec.

Lesueur, D., Petit, J., & Ritter, H.-J. (2013). The mechanisms of hydrated lime modification of asphalt mixtures: a state-of-the-art review. *Road Materials and Pavement Design*, *14*(1), 1–16. http://doi.org/10.1080/14680629.2012.743669

Li, Q., Lee, H. J., & Kim, T. (2011). A simple fatigue performance model of asphalt mixtures

based on fracture energy. *Construction and Building Materials*, 7.

Lira, B., Jelagin, D., & Birgisson, B. (2013). Gradation-based framework for asphalt mixture. *Materials and Structures*, *46*(8), 1401–1414. http://doi.org/10.1617/s11527-012-9982-3

Little, D. N., & Jones, D. R. I. (2003). Chemical and mechanical processes of moisture damage in Hot-Mix Asphalt pavements. In *Moisture Sensitivity of Asphalt Pavements: A National Seminar* (pp. 37–70). Washington, DC: Transportation Research Board.

Little, D. N., & Petersen, J. C. (2005). Unique Effects of Hydrated Lime Filler on the Performance-Related Properties of Asphalt Cements: Physical and Chemical Interactions Revisited. *Journal of Materials in Civil Engineering*, *17*(2), 207–218. http://doi.org/10.1061/(ASCE)0899-1561(2005)17:2(207)

Lottman, R. P. (1978). *Predicting Moisture-Induced Damage to Asphaltic Concrete*. *NCHRP Report*. Washington, DC: Transportation Research Board.

Lytton, R. L., Masad, E., Zollinger, C., Bulut, R., & Little, D. (2005). *Measurements of Surface Energy and Its Relationship to Moisture Damage* (Report 0-4). College Station, TX: Texas Transportation Institute.

Majidzadeh, K., & Brovold, F. N. (1968). *State of the art: effect of water on bitumen-aggregate mixtures* (Special Re). Washington, DC: Highway Research Board, National Research Council.

Mallick, R. B., Cooley, L. A., Teto, M. R., Bradbury, R. L., & Peabody, D. (2003). *An evaluation of factors affecting permeability of Superpave designed pavements*. Auburn, AL.

Mangiafico, S. (2014). *Linear viscoelastic properties and fatigue of bituminous mixtures produced with Reclaimed Asphalt Pavement and corresponding binder blends*. PhD Thesis, ENTPE/University of Lyon.

Mangiafico, S., Di Benedetto, H., Sauzéat, C., Olard, F., Pouget, S., & Planque, L. (2014). New method to obtain viscoelastic properties of bitumen blends from pure and reclaimed asphalt pavement binder constituents. *Road Materials and Pavement Design*, *15*(2), 312–329. http://doi.org/10.1080/14680629.2013.870639

Marmier, F. (2005). Colas innove sur la LGV Est européenne en testant une grave-bitume sous ballast [Colas innovates at the East European HSL by testing a bituminous sub-ballast layer]. *Revue Générale Des Routes et de L'aménagement (RGRA) - Vol. 840*, 20–22.

Masad, E., Castelblanco, A., & Birgisson, B. (2006). Effects of Air Void Size Distribution, Pore Pressure, and Bond Energy on Moisture Damage. *Journal of Testing and Evaluation*, *34*(1), 9. JOUR.

Masad, E., Jandhyala, V. K., Dasgupta, N., Somadevan, N., & Shashidhar, N. (2002). Characterization of Air Void Distribution in Asphalt Mixes using X-ray Computed Tomography. *Journal of Materials in Civil Engineering*, *14*(2), 122–129.

Masad, E., Muhunthan, B., Shashidhar, N., & Harman, T. (1999). Internal Structure Characterization of Asphalt Concrete Using Image Analysis. *Journal of Computing in Civil Engineering*, *13*(2), 88–95. http://doi.org/10.1061/(ASCE)0887-3801(1999)13:2(88)

Mauduit, C., Hammoum, F., Piau, J.-M., Mauduit, V., Ludwig, S., & Hamon, D. (2010). Quantifying Expansion Effects Induced by Freeze-Thaw Cycles in Partially Water

Saturated Bituminous Mix. *Road Materials and Pavement Design*, *11*(sup1), 443–457. http://doi.org/10.1080/14680629.2010.9690341

Mehrara, A., & Khodaii, A. (2013). A review of state of the art on stripping phenomenon in asphalt concrete. *Construction and Building Materials*, *38*(424), 423–442. http://doi.org/10.1016/j.conbuildmat.2012.08.033

Miner, M. A. (1945). Cumulative damage in fatigue. *Journal of Applied Mechanics*, *67*, 159–164.

Momoya, Y. (2007). New Railway Roadbed Design. *Railway Technology Avalanche, Newsletter from the Railway Technical Research Institute No. 20*, (20), 118.

Momoya, Y., Horike, T., & Ando, K. (2002). Development of solid bed track on asphalt pavement. *Quarterly Report of RTRI*, *43*(3), 113–118.

Monismith, C. L. (1992). Analytically based asphalt pavement design and rehabiliation: Theory to practice, 1962-1992. *Transportation Research Record*, (1354). Retrieved from http://trid.trb.org/view.aspx?id=370833

Mounier, D., Di Benedetto, H., & Sauzéat, C. (2012). Determination of bituminous mixtures linear properties using ultrasonic wave propagation. *Construction and Building Materials*, *36*, 638–647. http://doi.org/10.1016/j.conbuildmat.2012.04.136

Moutier, F. (1991). *Étude statistique de l'effet de la composition des enrobés bitumineux sur leur comportement en fatigue et leur module complexe [Statistical study of the effect of bituminous mixture composition on their fatigue behavior and complex modulus]*. *Bulletin des Laboratoires des Ponts et Chaussées*. Marne la Vallée, France.

Nadkarni, A., Kaloush, K., Zeiada, W., & Biligiri, K. P. (2009). Using Dynamic Modulus Test to evaluate moisture susceptibility of asphalt mixtures. *Transportation Research Record : Journal of the Transportation Research Board*, (2127), 29–35.

NF P98-231-2. Tests relating to pavements. Compaction tests on non-bituminous materials. Part 2 : compactibility using the gyratory testing machine. - Essais relatifs aux chaussées (1992). AFNOR - French Standard.

Nguyen, H. M. (2010). *Comportement cyclique et déformations permanentes des enrobés bitumineux [Cyclic behaviour and permanent deformation of bituminous mixtures]*. PhD Thesis, ENTPE/University of Lyon.

Nguyen, Q. T. (2011). *Comportement thermomécanique des enrobés bitumineux sous sollicitations cycliques dans les domaines linéaire et non-linéaire [Thermomechanical behavior of bituminous mixtures under cyclic loading in the linear and non-linear domains]*. PhD Thesis, ENTPE/University of Lyon.

Nguyen, Q. T., Di Benedetto, H., & Sauzéat, C. (2012). Determination of thermal properties of asphalt mixtures as another output from cyclic tension-compression test. *Road Materials and Pavement Design*, *13*(1), 85–103. http://doi.org/10.1080/14680629.2011.644082

Nguyen, Q. T., Di Benedetto, H., & Sauzéat, C. (2015). Linear and nonlinear viscoelastic behaviour of bituminous mixtures. *Materials and Structures*, *48*(7), 2339–2351. http://doi.org/10.1617/s11527-014-0316-5

Nguyen, Q. T., Di Benedetto, H., Sauzéat, C., & Tapsoba, N. (2013). Time Temperature

Superposition Principle Validation for Bituminous Mixes in the Linear and Nonlinear Domains. *Journal of Materials in Civil Engineering*, *25*(9), 1181–1188. http://doi.org/10.1061/(ASCE)MT.1943-5533.0000658

Nijboer, L. W. (1948). *Plasticity as a factor in the design of dense bituminous road carpets*. New York, NY: Elsevier.

Olard, F. (2003). *Comportement thermomécanique des enrobés bitumineux à basses temperatures: Relations entre les propriétés du liant et de l'enrobé [Thermomechanical behavior of bituminous mixtures at low temperatures: Relations between binder and mixture properties]*. PhD Thesis, ENTPE/INSA Lyon.

Olard, F. (2012). GB5 mix design: high-performance and cost-effective asphalt concretes by use of gap-graded curves and SBS modified bitumens. *Road Materials and Pavement Design*, *13*(sup1), 234–259. http://doi.org/10.1080/14680629.2012.657074

Olard, F., & Di Benedetto, H. (2003). General "2S2P1D" Model and Relation Between the Linear Viscoelastic Behaviours of Bituminous Binders and Mixes. *Road Materials and Pavement Design*, *4*(2), 185–224. http://doi.org/10.1080/14680629.2003.9689946

Olard, F., Di Benedetto, H., Dony, A., & Vaniscote, J.-C. (2005). Properties of bituminous mixtures at low temperatures and relations with binder characteristics. *Materials and Structures*, *38*(1), 121–126. http://doi.org/10.1007/BF02480584

Oldyrev, P. P. (1971). Self-heating and failure of plastics under cyclic loading. *Polymer Mechanics*, *3*(3), 322–328. http://doi.org/10.1007/BF00858775

Partl, M. N., Flisch, A., & Jönsson, M. (2007). Comparison of Laboratory Compaction Methods using X-ray Computer Tomography. *Road Materials and Pavement Design*, *8*(2), 139–164. http://doi.org/10.1080/14680629.2007.9690071

Partl, M. N., Pasquini, E., Canestrari, F., & Virgili, A. (2010). Analysis of water and thermal sensitivity of open graded asphalt rubber mixtures. *Construction and Building Materials*, *24*(3), 283–291. http://doi.org/10.1016/j.conbuildmat.2009.08.041

Petersen, D., Link, R., Lundström, R., Ekblad, J., & Isacsson, U. (2004). Influence of Hysteretic Heating on Asphalt Fatigue Characterization. *Journal of Testing and Evaluation*, *32*(6), 12284. http://doi.org/10.1520/JTE12284

Petersen, J. C. (1993). Asphalt oxidation – an overview including a new model for oxidation proposing that physicochemical factors dominate the oxidation kinematics. *Fuel Science and Technology International*, *11*(1), 57–87. http://doi.org/10.1080/08843759308916058

Pham, N. H., Sauzéat, C., Di Benedetto, H., González-León, J.-A., Barreto, G., Nicolaï, A., & Jakubowski, M. (2015). Reclaimed asphalt pavement and additives' influence on 3D linear behaviour of warm mix asphalts. *Road Materials and Pavement Design*, *16*(3), 569–591. http://doi.org/10.1080/14680629.2015.1021108

Phan, C. V., Di Benedetto, H., Sauzéat, C., & Lesueur, D. (2016). Influence of Hydrated Lime on Linear Viscoelastic Properties of Bituminous Mixtures (pp. 667–680). Springer Netherlands. http://doi.org/10.1007/978-94-017-7342-3_54

Piau, J.-M. (1989). Modélisation thermomécanique du comportement des enrobés bitumineux [Thermomechanical modelling of the behaviour of bituminous mixtures].

Bulletin de Liaison Des Laboratoires Des Ponts et Chaussees, (163), 41–54.

Prowell, B. D., & Brown, E. R. (2006). *Appendixes to NCHRP Report 573: Superpave Mix Design : Verifying Gyration Levels in the Ndesign Table - NCHRP Project 9-9(1)*. Washington DC, Etats Unis. Retrieved from http://onlinepubs.trb.org/onlinepubs/nchrp/nchrp_w96.pdf

Prowell, B. D., Brown, E. R., Anderson, R. M., Daniel, J. S., Swamy, A. K., Von Quintus, H., … Maghsoodloo, S. (2010). *Validating the fatigue endurance limit for hot mix asphalt*. *NCHRP Report*. Transportation Research Board.

Rail.One GmbH. (2012). GETRAC(R) Ballastless track system. Retrieved April 8, 2016, from http://www.railone.de/fileadmin/daten/05-presse-medien/downloads/broschueren/en/Getrac_EN2012_ebook.pdf

Raithby, K. D., & Sterling, A. B. (1972). Some effects of loading history on the fatigue performance of rolled asphalt.

Ramirez Cardona, D. A., Benkahla, J., Costa d'Aguiar, S., Calon, N., Robinet, A., Di Benedetto, H., & Sauzeat, C. (2014). High-speed ballasted track behavior with sub-ballast bituminous layer. In *Proceedings of the 2nd international symposium on railway geotechnical engineering - Georail 2014* (pp. 139–148). Marne la Vallée, France.

Ramirez Cardona, D. A., Di Benedetto, H., Sauzeat, C., Calon, N., & Saussine, G. (2016). Use of a bituminous mixture layer in high-speed line trackbeds. *Construction and Building Materials*, *125*, 398–407. http://doi.org/10.1016/j.conbuildmat.2016.07.118

Ramirez Cardona, D. A., Pouget, S., Di Benedetto, H., & Olard, F. (2015). Viscoelastic Behaviour Characterization of a Gap-graded Asphalt Mixture with SBS Polymer Modified Bitumen. *Materials Research*, *18*(2), 373–381. http://doi.org/10.1590/1516-1439.332214

Rayner, C., & Rowe, G. M. (2004). Properties of mastics using different fillers with both unmodified and EVA-modified binders. In *Proceedings of the 3rd Eurasphalt and Eurobitume Congress* (pp. 861–870). Vienna, Austria: Foundation Eurasphalt.

Read, J., & Whiteoak, D. (2003). *The Shell bitumen handbook*. (Shell Bitumen, Ed.) (5th ed.). London, UK: Thomas Telford.

Roberts, F. L., Kandhal, P. S., Brown, E. R., Lee, D.-Y., & Kennedy, T. W. (1996). *Hot mix asphalt materials, mixture design and construction*. (National Asphalt Pavement Association Research and Education Foundation, Ed.) (2nd ed.). Lanham, MD, USA.

Robinet, A., & Cuccaroni, A. (2012). L'expérience grave-bitume de la LGV Est Européenne [The bituminous mixture experience of the East European HSL]. *Revue Générale Des Chemins de Fer (RGCF), Vol. 220*, 44–50.

Romero, P., & Masad, E. (2001). Relationship between the Representative Volume Element and Mechanical Properties of Asphalt Concrete. *Journal of Materials in Civil Engineering*, *13*(1), 77–84. http://doi.org/10.1061/(ASCE)0899-1561(2001)13:1(77)

Roque, R., Birgisson, B., Kim, S., & Guarin, A. (2006). *Development of Mix Design Guidelines for Improved Performance of Asphalt Mixtures*. Tallahassee, FL.

Rose, J. G., & Bryson, L. S. (2009). Hot mix asphalt railway trackbeds: Trackbed materials, performance evaluations ans significant implications. In *International Conference on*

Perpetual Pavements (Vol. 7326, p. 19). Lexington, Kentucky, Etats Unis.

Rose, J. G., Li, D., & Walker, L. (2002). Test measurements and performance evaluations of in-Service railway asphalt trackbeds. In *Proceedings of the AREMA 2002 annual Conference* (p. 30). Washington, DC.

Rose, J. G., & Souleyrette, R. R. (2015). Asphalt Railway Trackbeds : Recent Designs , Applications and Performances. In A. R. E. and M.-W. Association (Ed.), *Proceedings of the 2015 AREMA annual Conference*. Minneapolis, MN.

Rose, J. G., Teixeira, P. F., & Veit, P. (2011). International design practices, applications and performances of asphalt/bituminous railway trackbeds. In *Proceedings of the 1st international symposium on railway geotechnical engineering - Georail 2011*. Paris, France.

Said, S. (1988). Fatigue characteristics of asphalt concrete mixtures. *Swedish National Road and Transport Research Institute: VTI Meddelande*, (583A), 68.

Salençon, J. (2009). *Viscoélasticité pour le calcul des structures [Viscoelasticity for structural dimensioning]*. (Les Editions de l'Ecole Polytechnique, Ed.). Paris, France.

Santamarina, C., Klein, K. A., & Fam, M. A. (2001). *Soils and waves: particulate materials behavior, chracterization and process monitoring*. New York, NY: Wiley.

Sauzeat, C. (2003). *Comportement du sable dans le domaine des petites et moyennes déformations : rotations "d'axes" et effets visqueux [Behavior of sand in the small and medium strain domains: rotation of axes and viscous effects]*. PhD Thesis, ENTPE/INSA Lyon.

Sayegh, G. (1965). *Variations des modules de quelques bitumes purs et enrobés bitumineux [Modulus variations of some pure bitumens and bituminous mixtures]*. University of Paris.

Selig, E. T., & Waters, J. M. (1994). *Track Geotechnology and Substructure Management*. London, UK: Thomas Telford.

Sengoz, B., & Agar, E. (2007). Effect of asphalt film thickness on the moisture sensitivity characteristics of hot-mix asphalt. *Building and Environment*, *42*(10), 3621–3628. http://doi.org/10.1016/j.buildenv.2006.10.006

Shashidhar, N., & Romero, P. (1998). Factors Affecting the Stiffening Potential of Mineral Fillers. *Transportation Research Record: Journal of the Transportation Research Board*, *1638*, 94–100. http://doi.org/10.3141/1638-11

Soenen, H., de La Roche, C., & Redelius, P. (2003). Fatigue Behaviour of Bituminous Materials: From Binders to Mixes. *Road Materials and Pavement Design*, *4*(1), 7–27. http://doi.org/10.1080/14680629.2003.9689938

Soenen, H., & Teugels, W. (1999). Rheological investigation on binder-filler interactions. In *Eurobitume Workshop on Performance Related Properties for Bituminous Binders*. Luxembourg.

Sohm, J. (2013). *Prédiction des déformations permanentes des matériaux bitumineux.* PhD Thesis, Ecole Centrale de Nantes.

Solaimanian, M., Harvey, J., Tahmoressi, M., & Tandon, V. (2004). Test Methods to Predict

Moisture Sensitivity of Hot-Mix Asphalt Pavements. In *Moisture Sensitivity of Asphalt Pavements CD-ROM* (pp. 77–110). Washington DC, Etats Unis: Transportation Research Board, National Research Council.

Solaimanian, M., Kennedy, T., & Elmore, W. (1993). *Long-term evaluation of stripping and moisture damage in asphalt pavements treated with lime and antistripping agents*. Austin, TX.

Soltani, A., & Anderson, D. A. (2005). New Test Protocol to Measure Fatigue Damage in Asphalt Mixtures. *Road Materials and Pavement Design*, *6*(4), 485–514. http://doi.org/10.1080/14680629.2005.9690017

Sousa, J. B., Deacon, J. A., & Monismith, C. L. (1991). Effect of laboratory compaction method on permanent deformation characteristics of asphalt-aggregate mixtures. *Journal of the Association of Asphalt Paving Technologists*, *60*, 533–585.

Stastna, J., Zanzotto, L., & Vacin, O. J. (2003). Viscosity function in polymer-modified asphalts. *Journal of Colloid and Interface Science*, *259*(1), 200–207. http://doi.org/10.1016/S0021-9797(02)00197-2

Stuart, K. D. (1990). *Moisture Damage in Aspha t Mixtures*--. McLean, VA.

Tan, S.-A., & Fwa, T.-F. (1991). Influence of Voids on Density Measurements of Granular Materials Using Gamma Radiation Techniques. *Geotechnical Testing Journal*, *14*(3), 257–265. http://doi.org/10.1520/GTJ10570J

Tapsoba, N. (2012). *Comportement des enrobés bitumineux à base de matériaux recyclés et / ou fabriqués à température réduite*. PhD Thesis, ENTPE/University of Lyon.

Tapsoba, N., Sauzéat, C., & Di Benedetto, H. (2013). Analysis of Fatigue Test for Bituminous Mixtures. *Journal of Materials in Civil Engineering*, *25*(6), 701–710. http://doi.org/10.1061/(ASCE)MT.1943-5533.0000636

Tashman, L., Masad, E., D'Angelo, J., Bukowski, J., & Harman, T. (2002). X-ray Tomography to Characterize Air Void Distribution in Superpave Gyratory Compacted Specimens. *International Journal of Pavement Engineering*, *3*(1), 19–28. JOUR. http://doi.org/10.1080/10298430290029902a

Teixeira, P. F., López Pita, A., & Ferreira, P. a. (2010). New possibilities to reduce track costs on high-speed lines using a bituminous sub-ballast layer. *International Journal of Pavement Engineering*, *11*(4), 301–307. http://doi.org/10.1080/10298431003749733

Teixeira, P. F., Lopez-Pita, A., Casas, C., Bachiller, A., & Robuste, F. (2006). Improvements in high-speed ballasted track design : Benefits of bituminous subballast layers. *Journal of the Transportation Research Board*, (1943), 43–49. Retrieved from http://cat.inist.fr/?aModele=afficheN&cpsidt=18111911

Terrel, R. L., & Al-Swailmi, S. (1993). The role of pessimum voids concept in understanding moisture damage to asphalt concrete mixtures. *Transportation Research Record*, (1386).

Terrel, R. L., & Shute, J. W. (1989). *Summary Report on Water Sensitivity* (SHRP-A/IR-). Washington, DC: Strategic Highway Research Program.

Traxler, R. N. (1961). *Asphalt: its composition, properties and uses*. New York: Reinhold.

Trinh, V.-N. (2011). *Comportement hydromécanique des matériaux constitutifs de plateformes ferroviaires anciennes*. PhD Thesis, Paris-Est University.

University of Minho. (2009). Highways Research Group. Retrieved March 10, 2016, from http://www.civil.uminho.pt/highways/laboratory.htm

Vavrik, W. R., Pine, W. J., Huber, G., Carpenter, S. H., & Bailey, R. (2001). The Bailey method of gradation evaluation: the influence of aggregate gradation and packing characteristics on voids in the mineral aggregate. *Journal of the Association of Asphalt Paving Technologists*, *70*, 132–175.

Von Quintus, H., Scherocman, J., & Hughes, C. (1989). Asphalt-Aggregate Mixtures Analysis System: Philosophy of the Concept. In *Asphalt Concrete Mix Design: Development of More Rational Approaches* (pp. 15-15–24). 100 Barr Harbor Drive, PO Box C700, West Conshohocken, PA 19428-2959: ASTM International. http://doi.org/10.1520/STP20067S

Walubita, L. F., Jamison, B., Alvarez, A. E., Hu, X., & Mushota, C. (2012). Air void characterisation of HMA gyratory laboratory-moulded samples and field cores using X-ray computed tomography (X-ray CT). *Journal of the South African Institution of Civil Engineering*, *54*(1), 22–30.

Williams, M. L., Landel, R. F., & Ferry, J. D. (1955). The Temperature Dependence of Relaxation Mechanisms in Amorphous Polymers and Other Glass-forming Liquids. *Journal of the American Chemical Society*, *77*(14), 3701–3707. http://doi.org/10.1021/ja01619a008

Wöhler, A. (1870). *Über die Festigkeitsversuche mit Eisen und Stahl [On the strength tests with iron and steel]*. Berlin: Ernst & Korn.

Wong, W. G., Han, H. F., He, G. P., Qiu, X., Wang, K. C. P., & Lu, W. (2004). Effects of water on permanent deformation potential of asphalt concrete mixtures. *Materials and Structures*, *37*(October), 532–538.

World Road Association. (2007). Road Dictionary. Retrieved March 7, 2016, from http://www.piarc.org/en/Terminology-Dictionaries-Road-Transport-Roads/

Xiaohu, L., Talon, Y., & Redelius, P. (2008). Ageing of bituminous binders - laboratory tests and field data. In *Proceedings of the 4th eurasphalt and eurobitume congress*. Copenhagen, Denmark: European Asphalt Pavement Association (EAPA).

Yusoff, N. I., Mounier, D., Marc-Stéphane, G., Rosli Hainin, M., Airey, G. D., & Di Benedetto, H. (2013). Modelling the rheological properties of bituminous binders using the 2S2P1D Model. *Construction and Building Materials*, *38*, 395–406. http://doi.org/10.1016/j.conbuildmat.2012.08.038

Zanzotto, L., Stastna, J., & Vacin, O. (2000). Thermomechanical properties of several polymer modified asphalts. *Applied Rheology*, *10*(4), 185–191.

Zhao, Y., Ni, Y., & Zeng, W. (2014). A consistent approach for characterising asphalt concrete based on generalised Maxwell or Kelvin model. *Road Materials and Pavement Design*, *15*(3), 674–690. http://doi.org/10.1080/14680629.2014.889030

Appendix

Appendix I

Modelling of the LVE behaviour of bituminous mixtures

A brief overview of different existing models is proposed in this section.

- **Models with discrete relaxation spectrum**

The principal models with discrete relaxation spectrum are summarized in Table A- I.

Table A- I. Principal models with discrete relaxation spectrum (adapted from (Tapsoba, 2012))

Name	Schematic representation	Creep (J) and relaxation (R) functions	Complex modulus equation
Spring		$J(t) = 1/E$ $R(t) = E$	$E^* = E = \sigma/\varepsilon$
Dashpot	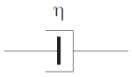	$J(t) = t/\eta$ $R(t) = \eta\delta(t)$	$E^* = j\omega\eta$
Maxwell		$J(t) = 1/E + t/\eta$ $R(t) = Ee^{-t/\tau}$ where $\tau = \eta/E$	$E^*(\omega) = E\frac{j\omega\tau}{1+j\omega\tau}$
Kelvin-Voigt	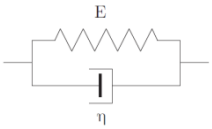	$J(t) = \frac{1}{E}\left(1 - e^{-t/\tau}\right)$ $R(t) = E + \eta\delta$	$E^*(\omega) = E + j\omega\eta$
Burgers	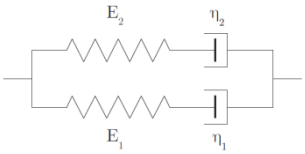	$R(t) = E_1 e^{\frac{-t}{\tau_1}} + E_2 e^{\frac{-t}{\tau_2}}$ where $\tau_i = \eta_i/E_i$	$E^*(\omega) = \frac{E_1}{1+j\omega\tau_1^{-1}} + \frac{E_2}{1+j\omega\tau_2^{-1}}$
Generalized Maxwell	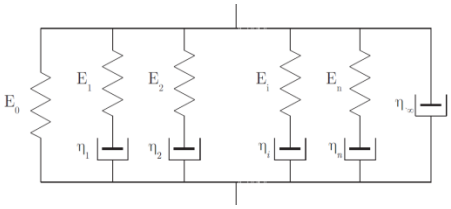	$R(t) = E_0 + \eta_\infty\delta + \sum_{i=1}^{n} E_i e^{\frac{-t}{\tau_i}}$	$E^*(\omega) = E_0 + j\omega\eta_{E_\infty} + \sum_{i=1}^{n} E_i \frac{j\omega\tau_i}{1+j\omega\tau_i}$
Generalized Kelvin-Voigt	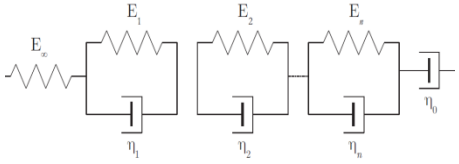	$J(t) = \frac{1}{E_\infty} + \frac{t}{\eta_0} + \sum_{i=1}^{n} \frac{1}{E_i}\left(1 - e^{\frac{-t}{\tau_i}}\right)$	$E^*(\omega) = \left(\frac{1}{E_\infty} + \frac{1}{j\omega\eta_0} + \sum_{i=1}^{n} \frac{1}{E_i + j\omega\eta_i}\right)^{-1}$

The Maxwell and the Kelvin-Voigt models alone fail in adequately describing the LVE behaviour of bituminous materials but are the base elements of more complex assemblies, such as the Burgers model, which consists of two Maxwell elements in parallel. However, Burgers model fails in describing the LVE behaviour of bituminous materials over the entire domain of frequency and temperature. The generalized Maxwell model, consisting of several Maxwell elements in parallel with, eventually, an isolated spring and an isolated dashpot, can provide a good approximation of the LVE behaviour of bituminous materials if enough elements are used. In fact, when the number of elements tends to infinite, the relaxation function tends to a continuous function which simulates better the LVE behaviour than discrete ones. The same is observed for the generalized Kelvin-Voigt model. However, the downside of these generalized models is that increasing the number of elements also increases the calculation time and efforts.

- **Models with a continuous spectrum**

Analogical models with continuous spectrum are those who can be represented by an assembly of infinite Maxwell or Kelvin-Voigt elements. They all have finite number of elements including at least one so-called "parabolic element". The parabolic element has a continuous creep function:

$$J(t) = a\left(\frac{t}{\tau}\right)^h$$

$$\text{so that } \tau(T) = \tau_0 a_T(T) \qquad \text{[A-1]}$$

where a is a dimensionless constant, h is a number between 0 and 1 and τ the characteristic time which depends in the temperature (T) and validates the TTSP

The Huet model (Huet, 1963) is an assembly of a spring and two parabolic elements of parameters h and k. It takes into account the maximum asymptotic stiffness value of bituminous materials at high frequencies and/or low temperatures (E_0). Nevertheless, the Huet model does not take into account the minimum asymptotic stiffness value of bituminous mixtures at low frequencies and/or high temperatures (E_{00}), which is provided by the granular skeleton of the mixture. The Huet-Sayegh model (Sayegh, 1965) corrected this drawback by adding an additional spring assembled in parallel as seen in Table A- II. However, for bitumen, the Huet-Sayegh model describes its behaviour at very low frequencies and/or high temperatures with a parabolic element whereas for these conditions bitumen behaves like a Newtonian fluid, which is better represented by a dashpot. This correction was integrated in the 2S2P1D (2 Springs, 2 Parabolic elements & 1 Dashpot) model (Olard & Di Benedetto, 2003; Olard, 2003) by integrating a dashpot to the Huet element.

Table A- II. Principal models with continuous relaxation spectrum (adapted from (Tapsoba, 2012))

Name	Schematic representation	Complex modulus equation
Parabolic element	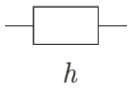	$E^*(j\omega\tau) = \frac{j\omega\tau^h}{a\Gamma(h+1)}$ $\Gamma(n) = \int_0^\infty x^{n-1}e^{-x}dx$ with $n > 0$
Huet	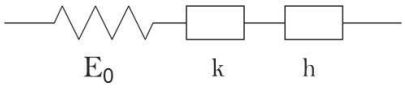	$E^*(\omega) = \frac{E_0}{1+\delta(j\omega\tau)^{-k}+(j\omega\tau)^{-h}}$
Huet-Sayegh	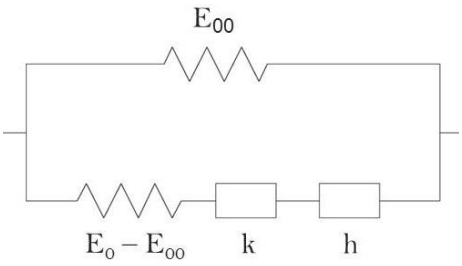	$E^*(\omega) = E_{00} + \frac{E_0 - E_{00}}{1+\delta(j\omega\tau)^{-k}+(j\omega\tau)^{-h}}$
2S2P1D	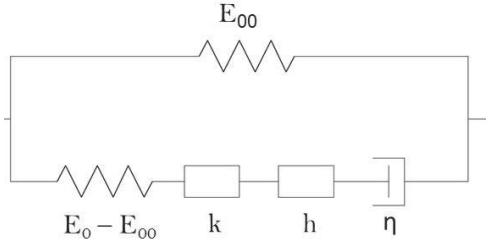	$E^*(\omega) = E_{00} + \frac{E_0 - E_{00}}{1+\delta(j\omega\tau)^{-k}+(j\omega\tau)^{-h}+(j\omega\beta\tau)^{-1}}$ with $\eta = (E_0 - E_{00})\beta\tau$

Appendix II

Measured temperatures for all complex modulus tests

Table A- III. Temperature at the surface of the samples and differences with respect to target temperatures in the temperature chamber

Mixture	Sample	Measured temperature per test stage									
		-25°C	-15°C	-5°C	5°C	15°C	25°C	35°C	45°C	55°C	65°C
GB3	GB3.1-I1-11.1%	-19.5	-15.0	-5.9	4.6	14.2	24.1	33.8	43.3	52.7	-
	GB3.1-I2-8.3%	-21.5	-15.5	-5.6	4.6	14.2	24.1	33.9	43.5	53.0	-
	GB3.1-I3-9.3%	-21.4	-15.8	-5.7	4.4	14.1	24.0	33.7	43.2	52.7	-
	GB3.1-C4-8.7%	-24.7	-15.2	-5.3	4.8	14.5	24.2	34.0	43.4	52.9	-
	GB3.1-D1-9.8%	-21.6	-14.4	-5.5	4.5	14.3	24.0	33.8	43.3	52.7	-
	GB3.1-D3-8.4%	-11.8	1.1	-4.6	4.9	14.5	24.2	33.9	43.5	52.8	-
	GB3.2-I1-9.4%	-21.2	-13.7	-4.6	4.9	14.9	24.0	33.6	43.1	52.4	-
	GB3.2-I3-8.5%	-21.6	-13.2	-4.9	5.1	14.5	24.8	33.9	43.7	53.1	62.4
	GB3.2-I4-8.8%	-4.1	4.3	-3.4	4.9	14.3	24.0	33.9	43.5	52.8	-
	GB3.2-D2-9.4%	-20.5	-13.5	-4.8	4.8	14.4	24.4	33.0	43.2	52.6	-
	GB3.2-D4-9.2%	-21.8	-14.2	-5.0	4.7	14.4	24.1	33.8	43.2	52.5	-
	GB3.3-C1-8.6%	-21.1	-14.0	-5.1	4.2	13.9	23.8	33.1	42.9	52.4	61.6
	GB3.3-D4-8.6%	-21.3	-14.1	-5.2	4.8	14.4	24.2	33.0	43.2	52.6	62.0
GB4	GB4.1-I4-5.2%	-23.5	-13.9	-4.2	5.3	14.7	24.1	33.6	43.0	52.1	61.2
	GB4.1-C1-5.4%	-23.6	-14.0	-4.5	5.1	14.6	24.0	33.5	43.0	52.2	61.4
	GB4.1-D1-5.5%	-22.5	-13.8	-4.2	5.2	14.7	24.1	33.6	43.0	52.2	61.2
	GB4.1-D4-5.0%	-	-	-	4.9	14.4	23.9	33.7	43.2	52.6	61.9
	GB4.2-I1-4.8%	-21.5	-14.0	-4.8	4.9	14.4	24.2	33.7	43.0	52.4	-
	GB4.2-I4-4.9%	-	-	-	-	14.5	24.3	33.8	43.2	52.9	61.9
GB PMB	GBPMB.1-I2-7.8%	-22.5	-15.0	-4.8	4.9	14.3	23.9	32.2	43.6	53.1	62.5
	GBPMB.1-I4-7.9%	-21.5	-14.0	-4.5	5.0	14.4	24.0	33.8	43.4	52.8	62.1

Appendix III

Complementary graphical representation of complex modulus test results

- GB3 mixture

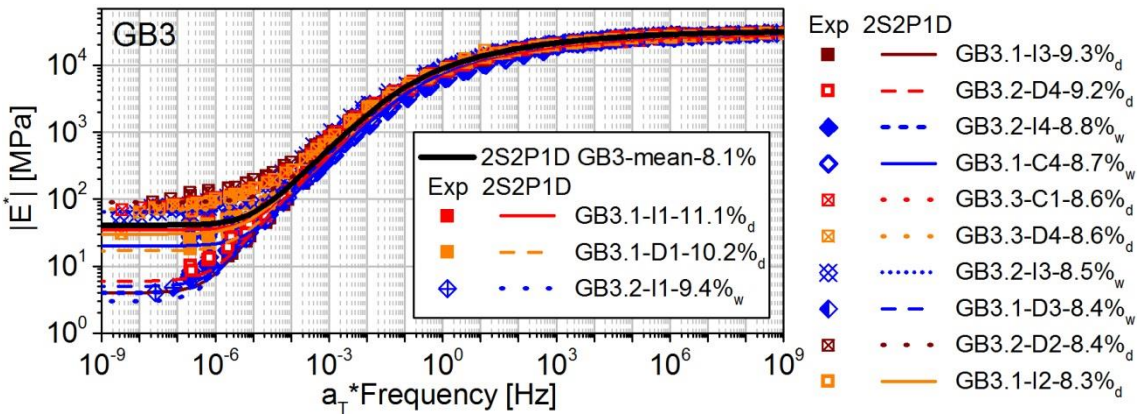

Figure A. 1. GB3 |E*| master curves

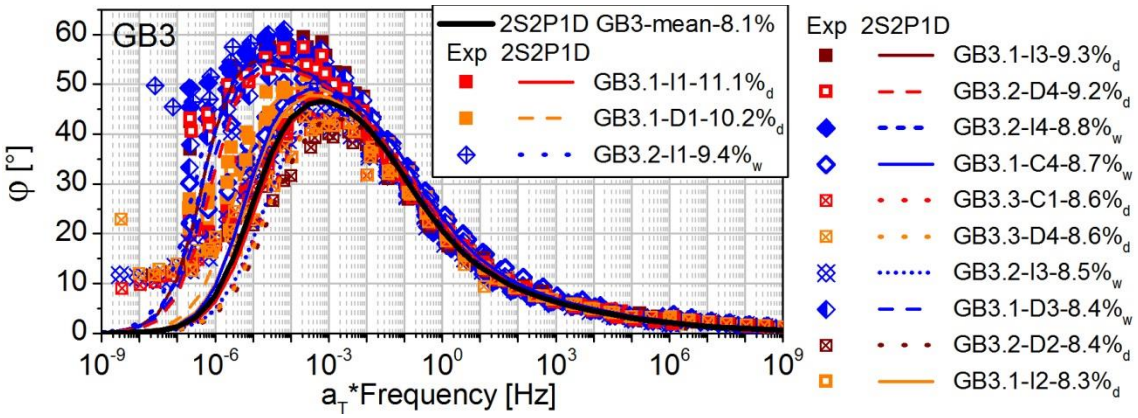

Figure A. 2. GB3 φ master curves

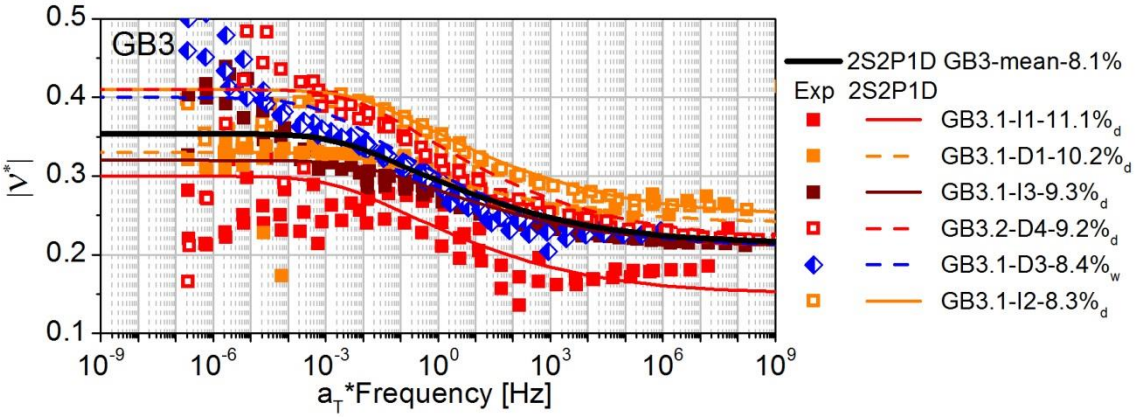

Figure A. 3. GB3 |v*| master curves

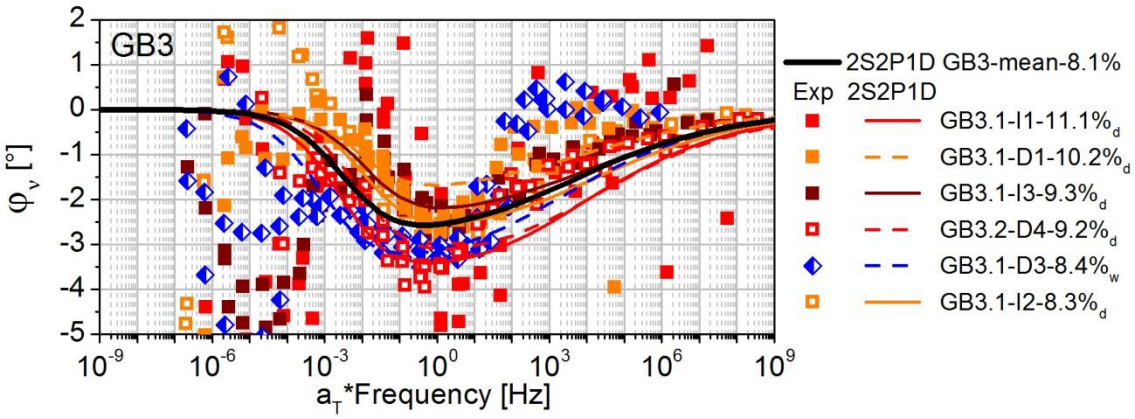

Figure A. 4. GB3 φ_v master curves

- GB4 mixture

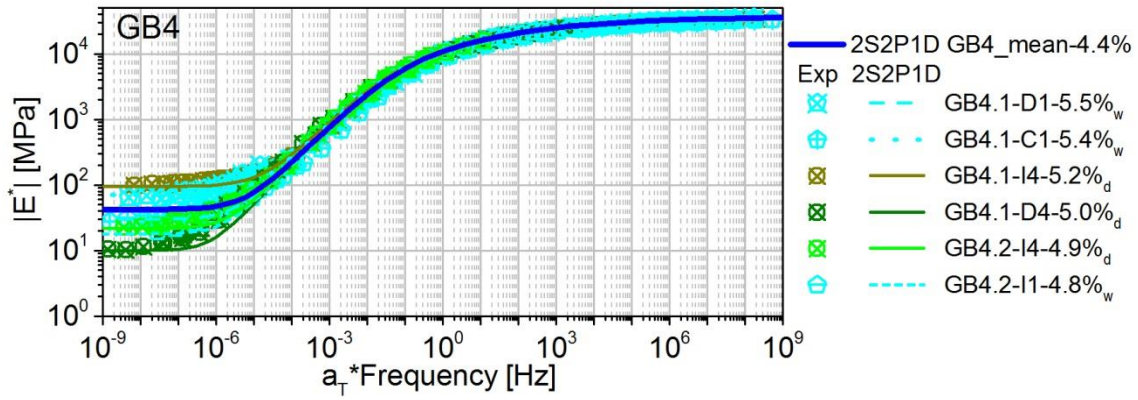

Figure A. 5. GB4 |E*| master curves

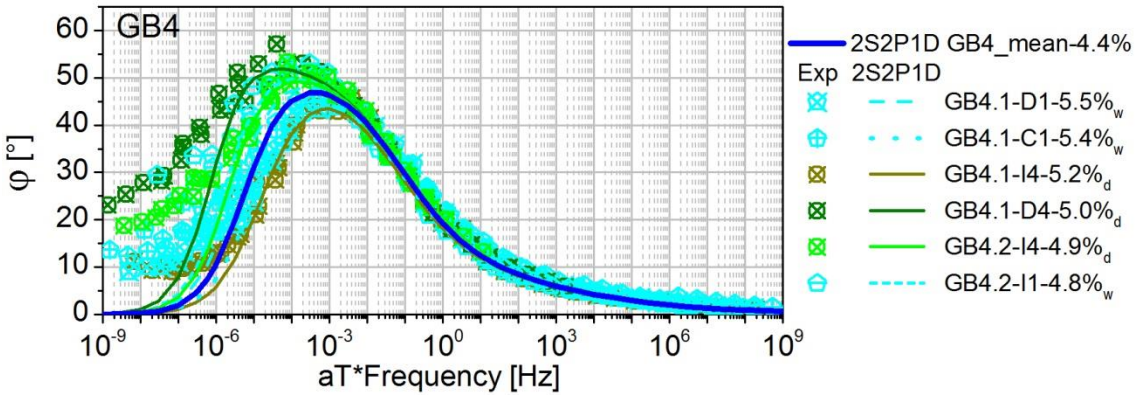

Figure A. 6. GB4 φ master curves

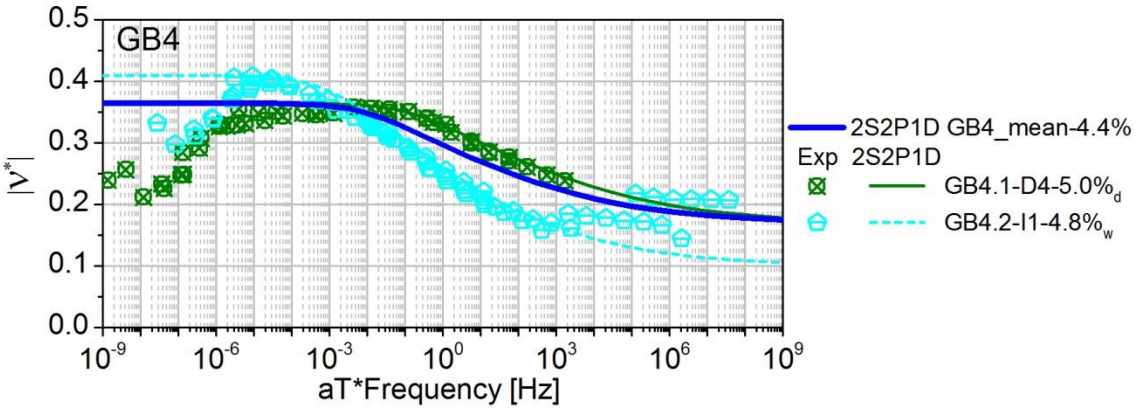

Figure A. 7. GB4 |v*| master curves

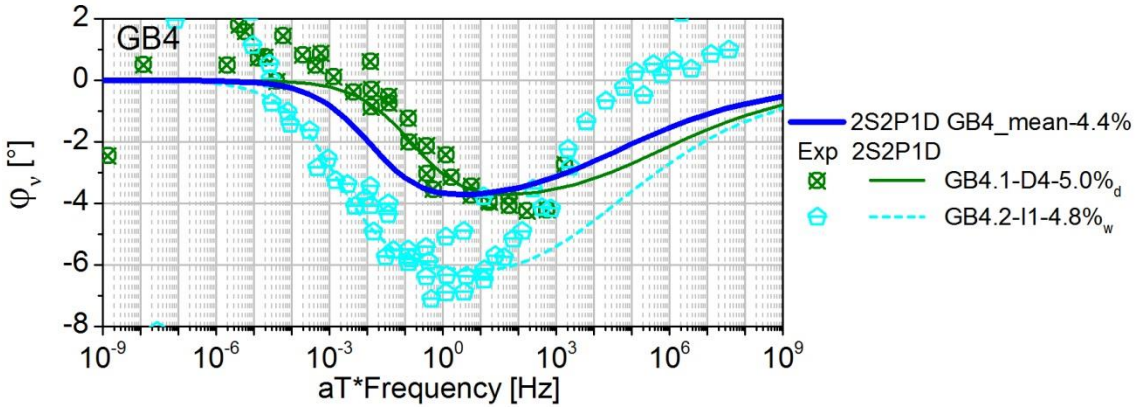

Figure A. 8. GB3 φ_v master curves

- GB PMB mixture

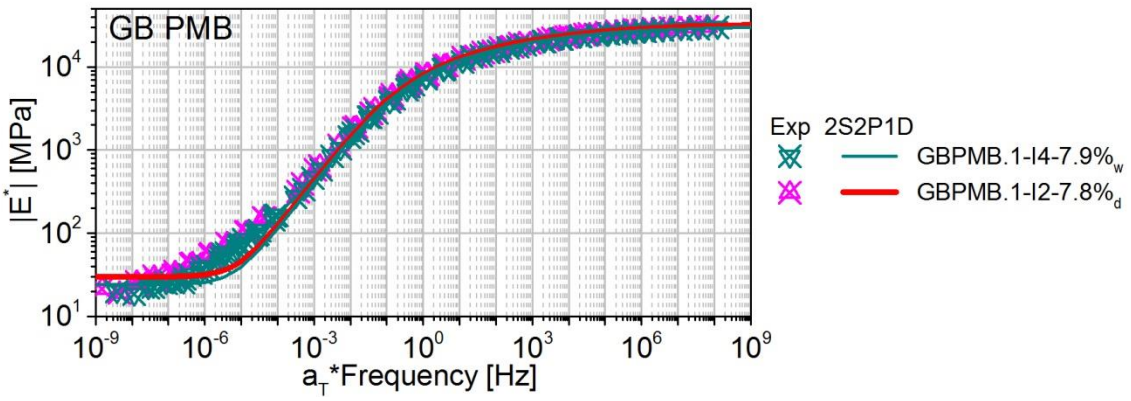

Figure A. 9. GB PMB |E*| master curves

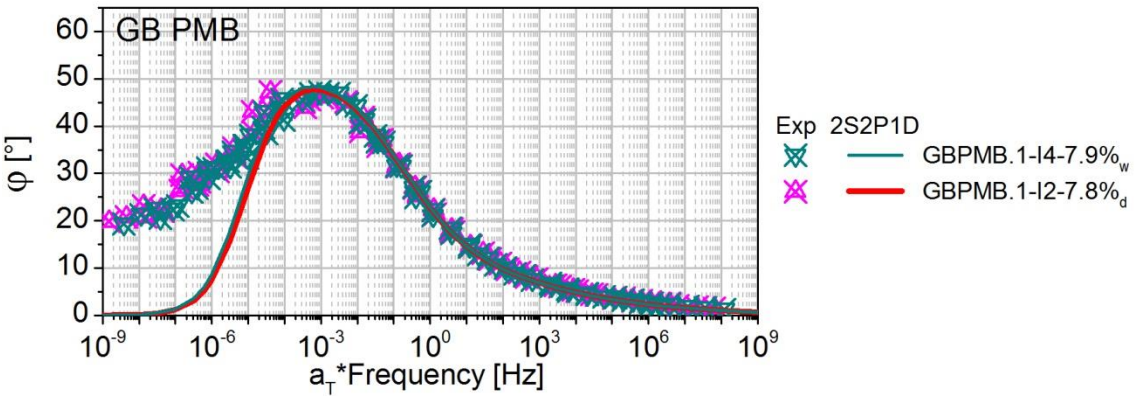

Figure A. 10. GB PMB φ master curves

Appendix IV

Complementary information of tension-compression fatigue test results

Table A- IV. GB3 N_f values from all failure criteria for all fatigue tests

Sample	Strain ε_0 [µm/m]	$N_{f\_50\%}$	$N_{f\_\phi Max}$	N_{f_Wn}	N_{f_r2Wn}	$N_{f\_\Delta\varepsilon}$	$N_{f\_\Delta\varepsilon\_ext}$	$N_{f\_\Delta\phi}$	$N_{f\_concavity}$
GB3-3-I4-8.3%d	60	4685001	4530001	3045001	-	1790000	2990001	-	2900000
GB3-3-D3-8.0%d	60	1940000	1925000	1900000	1900000	1910001	1925001	1915001	1900000
GB3-1-D2-8.0%d	70	1315001	1315001	1315000	1315000	742000	758000	826001	1250000
GB3-2-D3-8.1%d	70	1185001	1180001	1185001	1185001	1175000	1185000	1185000	1060000
GB3-2-D1-8.1%d	70	980000	974000	914000	978000	966001	962001	974001	920000
GB3-1-C2-7.5% d	90	664000	650001	404000	646000	288000	610000	490001	580000
GB3-2-C3-7.6%d	90	698000	678001	430001	426001	474000	512000	794000	440000
GB3-4-C1-7.5%d	90	352000	346000	350000	350000	196000	350000	350000	310000
GB3-1-C3-7.2%d	110	156000	154000	150001	150001	20000	148000	158000	130000
GB3-4-C2-7.3%d	110	232000	210000	134001	194000	186001	200000	294001	180000
GB3-4-C3-7.5%d	110	168000	162001	94201	154000	62600	96801	174000	150000
GB3-3-I1-8.0%w	60	1715000	1495001	1440000	1500000	1050000	1455000	-	1250000
GB3-1-C1-8.2%w	70	756000	754000	422001	756000	742000	754000	826001	700000
GB3-3-D1-8.1%w	70	888000	892001	498000	740000	69200	674000	796001	480000
GB3-4-I3-7.9%w	70	638001	642000	498001	574001	100	548001	-	520000
GB3-3-D2-7.7%w	90	154000	328001	90601	132000	136000	136000	180000	120000
GB3-2-C4-7.5%w	90	298001	292001	282001	268000	296000	296000	296000	160000
GB3-2-C2-7.3%w	110	358000	388001	116000	98000	55400	158000	-	82000
GB3-3-C2-7.2%w	110	56400	51401	45600	50400	26200	43801	34201	40000

Table A- V. GB3 D_{IIIc} values for all fatigue tests

Sample	Strain ε_0 [µm/m]	D_{IIIc}
GB3-3-I4-8.3%d	60	0.17
GB3-3-D3-8.0%d	60	0.12
GB3-1-D2-8.0%d	70	0.18
GB3-2-D3-8.1%d	70	0.18
GB3-2-D1-8.1%d	70	0.20
GB3-1-C2-7.5% d	90	0.19
GB3-2-C3-7.6%d	90	0.19
GB3-4-C1-7.5%d	90	0.21
GB3-1-C3-7.2%d	110	0.20
GB3-4-C2-7.3%d	110	0.17
GB3-4-C3-7.5%d	110	0.18
GB3-3-I1-8.0%w	60	0.19
GB3-1-C1-8.2%w	70	0.17
GB3-3-D1-8.1%w	70	0.20
GB3-4-I3-7.9%w	70	0.19
GB3-3-D2-7.7%w	90	0.20
GB3-2-C4-7.5%w	90	0.12
GB3-2-C2-7.3%w	110	0.18
GB3-3-C2-7.2%w	110	0.20

Table A- VI. GB4 N_f values from all failure criteria

Sample	Strain ε_0 [µm/m]	$N_{f\_50\%}$	$N_{f\_\phi Max}$	N_{f_Wn}	N_{f_r2Wn}	$N_{f\_\Delta\varepsilon}$	$N_{f\_\Delta\varepsilon\_ext}$	$N_{f\_\Delta\phi}$	$N_{f\_concavity}$
GB4-4-D3-4.6%d	60	7045000	6925001	-	-	6980000	6980000	6980000	6500000
GB4-1-I2-4.3%d	70	1290001	1290001	1295001	-	-	-	-	1210000
GB4-2-D1-4.2%d	70	1280001	1220000	1215000	1215001	1210001	1210001	1210001	1040000
GB4-4-I2-4.3%d	70	1950001	1820000	1280000	1430000	452000	1330001	452000	1140001
GB4-1-C4-3.9%d	90	636000	488001	406000	396000	17200	454000	17200	370000
GB4-3-I3-4.1%d	90	158000	158000	146000	152000	154000	154000	154000	106000
GB4-2-I3-4.0%d	90	144001	144000	140000	140000	110001	140001	110001	130000
GB4-1-C2-3.7%d	110	55400	55400	50401	55000	51600	-	51600	44000
GB4-1-C3-3.4%d	110	126001	73600	73600	72401	8080	74001	8080	70001
GB4-2-C2-3.7%d	110	110000	106001	99801	99801	102000	104000	102000	65000
GB4-2-D2-3.5%d	110	278000	276001	272001	272001	210000	268000	210000	238000
GB4-3-C3-3.7%d	110	136000	118001	90001	94200	84400	104000	84400	80000
GB4-2-D4-4.8%w	60	2285000	1635001	1400000	1560000	892000	1380001	892000	1900000
GB4-3-I1-4.7%w	60	1610000	1355001	1320000	1375000	1105000	976000	1105000	1200000
GB4-1-I3-4.3%w	70	3825000	3815000	2380001	3040001	2850001	3190000	2850001	3500001
GB4-1-D2-4.2%w	70	592001	588000	588001	588001	560001	586001	560001	550000
GB4-1-I1-4.5%w	70	2775000	2230001	1890000	2170000	1820000	2275000	1820000	1700000
GB4-4-D2-4.3%w	70	2700000	1630001	936001	1235000	560000	954000	560000	900000
GB4-3-D2-4.4%w	70	862000	688001	598000	708000	574000	608000	574000	540000
GB4-2-I2-4.1%w	90	372000	310001	230000	230001	2821	252000	2821	230001
GB4-1-D3-4.1%w	90	726001	726000	720000	720000	720001	724001	720001	680000
GB4-3-C2-4.1%w	90	332000	270001	212000	202000	168000	226000	168000	206000
GB4-2-C1-3.6%w	110	132000	114001	50001	82200	32801	67400	32801	60000
GB4-2-D3-3.7%w	110	106000	104001	104001	104001	92601	94600	92601	88000
GB4-2-C4-3.5%w	110	326000	316001	236000	250000	298000	298000	298000	280000

Table A- VII. GB4 D_{IIIc} values for all fatigue tests

Sample	Strain ε_0 [µm/m]	D_{IIIc}
GB4-4-D3-4.6%d	60	0.17
GB4-1-I2-4.3%d	70	0.15
GB4-2-D1-4.2%d	70	0.16
GB4-4-I2-4.3%d	70	0.18
GB4-1-C4-3.9%d	90	0.18
GB4-3-I3-4.1%d	90	0.03
GB4-2-I3-4.0%d	90	0.14
GB4-1-C2-3.7%d	110	0.06
GB4-1-C3-3.4%d	110	0.21
GB4-2-C2-3.7%d	110	0.16
GB4-2-D2-3.5%d	110	0.16
GB4-3-C3-3.7%d	110	0.18
GB4-2-D4-4.8%w	60	0.16
GB4-3-I1-4.7%w	60	0.17
GB4-1-I3-4.3%w	70	0.18
GB4-1-D2-4.2%w	70	0.13
GB4-1-I1-4.5%w	70	0.17
GB4-4-D2-4.3%w	70	0.19

GB4-3-D2-4.4%w	70	0.15
GB4-2-I2-4.1%w	90	0.17
GB4-1-D3-4.1%w	90	0.17
GB4-3-C2-4.1%w	90	0.18
GB4-2-C1-3.6%w	110	0.18
GB4-2-D3-3.7%w	110	0.18
GB4-2-C4-3.5%w	110	0.18

Table A- VIII. GB PMB N_f values from all failure criteria for all fatigue tests

Sample	Strain ε_0 [µm/m]	$N_{f\_50\%}$	$N_{f\_\phi Max}$	N_{f_Wn}	N_{f_r2Wn}	$N_{f\_\Delta\varepsilon}$	$N_{f\_\Delta\varepsilon\_ext}$	$N_{f\_\Delta\phi}$	$N_{f\_concavity}$
GBPMB-1-D2-7.9%d	70	4575001	4245001	3140000	4120000	2345000	3875000	-	3500000
GBPMB-1-D4-8.2%d	70	3325000	3320001	3310001	528001	3250000	3310000	3315000	2800000
GBPMB-3-D1-7.7%d	90	584000	474000	388000	458000	372000	424000	548000	390000
GBPMB-4-I3-7.8%d	90	522000	448001	462000	462001	510000	516000	520000	470000
GBPMB-2-D1-7.8%d	90	1160000	988001	632000	848001	278000	670000	1020001	850000
GBPMB-1-C2-7.2%d	110	304000	302000	270000	282000	294000	282000	302000	250000
GBPMB-1-C3-7.2%d	110	356000	340000	266000	266001	274000	304000	390000	240000
GBPMB-4-C4-7.1%d	110	88600	88201	84201	86600	85600	87600	87600	60000
GBPMB-1-C1-8.2%w	70	3920000	3830001	3435001	3575000	3615000	3520000	4450000	3000000
GBPMB-3-D3-7.9%w	70	2645000	2640000	2620000	2630000	2635000	2615000	2640000	2200000
GBPMB-1-D3-7.8%w	90	382000	380000	362000	364000	374000	372000	380000	340000
GBPMB-2-D4-7.7%w	90	464000	358000	338000	338000	336000	358000	504000	320000
GBPMB-4-I2-7.8%w	90	384000	300000	242001	286000	284000	292000	436000	270000
GBPMB-2-C4-7.4%w	110	75800	62000	59600	61800	53400	61800	84000	56000
GBPMB-4-C1-7.3%w	110	156000	152000	84401	86800	124000	95600	178000	80000
GBPMB-2-D3-7.3%w	110	64800	51000	30600	35601	24800	31000	114000	70000

Table A- IX. GB PMB D_{IIIc} values for all fatigue tests

Sample	Strain ε_0 [µm/m]	D_{IIIc}
GBPMB-1-D2-7.9%d	70	0.18
GBPMB-1-D4-8.2%d	70	0.17
GBPMB-3-D1-7.7%d	90	0.19
GBPMB-4-I3-7.8%d	90	0.13
GBPMB-2-D1-7.8%d	90	0.19
GBPMB-1-C2-7.2%d	110	0.18
GBPMB-1-C3-7.2%d	110	0.18
GBPMB-4-C4-7.1%d	110	0.12
GBPMB-1-C1-8.2%w	70	0.20
GBPMB-3-D3-7.9%w	70	0.16
GBPMB-1-D3-7.8%w	90	0.21
GBPMB-2-D4-7.7%w	90	0.17
GBPMB-4-I2-7.8%w	90	0.20
GBPMB-2-C4-7.4%w	110	0.19
GBPMB-4-C1-7.3%w	110	0.18
GBPMB-2-D3-7.3%w	110	0.19

N°d'ordre NNT : 2016LYSET009

THESE de DOCTORAT DE L'UNIVERSITE DE LYON
opérée au sein de
L'Ecole Nationale des Travaux Publics de l'Etat

Ecole Doctorale 162
Mécanique, Energétique, Génie Civil, Acoustique (MEGA)

Spécialité de doctorat : Génie Civil

Soutenue publiquement le 14/11/2016, par :
Diego Alejandro Ramirez Cardona

Characterisation of thermomechanical properties of bituminous mixtures used for railway infrastructures

Document résumé en français du manuscrit de thèse

Devant le jury composé de :

DOUADJI, Ali	Professeur	INSA Lyon	Président
CANESTRARI, Francesco	Professeur	Università Politecnica delle Marche	Rapporteur
HARVEY, John	Professeur	University of California Davis	Rapporteur
CALON, Nicolas	Docteur	SNCF Réseau	Examinateur
DI BENEDETTO, Hervé	Professeur	ENTPE	Directeur de thèse
SAUZEAT, Cédric	Docteur	ENTPE	Tuteur
OLARD, François	Docteur	EIFFAGE Infrastructures	Invité

Characterisation of thermomechanical properties of bituminous mixtures for railway infrastructures

Caractérisation des propriétés thermomécaniques des enrobés bitumineux pour infrastructure ferroviaire

Mots clé : Enrobé bitumineux, viscoélasticité, résistance à la fatigue, sous-ballast ferroviaire, plateforme ferroviaire

Introduction

Ce documente résume très brièvement le manuscrit the thèse intitulé « *Characterisation of thermomechanical properties of bituminous mixtures for railway infrastructures* » présenté à l'Université de Lyon pour l'obtention du titre de docteur en Génie Civil.

Le travail de recherche présenté dans ce document a été réalisé dans le cadre d'une collaboration entre l'ENTPE/Université de Lyon et la SNCF. L'objectif de l'étude est la caractérisation des propriétés thermomécaniques des enrobés bitumineux à être utilisés dans la construction de voies ferrées. Le comportement viscoélastique linéaire (VEL) et la résistance à la fatigue d'enrobés pour couche de base couramment utilisés en France ont été étudiés. L'influence de l'eau sur ces propriétés a été aussi étudiée du fait que l'exposition à l'eau des couches bitumineuses en structure ferroviaire peut les altérer et réduire la durée de vie de l'ouvrage.

La caractérisation du comportement VEL et de la résistance à la fatigue des matériaux a été faite en réalisant des essais mécaniques en traction-compression sur des éprouvettes cylindriques au laboratoire LTDS/ENTPE. Une nouvelle procédure de conditionnement à l'eau et au gel a été proposée sur la base des méthodes d'essai normalisées française et américaine. La susceptibilité à l'eau des matériaux a été obtenue par comparaison des résultats des essais mécaniques entre éprouvettes conditionnées et non conditionnées. Le comportement VEL des matériaux a été simulé avec le modèle 2S2P1D, développée à l'ENTPE.

Trois formules pour couche de base ont été testées : une GB3, une GB4 et une formule appelée GB PMB. Cette dernière est la même formule GB3 mais avec un bitume modifié aux polymères SBS. La GB3 sert comme matériau de référence. La GB4 est un matériau de meilleures performances que la GB3. La formule GB4 étudiée correspond à celle mise en place dans la couche sous-ballast de la Ligne à Grande Vitesse (LGV) Bretagne-Pays de Loire. L'intérêt d'étudier la GB PMB est de savoir si l'utilisation de bitumes modifiés aux polymères est pertinente dans un contexte ferroviaire ou pas.

La zone test construite dans la LGV Est-Européenne près de la ville de Reims avec une couche sous-ballast en enrobé bitumineux a servi comme cas d'étude pour cette thèse. Les différents avantages de l'utilisation de matériaux bitumineux en structure ferroviaire retrouvées dans la bibliographie ont été confirmés avec le retour sur l'expérience de cette zone test.

Les résultats obtenus des travaux expérimentaux montrent que les trois formules étudiées présentent des capacités portantes (rigidité) suffisantes pour leur utilisation comme couche sous-ballast. La méthode de conditionnement à l'eau et au gel utilisée n'a pas altéré le comportement VEL des matériaux. En ce qui concerne les essais de fatigue, les résultats ont montré que l'utilisation d'un bitume modifié aux polymères augmente sensiblement la résistance à la fatigue de la GB3. La GB PMB a aussi montré une plus faible susceptibilité de la résistance à la fatigue à l'eau et au gel que la GB3. Du fait que les niveaux de sollicitation de la base de la couche d'enrobé de la zone test LVG EE sont très faibles, tous les matériaux étudiés présentent des propriétés satisfaisantes de résistance à la fatigue en couche sous-ballast.

Dans ce résumé, les sections de ce résumé sont introduites sous forme de questions. Les principales points et résultats de l'étude sont présentés. Cela permet d'avoir une vision globale de ce qui a été réalisé et des conclusions qui ont été faites.

1. Quel est l'intérêt de l'utilisation d'enrobés bitumineux dans les structures ferroviaires ?

Le développement du transport ferroviaire implique des incrémentations de vitesse de circulation, de tonnage et de volume de trafic. La structure des voies doit être repensée pour assurer le confort, la régularité et la sécurité dans ces nouvelles conditions de service. L'utilisation d'enrobés bitumineux en sous-couche a été repérée comme une solution possible à ace besoin.

L'utilisation d'enrobés bitumineux dans la voie ferrée date de presque 40 ans dans certains pays. Leur expérience Leur expérience a permis d'identifier plusieurs avantages de cette technique, comprennent l'atténuation des vibrations, la réduction des efforts transmis au sol support, l'imperméabilisation de la Partie Supérieure des Terrassements (PST), la prévention du colmatage du ballast et la réduction des efforts de maintenance de la voie. En plus, des avantages constructives comme la possibilité de faire de la couche d'enrobé une voie d'accès circulable au chantier rendent cette technique très attractive (Buonanno & Mele, 2000; EAPA, 2014; Fang, Fernández Cerdas, & Qiu, 2013; Huang, Lin, & Rose, 1984; Robinet & Cuccaroni, 2012; Rose & Bryson, 2009).

2. Qu'est-ce que la susceptibilité à l'eau des enrobés bitumineux ?

La définition la plus acceptée d'endommagement par l'eau des enrobés bitumineux est celle proposée par (Kiggundu & Roberts, 1988) : « la détérioration fonctionnelle progressive du mélange hydrocarbonée par la réduction de l'adhésivité entre le liant bitumineux et la surface des granulats et/ou la perte de la résistance cohésive dans le liant à cause de l'action de l'eau ».

Selon (Copeland, Youtcheff, & Shenoy, 2007), cités par (Bausano & Williams 2009), l'endommagement par action de l'eau se passe de deux manières différentes : soit par l'affaiblissement de l'adhésion entre le liant et le granulat, soit par la détérioration du mastic bitumineux. En concordance avec la définition précédente, la première fait appel à la diminution de l'adhésivité et la deuxième à la perte de cohésion entre les composants de l'enrobé.

Dans tous les cas, l'endommagement par effets de l'eau ne peux pas être expliqué par une seule théorie puisque c'est un phénomène complexe avec plusieurs mécanismes de natures différentes (Kiggundu & Roberts, 1988).

L'affaiblissement des liens adhésifs entre le bitume et les granulats s'appelle desenrobage. Au moins cinq mécanismes de desenrobage différents peuvent être identifiées (Kiggundu & Roberts, 1988; Little & Jones, 2003; Terrel & Al-Swailmi, 1993).

Selon (Solaimanian, Kennedy, & Elmore, 1993), il y a cinq facteurs déterminants de la susceptibilité à l'eau des enrobés bitumineux. Ceux-ci peuvent se regrouper dans deux catégories (Arambula, 2007) :

- Facteurs internes :
    - Les caractéristiques des granulats et leurs propriétés
    - Les caractéristiques du bitume
    - La formulation du mélange
- Facteurs externes
    - Les conditions environnementales
    - La nature et le volume du trafic

3. En quoi consiste le cas d'étude de la zone test de la LGV EE avec enrobé sous ballast ?

En 2004 la SNCF a construit une zone test avec enrobé sous ballast à proximité de la ville de Reims sur la LGV EE. Cette zone test de 3 km de long a été faite du fait que la SNCF avait identifié plusieurs avantages de l'utilisation d'enrobés sous ballast. En particulière ils se sont intéressés par la possibilité de se servir de la couche en enrobé pour accéder au chantier. Le fait que cette voie d'accès restait utilisable même par mauvais temps, permettait de mieux maîtriser les délais du chantier. Aussi, la réduction de la hauteur de la plateforme et la réduction du volume de matériaux nécessaires était une avantage intéressent qui prend beaucoup d'intérêt surtout lorsque les sites de production de granulats de qualité sont loin du chantier.

La zone a été instrumenté pour suivre le comportement mécanique de la voie et confirmer les hypothèses de dimensionnement de la zone avec enrobé. Du retour sur l'expérience, l'observation la plus importante est peut-être en rapport avec le faible effort de maintenance requis par cette zone test. En effet, la zone avec enrobé sous ballast a eu besoin de moins de maintenance que les zones conventionnelles autour. Les données relevées de l'instrumentation ont permis de valider le bon comportement mécanique de la voie. A ce jour, les référentiels de l'entreprise considèrent cette structure de voie comme une possible solution de dimensionnement pour les LGV.

Actuellement, quatre projets de LGV sont en phase de construction avec des sections avec enrobé sous ballast (Groupement Professionnel des Bitumes, 2014) :

- La phase 2 de la LGV Est-Européenne (EE) – 55 km (52%) d'enrobé sous ballast
- La LGV Brtagne-Pays de Loire (BPL) – 105 km (58%) d'enrobé sous ballast
- La LGV Sud-Est Atlantique (SEA) – 43 km (14%) d'enrobé sous ballast
- Le contournement Nîmes-Montpellier (CNM) – 80 km (100%) d'enrobé sous ballast

4. Quels matériaux ont été testés et quels essais ont été réalisés ?

L'objectif du travail expérimental de cette étude est de déterminer si les enrobés bitumineux disponibles actuellement sur le marché Français sont aptes pour leur utilisation en structure ferroviaire. Différents aspects sont pris en compte dans l'analyse : module, dépendance de la température, effet de la vitesse de circulation ou de la fréquence de sollicitation, durée de vie et susceptibilité à l'eau et au gel.

Trois mélanges bitumineux différents ont été étudiés. Deux entre eux, la GB3 et la GB4, correspondent à des formules d'enrobé utilisées couramment comme des couches de base routières en France. Le troisième matériau, la GB PMB, est la même formule que la GB3 sauf que son bitume a été modifié aux polymères SBS réticulés.

Une procédure de conditionnement à l'eau et au gel a été développée et appliqué aux trois matériaux pour les endommager en présence d'eau. Leur susceptibilité à l'eau et au gel a été déterminé par la comparaison de leur propriétés thermomécaniques avec et sans endommagement.

Deux types d'essai mécaniques en traction compression ont été réalisés : des essais de module complexe et des essais de fatigue en traction-compression.

Les mélanges bitumineux testés ont été faits à partir des mêmes composants (bitume de base et granulats). Les granulats proviennent d'une carrière en Mayenne et sont les mêmes que ceux utilisés dans le mélange appliqué pour la couche sous ballast de la LGV BPL. Tous les mélanges ont une taille nominale de 14 cm (0/14). Le filler est de nature calcaire, ce qui est courant dans les formulations françaises.

La Figure 1 présente les courbes granulométriques des mélanges étudiés. Les tableaux 1, 2 et 3 résument leur composition. Comme expliqué avant, les formules GB3 et GB PMB ont la même courbe granulométrique et la seule différence entre les deux c'est la modification aux SBS du bitume de la GB PMB. La formule GB4 a une discontinuité dans la fraction granulaire 2-6 ce qui lui confère un squelette granulaire optimisé. Cela veut dire que les contacts entre les gros granulats sont privilégiés et que la compacité est augmentée. La plus abondante fraction fine de la formule GB4 lui confère aussi une plus grande compacité. Par rapport aux autres formules, la GB4 a une teneur en fines calcaires (basique) plus grande. Du fait que l'eau a une plus grande affinité pour les granulats de nature acide, ceci doit être pris en compte lors des analyses de susceptibilité à l'eau.

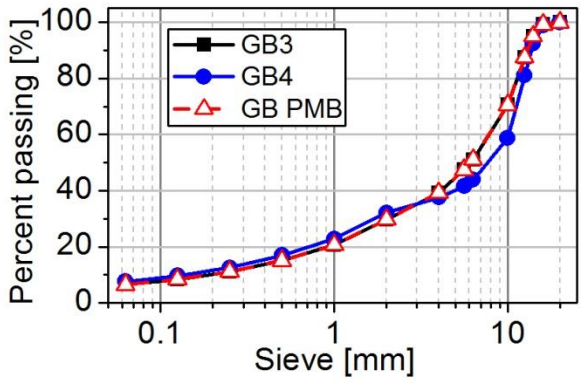

Figure 1. Courbes granulométriques des formules étudiées

Tableau 1. Granulats des trois formules étudiées

Elément	Type	Fraction [mm]	% masse totale		
			GB3	GB4	GB PMB
Granulats gros/fins (0/14)	Rhyolite – Carrière Baglione (53 Mayenne) – Nature acide	0-2	26.3	28.1	26.3
		2-6	21.2	10.0	21.2
		6-10	18.4	12.0	18.4
		10-14	27.2	41.7	27.2
Filler d'apport	Calcaire – Carrière Haut Lieu (59 Nord) – Nature basique	<0.063	2.5	3.4	2.5

Tableau 2. Fines dans les formules étudiées

Nature	Type	% masse totale			% masse de filler		
		GB3	GB4	GB PMB	GB3	GB4	GB PMB
Acide	Rhyolite	4	4.3	4	61.5	55.8	61.5
Basique	Calcaire (filler d'apport)	2.5	3.4	2.5	38.5	44.2	38.5
Total		6.5	7.7	6.5			

Les trois formules ont le même bitume de bas : 35/50 Total Donges. La modification aux polymères dans le bitume de la GB PMB est à 2.5% de SBS réticulé. Les mélanges ont été fabriqués par l'entreprise EIFFAGE Infrastructures dans le Centre de Recherche et Innovation situé à Corbas (69).

Tableau 3. Bitume et MVR des mélanges étudiés

Formule	Bitume	% masse totale	MVR [Mg/m^3]
GB3	Total Donges 35/50	4.4	2.486
GB4	Total Donges 35/50	4.8	2.476
GB PMB	Total Donges 35/50 avec 2.5% SBS réticulé	4.4	2.486

5. Quels sont les résultats les plus importants des essais de module complexe ?

Les résultats des essais de module complexe ont été simulés avec le modèle rhéologique 2S2P1D (Olard & Di Benedetto, 2003; Olard, 2003) développé à l'ENTPE/Université de Lyon. Les paramètres de forme du modèle ne varient pas entre un matériau et l'autre ni dépendent du conditionnement à l'eau et au gel des échantillons. Les paramètres du modèle E_0 (module vitreux) et τ (temps caractéristique) ont été trouvés comme dépendants de la teneur en vides des échantillons. Leurs valeurs diminuent avec l'augmentation de la teneur en vides.

Le conditionnement à l'eau et au gel n'a pas affecté le comportement viscoélastique linéaire des matériaux testés. Les figures 2 et 3 montrent comment tous les résultats de module complexe de toutes les éprouvettes testés de tous les matériaux se confondent dans les plans complexes normalisés (Cole-Cole et Black).

Les trois matériaux testés présentent des modules élevés pour les conditions de température et fréquence normales associés au trafic ferroviaire.

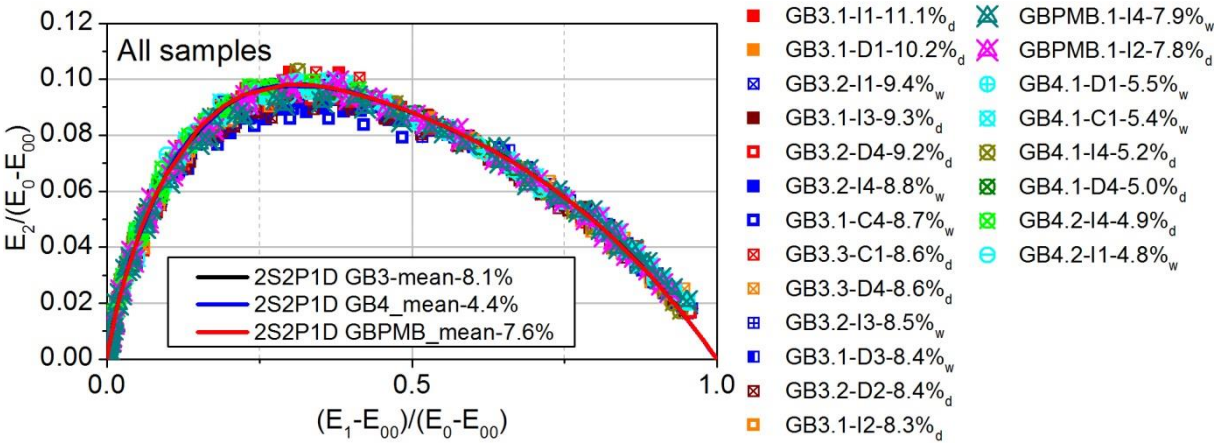

Figure 2. Résultats normalisés de tous les essais de module complexe dans un plan Cole-Cole et résultat de la simulation 2S2P1D valable pour tous les essais

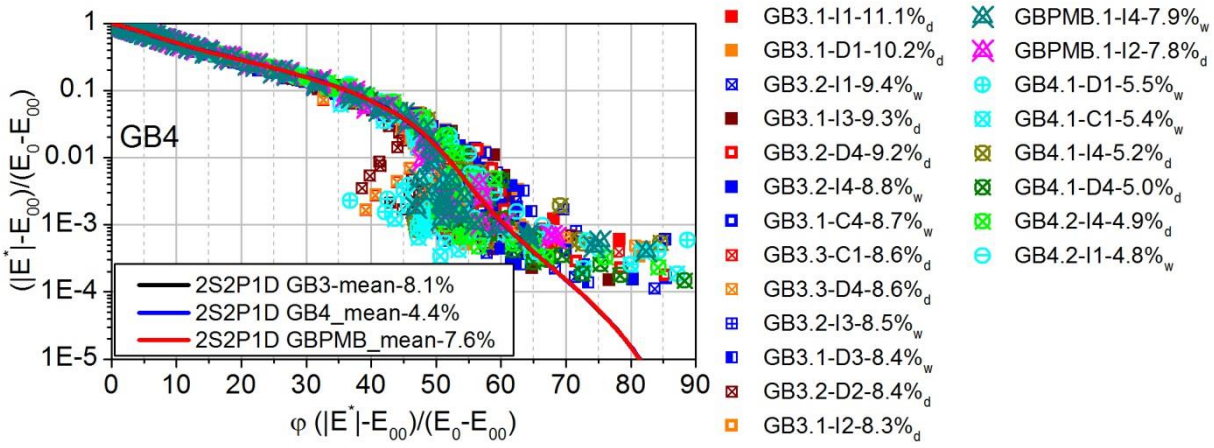

Figure 3. Résultats normalisés de tous les essais de module complexe dans un plan Black et résultat de la simulation 2S2P1D valable pour tous les essais

6. Quels sont les résultats les plus importants des essais de fatigue ?

La GB3 est le matériau qui présente la plus grande susceptibilité à l'eau et au gel des matériaux testés. La GB4 est celui qui en présente la moindre. Toutefois, les résultats de la GB4 sont très dispersés. Les figures 4, 5 et 6 présentent les droites de Wöhler pour les trois matériaux dans les deux états de conditionnement.

La GB PMB présente les meilleures propriétés de résistance à la fatigue. La GB PMB conditionnée à l'eau et au gel présente même une résistance à la fatigue supérieure que les formules GB3 et GB4.

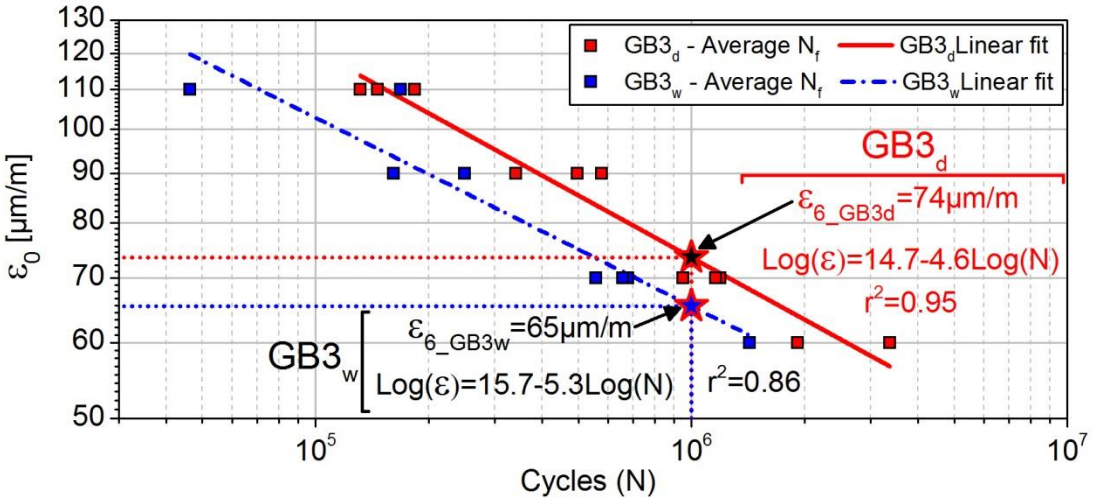

Figure 4. Droites de Wöhler GB3 - conditionnée (bleu) et une non-conditionnée (rouge)

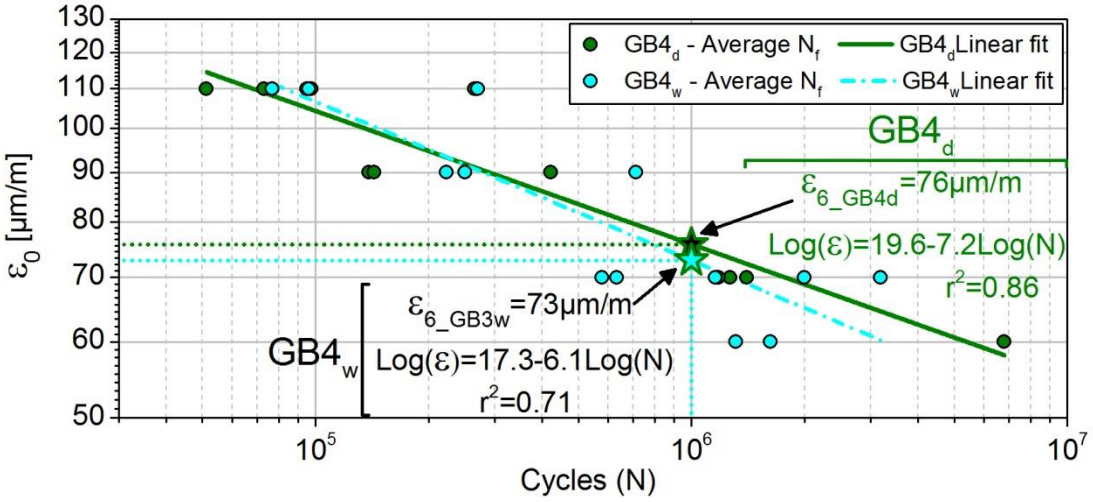

Figure 5. Droites de Wöhler GB4 - conditionnée (bleu clair) et une non-conditionnée (vert)

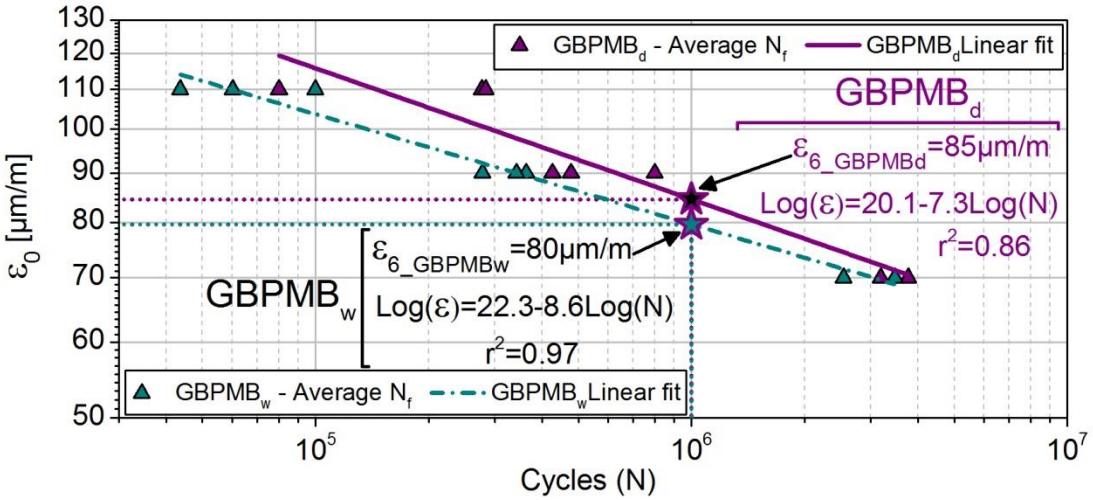

Figure 6. Droites de Wöhler GB PMB - conditionnée (cyan) et une non-conditionnée (violet)

Tableau 4. Paramètres des droits de Wöhler avec $N_{f\_average}$ pour tous les matériaux testés

Matériau	Etat de conditionnement	ε_6 [µm/m]	1/b	$\Delta\varepsilon_6$ [µm/m]	r^2	Teneur en vides moyenne [%]
GB3	Non-conditionné	73.6	-0.21	3.8	0.95	7.7
	Conditionné	66.1	-0.19	8.6	0.86	7.7
GB4	Non-conditionné	76.0	-0.14	7.1	0.85	4.0
	Conditionné	73.4	-0.17	10.2	0.70	4.2
GB PMB	Non-conditionné	84.7	-0.14	6.8	0.86	7.6
	Conditionné	79.7	-0.12	3.3	0.96	7.7

7. Quelles sont conclusions de l'étude et quelles sont les recommandations pour des futurs travaux de recherche sur me sujet ?

L'objectif de cette étude était de caractériser les propriétés thermomécaniques des enrobés bitumineux pour infrastructure ferroviaire. Le comportement viscoélastique linéaire (VEL) et les propriétés de résistance à la fatigue ont été investigués. Des mélanges pour couche de base routière ont été testés pour évaluer si les matériaux disponibles dans le marché français répondent bien aux sollicitations ferroviaires. Les matériaux testés ont donc des caractéristiques similaires à celles des matériaux couramment utilisés dans le domaine routier en France. Du fait que la durée de vie de dimensionnement des structures ferroviaires est plus élevée que pour les chaussées (100 ans contre 30), l'étude a porté spéciale attention à la pérennité des enrobés bitumineux. L'endommagement par exposition à l'humidité a été identifié comme un déclencheur potentiel de la détérioration du matériau dans une structure ferroviaire. Un nouveau protocole de conditionnement à l'eau et au gel a donc été proposé pour l'évaluation des propriétés thermomécaniques des enrobés bitumineux ayant été exposés à l'humidité. Ce protocole est basé sur les procédures de conditionnement des essais standard Français et Américain et sur les pratiques repérées dans l'état de l'art sur le sujet.

Des essais sinusoïdaux en traction-compression ont été réalisés sur des éprouvettes cylindriques d'enrobé. Le comportement VEL a été caractérisé par voie de l'essai de module complexe à différentes températures et fréquences. Les propriétés de résistance à la fatigue ont été obtenues par voie de l'essai de fatigue continue à 10°C et 10 Hz à différentes amplitudes de déformation. Les matériaux ont été testés à l'état conditionné et non-conditionné à l'eau et au gel pour caractériser leur susceptibilité à l'humidité.

Dans cette section, les principales conclusions de l'étude sont présentées.

a. Par rapport à l'analyse du retour sur l'expérience (REX) de la zone test de la LGV EE

Le REX de 8 ans de service de la Ligne à Grande Vitesse Est-Européenne (LGV EE) a mis en évidence certaines avantages de l'utilisation d'enrobés bitumineux sous ballast dans la structure LGV. En faisant la comparaison avec des zones voisines faites en structure granulaire, la zone test de la LGV EE présente les points suivants :

- Rigidité verticale plus importante et plus homogène
- Efforts verticaux transmis au sol support de plus faible amplitude
- Accélération verticale de la superstructure plus faible
- Plus faible vitesse de dégradation de la géométrie de la voie
- Plus grande efficience des opérations de bourrage dans le rétablissement de la géométrie de la voie

D'un point de vue industriel, l'observation la plus importante du REX de la LGV EE est l'importante réduction de la vitesse de dégradation de la voie avec enrobé sous ballast par rapport à la voie en structure granulaire adjacente. Pour des conditions de température moyennes (autour de 15°C) et pour un chargement à des fréquences typiques du trafic ferroviaire, l'enrobé présente une plus grande rigidité que le sol compacté ce qui

proportionnerait un meilleur support et confinement à la couche de ballast. Ceci entraîne une augmentation du réseau de force dans le ballast et une augmentation de la friction interne. En conséquence, la couche de ballast est moins susceptible de se désagréger au passage des trains. La faible vitesse de dégradation de la géométrie de la voie avec enrobé sous ballast après bourrage implique aussi que les effets nocifs du bourrage sur la qualité du ballast sont réduits.

La zone test de la LGV EE présente en général un bon comportement, similaire ou parfois meilleur que celui des zones en structure granulaire qui présentent se comportent le mieux.

b. Par rapport aux propriétés VEL des enrobés bitumineux testés

Des essais de module complexe à différentes températures et fréquences ont été réalisés pour les trois formules étudiées. Des éprouvettes conditionnées à l'eau et au gel et non-conditionnées ont été testées.

Le Principe de Superposition Temps-Température (PSTT) a été validé pour tous les matériaux étudiés, même après exposition à l'humidité. Les résultats des éprouvettes conditionnées n'ont pas montré de discontinuité dans le plan Cole-Cole (plan complexe). Il n'y a pas eu d'augmentation de la rigidité du matériau partiellement saturé à des températures négatives à cause de la présence de glace dans les interstices Le faible niveau de saturation des éprouvettes conditionnées au moment de l'essai peut en être la cause. Ceci est évidence du caractère imperméable des matériaux.

Le facteur de translation a_T des éprouvettes conditionnées n'a pas présenté des différences par rapport à celui des éprouvettes non-conditionnées. Ceci implique que le bitume n'a pas été affecté par la procédure de conditionnement. Il est pertinent de rappeler que cette procédure combine les conditions les plus extrêmes d'exposition à l'humidité des essais standard français et américain de sensibilité à l'eau.

Tous les matériaux étudiés ont présenté des valeurs de module élevées à des conditions de température normales (atour de 15°C) et pour des fréquences de sollicitation typiques ferroviaires en France. Le rang de température dit normale provient des mesures de température de la couche d'enrobé sous ballast de la LGV EE.

En général, la procédure de conditionnement à l'eau et au gel utilisée n'a pas affecté le comportement VEL des matériaux étudiés. La représentation des résultats des essais de module complexe dans le plan normalisé de Cole-Cole permet de justifier ceci. Les résultats des essais, sur des éprouvettes conditionnées et non-conditionnées, ont pu être modélisés avec le modèle 2S2P1D en utilisant les mêmes paramètres de forme (h, k, β and δ) pour tous les matériaux. La modification avec polymères du bitume de la GB PMB n'a pas altéré ces paramètres.

Le module vitreux E_0 et le paramètre τ ont été trouvés dépendants de la teneur en vides des éprouvettes. La valeur des deux paramètres décroit avec l'augmentation de la teneur en vides. Toutefois, les valeurs de τ pour la BG PMB ne corrèlent pas avec les valeurs des autres deux formules. Ceci est une évidence de la modification par polymères du bitume GB PMB.

Le module statique E00, par contre, n'a pas présenté de relation directe avec aucune des caractéristiques des éprouvettes. Il ne dépend pas non plus de l'état de conditionnement des éprouvettes. Le a haute dispersion des valeurs de E_{00} est, en partie, cause des limitations des

capteurs de mesure, notamment du capteur de force. Dans les conditions associés à E_{00} (haute température/basse fréquence) les amplitudes de force sont très faibles et les mesures imprécises. Toutefois, il a été identifié que les éprouvettes souffrant de l'extension pendant les essais présentaient des faibles modules statiques. Les résultats des essais de sollicitation cyclique à des différents niveaux de déformation moyenne et de relaxation ont permis de confirmer le fait que le module E_{00} décroit considérablement avec l'extension de l'échantillon.

c. Par rapport aux propriétés de fatigue des enrobés bitumineux testés

Les résultats des essais de fatigue réalisés sur des éprouvettes conditionnées à l'eau et au gel présentent, en général, plus de dispersion que ceux des éprouvettes non-conditionnées. Ceci peut être attribué aux différences dans la disposition interne des vides dans les échantillons, ce qui fait varier l'exposition effective à l'eau d'une éprouvette à l'autre.

La formule GB3 présente la plus grande susceptibilité à l'humidité des trois formules étudiées. Les propriétés de résistance à la fatigue de la GB4 ne semblent pas avoir été affectées par la procédure de conditionnement. Du fait que la GB4 est l'éprouvette la plus compacte, ceci implique que l'augmentation de la teneur en vides favorise la réduction de la résistance à la fatigue des matériaux par exposition à l'humidité. Toutefois, la formule GB4 a aussi présenté la plus grande incertitude de ε_6 parmi les trois matériaux.

La GB PMB présente une susceptibilité à l'eau et au gel moindre que la GB3. Néanmoins, elle présente des propriétés de résistance à la fatigue plus élevées que les formules GB3 et GB4, même après conditionnement. L'utilisation du bitume modifié aux polymères a réellement amélioré la résistance à la fatigue de la formule GB3.

Les niveaux de déformation mesurés à la base de la couche d'enrobé sous ballast de la LGV EE sont très faibles. Ces résultats ont été corroborés par des travaux de simulation de la voie. Sur la base de la méthode française de dimensionnement des chaussées, les propriétés de résistance à la fatigue des enrobés testés, même après conditionnement, semble adéquate pour leur utilisation en couche sous ballast. Toutefois, les mesures de la LGV EE devraient être confrontées à des nouvelles mesures dans d'autres projets comme la LGV Bretagne – Pays de Loire (BPL).

d. Contributions générales de l'étude

Cette étude a été réalisée en collaboration avec la Direction de l'Ingénierie de la SNCF. Ses résultats fournissent à l'industrie des informations de valeur sur le comportement thermomécanique des enrobés bitumineux pour infrastructure ferroviaire. Ces informations sont d'utilité pour l'établissement de documents référentiels en relation avec l'utilisation de matériaux bitumineux en couche sous ballast. Cette étude sert aussi de référence pour l'établissement des conditions requises des formulations d'enrobés pour le ferroviaire (teneur en liant, type de liant, teneur en vides). Les résultats de la caractérisation du comportement thermomécanique des enrobes peuvent aussi être intégrés dans les bases de données matériaux pour des futurs projets de modélisation numérique des voies.

Les conclusions de cette étude corroborent le fait que les formules d'enrobé bitumineux actuellement disponibles dans le marché français présentent des propriétés adéquates pour leur

utilisation en couche sous-ballast. Plus spécifiquement, la formule GB4, déjà utilisé dans la construction de la LGV BPL, a été trouvée très performante. L'information fournie sur la GB4 servira dans l'interprétation du REX de la LGV BPL.

Des nouvelles méthodes d'essai en laboratoire ont aussi été proposées dans le cadre de cette étude. Une nouvelle procédure de conditionnement à l'eau et au gel a été développée. Elle est considéré comme agressive mais respectueuse de l'intégrité des éprouvettes et simple d'utilisation.

De plus, deux protocoles d'essai mécaniques ont été développés pur accéder au module statique des enrobés bitumineux en fonction de l'état de déformation des éprouvettes. Les résultats de ces essais montrent une réduction du module statique avec l'extension de l'échantillon. Plus de travail expérimental devrait être réalisé sur ce sujet, spécialement des essais en contraction.

Les conclusions de cette étude ouvrent des portes à nombreux projets de recherche comme la viabilité de l'utilisation d'enrobés à fort taux de recyclés en structure ferroviaire, l'utilisation d'enrobés bitumineux comme assise des voies sans ballast, ou encore, leur utilisation dans des voies sans traverses avec rails en appui en continu sur la couche d'enrobé.

e. Recommandations pour des travaux futurs

Plusieurs points de cette étude méritent plus d'investigation, en particulier les suivants :

- La création et le suivi de zone instrumentés dans des voies avec enrobé sous ballast. Ceci fournira des informations supplémentaires par rapport au comportement de ces structures et leur durée de vie.
- Le développement des essais mécaniques pour la détection du module statique des enrobés bitumineux et de sa dépendance de l'état de déformation de l'échantillon. La procédure de l'essai de module complexe doit être modifiée pour éviter l'extension des échantillons pendant l'essai.
- L'utilisation d'agents anti-desenrobage dans des enrobés bitumineux à usage ferroviaire.
- La caractérisation des vides dans les éprouvettes par tomographie CT en complément de la procédure de conditionnement à l'eau et au gel proposée. Du fait que la saturation n'est pas imposé ni forcé, connaître la disposition des vides dans les éprouvettes permettrait d'avoir une idée sur l'exposition effective du matériau à l'eau pendant le conditionnement.
- La caractérisation des propriétés du bitume récupéré des éprouvettes conditionnées à l'eau et au gel pour quantifier les effets de la procédure sur le bitume.
- L'association des résultats de l'essai de fatigue avec l'analyse d'images des fasciés de rupture.